MULTITECHNIQUE STUDIES OF IONOSPHERIC PHENOMENA

Thesis
Submitted to

SAURASHTRA UNIVERSITY
Rajkot, India

For the Award of the Degree of
DOCTOR OF PHILOSOPHY
in
PHYSICS
by

Mala S. Bagiya

Guide
Dr. H. P. Joshi
Professor
Department of Physics
Saurashtra University
Rajkot – 360 005
India

September – 2010

MULTITECHNIQUE STUDIES OF IONOSPHERIC PHENOMENA

Thesis
Submitted to

SAURASHTRA UNIVERSITY
Rajkot, India

For the Award of the Degree of
DOCTOR OF PHILOSOPHY
in
PHYSICS
by

Mala S. Bagiya

Guide
Dr. H. P. Joshi
Professor
Department of Physics
Saurashtra University
Rajkot – 360 005
India

September - 2010

Dedicated To Mummy, Papa, Neetu and God

CERTIFICATE

This is to certify that the present work submitted for the award of Ph. D. degree of Saurashtra University, Rajkot by Miss Mala S. Bagiya has been the result of about 3 years of work under my supervision and is a valuable contribution in the field of IONOSPHERIC PHYSICS.

Dr. H. P. Joshi
Research Guide
Professor
Department of Physics
Saurashtra University
Rajkot – 360 005
INDIA

Acknowledgements

I wish to thank profusely and acknowledge with deep sense of gratitude to my guide, Prof. H. P. Joshi, Department of Physics, Saurashtra University, Rajkot for his guidance and patience throughout the course of this research effort. His constant monitoring and the valuable advices ensured the completion of this thesis. I thank him for setting high standards and motivating me to do the best.

I take this opportunity to acknowledge with thanks and deep sense of gratitude to Prof. K. N. Iyer, Head, Department of Physics, Saurashtra University, Rajkot for his constant encouragement and guidance during this work. I pay my heartily gratitude to Mrs. Girija. N. Iyer madam for her strong support and love.

I express my gratitude and high regards to Prof. R. Sekar, Physical Research Laboratory, Ahmedabad, in giving me vision towards research during UN course at PRL. His clear guidance and comprehensive knowledge has always helped me in understanding the subject.

I express my heartfelt gratitude to the late Dr. Sudha Ravindran, Space Physics Laboratory, Trivandrum, for her cooperation and for providing the GAGAN data. You will be always remembered and the memories always on my mind.

I am thankful to Dr. Smitha Thampi, Kyoto University, RISH, for her keen interest and encouragement. I thank her for sparing her valuable time and going through my work and making useful suggestions.

I gratefully acknowledge Dr. A. K. Patra, NARL, Gadanki for providing radar data and logistic facility during the campaign. He always kindly grants me his time even for answering some of my unintelligent questions about radar systems. I am grateful to Prof. Harish Chandra, Physical Research Laboratory, Ahmedabad for his ready cooperation and invaluable suggestions in carrying out my research work. I

would like to thank Dr. Dipu Chakrabaty, Physical Research Laboratory, Ahmedabad for his belief and generosity in sharing knowledge and experience. I am grateful to Prof. P. V. S. Ramarao, Andhra University, Visakhapatnam for his constant encouragement during the work. I thank Dr. B. M. Pathan, Indian Institute of Geomagnetism, Mumbai for providing the electrojet and magnetic data.

I sincerely thank Prof. H. H. Joshi, Prof. M. J. Joshi, Prof. D. G. Kuberkar, Dr. G. J. Baldha, Dr. K. B. Modi, Dr. J. A. Bhalodia, Department of Physics, Dr. M. N. Jivani, Department of Electronics, Saurashtra University, Rajkot for their strong support and inspiration throughout my research work. The cooperation from the non-teaching staff of the physics department is duly acknowledged. The library facilities and computer facilities of the university have been indispensable.

I would like to take this opportunity to convey my appreciation to Dr. Ritweej, Savan, Prakash, Sonal Saurashtra University, Rajkot, Mr. Satya Srinivas, NERTU, Heydrabad, for their kindness and help.

Special thanks are due to Drs. Debashish Nath, Phanikumar NARL, Gadanki, Malini Aggarwal, Yogesh Jani, Ravi Jadav, Niraj Pandya Saurashtra University Rajkot, Mr. Ribu Cherin IIT Mumbai, Mr. Ajeet Maurya IIG Mumbai, Mr. Sumanta Sarkhel, PRL, Ahmedabad for their honorable support to complete this thesis.

I am indebted to Dr. Pooja, Dr. Rujuta, Dr. Piyush, Purvi, Kashmira, Megha, Jayant, Jagdish, Ashish, Poorvesh, Sanjay, Nimish, Kamlesh, Vinay, Pooja, Jesica, Uma for making my stay here a memorable one. The company of Bansari H. Joshi, Hemangi H. Joshi, and Krutarth H. Joshi always made my vacation days very joyful. I also extend my gratitude to my M.Sc. classmates, and M.Sc. students for the support they have lent me during my stay in the university.

I wish to thank my childhood friends Ravi, Mayank, Mrs. Manisha, Mrs. Meeta, Mrs. Jigu, Kosha, Juhi, Raju, Nishith for helping me get through the difficult

times, and for all the emotional support, camaraderie, entertainment, and caring they provided.

I am happy to express my gratitude to Miss Neha Shukla for holding my hand and showing me the right direction at several critical dual paths of the life. I would like to take the opportunity to thank all my teachers for shaping my carrier to this point.

Finally, I am in short of words in expressing my thanks to my parents and other family members. The unflinching love and support received from my father and mother is enormous. Their unwavering faith and confidence in my abilities and in me is what has shaped me to be the person I am today. Thank you for everything. My thanks also go out to my grandparents who showed me the true worth of hard work. I thank my younger sister Neetu for her love and affection. The moral support and encouragement of her has always been a great source of inspiration. I thank my cousin Kaval for his constant monitoring in providing all the comforts during the work. Finally, thank you God.

Mala S. Bagiya

CONTENTS

Chapter 3

TEC variations during low solar activity period (2005-2009) near the EIA crest region in India

Chapter 4

A Multitechnique investigation on ESF irregularities

Chapter 5

Low Latitude ionospheric-thermospheric response to storm time electrodynamical coupling between high and low latitudes

Preface

The ionospheric plasma density shows temporal variability (with time of the day, season and solar cycle), latitudinal variability and variations during geomagnetic disturbances. In addition to this there is a presence of moving ionospheric plasma density irregularities in the night time equatorial and low latitude ionospheric F region on certain days. All these result in to the degradation of the strength of the satellite signals coming towards the earth. Hence from the point of view of satellite based navigation issues such as GPS based navigation, it is important to study the various ionospheric variability, evolution and growth of equatorial ionospheric F region irregularities and associated radio wave scintillation and geomagnetic storm time ionospheric behavior. The present thesis deals with above mentioned objectives.

Ionosphere has been studied by various ground based techniques during the past 4-5 decades. With advent of satellite era, space based techniques have been evolving which provide better global coverage. The multitechnique studies of ionosphere provides diagnostic tool for better understanding of the ionospheric variability and various ionospheric phenomena. The present study has been carried out using GPS - TEC and scintillation monitor, VHF coherent back scatter radar and Ionosonde techniques. The in-situ measurements and optical techniques have also been used.

The thesis consists of six chapters:

Chapter 1 gives the brief introduction of the earth's atmosphere and ionosphere. The various ionospheric characteristics along with the various phenomena that are common in equatorial and low latitude ionosphere are briefly reviewed. The scintillation and geomagnetic storm and its effects on ionosphere are highlighted.

Chapter 2 describes the various techniques used for the present study. The GPS – TEC and scintillation measurement technique along with the VHF coherent back scatter radar and ionosonde techniques are discussed in detail. In-situ and optical techniques are also highlighted.

Chapter 3 describes the ionospheric variability in terms of TEC near the northern EIA crest region, Rajkot (22.29^0N 70.74^0E, sub-ionospheric dip latitude 15.8^0N) in India for low solar activity period of 2005-2009. The diurnal and seasonal variations of TEC and solar activity dependence of TEC are discussed. It is seen that TEC shows positive solar activity dependence. The control of EEJ on EIA development is described. The influence of EEJ on low latitude TEC is also discussed. The low latitude L-band scintillation study describes that the observed amplitude of scintillation and occurrence frequency both remain low due to the low solar activity period.

Chapter 4 describes multitechqniue studies of ESF irregularities. The evolution and growth of ESF irregularities of various scale sizes are discussed in detail. The inhibition of E region instability in the presence of vertically rising ESF plumes is observed. The detail investigation on TEC depletions and L-band scintillation in association with the ESF plume structures are carried out. These results are presented and discussed in detail in chapter. In addition to TEC depletions, TEC enhancement during ESF is also addressed and discussed in detail. The latitudinal extent of L-band scintillation using GAGAN GPS receivers has been studied. The result says that L-band scintillation maximizes at low latitudes. The ESF and L-band scintillation both shows positive solar activity dependence.

Chapter 5 describes the geomagnetic storm time electrodynamical and neutral dynamical coupling between high and low latitudes and its effects on low latitude ionosphere – thermosphere system. The storm time ionospheric electric field perturbations either due to prompt penetration electric field or disturbance dynamo electric field redistributes the ionospheric plasma and creates positive or negative

ionospheric storm respectively. The prompt penetration electric field effect is observed to be occurred immediately while the disturbance dynamo electric field shows the delayed effect. It is observed that the storm time thermospheric neutral composition changes have great influences on ionospheric electron density. The prompt penetration of eastward electric field to equatorial and low latitudes leads to development of strong ESF where conditions was not much conducive for strong ESF generation before the onset of storm.

Chapter 6 summarizes the main results.

The results presented and discussed in this thesis bring out the significance of various equatorial and low latitude ionospheric phenomena which degrade the accuracy of satellite (for example, GPS) based positioning and navigation.

List of Abbreviations

IST	:	Indian Standard Time [IST= UT (Universal Time) + 5.5 hrs]
EEJ	:	Equatorial electrojet
CEJ	:	Counter electrojet
EIA	:	Equatorial ionization anomaly
ESF	:	Equatorial spread-F
SSC	:	Storm sudden commencement
TEC	:	Total Electron Content
IPP	:	Ionospheric Pierce Point
GPS	:	Global Positioning System
VHF	:	Very High Frequency
UHF	:	Ultra High Frequency
ISR	:	Incoherent Scatter Radar
MST radar	:	Mesosphere Stratosphere Troposphere radar
RTI	:	Range-Time-Intensity
TIMED	:	Thermosphere, Ionosphere, Mesosphere, Energetics and Dynamics
GUVI	:	Global Ultraviolet Imager
GAGAN	:	GPS Aided Geo Augmented Navigation
IMFBz	:	Interplanetary Magnetic Field – Z component
AE	:	Auroral electrojet index
IEFy	:	Interplanetary Electric Field- Y component
SYM-H	:	Symmetric ring current index

List of Figures

List of Tables

Chapter 1
Introduction

1.1 Introduction

The age of radio communication has been started with the discovery of ionized medium in the earth's upper atmosphere which contains free electrons in numbers sufficient to influence the propagation of the radio waves. This ionized medium is known as the ionosphere. The first credit to postulate the existence of the ionosphere goes to *Stewart* [1882]. *Marconi* [1901] had given an evidence for the existence of the ionosphere by conducting an experiment to transmit a radio signal from England to Canada. The independent evidences provided by *Kennelly* [1902] and *Heaviside* [1902] for the existence of the ionosphere offered more correct explanation for Marconi's radio communication experiment. They suggested that long range propagation could be due to the reflection of the radio signals from the ionized medium in the upper atmosphere. The final confirmation for the existence of the ionosphere emerged with the radio sounding experiments of *Appleton and Barnett* [1925] in England and *Breit and Tuve* [1925 & 1926] in America. These experiments revealed the distinct regions of the ionosphere conventionally designated as D (70 to 90 km), E (90- 150 km) and F (150 to not well defined but ~ 1000 km). *Chapman* [1931] presented a theory for the formation of the ionospheric regions based on the action of solar UV radiation. It was discovered that the F region splits into two regions at different altitudes during the day; the lower was labeled as F_1 region and the upper as F_2 region. There was rapid progress in obtaining an overall grasp of the behavior of the ionosphere and its effects on the propagation of radio signals. Appleton – Hartee equations were established [*Appleton,* 1932], which gave the complex index of refraction and the polarization for a plane wave propagated in the ionosphere in the presence of the earth's magnetic field.

Conventionally, the ionosphere has been considered as good reflector - under suitable conditions - of long, medium and short waves used for broadcasting

and radio communication. But in the present scenario of satellite based communication and navigation, the ionosphere is the major debilitating factor. In general, the satellite communication systems operate at sufficiently high radio wave frequencies which can propagate through the ionosphere unobstructed. But during their propagation, the radio signals experience a group delay due to the presence of free electrons in their propagation path. This behavior is not tolerable considering the demands of the modern satellite based communication and navigation systems. If the ionosphere is stationary, one could have estimated the number of electrons which the radio waves encounter during their propagation from the ionosphere and thus the group delay. With the help of this estimated group delay, the required correction could be done to acquire better accuracy of satellite based communication and navigation system. But this is not the case. Since the ionosphere is highly dependent on the input energy from the sun, it has great temporal variability ranging from min (during geomagnetic storms) to 11 years (solar cycle) and remarkable spatial variability that depends on the geometry of the earth's magnetic field. In addition to this, ionospheric plasma irregularities drifting in front of the satellite radio signals, scintillate the radio wave signals and causes unevenness of the signals at the receiver end. Therefore the behavior of the ionosphere under different geophysical conditions at different geographical locations needs to be understood carefully. The present study is centered on the ionospheric variability and the behavior of the ionosphere during various ionospheric phenomena. The thermospheric behavior during geomagnetic storms and its effects on the ionosphere are also presented. The following sections described the earth's atmosphere and ionosphere and its various characteristics in detail.

1.2 The structure of the neutral atmosphere

The earth is enveloped by its atmosphere which is bound to it due to its gravity. The earth's atmosphere which co-rotates with it can be classified according to various schemes based, in particular on, temperature, composition and state of mixing. The classification of different regions of the earth's atmosphere on the basis of temperature and state of mixing along with the

distribution of various neutral species with respect to height is shown in Figure 1.1. The total neutral gas density is ~10^{19} cm^{-3} near the ground and it decreases exponentially with height. As shown in the Figure 1.1, on the basis of the neutral temperature variation with height, the atmosphere can be subdivided in the troposphere, stratosphere, mesosphere and the thermosphere. The average height of troposphere varies from ~ 15 km at the equator to ~ 8 km at the poles. Tropopause occurs at these values of height respectively. Troposphere is the region of negative lapse rate (-6 K/km) due to the decrease in infra-red radiation as a function of height from the surface of the earth. This region consists of about 85-90% of the atmospheric mass. Weather occurs in the troposphere. The stratosphere starts after the tropopause, here the temperature increases with height and obtains a value of ~260 K near the stratopause (~ 50 km) from ~170 K at the tropopause (~15 km) due to the absorption of solar UV radiation by ozone. Stratosphere contains 90% of the atmospheric ozone with a peak ozone density at ~25 km. In mesosphere, which starts after the stratopause, temperature again decreases with height and reaches a minimum value of ~180 K near the mesopause at ~85 km. In the thermosphere, temperature increases monotonically with height due to the direct heating from the sun and obtains its highest value. The energy budget of the thermosphere is highly dependent on input solar energy.

The region of the atmosphere up to ~ 100 km is subjected to turbulent mixing. Therefore the lower atmospheric species in the atmosphere are well-mixed and this is the region of uniform composition, known as the homosphere or turbosphere. The mean free path (the average distance between successive collisions of the particles) is given by the following equation for molecular of diameter d at pressure P and temperature T.

$$\lambda_m = \frac{1}{\sqrt{2}\pi d^2}\frac{KT}{P} \tag{1.1}$$

From the above expression the mean free path increases with altitude as pressure decreases. The mean free path of the major atmospheric species is small in the lower dense atmosphere. The upper boundary of the homosphere is known as the turbopause (~110 km). Above the turbopause, the mean free path becomes

large and the molecular diffusion process becomes dominant. This region is known as the heterosphere. The mass discrimination is observed in the heterosphere and the vertical distribution of the atmospheric species is governed by their molecular masses and their diffusion, hence diffusive separation occurs, i.e. the heavier constituents start decreasing fast with altitude followed by the lighter species as shown in Figure 1.1.

This region is gravitationally separated with height, hence the situation arrives where the atomic and molecular motions - which are constantly under the influence of gravity - becomes almost collision free. Due to this, the atoms and molecules with larger kinetic energy can escape from the earth's atmosphere. This region is known as the exosphere and starts at ~ 600-700 km.

In general the region between (0-15 km) is called the lower atmosphere, (15-90 km) is the middle atmosphere, and the region above the 90 km is referred to as the upper atmosphere. Now it is known that the solar UV radiation from the sun is being absorbed in the altitude range of 15-60 km where the ozone concentration is significant. Before getting absorbed by the ozone, solar UV photons have sufficient energy to break the neutral species of the atmosphere above the altitude of ~60 km i.e. upper atmosphere. This reaction creates the free electrons and ions in the upper atmosphere and this part of the atmosphere which extends up to ~ 1000 km is known as the ionosphere. The ionosphere will be dealt in detailed in section 1.3. The region of the atmosphere where the present study is centered is the ionized part of the upper atmosphere - ionosphere.

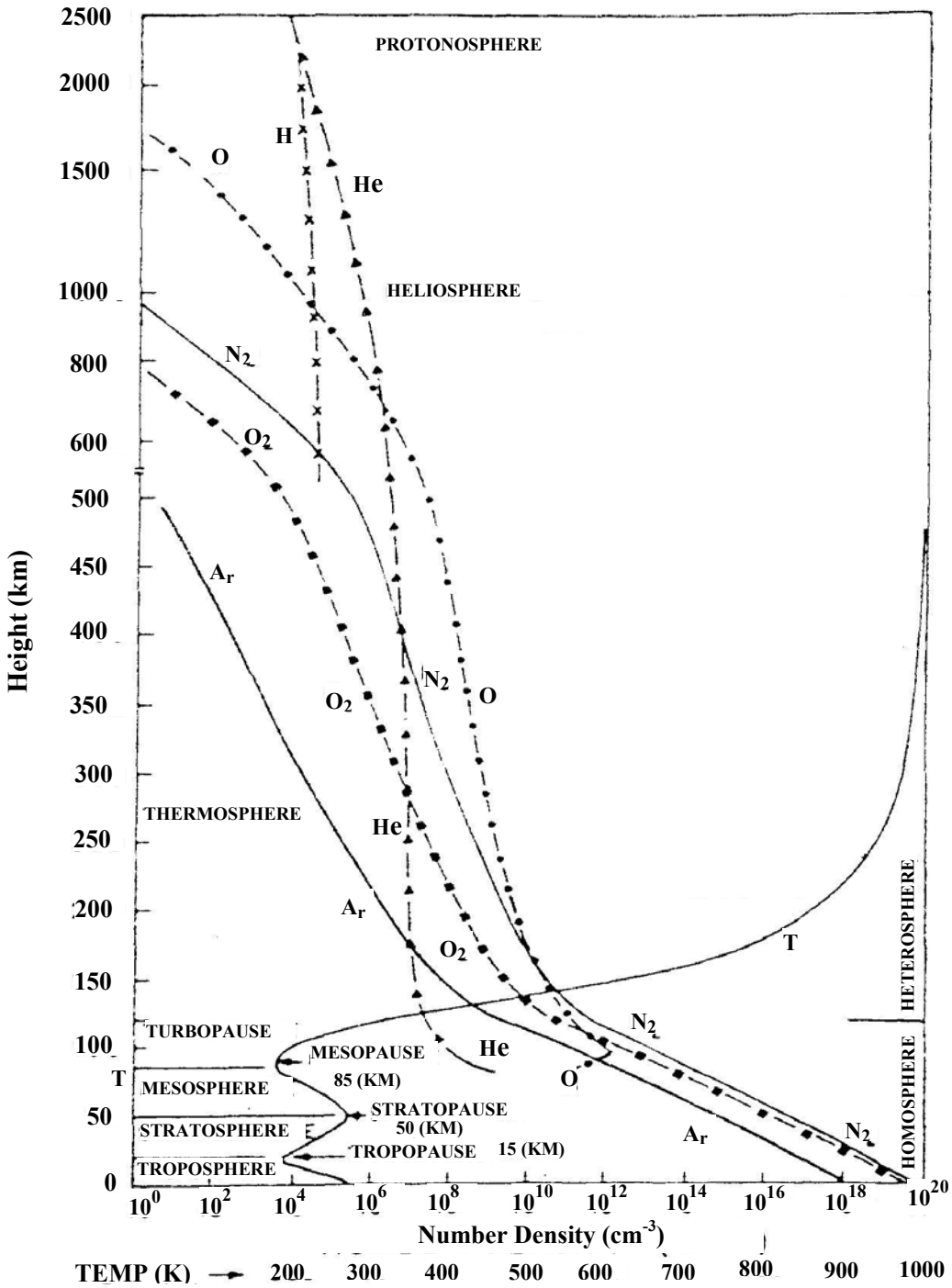

Figure 1.1: Temperature profile of the earth's atmosphere along with the density distribution [reproduced after *Pant,* 1998]

1.3 Ionosphere

The solar EUV photons ionize the neutral upper atmosphere through the process of photoionization in the day time hemisphere and creates ionosphere within it. In other words the ionosphere can be defined as the ionized part of the upper atmosphere which contains free electrons and ions. It begins at a height of ~60 km with no well defined upper limits but ~1000 km. Since the main energy source for the ionosphere is the incoming solar energy, the ionosphere has strong solar dependence. Once absorbed the solar EUV photons (in the process of photoionization), the intensity of the photon-beam deceases as it penetrates further in the region of increasing neutral density with decreasing altitude. The peak of the ionization occurs ~350 km i.e. the ions and electrons are most abundant at this level, with value of $10^6 cm^{-3}$ [*Kelley* 1989].

But they represent only one thousand of the total neutral density even at that level, so the ionosphere can be regarded as weakly ionized plasma. The peak plasma density is limited by the recombination rate at which the ions and electrons recombine to form a neutral molecule or atom.

The ionospheric radio sounding using the ionosonde revealed the distinct regions of the ionosphere [*Appleton and Barneet,* 1925, *Breit and Tuve,* 1925 & 1926]. Conventionally, these regions are known as the D, E and F regions. During day time the F region splits into F_1 and F_2 regions. Though the boundary of these regions gradually merges into each other, the boundary between D and E regions is assumed ~90 km altitude and the boundary between E and F regions is ~150 km. After sunset when the production stops, the D and E regions recombine fast while F_1 and F_2 regions merge into single F region which sustains throughout the night. Figure 1.2 shows electron density distribution in D, E and F regions of the ionosphere during day time and night time during solar maximum (maximum sunspot) and solar minimum (minimum sunspot) conditions.

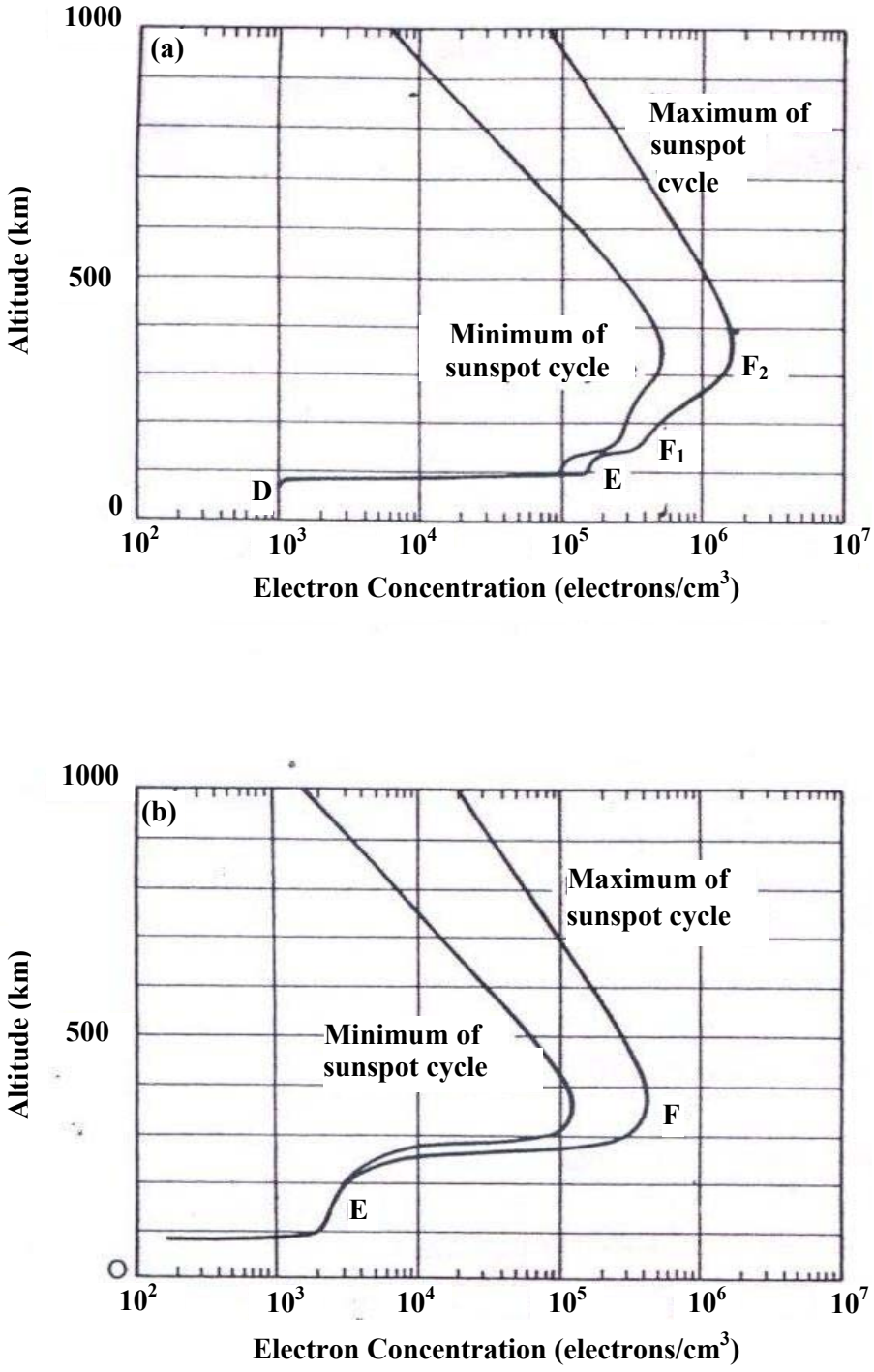

Figure 1.2: Electron density distribution in different regions of ionosphere with respect to solar activity (a) during daytime (b) during nighttime [After *Kelley,* 1989]

An excellent description on formation of ionosphere is given in *Hargreaves* [1992]. The ionosphere is produced by a wide spectrum of solar radiation. D region ionization is highly sensitive to the phase of the solar activity. During solar maximum the major ionization of D region is produced by the solar hard X-rays (0.1-1 nm). During solar minimum Ly-α (121.6 nm) ionizes the NO only and provides the major ionization source. O_2 ($^1\Delta$) metastables ionization by UV radiation < 111.8 nm and cosmic rays as well contributes to D region ionization.

The E region ionization is produced by the solar UV radiation between 91.1 – 102.7 nm. During solar maximum soft X-rays (1-20 nm) provides an important source of ionization. The F region ionization is produced by the EUV radiation of solar spectrum in 20-91.1 nm range. He I (~30.4 nm) and He II (~58.4 nm) are also source of ionization for F region. The negative ions exist only in D region and not in E and F regions.

The plasma which is dominant above 150 km is represented by O^+. The ionospheric peak production occurs in the F_2 region around 350 km for vertically incident solar radiation. The production rate above this altitude is limited by the available neutral species while that below by the available solar flux. This altitude has solar zenith angle dependency and it rises up with increase in solar zenith angle. However, the altitude of the ionization peak is much higher than the production peak, as the ionization is controlled by production as well as by loss and transport also. Due to these reasons ionization peak is highly variable with time of the day, season and solar activity.

At lower altitudes (E and lower F regions), dissociative recombination reduces the plasma density during nighttime. At higher altitude (upper F region) the plasma i.e. O^+ and H^+ ions sustains throughout the night. In this region the ionization loss is governed by charge exchange reaction.

The transition between these two regions occurs in the F region at about 160-200 km. When this transition region coincides with F region production peak,

the F region splits in to F_1 and F_2 regions [*Ratcliffe,* 1956]. In the upper F region, the recombination rate becomes lower than the ionization rate as altitude increases. Hence, there will be a larger ion density at altitude above F_1 region.

The atmospheric dynamos are active in the ionosphere, in which the motions of the neutral atmosphere across the earth's magnetic field lines produce the electric fields. These electric fields induce currents and motions in the ionospheric plasma. In E region the collision frequencies of ions with neutral (ν_{in}) is higher as compared to their gyrofrequencies (Ω_{in}) and the ions move with neutral wind. In case of electrons, their gyrofrequencies (Ω_e) are larger as compared to their collision frequencies with the neutrals (ν_e). In F region, the ion and electron motions are governed by geomagnetic field as their gyrofrequencies are higher than their respective collision frequencies with neutrals. The motions of the plasma initiate the various types of plasma instabilities in E and F regions at the time. The ionospheric E and F region's dynamo and plasma density irregularities will be discussed in detail in following sections.

It is known that at the magnetic equator the earth's magnetic field is horizontal, at mid latitudes it is inclined to the normal, and at polar latitudes it is almost vertical. Due to the difference in geometry of the earth's magnetic field at the magnetic equator and elsewhere, the behavior of the equatorial and low latitude ionosphere differs to a great extent from that of the mid and high latitudes. Therefore the regular investigations on the ionosphere have become extensive. In general the ionosphere from 0^0 to $\leq 20^0$ geomagnetic latitudes represents the equatorial and low latitude ionosphere, from 20^0 to 50^0 geomagnetic latitudes represents the mid latitude ionosphere and over 50^0 geomagnetic latitudes represents polar or high latitude ionosphere. India falls in the equatorial and low latitude zones with the magnetic equator at Trivandrum (8.5^0N, 77^0E, dip latitude 0.5^0N). Due to the different magnetic field geometry with latitudes, the ionosphere shows great spatial variability and due to the variable solar input energy it shows great temporal variability.

1.4 Electrical conductivity of the ionosphere

Due to the presence of free electrons and ions, the ionosphere emerges as an excellent conductor of electricity. The conductivity of the ionosphere is determined from the basic equations of motion for electrons and ions under the action of an applied electric field E [*Cowling,* 1945; *Baker and Martyn,* 1952, 1953; *Chapman,* 1956]. The ionospheric conductivity occurs due to the motions of free electrons and ions under the effects of two driving forces, first one is the presence of an electric field and the second is the neutral wind. However there are two complicating factors which one should consider while taking care of ionospheric conductivity, one is the collision between the charged and neutral particles and the second is the presence of geomagnetic field. The first one is characterized by the collision frequency and the second one is by the gyrofrequency. The electric conductivity of the ionosphere in the presence of a geomagnetic field depends on the number density of the charged particles (N_e, Ni), electric charge (e), mass (m), mean collision frequency (ν), and gyrofrequency ($\Omega = eB/m$).

Consider the case when the driving force **F** is parallel to the geomagnetic field **B**. Under this situation the drift velocity **V** of a charged particles can be approximated by equating the driving force F to the drag force due to collisions, $m\mathbf{V}\nu$.

$$\mathbf{V} = \mathbf{F}/m\nu \tag{1.2}$$

The effect of magnetic field is neglected since it is parallel to the direction of motion. On the other hand, when driving force **F** is perpendicular to geomagnetic field **B**, one should consider the effect of both the drag force (due to collisions) and the Lorentz force (due to geomagnetic field). The motion can be estimated to a steady drift with a velocity **V** given by

$$(\mathbf{F} \pm e\mathbf{V} \times \mathbf{B} - m\mathbf{V}\nu) = 0 \tag{1.3}$$

The + sign corresponds to the ions and the – sign corresponds to the electrons. The angle between the driving force **F** and the resulting velocity is given by

$$\tan\theta = \Omega/\nu \tag{1.4}$$

Since $\Omega = eB/m$ $\quad\quad$ $\tan\theta = eB/m\nu$

The ratio in equation (1.4) varies with altitudes because collision frequencies for both electrons (ν_e) and ions (ν_i) decreases rapidly with altitudes while Ω remains almost constant for both of it. Thus θ varies between 0^0 and 90^0, being very small at lower heights and very large at higher heights.

As mentioned earlier, the driving force **F** is either due to electric field **E** (**F** =e**E**) or due to a wind of velocity **U** (**F** = m**U**ν). The drift velocity obtained by a charged particle at any value of height, under the action of the wind of velocity **U**, is given by

$$\mathbf{V} = \left[\frac{\nu}{(\nu^2 + \Omega^2)^{\frac{1}{2}}}\right]\mathbf{U} \tag{1.5}$$

The amplitude of velocity **V** for both ions and electrons at any value of height depends on the ratio of ν/Ω.

Considering the case of an electric field as a driving force, the drift velocity can be estimated as

$$\mathbf{V} = \left[\frac{\Omega}{(\nu^2 + \Omega^2)^{\frac{1}{2}}}\right]\left[\frac{\mathbf{E}}{\mathbf{B}}\right] \tag{1.6}$$

The current produced in the ionosphere - either due to neutral wind or electric field - varies with altitude in direction as well as in magnitude.

The electric conductivity can be defined as $\sigma = \mathbf{I}/\mathbf{E}$, where **E** is the electric field and **I** is the current density. In the presence of the geomagnetic field **B** the ionospheric conductivity can be categorized as (i) Longitudinal or Direct conductivity (σ_0) for motion parallel to **F**, (ii) Pederson conductivity (σ_p) for motion perpendicular to **B** and parallel to **F**, (iii) Hall conductivity (σ_H) for motion perpendicular to both **B** and **F**. The expressions for all these three are given below:

$$\left.\begin{aligned} \sigma_0 &= \left(\frac{N_e}{m_e \nu_e} + \frac{N_i}{m_i \nu_i}\right) e^2 \\ \sigma_P &= \left(\frac{N_e}{m_e \nu_e}\frac{\nu_e^2}{(\nu_e^2+\omega_e^2)} + \frac{N_i}{m_i \nu_i}\frac{\nu_i^2}{(\nu_i^2+\omega_i^2)}\right) e^2 \\ \sigma_H &= \left(\frac{N_e}{m_e \nu_e}\frac{\omega_e \nu_e}{(\nu_e^2+\omega_e^2)} - \frac{N_i}{m_i \nu_i}\frac{\omega_i \nu_i}{(\nu_i^2+\omega_i^2)}\right) e^2 \end{aligned}\right\} \quad (1.7)$$

At any height in the ionosphere, the conductivity depends on the values of collision frequency as well as of gyrofrequency of both electrons and ions. For instance below ~80 km, $\nu_e >> \Omega_e$ and $\nu_i >> \Omega_i$, hence the motion of electrons and ions is controlled by the collisions. As a result, the current value is very small in response to an applied electric field. Above 140 km, the condition is reversed, the collision frequencies of both electrons and ions are very much smaller than their respective gyrofrequencies, $\nu_e << \Omega_e$ and $\nu_i << \Omega_i$. Hence the motion of electrons and ions is controlled by geomagnetic field only, because the effects of collisions are not present. Note that the net current is nearly zero in response to an applied electric field in this region because the electrons and ions have nearly the same Hall drift $\mathbf{E} \times \mathbf{B}/B^2$.

In the region between ~80 km and 140 km, the collision frequency of ions with neutrals (ν_i) is higher compared to their gyrofrequency (Ω_i), $\nu i > \Omega i$, and the ions move with neutral wind. While for electrons, their gyrofrequency (Ω_e) is larger compared to their collision frequency (ν_e) with the neutrals, $\nu_e < \Omega_e$, and they move nearly across the wind. Therefore, electrons and ions have differential

motion in this region. As a result of this charge separation, an electric polarization field $\mathbf{E_p}$ is created in such a way that at steady state the current is divergence free, i.e.,

$$\nabla.J= 0 \tag{1.8}$$

The total electric current **J** can be stated as

$$\mathbf{J} = \sigma \mathbf{E} \tag{1.9}$$

Here **E** consists of polarization electric field $\mathbf{E_p}$ and induced component (**U**×**B**) due to the effect of wind **U** i.e.

$$\mathbf{E} = \mathbf{E_p} + (\mathbf{U} \times \mathbf{B}) \tag{1.10}$$

The polarization electric field $\mathbf{E_p}$ and the electric current **J** have only horizontal components and $\mathbf{E_p}$ can be derived from an electrostatic potential ϕ produced by the charge distribution, i.e.

$$E_p = -\nabla\phi \tag{1.11}$$

Here potential ϕ depends on the global distribution of wind and conductivity.

In the presence of an applied electric field perpendicular to the geomagnetic field, the current is mainly by the Hall drift of electrons and there is minor contribution by the Pederson drift of ions. This region between 80 km and 140 km, which is highly conductive and bounded on either side by comparatively non conducting regions is known as the dynamo region of the ionosphere The current produced here is known as the S_q (solar quite) current of the ionosphere. A calculated height distribution of conductivity for the mid latitude ionosphere at noon is shown in Figure 1.3. It can be seen that the Pedersen and Hall conductivities peak in the E region where the direct conductivity continues to increase with altitude and is of much greater magnitude.

Near the magnetic equator due to the perpendicular geometry of global scale dynamo electric field E_y (east – west direction) and the geomagnetic field B_z (north-south horizontal direction), electrons drifts vertically with respect to ions. Since the vertical extent of E region dynamo is bounded by comparatively non conducting regions, vertical polarization electric field E_z is set up. This vertical polarization electric field sets up a Pederson current of ions so that the Hall current due to electrons is balanced by the Pederson current due to ions at equilibrium. So,

$$\sigma_H E_y = \sigma_P E_z \text{ or } Ez = (\sigma_H/\sigma_P)E_y \tag{1.12}$$

This induced vertically directed polarization field drives a Hall current in the east – west direction. Thus the total horizontal current in the east–west direction is the summation of the Pederson current due to an applied electric field and the Hall current due to an induced vertical polarization field.

The resultant effective conductivity is known as the Cowling conductivity, given by,

$$\sigma_C = \sigma_P + \frac{\sigma_H^2}{\sigma_P} \tag{1.13}$$

Considering a rectangular co-ordinate system with its X-Y plane coincides with the ground, the positive Z-axis is vertically upward, the positive Y direction is eastward and positive X direction is southward. The resultant conductivity along the co-ordinate axes can be shown to be

$$\left.\begin{aligned} \sigma_{XX} &= \frac{\sigma_0 \sigma_P}{\sigma_o \sin^2 I + \sigma_P \cos^2 I} \\ \sigma_{YY} &= \frac{\sigma_H^2}{\sigma_0 \tan^2 I + \sigma_P} + \sigma_P \\ \sigma_{XY} &= \frac{\sigma_0 \sigma_H \sin I}{\sigma_o \sin^2 I + \sigma_P \cos^2 I} \end{aligned}\right\} \tag{1.14}$$

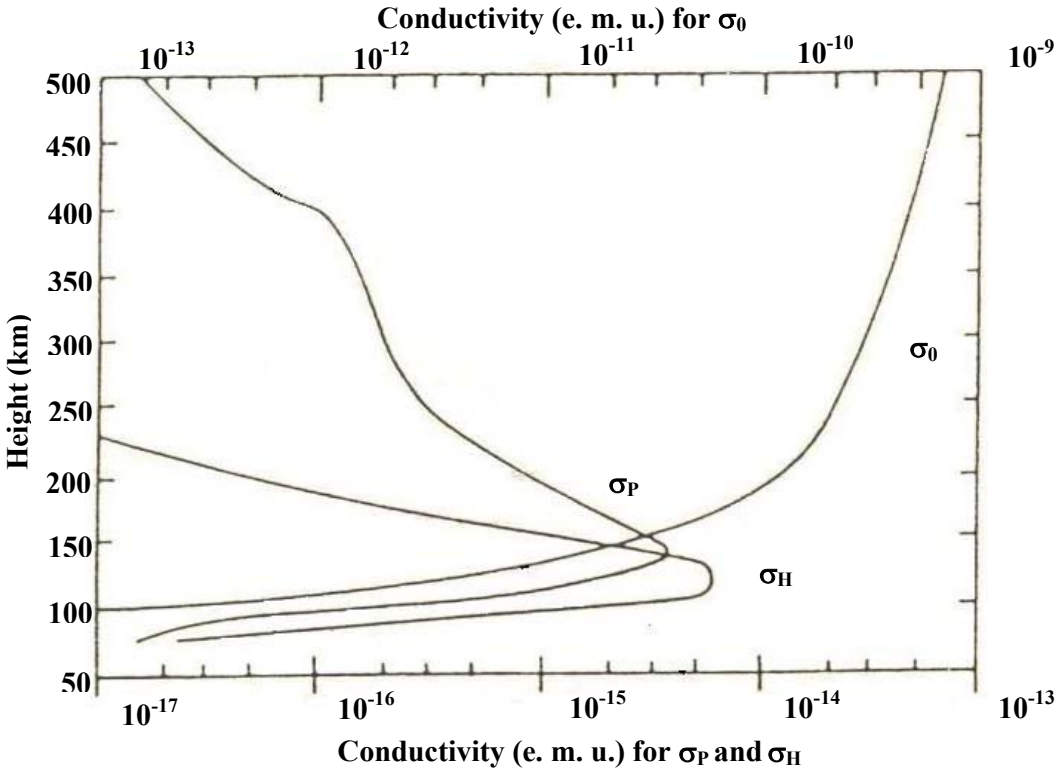

Figure 1.3: Conductivity profile calculated for middle latitude at noon [After *Hargreaves,* 1992]

At the magnetic equator, dip magnetic angle I =0 and

$$\left.\begin{aligned} \sigma_{XX} &= \sigma_0 \\ \sigma_{YY} &= \frac{\sigma_H^2}{\sigma_P} + \sigma_P = \sigma_C \\ \sigma_{XY} &= 0 \end{aligned}\right\} \quad (1.15)$$

This leads to two main consequences. First, the very high conductivity along the magnetic field lines makes them electrically equipotential. Second, the eastward conductivity becomes very large, comparable to direct conductivity σ_0. This results in to the intensification of east – west directed current within $\pm 3^0$ of magnetic equator. This large eastward current is known as the Equatorial Electrojet (EEJ).

1.5 Equatorial Electrojet and Counter Electrojet

Ground based magnetometer when placed near the magnetic equator showed abnormally large amplitude for the daily variation of the horizontal component (H). The enhancement was caused by a band of electric current at an altitude of ~ 105 km within $\pm 3^0$ of magnetic equator.

As we have discussed in section 1.4 that due to the special geometry of global scale dynamo electric field E in the east – west direction and the geomagnetic field B in the north – south direction over the magnetic equator, electros drift vertically with respect to ions and due to limitation of vertical extent of dynamo E region, a vertical polarization electric field sets up. This vertical polarization electric field results in the enhanced conductivity in the eastward direction. This large current is known as the Equatorial Electrojet (EEJ) [*Chapman,* 1951a]. The EEJ leads to many interesting phenomena in the equatorial and low latitude ionosphere.

There is an unusual reversal of EEJ current direction (westward from eastward) during day time on some days. This phenomenon is known as Counter Electrojet (CEJ). When CEJ occurs, the ground magnetic field value during the day goes below the nighttime level. *Gouin and Mayaud* [1967] reported a negative depression of H in observations of daily magnetic variations when CEJ was present. *Rastogi* [1971a] confirmed the westward electric field on the days of CEJ.

1.6 F region Dynamo

The F region has its own dynamo. This was first postulated by *Rishbeth* [1971]. Like the E region, the F region dynamo is also driven by the neutral winds which can generate the current while blowing across the magnetic field lines but the mode of operation are different for both of the regions. At the equatorial F region, around the sunrise and sunset, the pressure gradients in the neutral air produce zonal winds which give rise to vertical currents and polarization electric fields on both sides of the terminators [*Rishbeth,* 1971; *Farely et al.,* 1986; *Eccles,*

1998]. The equatorial F region vertical current is mapped to the magnetically conjugate E region (off equatorial E region) connected to the equatorial F region by the electron flow via the equipotential magnetic field lines constituting a field aligned current as depicted in Figure 1.4(a). When the E region is sunlit, it almost entirely short circuits the F region polarization electric fields [*Rishbeth,* 1971]. After sunset the E region conductivity may become too small that cannot support the field aligned currents. This results in the development of vertical polarization electric field at the F region. The night time enhancement in zonal plasma drift can be explained in terms of this vertical polarization electric field [*Rishbeth,* 1971; *Heelis et al.,* 1974].

To understand the F region, dynamo theory let us follow the simple explanation given in *Kelley* [1989]. Consider a simple model in which the thermospheric wind is eastward having uniform magnitude U with height. The vertical component of the large scale neutral wind field in the atmosphere is always small. Therefore the wind driven current is vertically upward with magnitude

$$J_z = \sigma_p UB \tag{1.16}$$

As σ_p depends on the product $n\nu_{in}$, it varies considerably with height. The zonal wind component U may also vary with height. Thus $d(\sigma_p UB)/dz \neq 0$ and an electric field must built up in the z direction to produce a divergence free current. In the F region $\sigma_p >> \sigma_H$ and $\sigma_p << \sigma_0$. The horizontal magnetic field lines over the equator bend and enter the E region at high latitudes, which has a finite conductivity. During night time, the field aligned current $J_y = 0$.

In the post sunset equatorial F region, gravitational forces do not cause the plasma (more precisely collisionless plasma) to fall at the magnetic equator since the velocity due to gravity is perpendicular to the gravitational force. The E-region ionization almost dies out due to the recombination. The situation resemblance the assumption of slab geometry and the F region plasma shapes a layer with a well defined lower boundary as shown in Figure 1.4 (b).

The F region plasma has a constant, finite Pederson conductivity σ_p inside the slab and zero elsewhere and zonal wind U is constant everywhere. The eastward zonal wind U forces the plasma across the magnetic field B; this generates a polarization electric field E. This gives rise to a zonal drift motion V in the F- region plasma.

During night time this induced zonal motion in plasma follows the direction as that of the zonal wind i.e. eastward direction. Since the current is upward inside the layer and zero elsewhere, charges pile up at the two boundaries as shown in Figure 1.4 (c), which in turn generates the electric field such that

$$Jz = \sigma_p Ez + \sigma_p uB = 0 \qquad (1.17)$$

This implies that

$$E_z = -uB \qquad (1.18)$$

The plasma inside the slab will drift with an $\mathbf{E} \times \mathbf{B}/B^2$ velocity which is equal in magnitude and direction to the zonal wind speed. Furthermore, the electric field in the frame of reference of the neutral wind, $\mathbf{E'} = \mathbf{E} + \mathbf{U} \times \mathbf{B}$, vanishes. The insulating end plate assumption is valid mostly in the night time E region, when rapid recombination takes place between molecular ion and electron. The F region dynamo is supported by O^+ ions which are dominant over there and having much longer life. However, during the day time, the E region entirely short circuits the magnetic field line integrated F region conductivity and the resulting electric fields are determined by winds in the E region. The E region tidal wind is weak hence the plasma drift is smaller during the day than at night. An alternative suggestion by *Haerendel et al.,* [1983] says that the large vertical electric field in the F region is due to partial closure of the vertical equatorial electrojet current in the F region.

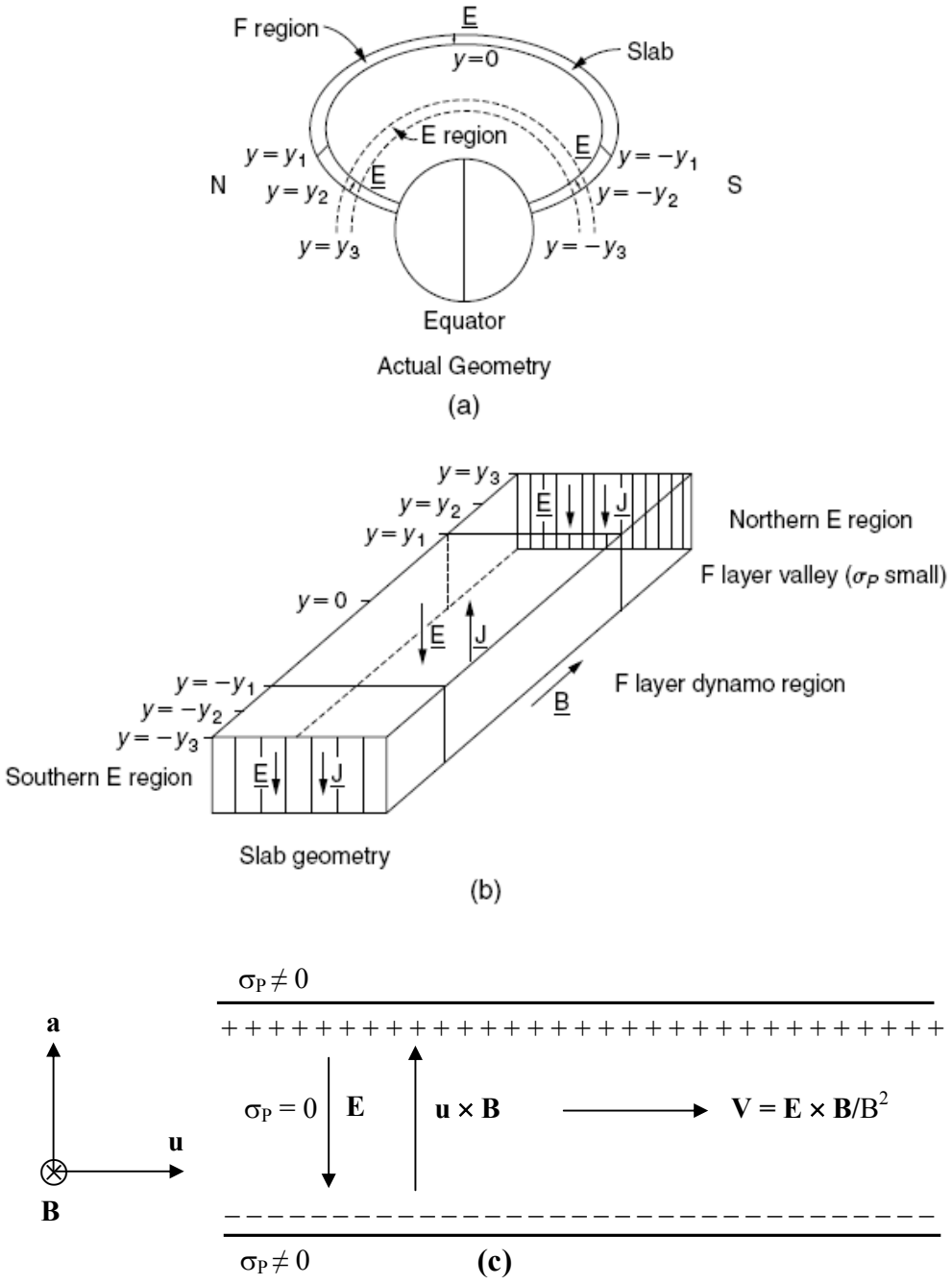

Figure 1.4: (a) Actual magnetic field lines geometry near the magnetic equator (b) F region slab geometry [After *Kelley*, 1989] (c) the schematic of equatorial F- region dynamo

1.7 Equatorial Ionization Anomaly

Due to the unique geometry of horizontal north-south magnetic field and an east-west (zonal) electric field perpendicular to it at the geomagnetic equator, the equatorial ionosphere shows some characteristics phenomena, (i) EEJ that we have already discussed in section 1.5, (ii) Equatorial Ionization Anomaly (EIA) and (iii) Equatorial Spread – F (ESF) etc.

EIA is the redistribution of ionospheric plasma with trough at the magnetic equator and crests on either side of it. In other words, EIA can be defined as double humped structure of ionization on either side of the magnetic equator. The anomalous behavior is seen as less electron density at the magnetic equator during the noon of a day and more on either side of it. It is confined to narrow belt of $\pm 15^0$ magnetic latitudes. *Appleton* [1946] first put forward the idea of a characteristic 'bitten out' look in the diurnal variation of electron density in the ionospheric F region over the magnetic equator. Due to transverse electric and magnetic field at the magnetic dip equator, plasma experiences the upward plasma drift i.e. $\mathbf{E} \times \mathbf{B}$ drift perpendicular to the plane containing electric and magnetic field. Due to the vertical $\mathbf{E} \times \mathbf{B}$ drift which is independent of charge and mass, both the electrons and ions lift up at the magnetic equator simultaneously to greater heights. The resultant is the fountain of equatorial ionospheric plasma under the action of vertical drift. When the meridional pressure gradients become strong enough, the plasma start diffusing down along the geomagnetic field lines away from the magnetic equator assisted by gravity and pole ward winds towards the low latitude ionosphere. This process creates trough at the magnetic equator with two crests on either side of it. Figure 1.5 (a) shows the EIA formation with the involved electrodynamical processes and Figure 1.5 (b) shows pictorial representation of EIA with trough at the magnetic equator due to vertical transport of plasma and two crests on either side of it due to subsequent diffusion.

The EIA was first explained by *Mitra* [1946], who suggested that the ionization produced by solar UV radiation in the upper atmosphere above the magnetic equator was capable of guided towards north and south along the

magnetic field lines of force. *Martyn* [1947] proposed the drift theory and showed that the vertical plasma drift over dip equator followed by diffusion along magnetic field lines is responsible for the double humped anomalous structure of electron density. *Croom et al.,* [1959] first observed EIA experimentally during noontime at different altitudes by using a chain of ionosondes in a longitudinal region. Several observations have shown the day to day, seasonal and solar cycle dependence of EIA [*Rao and Malhotra,* 1964; *Sivaraman et al.,* 1976; *Rastogi and Klobuchar et al.,* 1990; *Walker et al.,* 1994]. *Rush and Richmond,* [1973] have defined the strength of EIA as the product of the ratio of plasma at the crest to that at the trough of EIA and the dip latitude of the crest. EIA longitudinal dependence has been also investigated [*Lyon and Thomas,* 1963; *Lockwood and Nelms,* 1964; *Walker et al.,* 1980; *Sharma and Raghavarao,* 1989]. In addition to the previous observations with ionosonde, TEC and vertical top sounders measurements, ground based optical techniques have also been used to elaborate various EIA characteristics [*Kulkarni,* 1975; *Sridharan et al.,* 1993a; *Pallam Raju et al.,* 1996].

The EIA is predominantly day time phenomenon but it can be seen well beyond the post sunset and predawn hours depending on the season and solar activity phases. During daytime, it is produced by E region dynamo electric field while at post sunset period it is caused by the complex compound ion-neutral dynamics near sunset hours when F region dynamo takes control from the day time E region dynamo

In general, during night time when the eastward electric field reverses and becomes westward, the resultant downward $\mathbf{E} \times \mathbf{B}$ drift gives reverse fountain effect. This causes the retrieval of EIA. The EIA crests and their latitudinal movement had been observed by both ground based and satellite borne optical measurements of airglow emissions [*Chandra et al.,* 1973b; *Kulkarni,* 1975]. *Sridharan et al.,* [1993a] had shown the movement of EIA crest (high intensity regions) from north to south using an all sky imaging Fabry-Perot spectrometer.

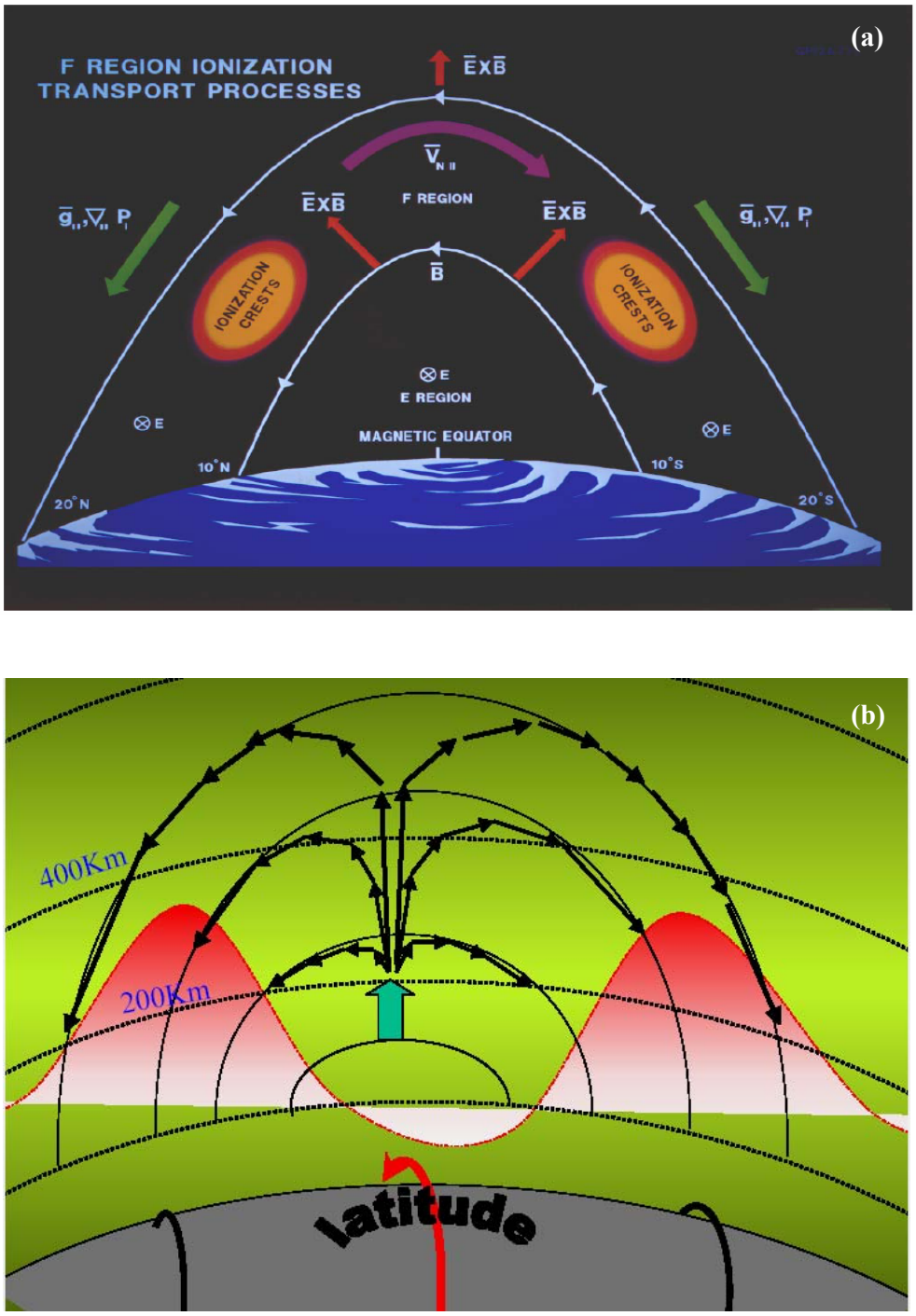

Figure 1.5: (a) Formation of EIA with involved electrodynamical processes (b) pictorial representation of EIA with trough at the magnetic equator and two crests on either side of it due to subsequent diffusion (*www.iiap.res.in/ihy/talks/Session8/Sridharan.pdf*)

Hines [1960] observed that the movements of the EIA crests trigger the gravity waves which in turn modulate both the neutral and ion densities. The latitudinal extent of EIA crests tend to stretch farther during high solar activity period. During geomagnetically disturbed period the EIA development inhibits or enhances that depends on the polarity of penetrated solar wind electric field from high latitudes to low and equatorial latitudes. In addition to electric field the equatorial plasma distribution is controlled by the neutral winds as well. The trans-hemispheric neutral winds induce the hemispheric asymmetry of the EIA. The transequatorial meridional winds produce the north-south asymmetry in the EIA crests.

1.8 Ionospheric irregularities

The ionospheric plasma are in continuous motion due to presence of electric fields, neutral winds etc. At the time, it pursues various kinds of instabilities which can depart the ionosphere from its equilibrium state. These plasma instabilities arise because the plasma in space is not in their thermoequilibrium state and contains definite amount of free energy. To reach into an equilibrium state, the plasma shed some of its energy to some wave modes, thereby making their amplitude grow in time. A growing plasma wave is called an unstable mode. In other way, the plasma instability is the process by which the free energy of the plasma gets converted into a growing mode in a collective way. These instabilities create fluctuations and structures in plasma density, commonly known as irregularities. These irregularities are global i.e. seen at all latitudes, longitudes. The scale sizes of these irregularities range from centimeters to kilometers. Ionospheric irregularities are grouped under E region and F region instability processes. In the last two decades considerable information about ionospheric irregularities has been obtained and considerable progress has been made at equatorial latitudes.

Investigations on equatorial ionospheric irregularities started with ionosonde observations of Equatorial Spread F [*Berkner and Wells,* 1934; *Booker and Wells,* 1938] and Equatorial Sporadic E [*Berkner and Wells,* 1937]. From

1960s, rocket, satellite, radar and scintillation measurement techniques have been used extensively to update our knowledge about the irregularity structures. As mentioned by *Patra* [1997], measurements with rocket and satellite provide estimation of ionospheric parameters such as density, electric fields, magnetic fields etc. A one dimensional k-spectrum of the waves over a wide range of wavelength can be derived from the density data. *Mitra* [1949] introduced the spaced receiver method to estimate drift velocity of ionospheric irregularities from the recording of the fading from spaced receivers. High power coherent VHF radar scatters from irregularities having scale sizes of half of the radar wavelength, i.e. the scattering wavelength is one half of the transmitted wavelength. Backscattered signal power is related to the strength of the irregularities and the Doppler shift corresponds to the drift velocity. When the radio signals encounter the ionospheric irregularities in its way from satellite to the receiver, they suffer phase modulations. The phase modulations give rise to intensity fluctuations as the wave propagates further, resulting in a diffraction pattern at ground. The temporal fluctuations in phase and intensity arise because the diffraction pattern moves due to the horizontal movement of the irregularities. The total number of fluctuations is related to the strength of irregularities. The amplitude and phase scintillation both have been used to study the ionospheric irregularities. The following sections describe the E and F region irregularities.

1.9 E region irregularities

The ionospheric E region irregularities are commonly known as Sporadic-E (Es). In general, Es is observed at all the latitudes and normally found between 100 km to 120 km altitudes. In its weaker form, Es consists of cloud of ionization and in its most intense form consist of a thin sheet of ionization some tens or hundreds of meters in thickness. On ionograms Es is seen as an echo at constant height which extends to a higher frequency than is usual for the E region; for example above 5 MHz. An example of Es observed at Rajkot (22.29^0N 70.74^0E, sub-ionospheric dip latitude 15.8^0N) is shown in Figure 1.6. A thin region is observed at constant height of ~100 km. The second region at ~200 km is the

reflection of the below region. The observed sporadic-E completely absorbs the transmitted frequencies and F region is totally absent.

A brief review on different type of E-region irregularities is given by *Fejer and Kelley* [1980]. *Whitehead* [1970] has given a summary of Es types in all the three latitude regions viz. high, mid and low. As shown by *Mathew* [1998], at high latitudes such ionization is often associated with the appearance of the aurora. This suggests that polar Es might be caused due to particle precipitation. At mid latitudes, one of the prime causes of Es is believed to be horizontal wind movements across the earth's magnetic field, coupled with the existence of large vertical gradients in velocity - "wind shears". *Berkner and Wells* [1937] reported an anomalous scattering region in the equatorial ionospheric E region from ionosonde observations. This scattering region was known as the Equatorial Sporadic –E (Esq). The Esq is believed to be due to plasma instabilities associated with EEJ and present during both day and night even when the electron densities are greatly reduced. VHF forward scattering experiments revealed that the echoes from the Esq region are field aligned and are caused by scattering from electron density irregularity immersed in the equatorial electrojet [*Bowles et al.,* 1960; *Bowles and Cohen,* 1962].

The occurrence of Es is mostly during daytime [*Smith*, 1957] as seen in the ionogram. *Matsushita* [1957] showed that the occurrence of Esq is negatively correlated with geomagnetic disturbances. Occasionally, even on quiet days disappearance of Esq for short periods are associated with low values of horizontal magnetic field intensity or even the reversal of the normal electrojet current (CEJ) [*Cohen et al.,* 1962; *Rastogi et al.,* 1971; *Krishna Murthy and Sen Gupta,* 1972]. This disappearance of Esq is attributed to the reversal of electrojet, i.e. CEJ [*Gouin and Mayaud,* 1967; *Rastogi,* 1972].

In general Es appears as a patchy and particularly transparent region, while sometime it appears in sheets which completely blankets the overlying F region and is known as blanketing type Es or Esb. The generation mechanism of Esb region at the magnetic equator has been proposed to be due to the local action of east west winds with large vertical shears on the electrojet plasma resulting in the

generation of substantial wind induced polarization electric fields perpendicular to the geomagnetic field in the magnetic meridional plane [*Reddy and Devasia,* 1981]. The electric fields generated due to these winds can modify the vertical and latitudinal structure of the electrojet current and can also lead to ionization convergence and divergence and the eventual formation of Esb region [*Somayajulu et al.,* 1993].

Radar spectral studies have shown existence of two classes of irregularities called type I and type II associated with the electrojet. The characteristics of the type I or two stream irregularities were determined in the early measurements at Peru [*Bowles et al.,* 1960, 1963; *Bowles and Cohen,* 1962].

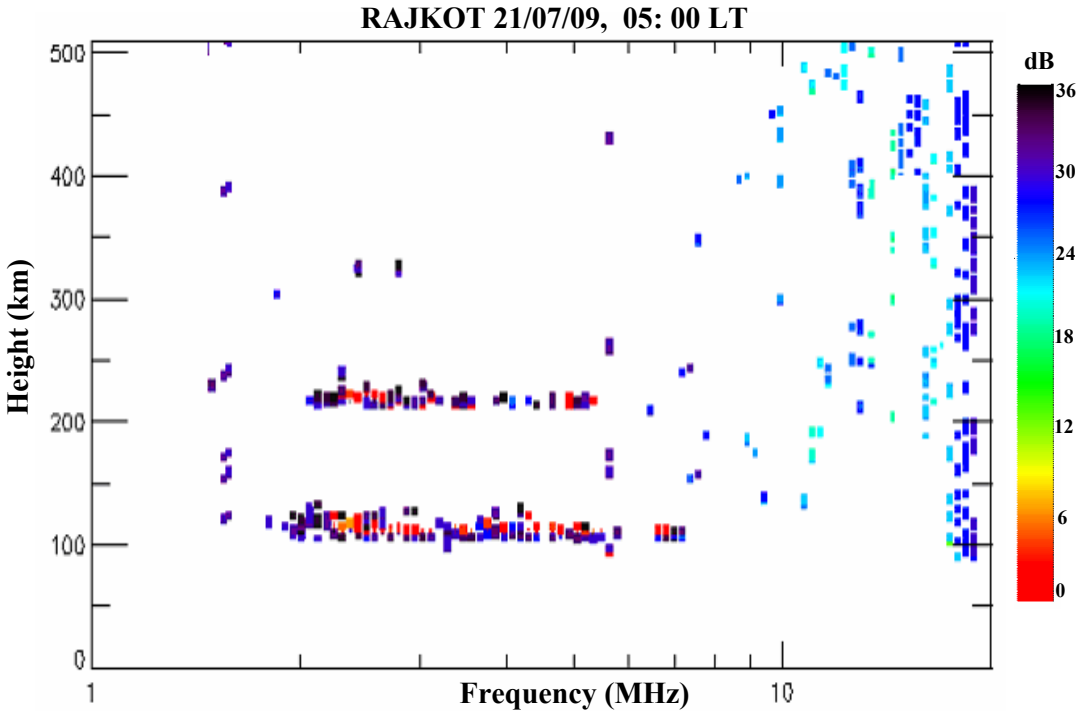

Figure 1.6: An example of Sporadic –E irregularities on ionograms observed at Rajkot on 21 July 2009, 05:00 LT

The type II irregularities have been studied in detail with the advent of improved spectral measurements at Jicamaraca [*Cohen and Bowles,* 1967; *Balsley,* 1969]. A detailed account of these two types of E region irregularities is given by *Fejer and Kelley* [1980].

1.10 F region irregularities

During normal ionospheric conditions, the ionograms show discrete and well behaved trace for ionospheric F region after sunset. But in the presence of ionospheric F region irregularities, a spread is observed in radio echoe from F region as seen in the ionograms. This event is commonly referred to as spread- F [*Berkner and Wells,* 1934; *Booker and Wells,* 1938]. Figure 1.7 shows an example of spread-F irregularities on ionograms observed at Rajkot on 26/12/2008. The ionospheric F region is normal at 19:45 LT. By 02:45 LT a spread is observed in F region echoes.

It is well proved from many studies that spread-F occurs due to the presence of wide range of plasma density irregularities starting from few centimeters to few hundred kilometers. Based on observed features on ionograms spread-F has been divided into two types, range type spread and frequency type spread [*Calvert and Cohen,* 1961; *Rastogi,* 1980]. Range spread F occurs when there are multiple echoes at different heights related to same frequency. Frequency spread F occurs when there are multiple echoes at different frequencies related to each height. The spread-F observed at the equatorial F region is known as the Equatorial spread F (ESF). The generation of spread-F can be expected at any latitudes i.e. equatorial/low, mid, and high. But the probability of occurrence is least at mid latitudes between 20^0 and 40^0. The ESF is discussed extensively in the present study. The occurrence of ESF generally remains confined to the latitudinal extent of $\pm 20^0$ around the dip equator.

It is now well accepted that Rayleigh- Taylor (R-T) gravitational instability is the basic process for the generation of spread-F irregularities. The R-T instability gets generated in the bottom side of the F region and grows non-linearly encircling higher altitudes during the post sunset under favorable background ionospheric/thermospheric conditions. The parameters like background electron density gradients, electric fields, zonal winds and vertical winds play a very important role in the growth of R-T instability. The fully grown irregularities contain wide range of scale sizes which have been detected by

ground based radio sounders, night airglow measurements, satellite measurements and backscatter radar echoes. A wide number of theoretical studies have been carried out to understand the ESF phenomenon exclusively and these have been reviewed by *Ossakow* [1981]. Simulation studies by linear and non-linear models have revealed the significance of neutral parameters like vertically down ward winds [*Sekar and Raghavarao,* 1987], the role of topside plasma density gradients [*Sekar and Raghavarao,* 1995] and on the initial perturbation amplitudes in the triggering and evolution of ESF [*Sekar et al.,* 1995]. A detailed discussion on ESF and its generative mechanism will be carried out in Chapter 4.

1.11 Scintillation

Radio waves coming from discrete sources such as radiostar or a satellite and passing through a medium containing irregularities in electron density distribution (such as the ionosphere at times) show fluctuations of parameters like amplitude, phase and polarization etc. This phenomenon is termed as scintillation. It is similar to twinkling of starts due to the inhomogeneties in the troposphere.

The two regions on the globe one around the aurora and the other around geomagnetic equator are known for intense scintillation activity arising due to presence of moving irregularities of varied scale sizes in the ionosphere. The irregularities responsible for scintillations are predominantly in the F region, at altitudes between 250 and 650 km. These irregularities scatter radio waves from satellites in the frequency range of 100 MHz – 4 GHz [*Basu et al.,* 1988; *Aarons,* 1993; *Aarons and Basu,* 1994). Scintillation is observed mainly during night time in the Indian region and is observed more frequently during high solar activity equinoctial months as compared to other periods.

Figure 1.8 shows the of global scintillation occurrence pattern at L-band frequencies during high solar activity period and low solar activity period. It can be seen that during high solar activity period, scintillation is intense in auroral and equatorial region. During low solar activity period, the amplitude and occurrence of scintillation both are very less.

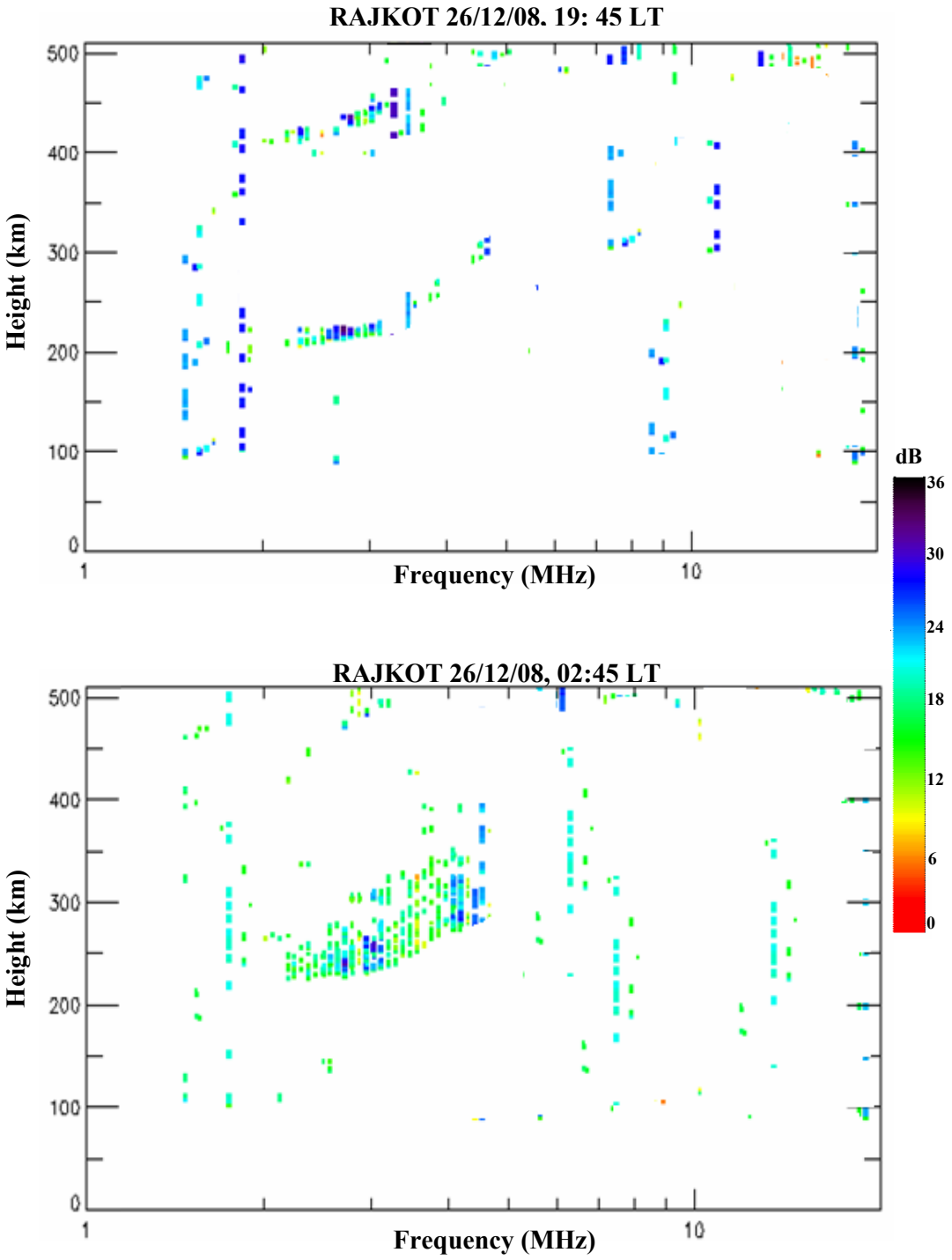

Figure 1.7: An example of Spread-F irregularities on ionograms observed at Rajkot on 26-12-2008. Ionogram in top panel shows well developed F –region at 19:45 LT while ionogram in bottom panel shows the F-region spread at 02:45 LT due to presence of irregularities

To understand scintillation, consider the medium to be equivalent to a diffracting screen with random density irregularities which are frozen in the uniform background and move with a fixed velocity. If the diffracting region is thin it causes phase fluctuations on the signal which when propagates beyond screen produces intensity fluctuations due to interference effects. Thus as a result of the phase fluctuations, intensity fluctuations build up as the wave propagates which results in a diffraction pattern at ground.

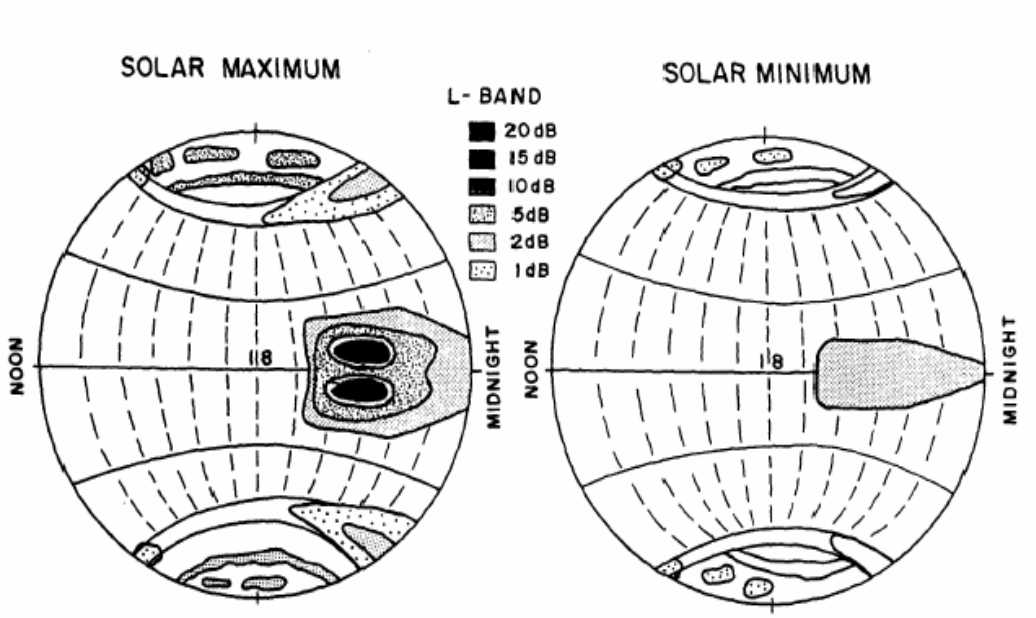

Figure 1.8: The global scintillation occurrence pattern at L-band during solar maximum and solar minimum [After *Basu et al.,* 1988a]

These fluctuations are known as scintillation. As the irregularities have horizontal movement, the diffraction pattern will move giving temporal fluctuations in phase and intensity. The amount of fluctuations is related to the strength of irregularities. The scintillation strength is given by number of indices. For example, the normalized RMS deviation of intensity fluctuations is generally used to describe the amplitude scintillation which is popularly known as the S4 index.

The phase scintillation is described by the RMS phase deviation. Both the phase and amplitude scintillation have been proved as one of the diagnostic tool to

study the ionospheric irregularities. When the depth of fading exceeds the fade margin of a receiver, the signal becomes buried in noise and signal loss and cycle slips are encountered. Phase scintillations induce a frequency shift and when this shift exceeds the phase lock loop bandwidth, the signal is lost and the receiver spends valuable time reacquiring the signal. Overall, in the presence of scintillation the performance of communication and navigation systems is degraded. A detailed account of scintillation results will be dealt in Chapter 4.

1.12 Geomagnetic Storm

Sudden transient changes in the earth's magnetic field after the impact of the solar wind on the earth's magnetosphere are known as the geomagnetic storms or magnetic storms. Magnetic storm typically last for tens of hours. The total duration of the magnetic storm is classified in four phases each with characteristic features. The first phase starts when solar wind plasma arrives at the boundary of the magnetosphere with a speed grater than the steady solar wind speed. At the epoch, outer part of the magnetosphere experiences strong impact and as a result sudden compression of the magnetic field occurs in that region. This sudden compression of the magnetic field propagates inward as hydromagnetic perturbations and reaches the earth. This causes a sudden increase in the horizontal component of the earth's magnetic field. This is known as the storm sudden commencement (SSC).

The second phase is the initial phase during which the disturbance in the H- component of the earth's magnetic field does not change significantly. The third phase is the main phase during which the value of the H-component of the earth's magnetic field depresses due to the enhanced westward ring current. The enhancement in ring current is due to the trapped solar wind particles by the strong earth's magnetic field within the magnetosphere. The main phase is followed by the fourth and last phase known as the recovery phase. During recovery phase the value of the H-component gradually recovers to the normal pre-storm level. Figure 1.9 shows the difference phases of geomagnetic storm in

terms of SYM-H index (SYM-H is the symmetric disturbance field in H with one minute time resolution).

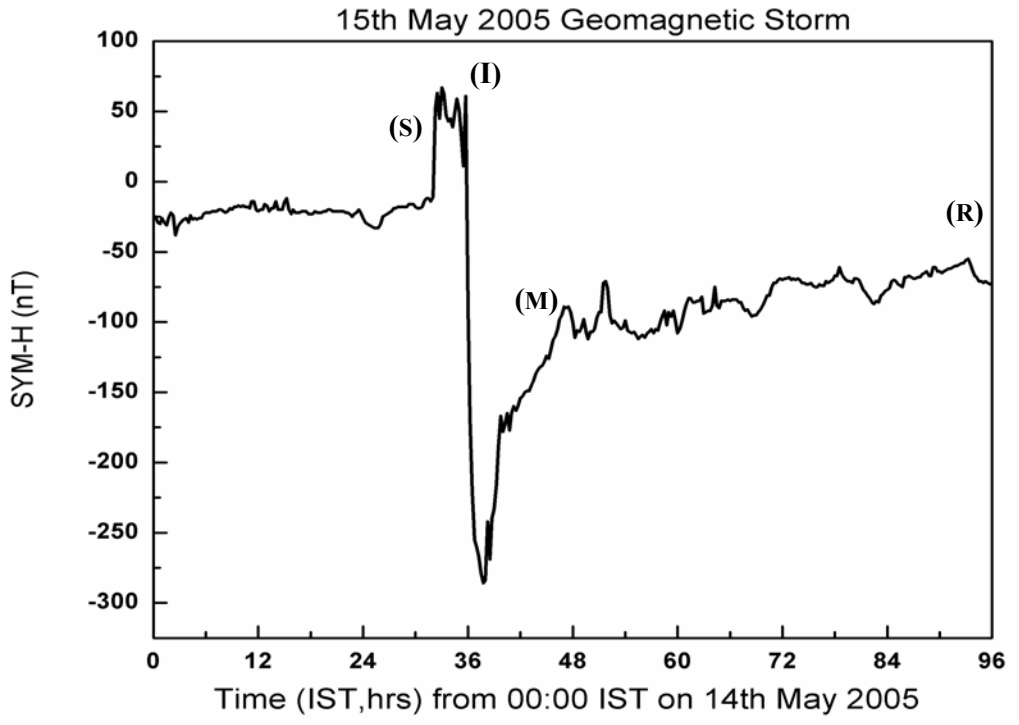

Figure 1.9: The different phases of geomagnetic storm in terms of SYM-H index during 15 May 2005 storm; (S)- storm sudden commencement, (I) – initial phase, (M)- main phase, (R)-recovery phase

The geomagnetic storm time ionospheric electric field perturbations redistribute the ionospheric plasma in some cases and in other cases they can create ionospheric irregularities depending on the local time of the onset of the storm. In addition to the ionosphere, thermosphere also undergoes drastic variations during geomagnetic storms. The excess energy input at high latitudes during geomagnetic storm lifts the neutrals their and drives them towards the low and equatorial latitudes. This changes the thermospheric composition globally. As the ionosphere and thermosphere behave as a coupled system, the thermospheric variations get reflected in the ionosphere also. The details of the processes that take place during geomagnetic storms and its effect on the ionosphere-thermosphere will be discussed in the Chapter 5.

1.13 Aim of the present study

The discussions on the various ionospheric phenomena in the above sections provide evidences for the complex nature of the equatorial and low latitude ionosphere system. The equatorial and low latitude ionospheric behavior during ESF and geomagnetic storms can not be predicted from the available ionospheric models. In recent times, from the point of view of satellite based navigation issues, such as Global Positioning System (GPS) based navigation, the need has been felt to understand the equatorial and low latitude ionosphere behavior thoroughly. In this context, the present thesis describes the significance of various ionospheric phenomena like EIA, ESF and geomagnetic storm time ionospheric behavior. The multitechnique studies provides diagnostic tool for better understanding of the various ionospheric phenomena.

.

Chapter 2
Experimental Techniques

2.1 Introduction

Ionosphere is one of the regions of the terrestrial atmosphere, in which photo-ionization creates plasma of sufficient density to have significant influence on dynamics of the region [*Louise and Keith,* 2004]. The temporal (with time of the day, seasons, solar cycle etc.) and spatial (with the latitude and longitude on the earth) variations of ionosphere have significant effect on radio waves propagating through it. Thus it becomes important to study the ionosphere on day to day basis under different geophysical conditions at different geographical locations. In-situ measurements using rockets give inclusive database of state and conditions of the ionosphere. The ground based remote sensing techniques like radars help to study the temporal variability of the ionosphere, but addressing spatial variability with this is impractical. Conversely, the study of ionosphere using orbiting satellites resolves the problem of spatial variability moderately well.

Remote sensing by radio waves includes some of the major techniques for studying the ionosphere. These techniques are generally classified in three groups [*Hargreaves,* 1992]. (1) The radio wave may be totally reflected within the medium, ionosonde works on this principle, (2) Most of the energy may travel through the medium and a small fraction being scattered or partially reflected by constituents of the medium or by irregular structures, incoherent and coherent radar works on this principle, (3) It may pass through the medium but emerge altered, for e.g. passage of satellite signals from the ionosphere.

The techniques in first and second groups involve a transmitter and receiver both sited below or above the ionosphere. Greater sensitivity is needed for techniques in second because the returned echoes are very weaker. Techniques in third group generally require a source or a receiver above the ionosphere.

The multi-technique studies of ionosphere provides diagnostic tool to understand the ionospheric variability and various ionospheric phenomena with better clarity. The present thesis work has been carried out using some of the techniques which fall under the above groups. The following sections describe these techniques in detail.

2.2 Radio wave propagation from the ionosphere

Propagation of radio waves through the ionosphere depends on the radio refractive index of the medium. The radio refractive index for an ionized medium can be expressed by the Appleton – Hartee equation [*Rishbeth and Garriott,* 1969]. This equation is based on a simple explanation of the cold plasma considering the electron motions only. In addition to this it is also assumed that the electromagnetic wave induced disturbances in the plasma are small and do not affect the propagation itself, i.e. the problem is linearized.

The Appleton – Hartree equation for the complex index of refraction is given by

$$\eta = 1 - \frac{X}{1 - jZ - \left[\frac{Y_T^2}{2(1 - X - jZ)}\right] \pm \left[\frac{Y_T^4}{4(1 - X - iZ)^2} + Y_L^2\right]^{1/2}} \qquad (2.1)$$

In general η is complex. X, Y and Z are dimensionless quantities defined as

$X = \omega_p^2 / \omega^2$

$Y = \omega_B / \omega$

$Y_L = \omega_L / \omega$

$Y_T = \omega_T / \omega$

$Z = \nu / \omega$

Here ω_p is the angular plasma frequency, ω_B is the electron gyrofrequency, and ω_L and ω_T are respectively the longitudinal and transverse components of ω_B

with respect to the direction of propagation. Here ν is the electron collision plasma frequency and ω is the angular wave frequency.

If θ is the angle between the propagation direction and the geomagnetic field than

$$\left.\begin{aligned} \omega_L &= \omega_B \, Cos\theta \\ \omega_T &= \omega_B \, Sin\theta \end{aligned}\right\} \qquad (2.2)$$

Neglecting the collisions Z = 0 and the geomagnetic field Y=0. Under this condition equation can be expressed as

$$\eta^2 = 1 - X$$

Where $X = \omega_p^2 / \omega^2$ and $\omega_p = \left[\frac{N_e e^2}{m_e \varepsilon_0}\right]^{1/2}$

Where N_e is the plasma density in cm^{-3}, m is the mass of the electron and e is the electron charge. ε_0 is the permittivity of a vacuum.

$$\eta^2 = 1 - \left[\frac{\omega_p^2}{\omega^2}\right] \qquad (2.3)$$

At the reflection level, radio refractive index η=0 therefore

$$\left.\begin{aligned} \omega_p &= \omega \\ &\text{or} \\ f_p &= f \end{aligned}\right\} \qquad (2.4)$$

Here, f_p is the local plasma frequency and f is the transmitted wave frequency. Therefore at the reflection level the local plasma frequency in the ionosphere is equal to the transmitted wave frequency.

The ionosphere consists of different regions. The maximum plasma frequency of a given region is called the critical frequency of that region. For vertical incidence, the maximum critical frequency of the whole ionosphere is called the penetration frequency. Thus, the waves whose frequency is greater than the penetration frequency can be received from a source in the space by a ground based receiver. The source may be satellite onboard transmitter, or an ascending rockets or the natural radio emission from the moon or galaxy. This is known as the trans-ionospheric propagation.

The total electron content (TEC, which is the line integral of electron density along the line-of sight between the satellite and the receiver) measurements techniques are based on the trans-ionospheric radio wave propagation. When a radio waves travel through the ionosphere, it experiences a group delay and a phase advance proportional to the TEC between the transmitter and the receiver. As the ray passes through the ionosphere, phase speeds up and the ray bends in accordance with Snell's law, as a result of the changing index of refraction of the ionosphere. If we ignore the bending and other higher order effects, we can get the TEC along the straight line between the transmitter and the receiver because the change in a phase is directly proportional to the TEC along the line of sight.

From equation 2.3

$$\eta = \sqrt{1 - \frac{\omega_p^2}{\omega^2}}$$

$$\eta \cong 1 - \frac{e^2}{2m_e\varepsilon_0}\frac{N_e}{\omega^2}$$

$$\eta \cong 1 - 40.3\frac{N_e}{f^2} \qquad (2.5)$$

Since the mid-1950s, the TEC measurements have been made, beginning with the Faraday rotation of the lunar reflected VHF waves. These techniques became popular to study the spatial variability of the ionosphere with the advent of artificial satellites. The following section describes the different TEC measurements techniques.

2.3 TEC measurement techniques

The conventional ground based techniques like ionosonde and radar can be used to investigate the various aspects of ionosphere up to F region peak and up to ~1000 km respectively. But with the advent of satellite orbiting round the earth it became possible to study the ionosphere beyond the F region peak due to the altitude of respective satellite in the orbits. For example geostationary satellite (altitude from the ground ~ 36,000 km) provides an opportunity to study the ionosphere as well as the plasmasphere also. By measuring some of the characteristics of the coherent transmissions from satellites, such as polarization, amplitude, phase, frequency etc., it becomes possible to study the ionospheric variability on short and long time scales.

The measured parameter for such studies is TEC of the ionosphere which is comprehensively defined as the total number of free electrons in a column of unit cross section area along the path of the electromagnetic wave between the satellite and the receiver [*Browne et al.,* 1956]. The satellite could be in low earth orbiting satellites, middle earth orbiting satellites for e.g. GPS etc. or Geo-stationary satellites for e.g. FLEETSAT (73^0E), MARSAT 1, ETS-II etc.

The study of TEC is important at different geographical locations on short and long time scale, as it throws light on the physical process at work in the ionosphere. TEC measurements have been made by simple recording of the Farady rotation (Plane of polarization) or by the recording of differential phase or group delay. An excellent review of these different techniques is provided by *Davies* [1980]. The Faraday rotation measurement technique was extensively used to measure TEC till the advent of Navy Navigation Satellite System (NNSS) and

later from Applications Technology Satellite – 6 (ATS-6). The differential phase or group delay which are directly proportional to TEC that require two coherent beacon frequencies. By measuring this delay using a dual frequency GPS receiver, properties of the ionosphere can be inferred, and these properties can be used to even monitor space-weather events. Therefore, GPS is a predominant technique for TEC measurement.

In view of the fact, that the ionosphere is characterized by large gradients, intense irregularities and equatorial anomaly conditions etc. These irregularities in the ionosphere produce short-time signal variations termed as scintillations. These scintillations affect the reliability of radio transmission between earth and spacecraft. Plasma irregularities in the ionosphere (like ESF, plasma bubbles etc.) are known to cause scintillation in VHF, UHF and L-band frequency range. The fluctuations of GPS signals during scintillation event can cause degradation in range measurements and in severe circumstances, cause discontinuity in phase of the signal. This discontinuity of phase can lead to loss of lock at receiver tracking circuitry. Due to loss of lock, cycle slips occur in phase measurements of GPS data. Thus in the present age of satellite based communication and navigation, it becomes important to study the characteristics morphology of scintillation to correct these errors.

2.3.1 GPS technique for TEC and scintillation measurements

The NAVSTAR GPS (Navigation Satellite Timing and Ranging Global Positioning System) is all weather, space based navigation system established by US Dept. of Defense. GPS system consists of three segments. (a) space segment (b) control segment and (c) user segment. Space segment consists of the GPS satellite constellation. Table 2.1 represents the salient features of GPS. Control segment consists of the master station (near Colorado Springs) which takes care of all data processing, worldwide network of monitor stations (Ascension Island, Diego Garcia, Kwajalein, Colorado Springs and Hawaii) and ground antennas. User segment includes the five main modules namely antennas, receiver, signal processing and data processing capabilities input/output device such as a control

display unit and a power supply. Figure 2.1 (a) shows the space segment of GPS system. Figure 2.1 (b), (c) and (d) are user segments of GPS system.

GPS satellite transmits two radio signals. These signals consist of a C/A (coarse acquisition) code at 1.023 MHz and a P (precision) code at 10.23 MHz bandwidths. The signals are transmitted at two carrier frequencies L1 (1576.42 MHz) wavelength ~ 19 cm and L2 (1227.60 MHz) wavelength ~24 cm. All the GPS users can access the C/A code. The P- code is accessible to only authorized users. Both C/A and P-codes are transmitted on the L1 frequency, either C/A or P-code is transmitted on the L2 frequency depending on the ground command [*Ananda,* 1988].

The user at the ground estimates the range to each satellite by measuring the transit time of the signal. This range is called the psuedorange, because the biases in the receiver clock prevent the actual range measurements. These pseudoranges are used to estimate the user's position in terms of latitude, longitude and height from the mean sea level and also the time offset between the transmitter and receiver clock.

The radio transmissions from GPS satellites are being used by worldwide ionospheric scientists groups to monitor the ionosphere. It is known that the ionosphere is a dispersive medium with respect to the GPS radio signal. As mentioned earlier, GPS radio signals when propagate through the ionosphere**,** the carrier experiences a phase advance and the codes experience a group delay. When the GPS code information is delayed, the measured psuedorange is quiet long as compared to the geometric range to the satellite [*Hofmann et al.,* 1992]. The group delay in the GPS code depends on the TEC along the signal path. The group delay due to the ionosphere is the most deleterious error in GPS applications.

The TEC can be given as

$$TEC = \int_{receiver}^{satellite} Nds \tag{2.6}$$

Where , N is the electron density. The unit of the TEC is TEC Unit (TECU).
1 TECU = 10^{16} electrons / m^2.

The TEC is proportional to the ionospheric differential delay between L1 and L2 signals and can be written as

$$I\rho = -I\varphi = \frac{40.3 \times TEC}{f^2} \tag{2.7}$$

Here Iρ represent the ionospheric delay term in measurements of pseudorange and Iφ represents the ionospheric delay term in measurements of carrier phase. The differential phase and group delay methods for TEC measurements are explained in later in the chapter.

GPS receiver computes the TEC from combined L1 and L2 pseudorange and carrier phase measurements. The carrier to noise (C/No) measurements can be used to calculate the amplitude scintillation. In the present wrok, the ionospheric TEC and S4 measurements have been carried out with the GSV 4000B GPS ionospheric scintillation and TEC monitor (GISTM). The detail description of GISTM receiver is given in the next section.

Features	Specifications
Number of Satellites	30 satellites
Orbital planes	6 circular orbital planes
Orbit inclination	55^0
Orbital Period	11 hrs. 58 min.
Altitude	~20,150 km
Velocity	~3.9 km/sec
GPS satellites transmit on two L-band frequencies	L1 (1576.42 MHz) L2 (1227.60 MHz) [As the ionosphere is a dispersive medium, there is a time delay at receiving end of both these frequencies. This time delay is directly proportional to the total number of free electrons encountered to the signals during their passage through the ionosphere]
Ionospheric Parameters derived from the GPS measurements	(i) Total Electron Content (TEC) (ii) Scintillation Indices (S4) (iii) TEC rate

Table 2.1: Specifications of Satellite Navigation System – GPS

2.3.2 GISTM GSV4004B receiver

The GISTM system provides the true amplitude, single frequency carrier phase measurements and dual frequency TEC measurements from 8 to 11 GPS satellites in view. The receiver and recording system estimate phase and amplitude scintillation parameters and compute TEC from the combined L1 and L2 pseudo ranges and carrier phases. The receiver uses wide band-width tracking loops and an internal phase stable, crystal oscillator to compare the phase measurements with the actual carrier phase GPS observations. Thus the real time values of the amplitude scintillation index, S4, and the phase scintillations index computed over periods of 1, 3, 10, 15, 30 and 60s are obtained.

In addition to that, 4 pairs of TEC and TEC rate computed every 15s are also obtained. Thus the equipment is ideally suited for studies of TEC, TEC rate and S4 index simultaneously. While TEC represents the total number of electrons along the signal path, the TEC rate and S4 represent the plasma irregularity structures weighted by F region.

In practice, STEC is obtained from the dual frequency code measurements, given by

$$\mathrm{STEC} = \frac{1}{40.3} * \left(\frac{1}{L_1^{\,2}} - \frac{1}{L_2^{\,2}} \right)^{-1} * (P_1 - P_2) + \mathrm{TEC}_{\mathrm{CAL}} \qquad (2.8)$$

P_1 = Pseudo range at L1 in meters

P_2 = Pseudo range at L2 in meters

For our purpose we use STEC measured by the receiver at every 30 seconds. The parameter $\mathrm{TEC}_{\mathrm{CAL}}$ in equation 2.8 represents the bias error correction and is different for different satellite–receiver pairs. In the present study, the receiver part of the above bias is corrected by taking the value of 0.793 TECU supplied by the manufacturer by calibrating the receiver against Wide Area augmentation system (WAAS). As we are mainly concerned with variations of TEC, the above approach is satisfactory. This procedure gives the corrected slant TEC. As slant TEC is dependent on the ray path geometry through the ionosphere, it is desirable to calculate an equivalent vertical value of TEC which is independent of the elevation of the ray path.

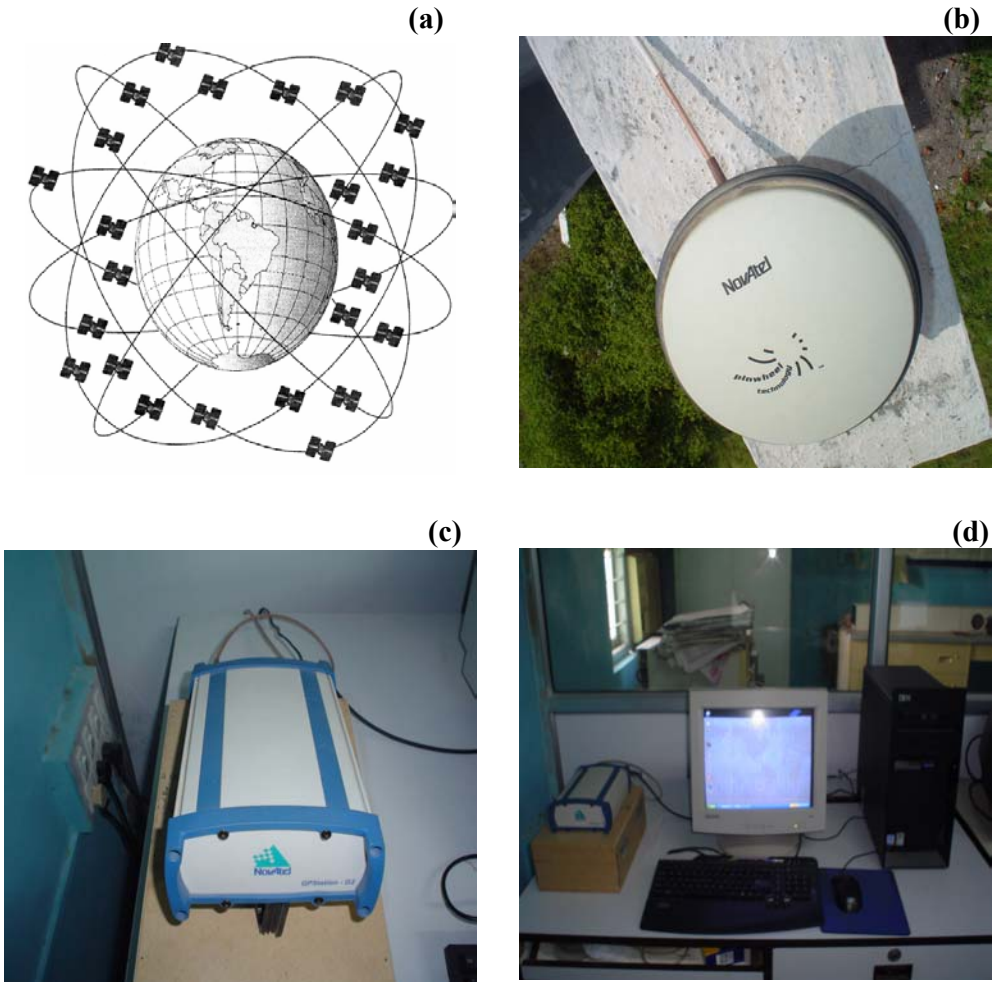

Figure 2.1: GPS includes (a) NAVSTAR Satellites Orbits Arrangement (b) L1/L2 GPS Antenna (NovAtel's Model GPS702) (c) GPS Ionospheric Scintillation and TEC Monitor (GISTM) GSV4004B (d) GPS setup at Rajkot

The Vertical TEC (VTEC) is obtained by taking the projection from the slant to vertical using the thin shell model assuming a height of 350 km, following the technique given by [*Klobuchar,* 1986]

$$VTEC = STEC^* \cos [\arcsin (R_e \cos \theta / Re + h_{max})] \quad (2.9)$$

Where R_e = 6378km, h_{max} = 350km and θ = satellite elevation angle at the ground station.

The amplitude scintillation index (S4) is defined as the normalized standard deviation of the received signal strength. The receiver collects the C/No measurements at 50 Hz rate to compute the S4 index. The formula for S4 calculation can be written as,

$$S4 = \frac{\text{Standard deviation of } C/N_{L1} \text{ or } C/N_{L2}}{\text{Mean of } C/N_{L1} \text{ or } C/N_{L2}}$$

$$S4 = \frac{\sqrt{\langle SI^2 \rangle - \langle SI \rangle^2}}{\langle SI \rangle^2} \quad (2.10)$$

Here, C/N_{L1} is the carrier to Noise ratio at L1

C/N_{L2} is the carrier to Noise ratio at L2

Here, < > denotes the average values of the detrended signal intensities over a 60 second period. In our study we have considered only amplitude scintillation. The signal intensities C/No are detrended with a 6^{th} order Butterworth low pass filter (with a cutoff frequency specified by user). If the cutoff frequency is zero or not specified then the signal intensities C/No are detrended with the measurement, averaged over the 60-second interval. This is the total S4 which also includes the effects of ambient noise as well as multipath. This is recorded every minute by the receiver for further analysis [*GSV 4004/GISTM User's Manual*].

The phase scintillation can be derived from dual frequency carrier phase measurements by calculating [*Doherty et al.,* 2000]

$$\Delta\phi(t) = \phi_{L1,L2(t)} - \phi_{L1,L2(t-1)}$$
$$\phi_{L1,L2(t)} = C\left(\phi_{L2(t)} - \phi_{L1(t)}\right) \quad (2.11)$$

Here $\phi_{L1(t)}$, $\phi_{L2(t)}$ represents the L1 and L2 carrier phase measurements respectively. C is a constant and it is used to calculate ionospheric phase delay. $\Delta\phi(t)$ at L1 and L2 are calculated using the 50 Hz raw carrier phase measurements at L1 and L2. The raw phase measurements are detrended with a 6^{th} order Butterworth high pass filter (with a cutoff frequency specified by user). Then, for every minute on the minute, the statistics of the residuals called phase sigma (of the previous 3000 detrended phase measurements) are computed over periods of 1 second, 3 seconds, 10 seconds, 30 seconds and 60 seconds. Thus for every 60 seconds, 5 values (1-sec, 3-sec, 10-sec and 60-sec phase sigma's) are recorded by the receiver [*GSV 4004/GISTM User's Manual*].

A MATLAB programme is developed to perform the data sorting and analysis for the long term study. To obtain the VTEC at any place we restrict to longitude grid of $\pm 2^0$ and latitude grid of $\pm 2^0$ from the observing station. Figure 2.2 represents GPS observations measured by PRN 8 at Rajkot on 01 June 2007.

The two subplots at the top reveal the elevation of the satellite from the GPS observational site and the variations in the amplitude scintillation given by scintillation index S4. The first subplot in the lower panel shows the temporal variations of the VTEC corrected from the slant-path values of the line-of-sight electron content for the GPS satellites in view. The second subplot in the lower panel reveals latitudinal/longitudinal coverage of the satellite. The VTEC will be denoted as TEC in rest of the thesis. The detail account of GPS observations will be dealt in detail in following chapters.

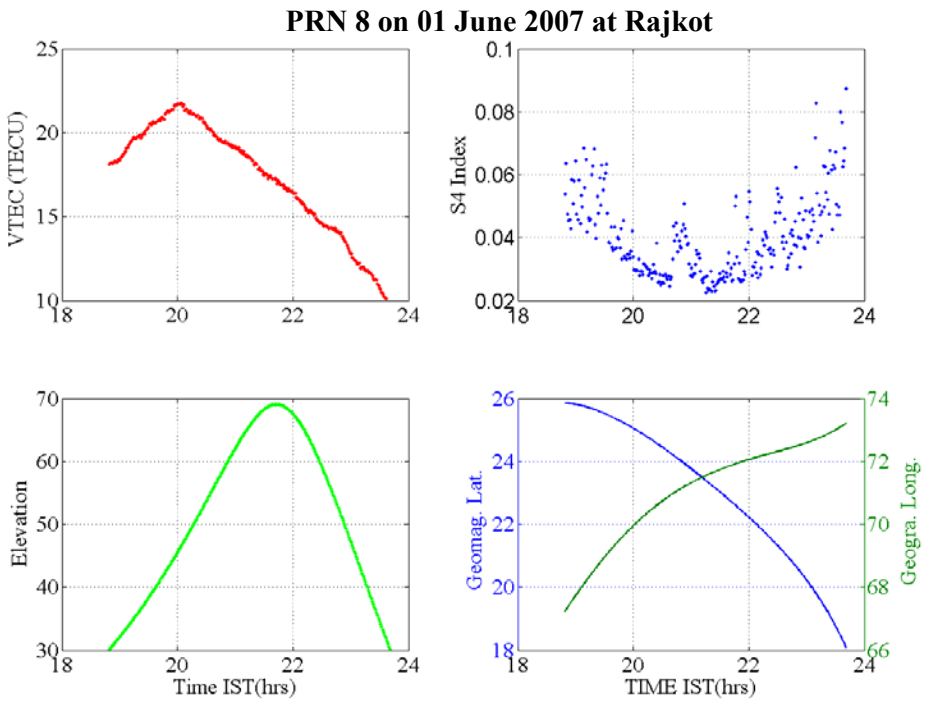

Figure 2.2: GPS observations at Rajkot measured by PRN 8 on 01 June 2007

2.3.3 Other TEC measurement techniques

(i) Farady Rotation

When a plane polarised radio wave travels through the magnetoionic medium like ionosphere, polarisation angle of it rotates depending approximately on the average magnetic field component in the direction of propagation and on the total number of free electrons along the ray path. This angular rotation of the plane of polarization is known as the Faraday rotation. The value of the earth's magnetic field is known. Therefore, the measurements of the angle of rotation of the plane of polarisation of a wave of known frequency gives direct measure of total number of free electrons in a unit column along the ray path from the satellite to a receiver at the ground. From this the vertical columnar electron content can be derived.

(ii) Differential Phase

When the radio waves propagate through the ionosphere their phase refractive index decreases due to the presence of plasma density in their propagation path. As a result of this, there is an increase in phase velocity of radio waves. If a radio wave travels a distance s in an ionized medium, its phase changes by phase ϕ of the carrier frequency f at the receiver can be expressed as

$$\left.\begin{aligned} \phi &= -2\pi f \int \frac{1}{v_\phi} ds \\ \phi &= -2\pi f \int \frac{\eta}{c} ds \end{aligned}\right\} \quad (2.12)$$

Here, v_ϕ is the phase velocity and η_ϕ is the phase refractive index. From equation (2.3), in the absence of collision and magnetic field the refractive index for a radio frequency f much higher than the plasma frequency fp is given by

$$\eta^2 = 1 - \left[\frac{f_p^2}{f^2}\right] \quad (2.13)$$

Thus

$$\eta = \left[1 - \frac{f_p^2}{f^2}\right]^{\frac{1}{2}}$$

$$= \left[1 - \frac{f_p^2}{2f^2}\right]$$

$$= \left[1 - \frac{1}{2f^2}\left[\frac{ne^2}{4\pi^2 \varepsilon_0 m}\right]\right]$$

$$\eta = \left[1 - \frac{40.3n}{f^2}\right] \quad (2.14)$$

Here, n is the electron density in m^{-3}, f is in cycles/s. Now, from equation (2.8),

$$\phi = -2\pi f \int \frac{1}{c}\left[1 - \frac{40.3n}{f^2}\right] ds$$

$$= -2\pi f \int \frac{1}{c}\left[1 - \frac{40.3n}{f^2}\right] ds$$

$$= -2\pi f \int \frac{1}{c} ds - 2\pi \int \frac{40.3n}{cf} ds \qquad (2.15)$$

The advance in phase is also frequency dependent. Therefore if two phase coherent transmissions are used, the differential phase is a measure of total columnar electron content from satellite to receiver. If there are two phase coherent transmissions at frequencies f and ηf respectively, and if the higher frequency divided by η, then the differential phase changes are,

$$\Delta \phi = \phi_1 - \phi_2$$

$$\Delta \phi = \left[-2\pi f \int \frac{1}{c} ds + 2\pi \int \frac{40.3n}{cf} ds\right] - \frac{1}{\eta}\left[-2\pi \eta f \int \frac{1}{c} ds + 2\pi \int \frac{40.3n}{c\eta f} ds\right]$$

$$\Delta \phi = \left[\frac{\eta^2 - 1}{\eta^2}\right] \frac{2 * 40.3}{cf} \int n ds \text{ radians} \qquad (2.16)$$

Here, η is known, the measurement of $\Delta\phi$ gives the value of TEC in a unit column along the line of propagation. It can be said that the differential phase changes are proportional to the TEC. The TEC values derived from the differential phase measurements are relative and need calibration.

(iii) Group Delay

The presence of electron density in the propagation path of radio waves from satellite to receiver at ground also results in to the decrease of group velocity of radio waves. The group delay from satellite to receiver is

$$\left.\begin{aligned} t &= \int \frac{ds}{v_g} \\ &= \int \frac{\eta_g}{c} ds \end{aligned}\right\} \qquad (2.17)$$

Here, v_g is the group velocity and η_g is the group refractive index. Following the same procedure as is done in the differential phase method, if there are two phase coherent signals transmitted from satellite at two different frequencies, then the differential group delay is proportional to TEC. This method gives absolute measurements of TEC.

2.4 VHF coherent back scatter radar technique

Ionosonde works on the principle of total reflection of radio frequency signals which occurs when transmitted frequency (f) is equal to the local plasma frequency (fp). For f >> fp, the waves almost pass through the ionosphere with a small amount of energy being scattered by random thermal motions of ionospheric plasma and this is incoherent in nature. This small amount of scattered energy is used by the incoherent scatter radar (ISR) technique. The total power in returned echo is proportional to the number density of electrons in the volume irradiated. As the electrons are consistently in thermal motion, the radiation is Doppler shifted from the incident frequency. The result is a spread in the returned echo spectrum which gives substantial information about the velocities in the medium. In addition to this, the returned echo spectrum contains the information of electron temperature and ion temperature also.

ISR technique sounds the ionosphere up to ~1000 km. As of now the lowest frequency used in ISR technique is ~50 MHz [*Kelley,* 1989]. These frequencies are almost unattenuated by the ionosphere and small amount of energy is scattered by the ionospheric electrons which is received back and used by the ISR.

This technique can be applied to the neutral atmosphere also because the turbulence within the homosphere – below about 100 km is able to scatter the radio wave signals. But in the case of neutral atmosphere the scattering mechanism is different from that of ionosphere, which gives incoherent scatter echoes. The radar primarily designed to study the echoes from the neutral air, in

other words to investigate the Mesosphere, Stratosphere and Troposphere is known as the MST radar.

The major disadvantage of ISR is that it has to work with a very weak signal. Therefore, it requires a transmitter of high power, a large antenna, and the most sensitive receiver and sophisticated data processing available, all of which add up to major technique and considerable expense.

If there is plasma irregularities present in the ionosphere, the electron density fluctuations in the medium can grow to values much greater than the thermal fluctuations. Radio signals backscattered from plasma irregularities with a spacing of half a radar wavelength will reinforce by constructive interference in the direction back to the radar and can produce signal strong enough to detect by smaller radar system. This phenomenon is known as the coherent backscatter and can be detected by coherent back scatter radar. Coherent back scatter radar is actually designed to receive echoes from physical structures within the ionosphere.

In last three decades, the high power VHF and UHF backscatter radars have been emerged to probe the ionosphere in order to provide better understanding of basic plasma processes associated with the ionosphere and to study the generation and dynamics of the small scale ionospheric irregularities. The observations at VHF and UHF frequencies correspond to irregularities with scale sizes of few meters to few centimeters. The investigations using Jicamarca radar (operating at 50 MHz), Altair and Tradex radars (155.5 MHz, 415 MHz, 1320 MHz) at Kwajalein, high power VHF radar (53 MHz) at Gadanki, India, HF and VHF radar (54.95 MHz) at Trivandrum, India, Portable Radar Interferometer (50 MHz) at Cornell University have contributed significant information to understand the low latitude ionospheric plasma processes.

2.4.1 Principle of Coherent backscatter

The atmosphere either ionized or not, contains irregularities of various scale sizes. It is to be believed that at each edge a small fraction of the incident energy scatters in all directions. If the numbers of field aligned irregularities are present, with spacing between them of, half of the transmitted wavelength then the resulting scattered signals will reinforce in the direction back to the radar. Thus, even the scattered energy is very weak, they can add up and the resulted signals will be strong enough to be detected by small radar system. Figure 2.3 represents the principle of volume scattering. It is not necessary for the electron density irregularities to be regularly spaced. The radar of wavelength λ_T will effectively select the spatial component of period $\lambda_T/2$, ignoring the others. Scatter in other directions will select some other spatial period. The signals from two scattering planes reinforce when their path difference is λ_T.

When the scattering is from structures within the medium then the coherence time is high, because the structures tend to vary more slowly in comparison to radar's ability to resolve those changes. Due to the high coherence, echoes will have the same amplitude and phase, as a result are added coherently.

The radar scatters from the irregularities in the medium, K_{MED}, according to the relationship

$$\mathbf{K_T = K_S + K_{MED}} \tag{2.20}$$

Here, K_T is the transmitted wave and K_S is the scattered wave. For backscatter, $K_S = - K_T$.

$$\mathbf{K_{MED} = 2K_T} \tag{2.21}$$

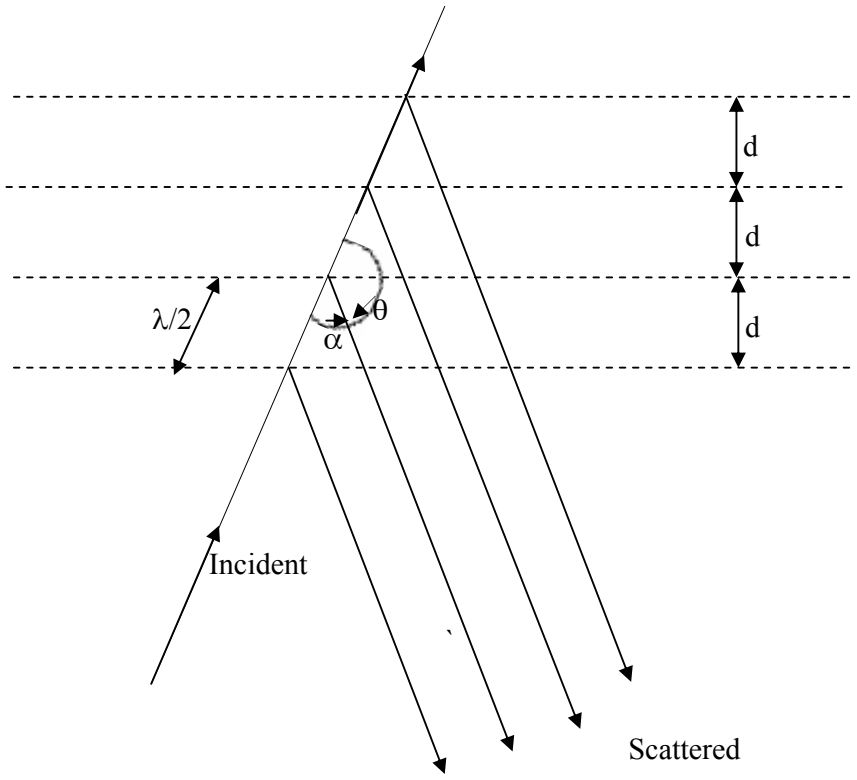

Figure 2.3: Principle of volume scattering

Equation 2.21 represents the conservation of momentum. Where $|K_T| = |K_S| = 2\pi/\lambda_T$, $|K_{MED}| = 2\pi/\lambda_{IRR}$. The backscattered wave vector will follow the Bragg condition i.e.

$$\lambda_T = 2\,\lambda_{IRR} \sin(\theta/2) \qquad (2.22)$$

From the above equation it also follows that the transmitted wavelength or radar wavelength determines the scale size of the irregularities that can be observed by this radar. For monostatic backscatter ($\theta = 180^0$), which is usually applicable for ionospheric experiments, $\lambda_{IRR} = \lambda_T/2$. Thus, the scattering wavelength is one half of the transmitted wavelength.

In backscatter radar, the scattering volume is determined by the antenna beamwidth, the transmitted pulse width as well as the vertical extent of the

echoing region under study. The mobility of the electrons is much higher along the magnetic field than perpendicular to it therefore the irregularities are elongated along the geomagnetic field lines. This fact leads to high aspect sensitivity in the backscatter. Thus, the radar line of sight has to be close to a direction normal to the field line. The radar power spectra provide information on the signal strength, mean Doppler shift and Doppler spectral width which correspond to the strength of the irregularities, line of sight phase velocity, and its variance respectively [*Patra*, 1997].

2.4.2 VHF coherent back scatter radar at Gadanki, India

Indian MST radar, situated at Gadanki (13.5^0N, 79.2^0E, dip latitude 6.3^0N) India, can be operated in ionospheric mode to study the ionospheric E and F region plasma irregularities. This high power VHF coherent backscatter radar has been established as MST (Mesosphere–Stratosphere–Troposphere) radar, primarily to study the lower and middle atmospheric dynamics. In addition to these studies, it was also meant for the coherent backscatter studies of the ionospheric irregularities. Accordingly, the phased antenna array has been aligned along the geomagnetic axis, 2^0 away from the geographic axis in anticlockwise direction [*Patra,* 1997]. The radar is highly sensitive, pulse coded, coherent VHF phased array radar operating at 53 MHz with a peak power aperture product of 3×10^{10} Wm^2.

To detect the backscatter from ionospheric field aligned irregularities, the radar beam has to be made transverse to the magnetic field lines. Thus the tilt of 14.8^0 N from the zenith has been given to the radar beam to satisfy the perpendicularity condition at 350 km. Since it is possible to orient the radar beam anywhere within 20^0 zenith angle, this condition can be satisfied easily. The radar beam geometry at Gadanki for the study of F region irregularities is shown in Figure 2.4. The beamwidth of radar is 2.8^0 in both east- west and north-south planes. Table 2.2 represents the main specifications of the MST radar [*Patra,* 1997].

The major subsystems of the MST radar can be listed as (i) the antenna and feeder network (ii) transmitters (iii) exciter and radar controller and (iv) the receiver and signal processor. The details of the radar and its subsystems are discussed by *Rao et al.,* [1995] and *Patra,* [1997].

The radar power spectra provide information on the signal strength, mean Doppler shift and Doppler spectral width which corresponds to the strength of the irregularities, line of sight phase velocity and its variance respectively.

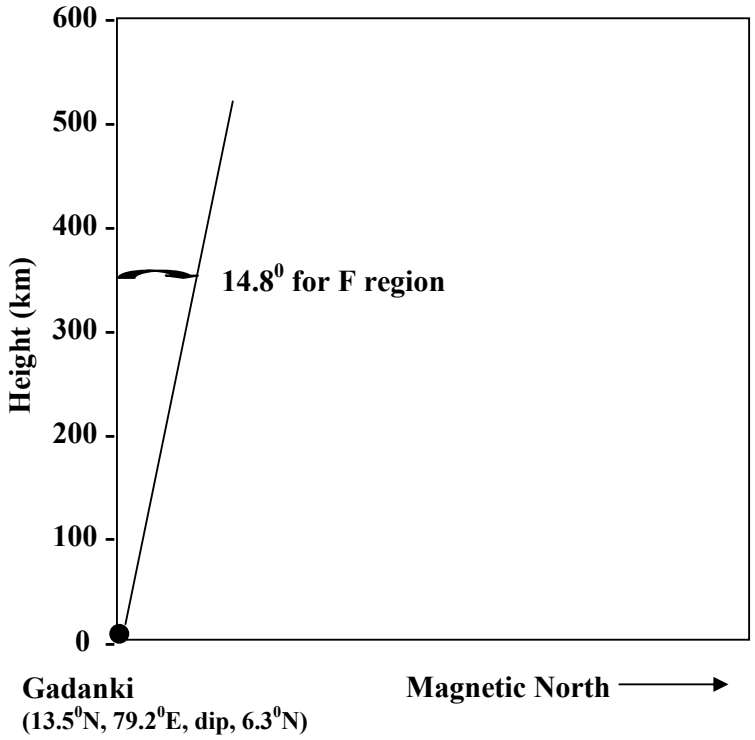

Figure 2.4: Geometry of the MST radar beam located at Gadanki for studying the ionospheric F region irregularities [reproduced after *Patra,* 1997]

Features	Specifications
Location	Gadanki (13.5^0N, 79.2^0E, Geomagnetic Latitude 6.3^0N)
Frequency	53 MHz
Peak Power	2.5 MW
Peak Power-aperture Product	3×10^{10} Wm^2
Maximum duty ratio	2.5%
Number of Yagi antennas	32 × 32, 3-element orthogonal Yagi arrays
Beam width	2.8^0
Beam position (zenith angle)	± 20^0 in both E-W and N-S planes in steps 1^0; 13.2^0 N and 14.8^0 N for ionospheric application
Receiver bandwidth	1.7 MHz
Receiver gain	120 dB
Receiver dynamic range	70 dB
Pulse width	1,2,4,8,16,31 μs uncoded; 16,32 μs coded with 1 μs baud
Pulse repetition frequency	62.5 Hz – 8 KHz
Maximum number of coherent integrations	512
Maximum number of range bins	512
Maximum number of FFT points	1024
Radar Controller	PC-AT Pentium – IV featuring programmable experiment specification file
Computer System	PC-AT Pentium – IV system with ADSP 21060 DSP processors for data acquisition and processing

Table 2.2: Main specifications of the Indian MST radar

The direction of arrival of the echoes being close to vertical, the line of sight phase velocity of the irregularities represents mostly the vertical component. The Range Time Intensity (RTI) map of ESF irregularities observed by VHF radar, Gadaki on 07 February 2008 is shown in Figure 2.5. The color code in the plot represents the strength of the irregularities in dB. The detail account of radar ESF observations will be dealt in Chapter 4.

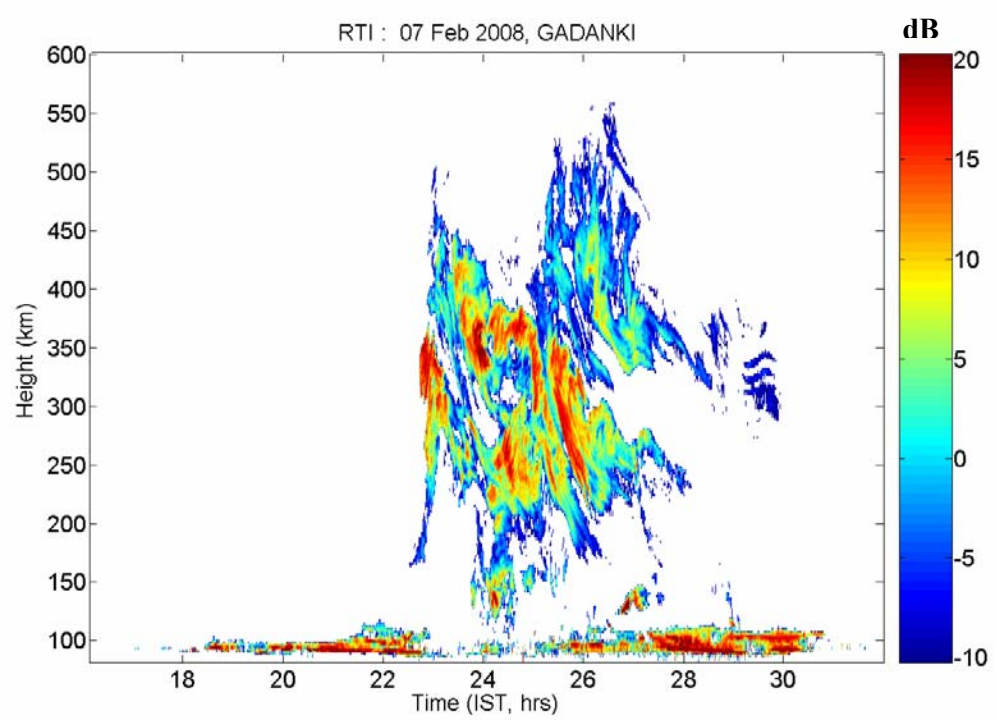

Figure 2.5: RTI map observed on 07 Feb 2008 using Indian MST radar. The color code in the plot represents the strength of the irregularities in dB

2.5 Ionosonde

An ionospheric sounder or ionosonde is the oldest ground based experimental technique for investigating the terrestrial ionosphere by means of radio waves. Ionosonde is basically variable frequency radar which transmits a signal vertically whose frequency varies from 1 to 22 MHz and measures the time delay between the transmission of radio frequency pulse and echo from a reflecting layer in the ionosphere. The limitation of the ionosonde is it can sound

the ionosphere only up to hpF2 (peak of the F region) height only. Thus there is a lack of information above the hpF2 height. The satellite based miniature ionosonde can provide the information above the F2 peak. This is called the top side sounding in contrast to the pervious one which is known as the bottomside sounding. In top side sounding also the information will be up to hpF2 only from topside. Thus, the combined observations, topside and bottomside, can give complete profile of the terrestrial ionosphere.

The topside sounding helps to study spatial variability but temporal variability is not visible with this. The bottomside sounding helps to study temporal variability but in general unable to address the spatial variability. Ionosonde operates on the principal of total reflection of radio signals from a reflecting level in the ionosphere.

2.5.1 Principle of ionosonde

The basic principle of the ionosonde is the reflection of radio signals by the ionospheric plasma when transmitted radio frequency f is equal to the local plasma frequency f_p. At the occasion of reflection the transmitted frequency is known as the critical frequency. The plasma frequency (f_p) is related to the electron density (N_e) of the reflecting layer as

$$f_p = \frac{1}{2\pi}\left(\frac{N_e e^2}{m_e \varepsilon_0}\right)^{1/2} \tag{2.23}$$

By substituting the standard values,

$$f_p = 9\ (N_e)^{1/2}\ \text{MHz} \tag{2.24}$$

From this the plasma density can be given by the following expression,

$$N_e = 1.24\times10^4\ f_p^{\,2} \tag{2.25}$$

As the electron density in the ionosphere increases monotonically with height, the reflection takes place for the higher values of plasma frequency f_p as

the height increases. Since the peak electron density in the ionosphere is few times 10^6 cm^{-3}, the plasma frequency $f_p \leq 12$ MHz. [*Kelley*, 1989]. If the transmitted frequency is higher than the peak plasma frequency (frequency corresponds to the peak electron density), the radio wave signals will penetrate through the ionosphere and escape in to the space. The lowest frequency which just penetrated the ionospheric layer, the penetration frequency, would provide a measure of the electron density at the peak. If there is a dense E region it can block the F region entirely by absorbing the transmitted radio frequencies as we have observed in Chapter 1-section 1.9.

The time delay measured by the ionosonde is converted in to the height. As the ionosphere is not vacuumed, the velocity of the radio waves in the ionosphere is not similar to that of the velocity of light. Therefore, the height measured by the ionosonde will not be a real height but it will be a virtual height. The plot of the transmitted frequency Vs virtual height is known as the ionogram. The ionograms are scaled for the different ionospheric parameters like virtual height of the ionospheric regions, critical frequency of the ionospheric regions etc. The typical ionogram recorded using CADI digisonde at Rajkot is shown in Figure 2.6. The different ionospheric regions can be observed. The E region is visible at ~100 km. F1 and F2 splitting is observed at ~ 325 km.

The virtual height can be converted into real height if required. The typical expression for the virtual height can be given by

$$h_v = c\frac{t}{2} \tag{2.26}$$

Here t is the time delay of the echoes. The group velocity of the radio waves is less than the velocity of light in the ionosphere due to the presence of free electrons in their path. Hence the virtual height h_v is always greater than the real height.

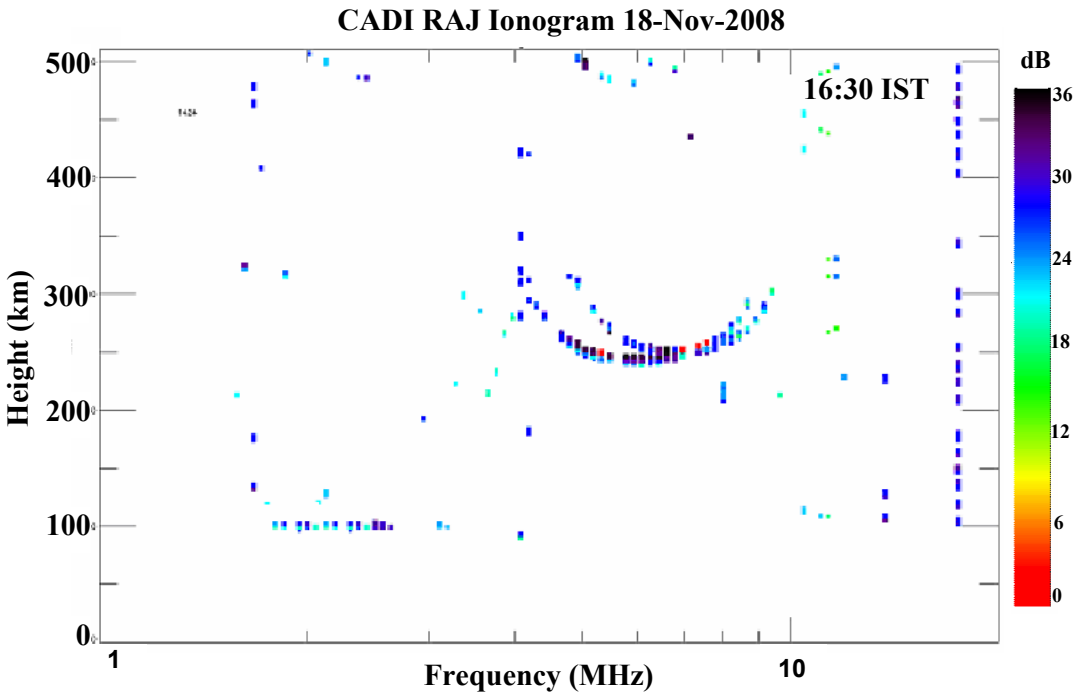

Figure 2.6: An example of typical ionogram at Rajkot

2.5.2 KEL IPS-42 ionosonde system

In the present study, the ionosonde data is obtained from KEL IPS-42 (Ionosphere Prediction Service) which has been in operation at Trivandrum. The instrument is a solid state, sweep frequency, pulsed ionosonde designed for routine vertical incidence sounding of the ionosphere. It employs a digital frequency synthesizer and programming control, signal processing and display technique. The main specifications of KEL ionosonde are given in Table 2.3

Features	Specifications
Frequency range	1 to 22.5 MHz
Frequency generation	Digital synthesizer
Frequency sweep time	12s
Transmitter pulse power	5 kW
Transmitter pulse width	41.67 μs
Pulse interval	5.33 ms, three on each channel
Maximum virtual height	800 km
Height marker interval	100 km
Programming options	(1) Ionograms at 15, 5 or 1 minute interval (2) 3 per minute (optional)
Date/Time identification	Recorded with each ionogram
Video display	High resolution green phosphor (12 cm) Video card extra 18 Kbytes of R.A.M.

Table 2.3: Main specifications of KEL IPS-42 ionosonde

2.6 Other techniques

2.6.1 In situ measurements

Instruments have been designed for the direct measurements of many variables of the atmosphere and ionosphere. A variety of instruments are used to measure the temperature, concentration, and drift velocity of either the ambient thermal electron or the thermal ions. When instruments are mounted on satellites they are most useful for long term monitoring above about 200 km. The parameters most frequently sought are the vertical distribution of each of the electrons and the ions and neutral species. To determine the composition one requires a mass spectrometer, but much information about concentrations and temperatures can be obtained from simpler devices variously known as ‘probes’, ‘traps’ and ‘analyzer’, and many such instruments have been flown on rockets and on satellites over the years. These instruments are mounted on satellites and

rockets that are moving through the plasma at velocities between 1 and 9 km/s [*Kelley,* 1989].

A probe is projected into the medium and draws from it an electric current of electrons or ions depending on the sign and magnitude of the potential applied to it. A trap collects ions from the medium because the vehicle in orbit moves faster than the ions and so sweeps them up from its path. Additional electrodes are often incorporated to enable a more detailed analysis to be made in real time, the results being transmitted to a ground station by telemetry. The examples of in situ instruments are Langmuir Probes, Retarding Potential Analyzer, and Drift Meters etc.

2.6.2 TIMED satellite

The thermospheric neutral composition variations in terms of $[O]/[N_2]$ presented in the present study have been obtained from Thermosphere, Ionosphere, Mesosphere, Energetics and Dynamics (TIMED) onboard Global Ultraviolet Imager (GUVI) instrument. The TIMED satellite is launched by NASA under Solar Terrestrial Probes Program. The purpose is to study the sun-earth system more thoroughly. The TIMED satellite is placed in a circular orbit at an altitude of ~625 km to observe the Mesosphere and Lower Thermosphere/Ionosphere (MLTI) region. It employs advance instruments in remote sensing technology. The parameters such as temperature, pressure, wind and chemical composition, along with its energy inputs and outputs of MLTI region's are acquired. The more details on TIMED satellite can be found on http://www.timed.jhuapl.edu/WWW/index.php

In the imaging mode the GUVI instrument of the TIMED satellite gives far ultraviolet images of thermosphere composition and temperature below about 625 km altitude. The details of the GUVI instrument, operation and example of data products are presented by *Paxton et al.,* [1999], *Christensen et al.,* [2003] and *Paxton et al.,* [2004]. The atomic oxygen to molecular nitrogen vertical column density ratio ($\sum O/N_2$) is one of the geophysical parameter obtained from data

products of the GUVI imager. The ratio of vertical column density of atomic oxygen (135.6 nm) to that of molecular nitrogen (174.3 nm) is proportional to ratio of emission rates within the airglow layer, extending from about 140 km to 250 km [*Meier et al.,* 2005]. A more detail on GUVI can be found on *http://guvi/jhuapl.edu/*.

2.6.3 Optical techniques

The study of atomic and molecular emissions in the upper atmosphere using optical techniques provides information on the chemical and physical processes going on in the atmosphere. These emissions are known as the airglow emissions. Optical investigations have a tremendous potential in inferring the behavior of the upper atmosphere. As the ionosphere is the part of the upper atmosphere, optical investigation of different emissions gives wealth of information on different chemical processes which plays a major role in sustaining the ionosphere during different time of the day. Optical techniques have been developed on different platform such as ground based, balloons, rockets and satellites.

Airglow emissions variability at any given place provides plenty of information on the behavior of the ionosphere – thermosphere system at the respective emitting altitudes. The ideal condition to study the airglow emission is the moon less clear night sky (no clouds). Dayglow study is the challenging task due to the presence of strong sunlight background. But with the development of unique Dayglow Photometer (DGP) and Multiwavelength Dayglow Photometer (MWDPM) [*Narayanan et al.,* 1989; *Sridharan et al.,* 1993, 1998], an investigation on various characteristics of dayglow emissions have been carried out.

The optical techniques observe fundamentally the total incoming photon flux at a particular wavelength and the variations of the photon flux with varying wavelength. The former is called the photometry while the later is called the spectrometry.

The basic parameter in the airglow study is the intensity of the emissions. The major optical instruments to study the airglow emissions at different altitude at a given place are (i) photometer (ii) imager and (iii) spectrometer. The intensity i.e. total or specific line emission of radiations is measured by photometers (with small field of view ~10^0 or less). The scanning photometer scans the sky at fixed angle to study the dynamics of the upper atmosphere. The schematic of night airglow photometer is shown in Figure 2.7. The different parts of the photomere are shown there.

Photometer measures integrated airglow brightness over its field of view. The photometer mainly consists of three major parts (i) front optics (ii) filter assembly (iii) detector section. The front end optics collects light from a small field of view. Collimating lens makes the light rays parallel hence a normal incidence to the filter. Narrow band interference filter is used to isolate unwanted wavelengths. Focusing lens directs all light towards the detector. Thus light is refocused on to detector (for example photomultiplier tube) which measures the intensity of incoming light. In case of scanning photometer, the scanning mirror scans the different parts of the sky at a given interval of time. The detector section has to be connected to the data acquisition system.

The bi-directional (zenith and 45^0 elevation towards west) measurements of night airglow emission at OI 777.4 nm are used to calculate the night time plasma drift. This drift value is used in the case study presented in section 4.4 of Chapter 4. These airglow emission measurements are done by Physical Research Laboratory group, Ahmedabad at low latitude station Gadanki. This is a multiwavelength photometer. The details of this photometer are described by *Sekar et al.,* [2004, 2008].

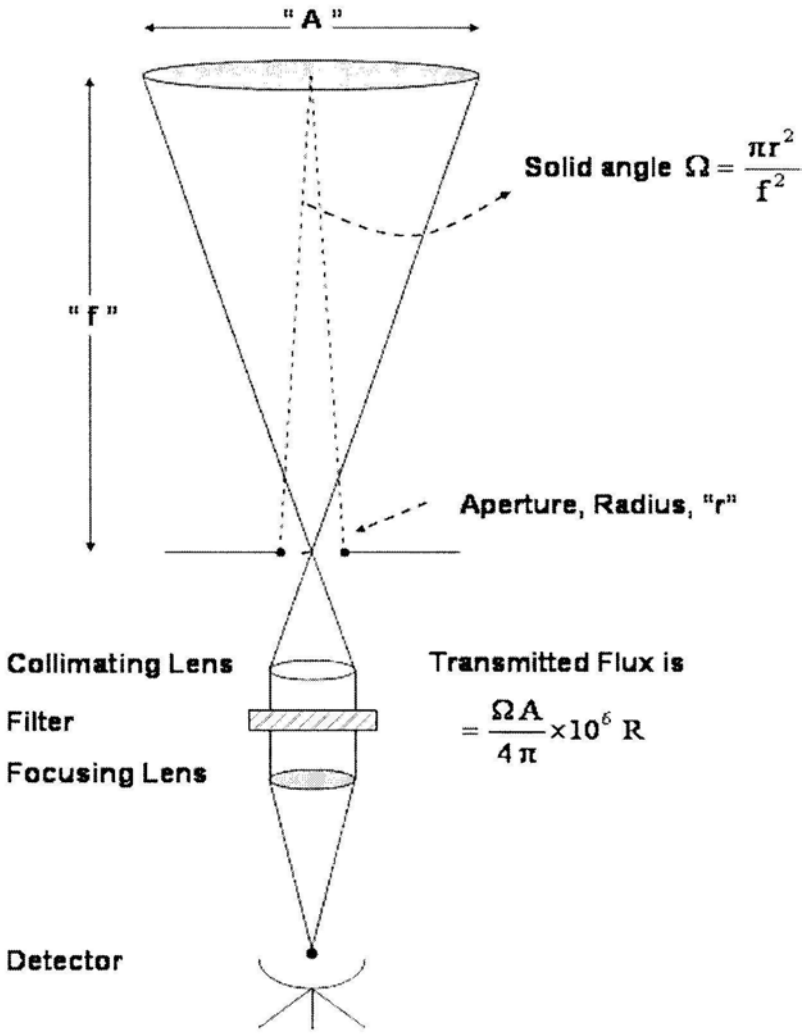

Figure 2.7: Schematic of night airglow photometer [CSSTEAP course material, Prof H.S. S. Sinha's notes]

2.7 Summary

In the present chapter the radio wave propagation from the ionosphere and the effects of ionosphere on it is discussed. The core part of the chapter contains the discussions on various techniques for studying the ionosphere. The GPS TEC and scintillation measurement technique is discussed in detail. The sample observations from the satellite (PRN 8) are shown and explained. The other TEC measurement techniques are also discussed. The VHF coherent back scatter radar technique for studying the F region irregularities is discussed along with the

principle. The ionosonde technique is also discussed along with its principle. The In situ techniques are highlighted. The thermospheric variation in terms of $[O]/[N_2]$ ratio are studied using TIMED/GUVI data. The glimpse of TIMED/GUVI system is given. At the end the optical technique to study the night time ionospheric variations is also highlighted.

Chapter 3

TEC variations during low solar activity period (2005-2009) near the EIA crest region in India

3.1 Introduction

As mentioned earlier, when the GPS satellite signals propagate through the ionosphere, the carrier experiences a phase advance and the code experiences a group delay due to the total number of free electrons along the path of the signals from the satellite to receiver at the ground. Therefore, the carrier phase pseudoranges are measured too short and the code pseudoranges are measured too long compared to the geometric range between the satellite and the receiver. This results in the degradation of the positional accuracy provided by the GPS receiver [*Hofmann-Wellenhof et al.,* 1992]. The domain of the effect on the range may vary from the furthest distance of more than hundreds of meters (at mid day, during the period of maximum sunspot activity, with the satellite near the horizon of the observer) to the closest distance of less than a few meters (at night, during the period of minimum solar activity, with the satellite at the zenith). Among the different sources of GPS positional errors, ionospheric delay, which is proportional to the TEC, is the highest contributor. Therefore, in order to get better GPS positional accuracy, it is necessary to have a precise knowledge of the accurate values and variations of the TEC at different geographical locations under different geophysical conditions.

3.2 Historical background

During past few decades an extensive study of TEC variations with local time, seasons, and solar activity has been made [*Rastogi et al.,* 1971; *da Rosa et al.,* 1973; *Van Velthoven,* 1990; *Feitcher and Leitinger,* 1997; *Warnant et al.,* 2000; *Gupta and Singh,* 2000; *Wu et al.,* 2008]. In the past three decades, several individual measurements of TEC at various locations in India have been made using the available low earth orbiting satellites as well as geostationary satellites

[*Rastogi and Sharma,* 1971; *Das Gupta and Basu,* 1973; *Rastogi et al.,* 1975; *Rama Rao et al.,* 1977; *Davies et al.,* 1979]. All these studies have shown the characteristic features of the TEC for the Indian region.

Equatorial Ionosphere exhibits large spatial gradients in electron density due to the well-known EIA with a trough at the equator and a crest at $\pm 15^0$ north and south geomagnetic latitudes of it. *Rastogi and Klobuchar* [1990], using ATS-6 TEC measurements from India, have shown a large day to day variability in the location of EIA crest in the Indian sector and its dependence on the EEJ and CEJ. *Sethia et al.,* [1980] and *Balan and Iyer* [1983] have shown that the EEJ has a pronounced influence on the development of EIA in TEC, based on the sparse data of previous satellites of opportunity.

With the advent of GPS satellites, a network of GPS stations monitoring TEC and scintillations in the Indian subcontinent have been established jointly by Indian Space Research Organisation (ISRO) and Airport Authority of India (AAI). This network is known as the GAGAN (GPS Aided Geo Augmented Navigation). Using GAGAN GPS TEC measurements [*Rama Rao et al.,* 2006] and other individual GPS TEC measurements [e.g. *Pandey and Dashora,* 2006], ionospheric TEC variations have been investigated at few Indian stations.

The dual frequency GPS signals recorded at Rajkot near the EIA northern crest in India have been analyzed to study the ionospheric variations in terms of TEC during the low solar activity period of April 2005 to April 2009. In this study, we describe the diurnal and seasonal variations of TEC, solar activity dependence of TEC. Some limited data set from the GAGAN GPS receivers is used to study the control of EEJ on EIA. The details of GAGAN GPS stations used in the present study are given in Appendix I (Table I.1). The observed low latitude L-band scintillation during the descend phase of the solar activity is also discussed

3.3 Diurnal variations of TEC

The diurnal variations of TEC exhibit a steady increase from about sunrise to an afternoon maximum and then fall to attain a minimum just before sunrise. The diurnal characteristics of TEC have seasonal, solar activity, geomagnetic activity and latitudinal dependence. Figure 3.1 shows the diurnal pattern for a typical quiet day of 17 April 2005 (Ap=4) derived from per minute TEC values. It is derived for $\pm 2^0$ latitude and $\pm 2^0$ longitude bin from the Rajkot for all the visible satellites. The variations can be divided into three different regions, namely: the build up region, the day time plateau and the decay region. The diurnal variations in TEC at Rajkot exhibits many characteristics typical to low latitude ionosphere such as TEC minimum at pre-dawn hours and gradual increase with the time of the day, attaining maximum in the afternoon and gradual decrease after sunset. The daily peak occurs around 14:00 IST hours (IST=UT+5.5 hrs).

At low latitude ionosphere the highest daytime peak TEC values greatly depend on the strength of the EIA. Figure 3.2 (a) and (b) shows the mass plots of TEC diurnal variations for the months of years 2005 to 2009.

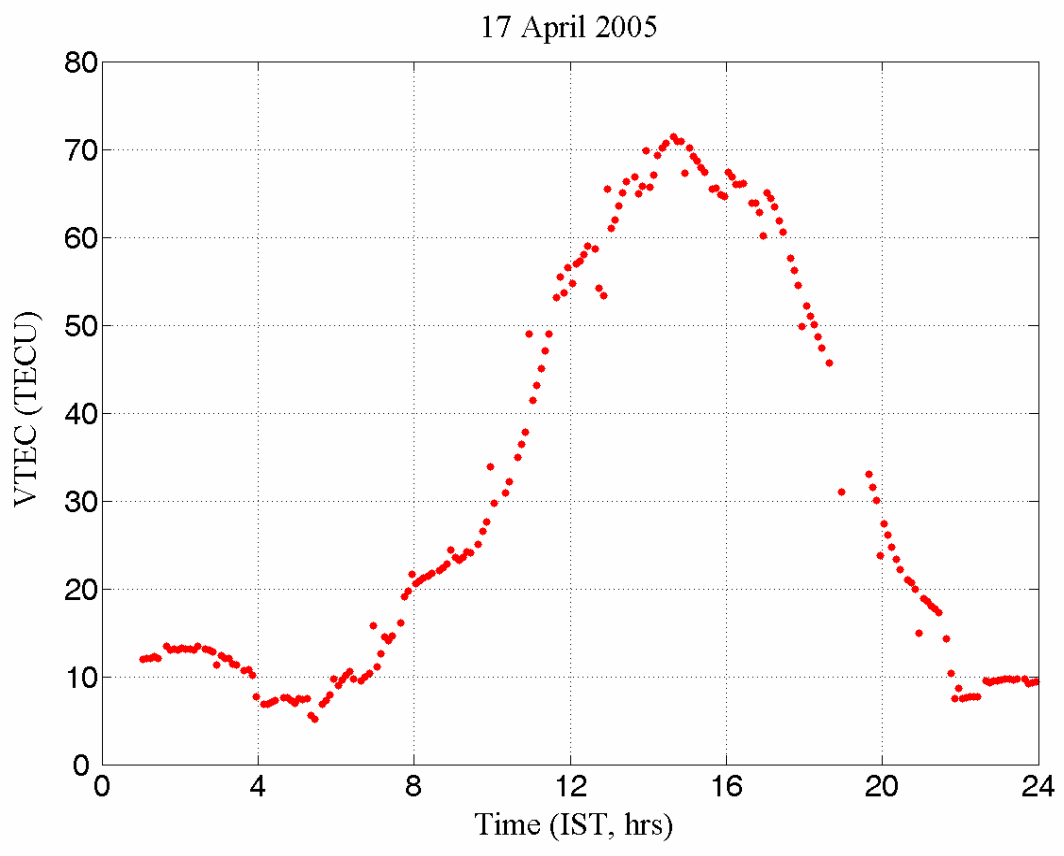

Figure 3.1: Diurnal variations of TEC observed for a $\pm 2^0$ latitude and $\pm 2^0$ longitude bin from the observing station Rajkot

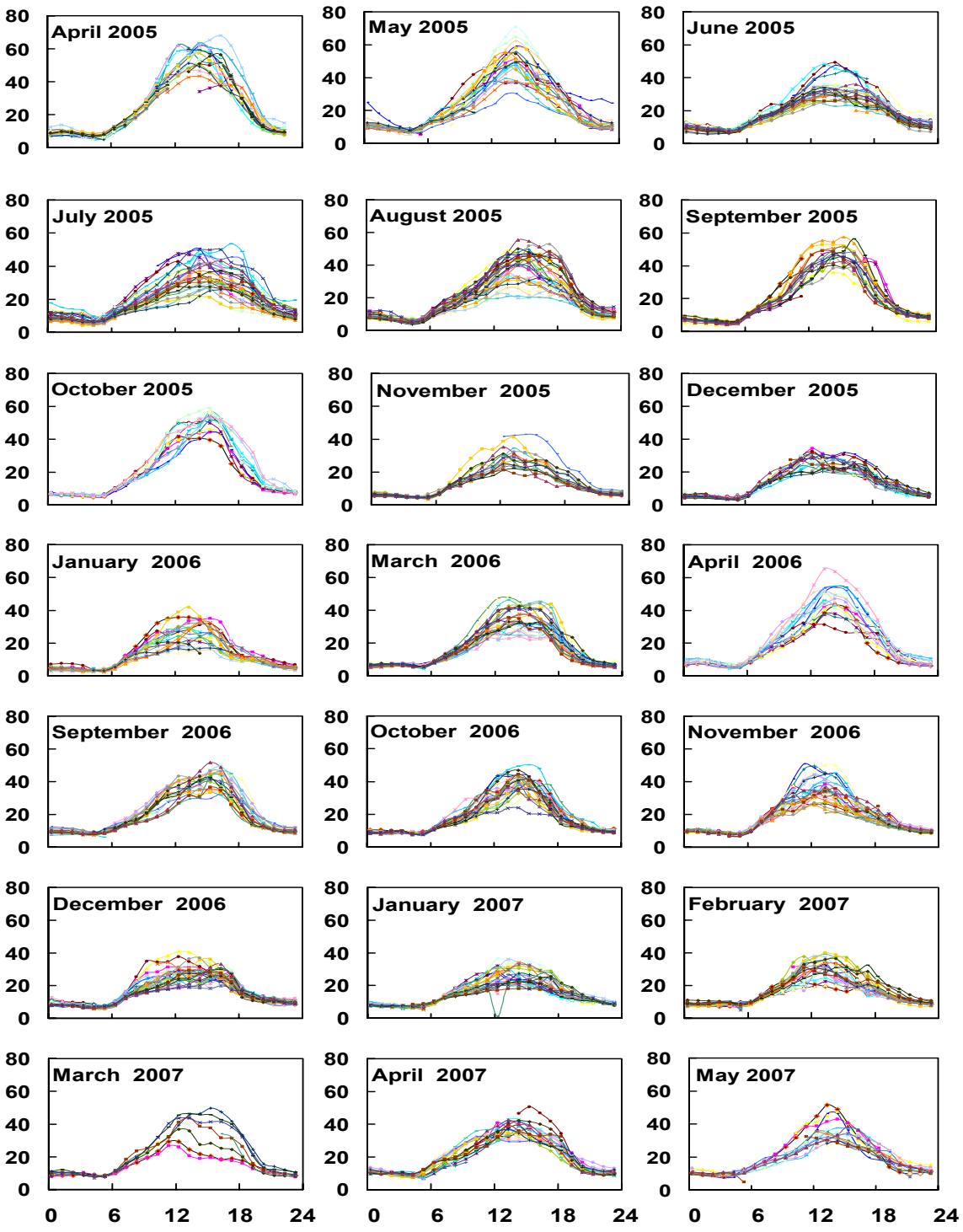

Figure 3.2 (a) : Mass plot of Diurnal variation of TEC at Rajkot from April 2005 to May 2007 with the exception of May to August 2006 due to instrument failure

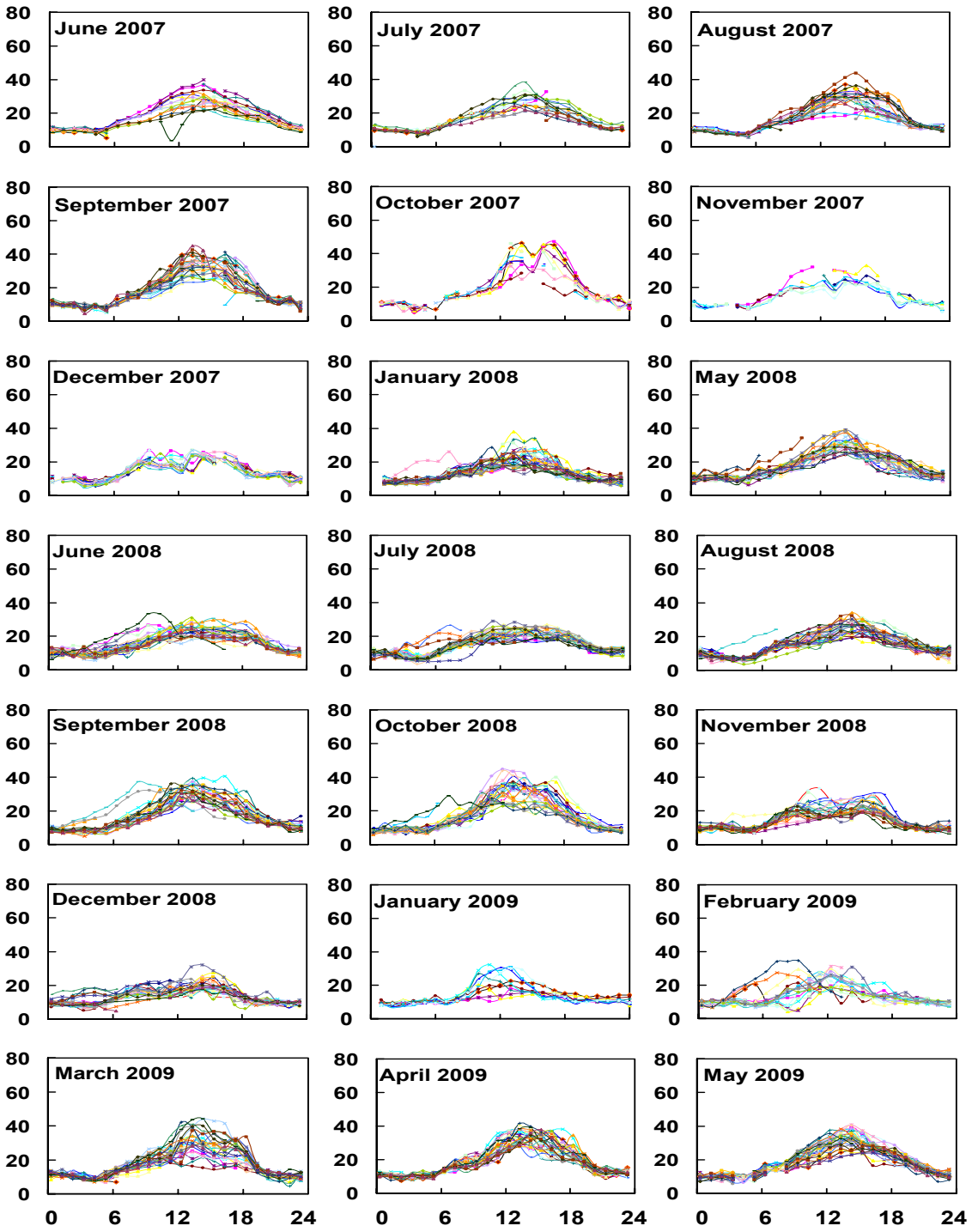

Figure 3.2 (b) : Mass plot of Diurnal variation of TEC at Rajkot from June 2007 to May 2009 with the exception of February to March 2008 (because during this period, GPS receiver operated from Gadanki for ESF campaign)

These curves show appreciable day to day variability. The day to day variability of TEC is contributed by the various parameters like EUV flux, geomagnetic activity [*Dabas et al.,* 1984], EEJ strength and local atmospheric conditions in the thermosphere [*Rama Rao et al.,* 1980] etc. It can be noticed that the day to day variability in TEC decreases with the phase of the solar activity. During 2005 to 2007 significant day to day variability is observed while during 2008 and 2009 the day to day variability is less. This is may be due to the variations of EUV flux with the phase of the solar activity.

3.4 Seasonal variations of TEC

The mean diurnal TEC variations during different seasons recorded at Rajkot for the years of 2005–2009 are shown in Figure 3.3. The equinox represents March, April, September, and October; the summer represents May, June, July, August; and the winter represents the January, February, November and December.

It can be seen from Figure 3.3 that TEC values are high in equinoctial months followed by summer and winter. Seasonal variations of TEC depend not only on production and loss of ionization but also on the transport of plasma through winds and on thermospheric neutral composition variations. The higher values of TEC in equinox months are due to high values of solar flux. During summer the meridional winds are equatorward. The equatorward winds push the plasma along the geomagnetic field lines i.e. at higher altitudes where production and loss ratio is high. This behavior increases the electron density at low latitudes [for e.g. *Ramarao et al.,* 1996]. During winter the meridional winds are poleward. The poleward winds push the plasma to lower altitudes where production and loss ratio is comparatively low. This behavior decreases the electron density.

The changes in the ratio of thermospheric $[O]/[N_2]$ due to differential heating between two hemispheres also influences the seasonal variations of TEC [for e.g. *Bhuyan and Borah*, 2007 ; *Mukherjee et al.,* 2010]. It is observed that at Rajkot, the winter anomaly is absence. Winter anomaly represents the higher

values of electron density in the winter months than in the summer. The detail description on winter anomaly can be found in literature.

There is a sharp daily maximum during 2005–2006 for all the seasons which is not seen for other observations. During the low solar activity period the seasonal variability of daily peak TEC is comparatively low. This agrees with the results shown by Modi and Iyer [1989]. One more interesting point here is that during 2008-2009 the observed TEC values for each season are little higher than the values observed during 2007-2008. This may be because the sun is approaching the next active solar cycle period and TEC at low latitudes has started to show the signatures of its. Figure 3.4 shows the month to month variations of monthly mean diurnal peak TEC values. This monthly mean diurnal peak TEC shows semiannual variations with a peak during the equinox period and a trough during the solstice period.

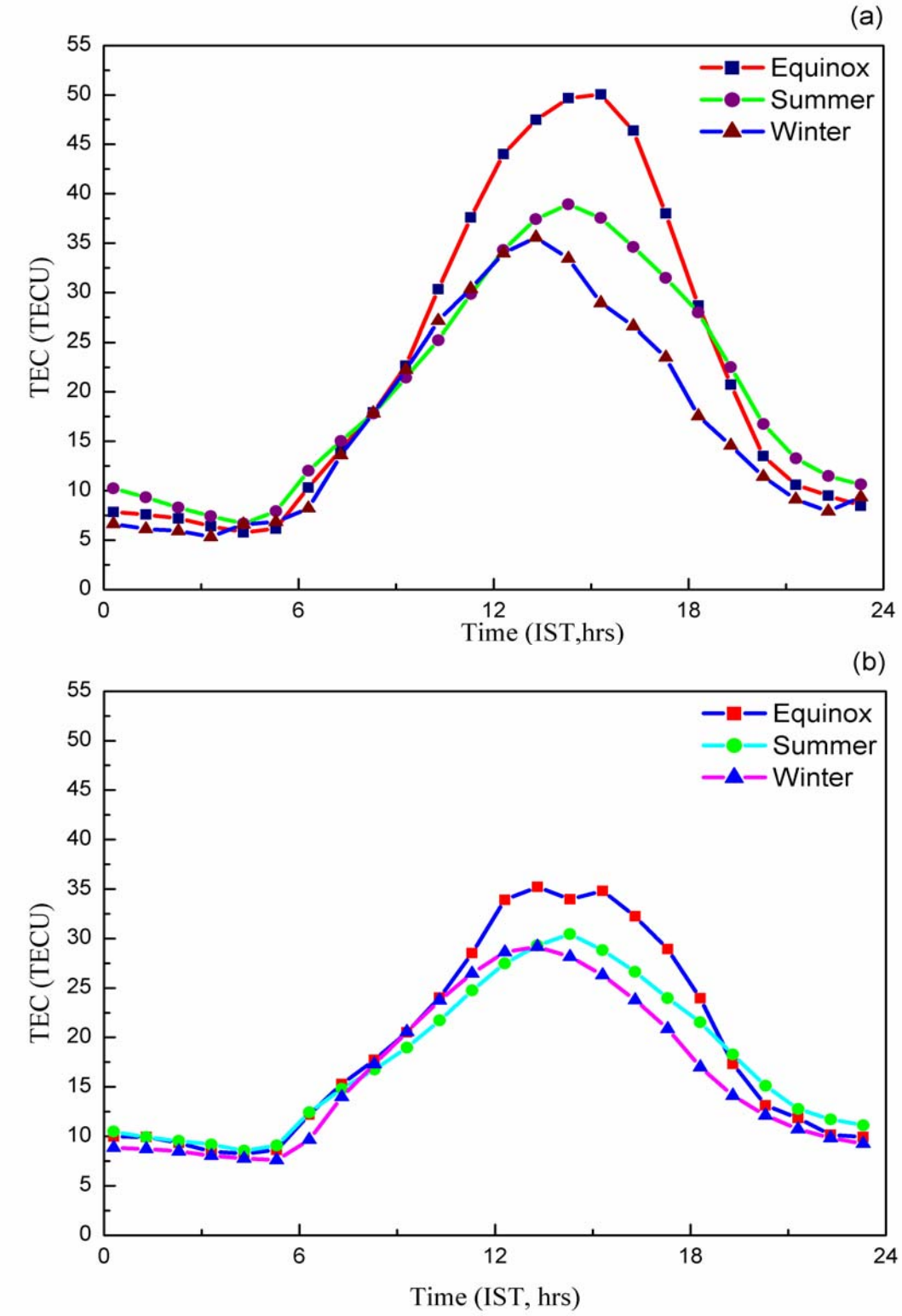

Figure 3.3: Seasonal mean diurnal variations of TEC during (a) 2005–2006 and (b) 2006–2007 at Rajkot

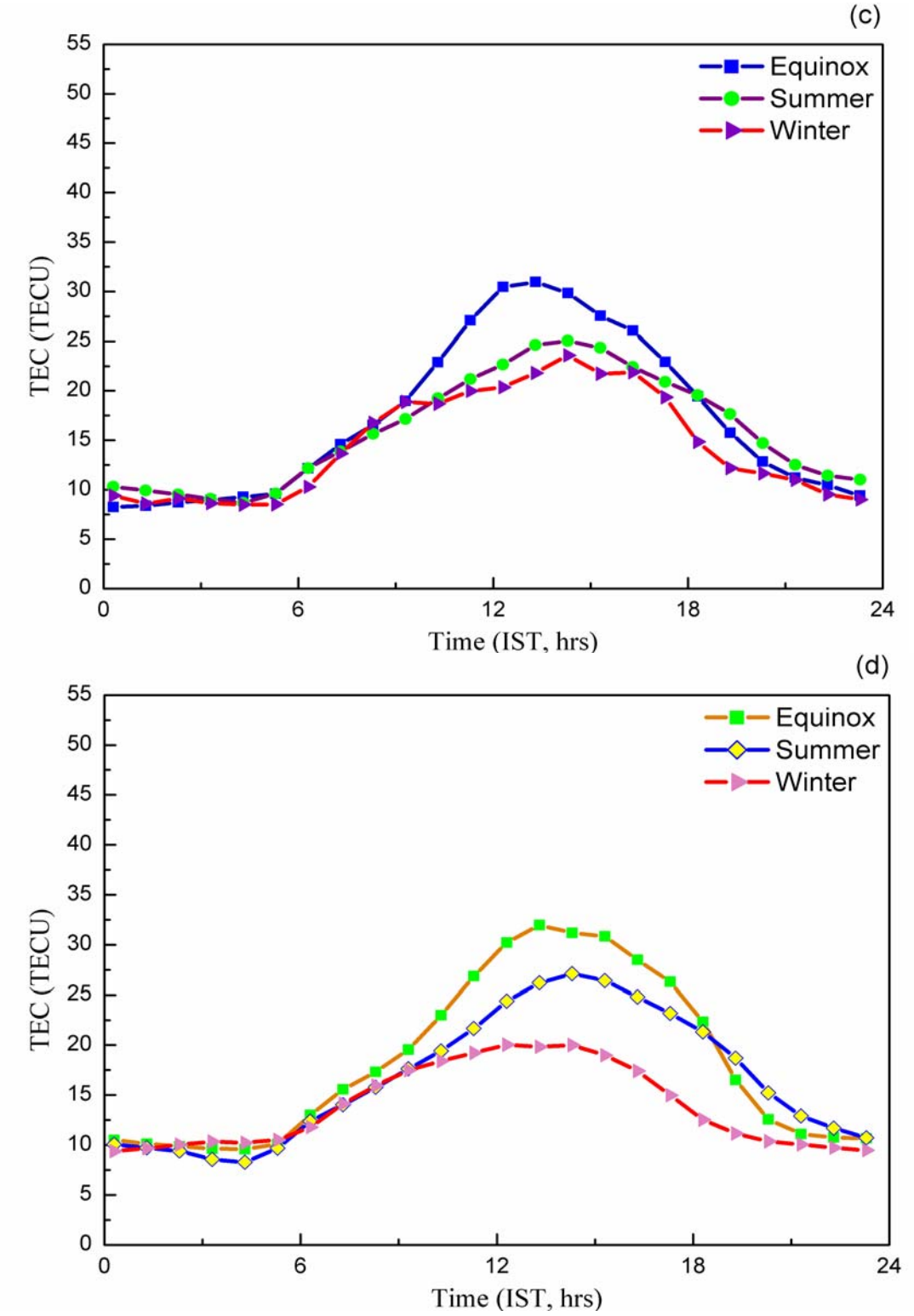

Figure 3.3: Seasonal mean diurnal variations of TEC during (c)2007 -2008 and (d) 2008–2009 at Rajkot

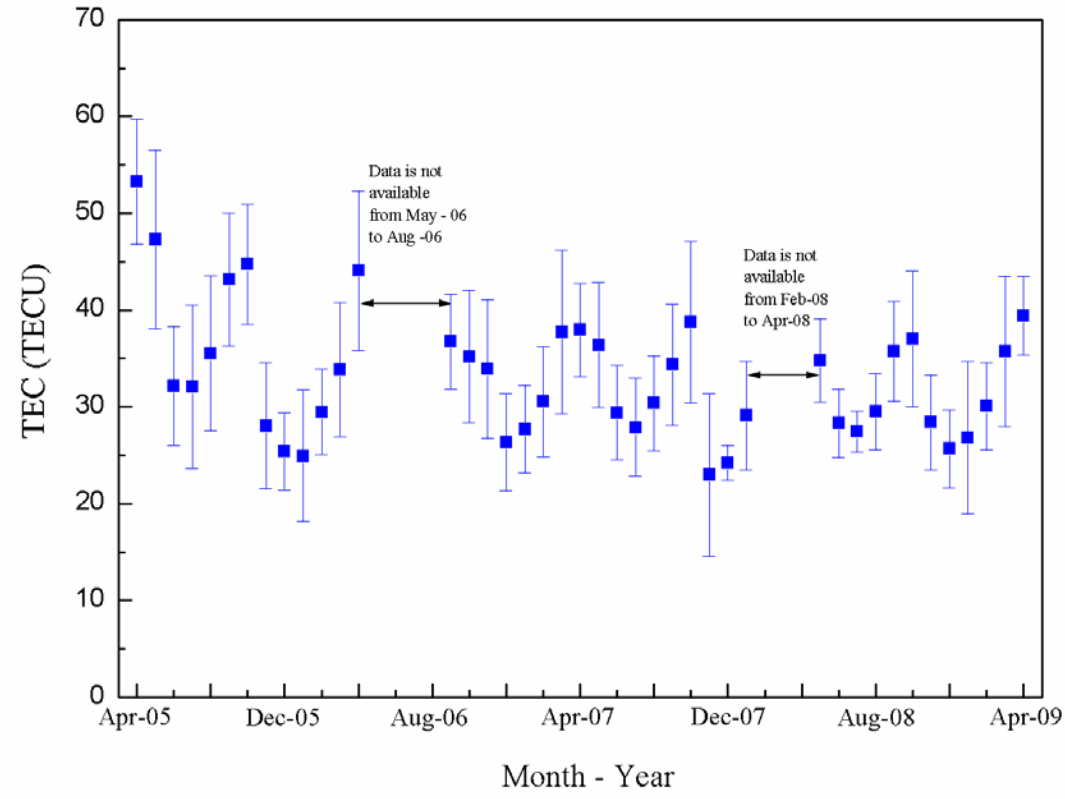

Figure 3.4: Month-to-month Variations of TEC, daily mean peak, (2005–2009) at Rajkot

3.5 Solar activity dependence of TEC

The sun emits a wide spectrum of radiation along with the high energy particles. In addition to the sunspot number, the flux of the sun's radio emission at a wavelength of 10.7 cm (2.8 GHz) is also a useful indicator to show the phase of the solar activity. We have used the solar F10.7 flux values to observe the variations of the present solar cycle. Figure 3.5 shows the correlation between the yearly mean daytime peak TEC and respective year's average solar flux values. The yearly mean TEC is derived from the average of the each month's daily peak TEC.

Rama Rao et al., [1985] reported the direct control of solar activity on the ionization level, with high electron density values during a high solar activity

period and low values during a low solar activity period. Although the range of solar flux variations during the present study is very limited but Figure 3.5 shows high positive correlation (Correlation Coefficient R=0.97) between daytime peak TEC and the solar F10.7 flux.

During the period of low sunspot numbers, TEC builds up quite slowly, resulting in the low values of day maximum. This can also be observed in Figure 3.4 where TEC values are decreasing consistently with the period of the years. But for the year of 2008-2009 it is observed that TEC values are increasing gradually. This shows clearly the solar activity dependence of electron density. *Warnant et al.,* [2000] have reported higher values of TEC with increasing solar activity.

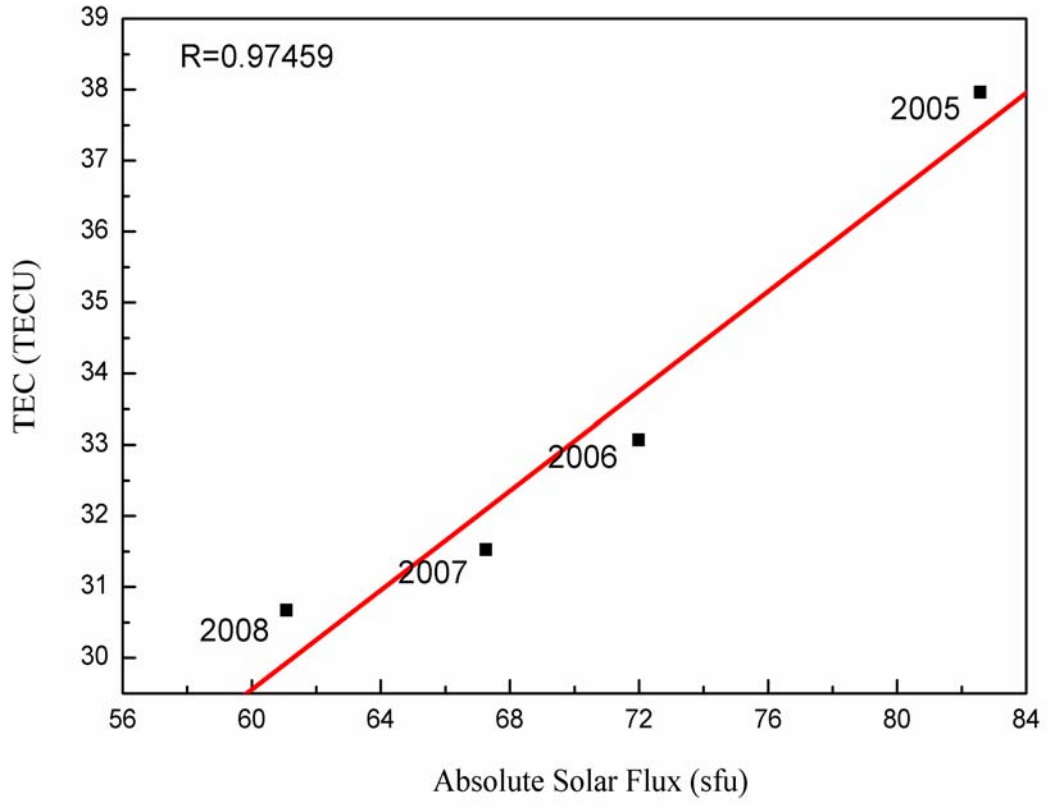

Figure 3.5: Solar cycle dependence of TEC observed at low latitude station Rajkot

3.6 EEJ control on development of EIA

In order to see the EIA development and influence of EEJ on it we have derived the contour plots of TEC with respect to local time and magnetic latitudes on three quiet days for different EEJ conditions, using GAGAN GPS data of five stations: Trivandrum (0.5^0 N Geomagnetic), Bangalore (4.32^0 N Geomagnetic), Hyderabad (9.22^0 N Geomagnetic), Bhopal (14.21^0 N Geomagnetic) and Delhi (20.32^0 N Geomagnetic). All these stations are around the common longitude belt of $77–78^0$ E. The details of these stations are given in Appendix-I (Table I.1).

In Figure 3.6, the first panel represents the contour TEC plot on 25 December 2005 along with the diurnal variations of EEJ on the day. It can be seen that due to the presence of CEJ, EIA peak occurred at lower value of ~35 TECU at ~1600 IST. This is the case of morning counter Electrojet. On the day anomaly is totally inhibited with a spatial extent of $\sim6^0$ N. Due to inhibition of EIA, plasma does not get transfer to more extended latitudes. Hence maximum of EIA occurs at lower latitude with low magnitude.

The second panel represents the contour TEC plot on 23 October 2005 along with the diurnal variations of EEJ on the day. This is the case of weak EEJ and EEJ peak value is ~ 31 nT. On the day, the EIA peak occurred at ~45 TECU at ~15:00 IST and it extended up to 10^0 N.

The third panel represents the contour TEC plot on 20 October 2005 along with the diurnal variations of EEJ on the day. This is the case of strong EEJ and EEJ peak values is 78 nT. On the day, the EIA peak occurred at ~55 TECU at ~13:00 IST. The latitudinal extent of EIA is up to $\sim14^0$ N.

The observed results clearly show the control of EEJ on development of EIA *Dabas et al.,* [1984] also reported that EEJ has a pronounced influence on TEC over a large latitudinal belt starting from the equator to 25^0N dip latitude. *Rama Rao et al.,* [2005] have shown that EEJ controls the altitude of the lifted plasma over the equator and hence the location of the crest of EIA. The higher the

EEJ strength, the higher the altitude to which plasma gets lift over the equator and farther the location of the crest of the EIA. They have shown the spatial variation of TEC and dependence of EIA on EEJ using GPS data of seven stations of the GAGAN network. Our results agree with this and showing positive dependence of EIA on EEJ.

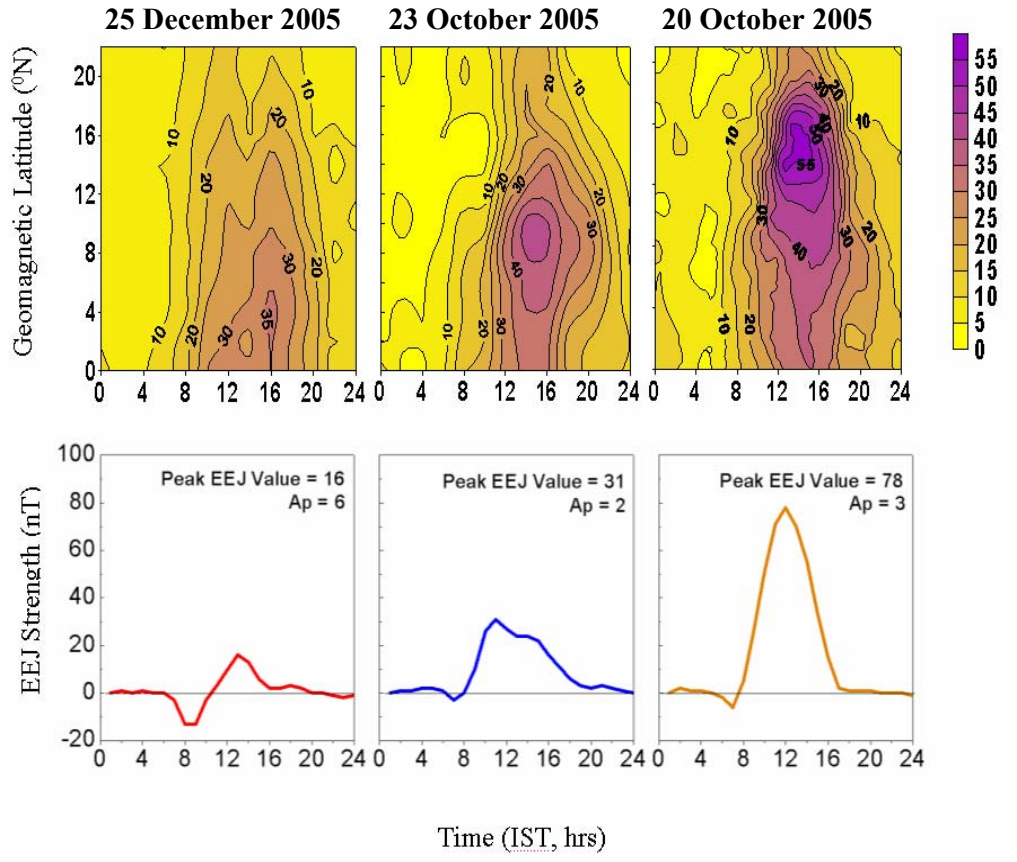

Figure 3.6: EIA development during three different EEJ conditions

The statistical correlation between EIA strength and EEJ strength is presented in Figure 3.7. The correlation (correlation coefficient (R) value of 0.71) shows that EIA strength increases with EEJ strength. There is a good linear correlation between EIA strength and EEJ peak value. The scattered points around the regression line may be due to other factors contributing to the day-to-day variability of TEC, although only magnetically quiet days are considered in this analysis.

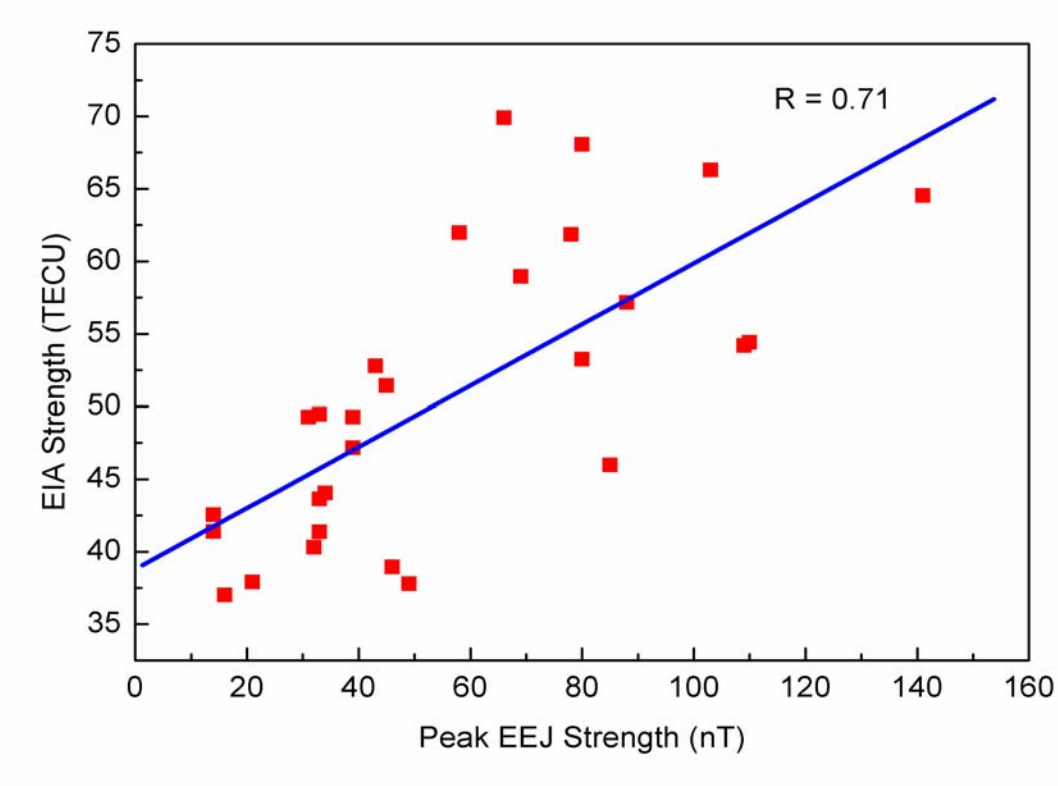

Figure 3.7: Statistical correlation between EIA strength and EEJ peak values. R shows the value of Correlation Coefficient

3.7 EEJ control on low latitude TEC

As discussed in the previous section, the strong EEJ results in to the strong **E**×**B** drift. Hence, EIA strength increases and more plasma will get transfer at low latitudes from equatorial latitudes. This process increases the low latitudes TEC. Now, in order to see the low latitude TEC variations during different EEJ conditions we have plotted the diurnal variations of TEC at Rajkot during strong, weak and counter EEJ conditions. Figure 3.8 shows these results.

Figure 3.8 (a) represents the diurnal variations of TEC on 9 April 2005 (Ap=3), a strong EEJ day with EEJ peak value of 81 nT. TEC attains the peak value of ~70 TECU on the day and the daily peak occurred at ~13:00 IST. On strong EEJ day, obviously the EIA strength will be high. The observed high value of TEC diurnal peak on 9 April 2005 is in agreement with this.

Figure 3.8 (b) represents the diurnal variations of TEC on 5 December 2005 (Ap=3), a day of weak EEJ. The TEC diurnal variations show two peaks one at ~12:30 IST with value of ~35 TECU and other at 16:30 IST with value of ~41 TECU on the day. As observed in the case of 23 October 2005 in the previous section, the EIA peak occurs at delayed time of ~15:00 IST. The observed two TEC peaks on 5 December 2005 day require further investigations.

Figure 3.8 (c) represents the diurnal variations of TEC on 3 July 2005 (Ap=7), an afternoon CEJ day. Here also two peaks have been observed with very short time gap. Diurnal TEC maximum occurred at 14:00 IST with value of ~50 TECU. Figure 3.8 (d) represents the diurnal variation of TEC on 31 December 2006 (Ap=2), a morning CEJ day. On the day, prominent daytime TEC peak has not seen. The broad and flat TEC curve is observed. This may be due to the inhibition of EIA on this day. The morning CEJ results in to the downward **E**×**B** drift in the fore noon hours.

On strong EEJ days, EIA intensifies and transfers more plasma in to the crest regions. On CEJ days, EIA suppressed and TEC shows low values near the crest region. Thus the results suggest that EEJ fully controls the EIA development, and hence the distribution of F region plasma in the low latitude ionosphere. This agrees with the results shown by *Rama Rao et al.* [1983] and *Rastogi and Klobuchar* [1990].

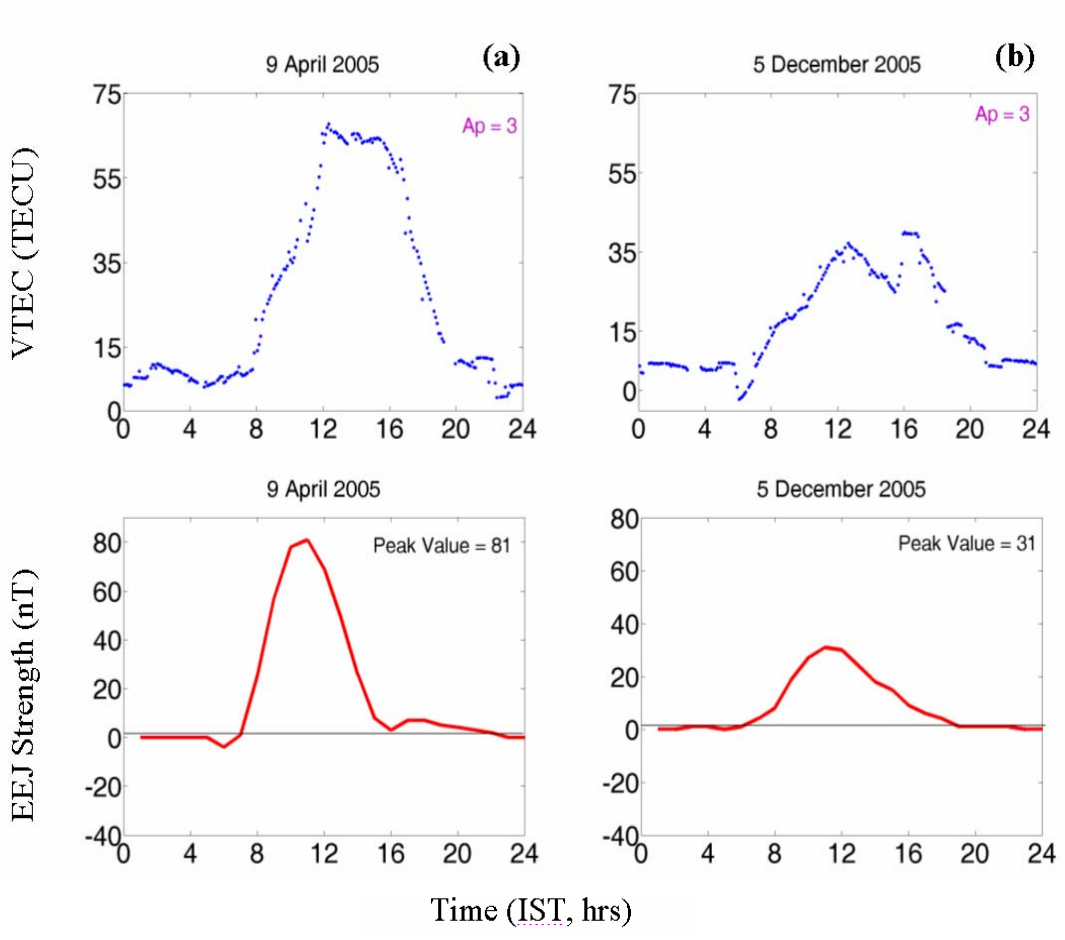

Figure 3.8: EEJ influence on diurnal variations of TEC on the day of (a) 9 April 2005, (b) 5 December 2005, representing strong and weak EEJ conditions respectively

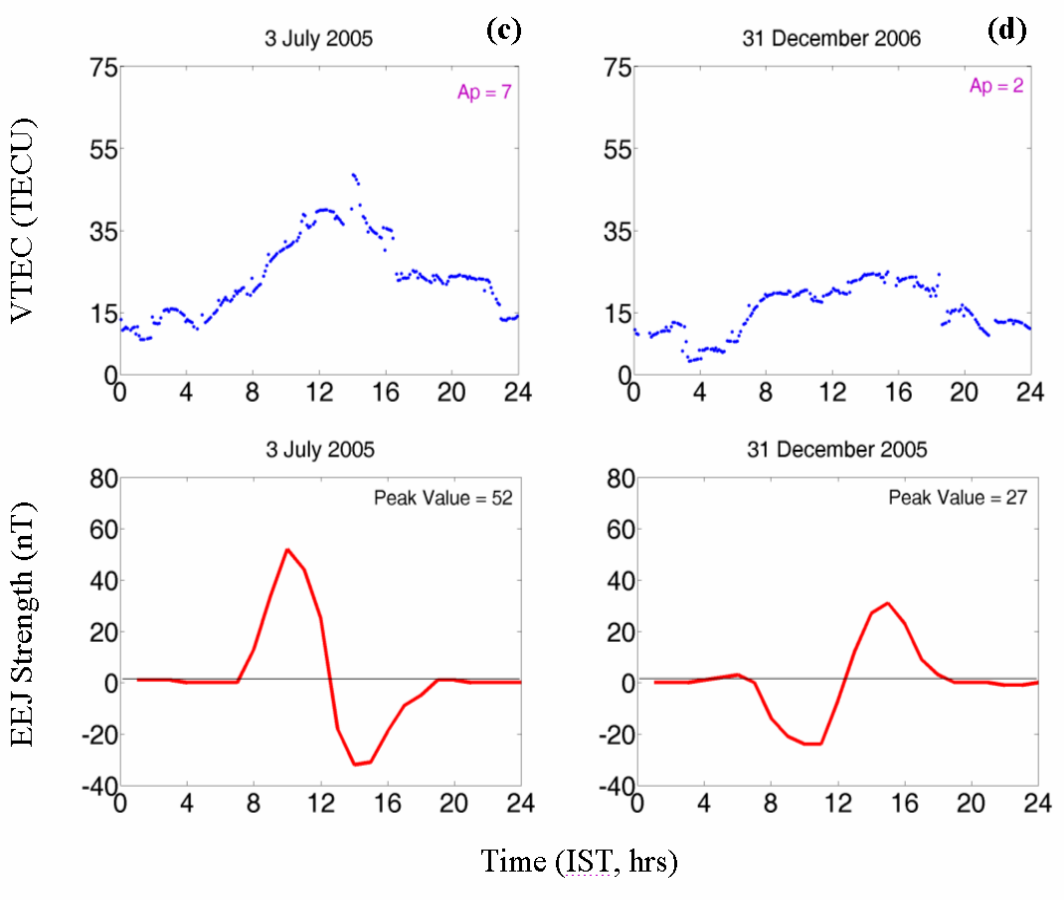

Figure 3.8: EEJ influence on diurnal variations of TEC on the day of (c) 3 July 2005 (d) 31 December 2006, representing afternoon CEJ and morning CEJ conditions respectively

3.8 Low Latitude L-band scintillation and associated TEC depletion

When a radio wave propagates through electron density irregularities presence in the ionosphere, it suffers from phase and amplitude fluctuations. As we have discussed in Chapter 1, if the ionospheric irregularities are present in the path of the radio wave signals, they experience phase and amplitude fluctuations, onset angle variations and also the signal loss on some occasions. The understanding of these signal fluctuations i.e. ionospheric scintillation is necessary in order to provide the better and accurate GPS positioning and navigation and also to study the nature and dynamics of ionospheric irregularities. The detailed discussion on ionospheric F region irregularities i.e. ESF responsible for radio wave scintillation is given in Chapter 4. In this section we present GPS L-band scintillation and associated TEC depletion observed at low latitude station Rajkot during April-2005 to April-2009.

The GPS observations from April – 2005 to April - 2009 at Rajkot show only 30 scintillation days. Almost all the events are observed during post-sunset-pre-midnight hours. The observed scintillation by different PRN's for four different days during April 2005 to April 2009 are presented in Figure 3.9. The left panel of each figure shows the temporal variations of TEC and scintillation index S4. The right panel of each figure shows the temporal variations of satellite elevation angle and geomagnetic latitude (solid line) and geographic longitude (broken line) of the ionospheric pierce point (IPP) computed from the elevation and azimuth angles of the satellite at each instant of its pass, as seen from Rajkot. For IPP computations a thin ionospheic shell at an altitude of 350 km has been understood. The observations below 30^0 have been omitted in order to take care the effect of multipath reflections.

Figure 3.9 (a) represents the scintillation event observed by PRN 5 on 06 October 2005. It can be seen that TEC depletion of magnitude ~3 TECU has been observed between 2125 IST and 2150 IST. On the occasion S4 enhanced up to the magnitude of ~0.18. At 2150 IST, TEC enhancement is observed. The noteworthy feature here is that TEC enhancement is associated with the depletion in S4 to

~0.025. After this again TEC depletion of ~4 TECU is seen with S4 enhancement up to ~0.24. The elevation information describes that the depletion is observed at high elevation angles (between 45^0 and 65^0). The latitude-longitude (lat-long) information describes that the depletion is observed at lower latitudes than the Rajkot i.e. equatorward and west of Rajkot.

Figure 3.9 (b) represents the scintillation event observed by PRN 31 on 24 December 2006. TEC depletion of magnitude ~1 TECU and S4 enhancement of ~0.12 is observed between 2200 IST and 2300 IST. The temporal variations of elevation angle describes that the depletion is observed at elevation angles between 65^0 and 50^0. The lat-long variations describe that depletion is observed between 8^0 N and 13^0N and east of Rajkot.

The strongest scintillation event observed during 2005-2009 is on 25 September 2007 which is shown in Figure 3.9 (c) and Figure 3.9 (d). TEC depletion of ~6 TECU and S4 enhancement up to 0.29 is observed by PRN 5 between 2075 IST hrs and 2125 IST hrs as shown in Figure 3.9(c). TEC depletion of ~2 TECU and S4 enhancement up to 0.12 is observed by PRN 30 in Figure 3.9(d) almost at the same time. The elevation angle variations of PRN 5 show that the depletion is occurred at elevation angles between 55^0 and 40^0. The latitude - longitude curves of PRN 5 shows that the depletion is occurred between latitude range of ~12^0N to ~11^0N and west of Rajkot. The elevation variations of PRN 30 describes that the depletion is occurred at elevation angles between 55^0 and 50^0. The lat-long variations of PRN 5 describes that the depletion is occurred between latitude range of 13.5^0N and 12.5^0N and west of Rajkot. PRN 30 has come across of two TEC depletions. The second is observed at quite low elevation angle of ~30^0-35^0. The depletion magnitude is ~4 TECU which is accompanied by S4 value of ~0.18. It is observed at lower latitudes than the Rajkot and west of it.

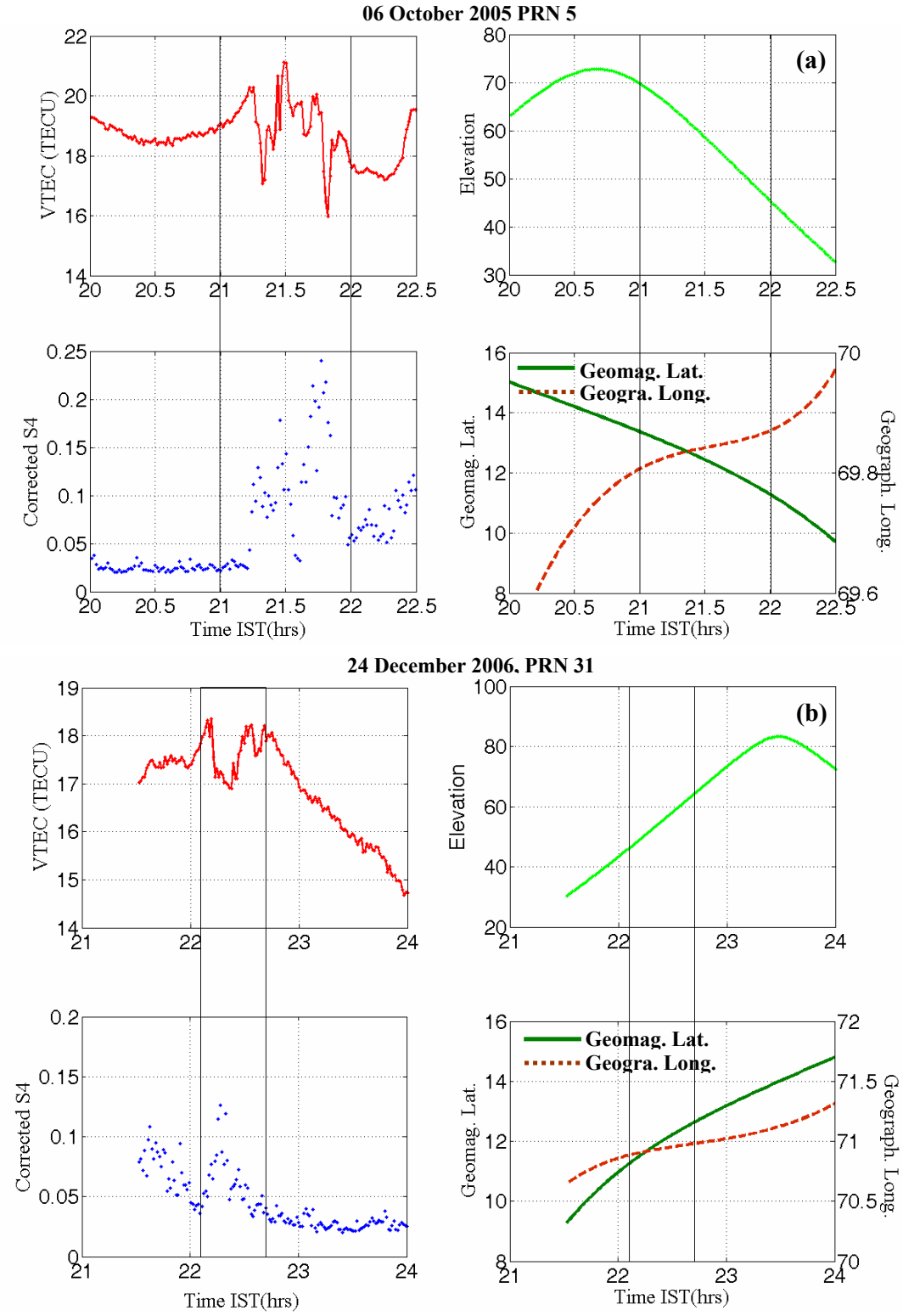

Figure 3.9: Low latitude L-band scintillation observed on (a) 06 October 2005 (b) 24 December 2006 at Rajkot

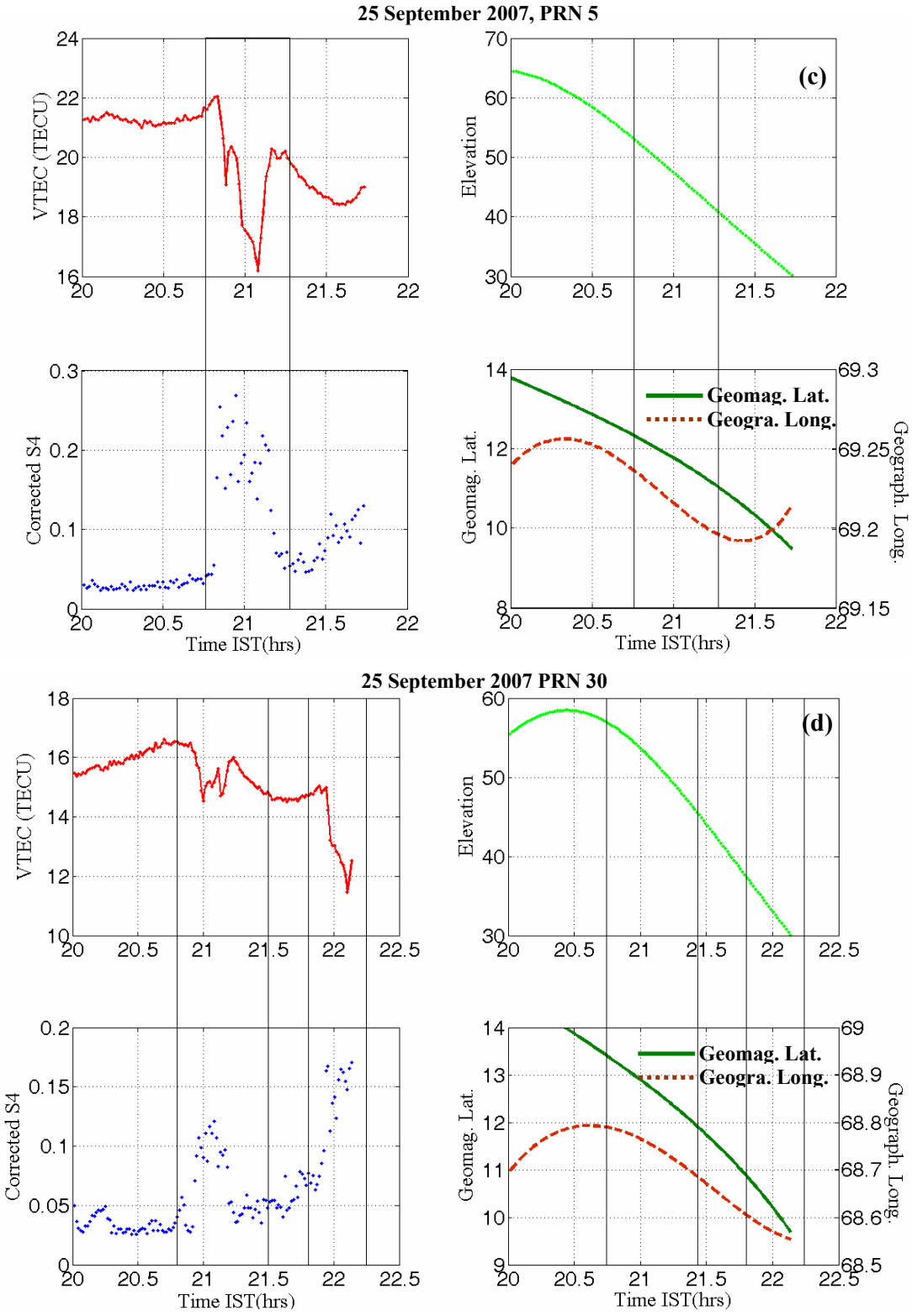

Figure 3.9: Low latitude L-band scintillation observed on (c) and (d) 25 September 2007 at Rajkot

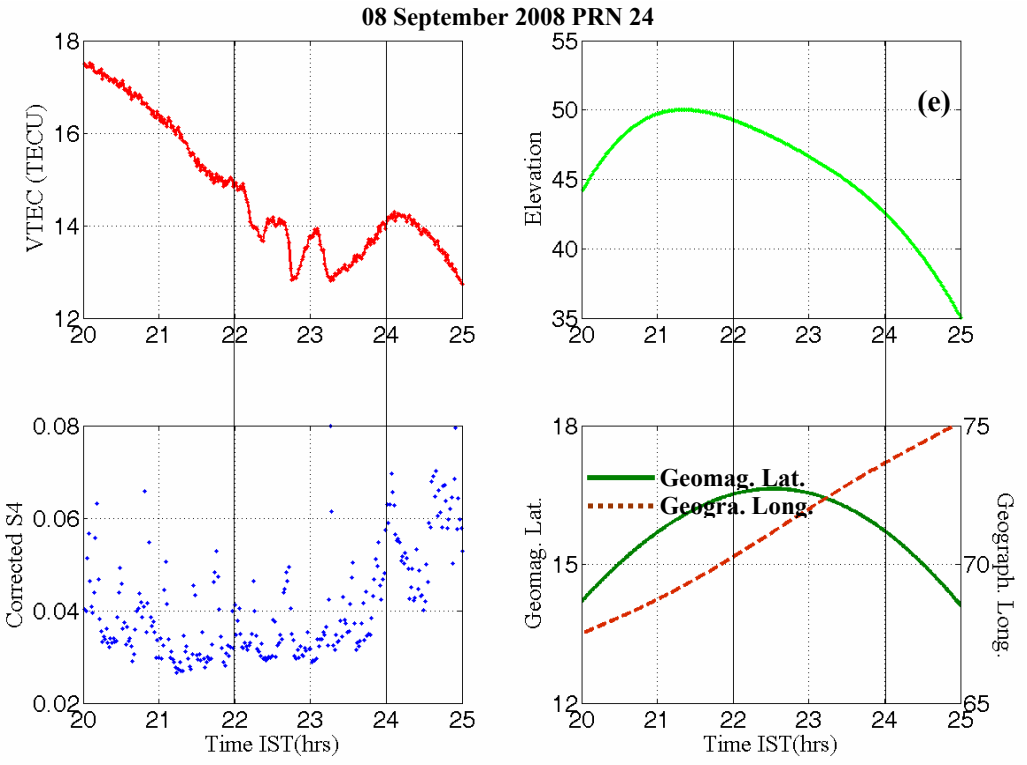

Figure 3.9: Low latitude L-band scintillation observed on (e) 08 September 2008 at Rajkot

Figure 3.9 (e) represents the scintillation event observed by PRN 24 on 08 September 2008. Three clear depletions are observed between 2200 IST and 2350 IST. The magnitude of TEC depletion is ~ 1 TECU. The S4 values are not showing any noticeable enhancement during this event. The depletions are at quite high elevation angles and higher latitudes than the Rajkot. The low S4 values indicate that the observed TEC depletions might be due to some ionospheric wave like features which require further investigations.

In this investigation, it has been observed that on most of the days scintillation is observed between 21:00 to 22:00 IST. The observed scintillation amplitude is very low and only 30 events of scintillation are observed during 2005-2009. One of the reasons for the low scintillation amplitude and less occurrence frequency is the current low solar activity period. Due to the low solar activity period, the occurrence frequency of ESF also becomes low .Even if the irregularities occur at the equator, the height which they attain over the equator

that only decides the latitudinal extent of irregularities and hence scintillation if any.

An attempt has been made to describe the latitudinal extent of L-band scintillation in Chapter 4. The results from the multitechnique campaign conducted for the study of ESF irregularities are discussed in Chapter 4. During the campaign period, it is observed by radar, located at off equatorial station Gadanki (13.5^0N, 79.2^0E; geomagnetic dip 6.5^0N) in India, that the ESF irregularities' height mostly confined to 500-600 km. Thus, due to this lower confined height of ESF irregularities, they may not expand up to Rajkot latitude and die out over lower latitudes only. The observed lower occurrence frequency of L-band scintillation at Rajkot may be due to this reason.

Dasora and Pandey [2005] reported the UHF scintillation and associated TEC depletions near the northern crest region of EIA, Udaipur (26.4^0N 73.7^0E, Geographic, 15.6^0N Geomagnetic), in India. They have shown a one to one correspondence between the TEC depletion and the increase in S4 index.

3.9 Conclusion

The present chapter describes the temporal and spatial variations of GPS derived TEC during the low solar activity period (2005–2009).The temporal variations are recorded at Rajkot (22.29^0N 70.74^0E, sub-ionospheric dip latitude 15.8^0N) near the northern crest of EIA. The diurnal variations of TEC show a steady increase from about sunrise to an afternoon maximum and then fall to attain a minimum just before sunrise. A significant day to day variability in diurnal pattern has been observed which decreases with descend phase of solar activity. The seasonal variations of TEC show that TEC values are high in equinoctial months followed by summer and winter. The month to month variations of mean diurnal peak TEC shows semiannual variations with a peak during the equinox period and a trough during the solstice period. The high positive correlation between TEC peak and solar F10.7 flux shows high solar

cycle dependence of TEC. The gradual increase in TEC observed in the year 2009 provides the indication of the starting of new solar cycle.

The latitudinal variations of TEC derived from the GAGAN GPS stations, further show that the EIA parameters, viz, the anomaly peak value, time and latitudinal extent are greatly controlled by EEJ. Our results indicate that low latitude TEC magnitude and daily peak time depends on the EEJ conditions. EIA is completely inhibited on the day of morning CEJ, resulting in a lower TEC value at Rajkot. The low latitude L-band scintillation is low both in amplitude as well as occurrence frequency due to the low solar activity period. Most of scintillation events are observed between post sunset and pre-midnight hours.

Chapter 4
A Multitechnique investigation on ESF irregularities

4.1 Introduction

The sunset in the equatorial and low latitude ionosphere is characterized by the pre-reversal enhancement (PRE) in vertical drift velocity/eastward electric field before it turns to westward [*Fejer*, 1991]. The rapid bites out of E-region ionization due to fast chemical recombination of dominant molecular ions after sunset and the PRE in vertical drift velocity create steep plasma density gradient at the bottom side of equatorial F region. This plasma density gradient is anti-parallel to gravity and provides platform for the generation of wide spectrum of field aligned plasma density irregularities in the night time equatorial F-region [*Haerendel,* 1974; *Woodman and LaHoz,* 1976]. These irregularities are known as Equatorial Spread-F (ESF).

The ESF was first discovered by *Booker and Wells* [1938] as diffuse echoes on ionograms. With the advancement of time, it was understood that the ESF manifests itself as spread in range or frequency on the ionograms [*Booker and Wells*, 1938], plume like structures in coherent backscatter radar echoes [*Woodman and LaHoz*, 1976], intensity bite-outs in OI 630.0 nm night airglow [*Weber et al.,* 1978], and scintillations on amplitude and phase of VHF, UHF and L bands [*Su. Basu and Kelley,* 1977; *Yeh and Liu,* 1982; *Aarons,* 1982].

Booker and Wells [1938] associated the occurrence of spread F with post sunset rise of the F region. Number of studies revealed that the $\mathbf{E}\times\mathbf{B}$ drift is the primary mechanism [*Fejer et al., 1999; Whalen, 2002; Lee et al., 2005*] which directly uplifts the F region and creates required electron density gradient. The PRE in the vertical drift results in to the decrease of the collision effect [*Kelley,* 1989] which positively takes part in ESF development. *Spencer* [1955] was the first to suggest that ESF is a manifestation of the field aligned irregularities.

Though spread-F can occur at any latitudes, the maximum and intense occurrence is around $\pm 20^0$ geomagnetic latitudes. The ESF shows variability with season, local time, geographical location and solar activity. [*Chandra and Rastogi,* 1970; *Woodman and LaHoz*, 1976; *Fejer and Kelley* 1980; *Basu and Coppi, 1999*; *Hysell and Burcham*, 2002]. The maximum probability of occurrence of ESF is during equinoxes, moderate during summer and minimum during winter.

Generation mechanism of ESF

The primary mechanism which plays role in the initiation of ESF is collisional Rayleigh-Taylor instability. This instability perturbs the bottom side of the F region followed by secondary instabilities, one feeding on the other. An excellent explanation of these processes is given by *Kelley* [1989]. Figure 4.1 shows the schematic representation of the processes playing roles in the ESF generation.

As mentioned earlier, the steep plasma density gradient at the bottom side of the F region, a combined effect of PRE and rapid recombination of E-region ionization, is anti-parallel to gravity. The situation is analogues to a heavier fluid supported by a lighter fluid. In case of ionosphere, the magnetic field is the 'light fluid'. This configuration of plasma density builds the platform for the generation of well known Rayleigh - Taylor (R-T) instability. This plasma density configuration is same for all the nights. But on some nights, when both the conditions i.e. steep plasma density gradient at the bottom side of the F region and F region height, along with the other background conditions are conducive, a small perturbation in the bottom side of the F region can give rise to R-T instability.

The expression for the linear growth rate 'γ_g' for the collisional R-T instability has been shown [*Haerendel*, 1973; *Ossakow et al*., 1979] to be

$$\gamma_g = \frac{1}{L}\frac{g}{\nu_{in}}\frac{k_x^2}{K} \tag{4.1}$$

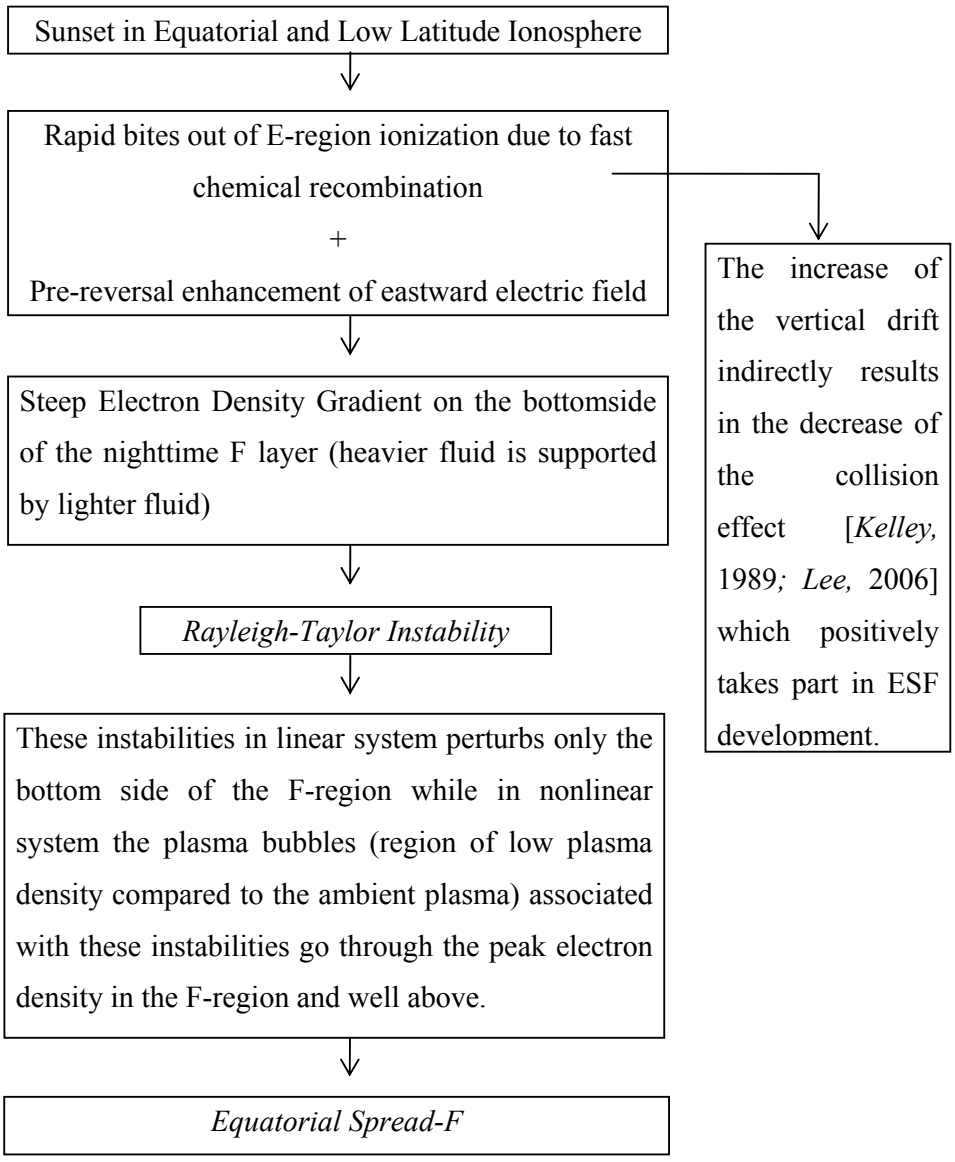

Figure 4.1: Schematic representation of the processes playing roles in the ESF generation

where ν_{in} is the ion-neutral collision frequency, g is the acceleration due to gravity, L is the ambient plasma density scale length which is inversely proportional to the plasma density gradient dn_0/dz and is given by $L = \left[\frac{1}{n_0} \left(\frac{dn_0}{dz} \right) \right]^{-1}$. The zonal component of the total wave vector K, whose magnitude represents the wave number, is denoted by k_x.

The collision Rayleigh-Taylor instability can be described as follows. Consider a sinusoidal perturbation in the ion and electron densities (n'), over the steady state value (n_0) in the F- region along the zonal direction as depicted in Figure 4.2. The ∇n_0 is directed anti-parallel to the gravity. The magnetic field B is into the plane of the paper. Under the action of gravitational drift, perturbations in ion and electron densities move eastward and westward with a gravitational drift velocity of $\mathrm{g}/\Omega_{\mathrm{i}}$ and g/Ω_e respectively; Ω_{i} and Ω_{e} being the ion and electron gyro frequencies respectively. Since gravitational drift is inversely proportional to the gyro frequency, the perturbation in ion densities moves faster than those of electron and lead to the charge separation. Due to this charge separation, polarization electric fields get generated which are directed eastward in the density depleted and westward in the enhanced regions. These polarization electric fields make the depleted region to drift upward and bring the enhanced density region downward, amplifying the density perturbation. In order to sustain the growth, this process should be faster than the effective lifetime of the ions *i.e.* $1/\nu_R$ (ν_R is the recombination rate), otherwise the ions would be lost by recombination inhibiting the growth of the perturbation. The plasma-depleted region is called a bubble in analogy to the hydrodynamic case. The upward drift of the plasma ceases at the altitudes where the ambient electron density becomes equal to that inside the bubble. This determines the maximum altitude of plasma bubbles and the altitudinal extent of ESF.

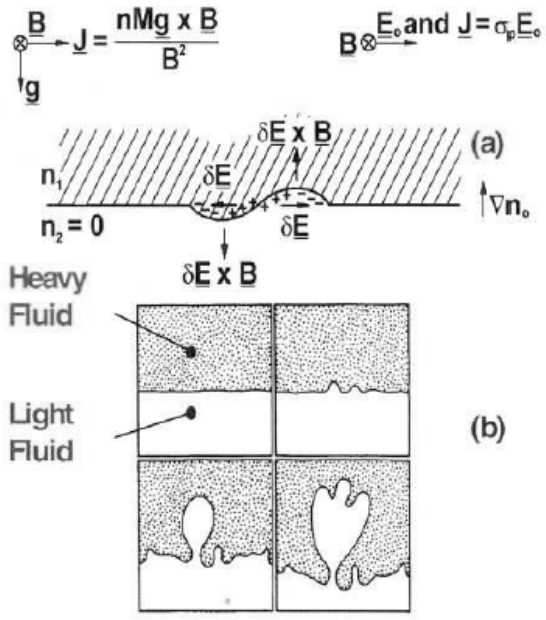

Figure 4.2: Schematic diagram of the plasma analog of the R-T instability in the equatorial geometry (b) Sequential sketches from photos of the hydrodynamic R-T instability. A lighter fluid is initially supports a heavy fluid [After *Fejer and Kelley,* 1980]

The growth rate is shown to be maximum when the perturbation is along the zonal direction and becomes independent of wavelength for horizontally propagating wave [*Ossakow*, 1979] and hence the equation 4.1 becomes

$$\gamma_g = \frac{1}{L}\frac{g}{\nu_{in}} \tag{4.2}$$

Apart from gravity, eastward electric field also contributes to the growth of the amplitude of the density perturbation. However, the mechanism is slightly different. Due to the Hall drift ($\mathbf{E} \times \mathbf{B}/B^2$) the plasma is lifted up to higher altitudes to a region of smaller ion neutral collision frequencies, thereby increasing the growth rate of the R-T instability. This drift is independent of the mass and charge of the species; however a charge separation does occur along the direction of the electric field due to the differences in the Pederson mobility $\left(\frac{1}{eB}\frac{\nu_{\alpha n}}{\Omega_\alpha}\right)$ of ions and electrons. Here, '$\nu_{\alpha n}$' can be either ion-neutral or electron-

neutral collision frequency (ν_{in}, ν_{en}) as the case may be. Due to this charge separation, eastward polarization electric fields get set up in the density troughs and westward in the density crests. This results in the differential vertical drifts as discussed in the case of gravity, affecting the growth of the perturbation amplitude. The effect of the primary eastward electric field E_x [*Ossakow*, 1979; *Kelley*, 1989] in enhancing the growth rate of the R-T instability is written as

$$\gamma_E = \frac{1}{L}\frac{E_x}{B} \tag{4.3}$$

In addition to the electric field, neutral parameters like eastward zonal wind W_x can also drive the instability when the background electron density gradient is westward. The growth rate is given as:

$$\gamma_{w_x} = \frac{1}{L} W_x \left(\frac{\nu_{in}}{\Omega_i}\right) \tag{4.4}$$

The vertical wind (W_z), though small in magnitude, exists in the equatorial ionosphere [*Biondi and Sipler*, 1985; *Raghavarao et al*., 1987; *Raghavarao et al*., 1993; *Sekar and Raghavarao* 1987]. Thus an expression for the growth rate of the generalized R-T instability including all the above-mentioned parameters is given as [*Sekar and Raghavarao*, 1987] :

$$\gamma = \frac{1}{L}\left[\frac{g}{\nu_{in}} + \frac{E}{B} + W_x\left(\frac{\nu_{in}}{\Omega_i}\right) - W_z\right] \tag{4.5}$$

However, this expression takes care of the linear growth of the R-T instability, which is the primary mechanism for the generation of ESF. A 'hierarchy of plasma instabilities' is believed to be the cause for the observed wide range of scale sizes, extending to shorter scale lengths through secondary plasma processes [*Haerendel*, 1973; *Chaturvedi and Kaw*, 1976; *Costa and Kelley*, 1978]. The hierarchy is as follows:

(1) Collisional R-T instability mechanism driven by the zero order electron density gradient

(2) The (**E** × **B**) gradient drift instability due to the sharp density gradients set up by the collisional R-T instability mechanism

(3) Collisionless R-T instability in the region where collisions become negligible and grows due to the sharp density gradients, and finally

(4) Kinetic drift waves grow off these irregularities as they attain large amplitudes

The basic idea of the multi-step (hierarchy) process for the growth of ESF irregularities is now well accepted though there are some differences regarding the details of the processes. By far, the nonlinear theories of ESF have been very successful in explaining different kinds of observations on ESF irregularities at various altitudes from different longitude regions across the globe.

Plasma bubbles are the manifestation of non linear irregularities development. The bubbles are magnetic flux tubes aligned and cover north-south distances across the magnetic equator of several thousand kilometers, with east-west dimensions of up to a few hundred kilometers. As plasma bubbles buoyantly rise upwards, they become highly elongated in the vertical direction [*Tsunoda & Towle,* 1979], sometimes attaining very high altitudes (>1500 km) at the magnetic equator [*Mendillo & Tyler,* 1983], and the depleted regions extend poleward in the flux tubes [*Sales et al.,* 1996], reaching dip latitudes of over $\pm 15^0$ [*Rohrbaugh et al*., 1989]. The regions of the strong plasma density gradients are known as plasma bubble walls, separating the inside and outside of the plasma bubble structures. The steep plasma density gradient of the walls of a developing plasma bubble becomes unstable under secondary instability processes, this provides platform for the development of a spectrum of irregularities falling into a smaller scale sizes.

Satellite signals, during their earth-space propagation path, experience amplitude and phase fluctuations due to the presence of these plasma bubble irregularities in their propagation way. If the level of the irregularity is low, only

the phase and angle of arrival are changed (thin phase screen). If the level of structuring is strong, the amplitude of the signal also varies (thick phase screen). After crossing the phase screen, the electromagnetic wave makes a diffraction pattern in both intensity and phase at the ground. These fluctuations of the radio signals are known as scintillations.

The scintillations vary widely with frequency, time of the day, season, geographical place and magnetic as well as solar activity, [*Basu and Kelley,* 1979; *Aarons,* 1982; *Das Gupta et al.,* 1982]. According to *Sripathi et al.,* [2008] if irregularities are confined to a layer of less than ~100 km thickness, only phase fluctuations get emerged and further propagation of radio waves to the plane of the receiver produces amplitude fluctuations also.

Fluctuations of GPS signals cause in some cases an additional error in finding the exact position of an object, which could be as large as tens of meters. In other cases a complete loss of the navigation signal also may occur. Since these plasma bubble irregularities cause disruptions/degradations of the navigation signals, understanding the evolution and dynamics of this phenomenon and its variability are of considerable practical importance.

In this context, the present chapter deals with the multitechnique investigation on ESF phenomenon. The multitechnique campaign from India involving VHF radar at low latitude station Gadanki (13.5^0N, 79.2^0E, dip latitude 6.5^0N), GPS TEC and scintillation monitor from the similar place and digital ionosonde at equatorial station Trivandrum (8.55^0N, 76.9^0E, dip latitude 0.5^0N) is conducted during the equinox season of 2005 to 2008 to further elucidate the evolution and dynamics of ESF irregularities. TEC enhancement associated with ESF plume structures is observed during the investigation. GAGAN GPS TEC and L-band scintillation data has been used to investigate the latitudinal extent of ESF associated L-band scintillation. Solar activity dependence of L-band scintillation is also presented.

4.2 Historical background

In past few decades, ESF has been extensively studied using various techniques, like VHF radars [for example, *Woodman and LaHoz*, 1976; *Patra et al*., 1997; *Hysell and Burcham*, 1998 and references therein, *Rao and Patra*, 1998], incoherent scatter radars [*Tsunoda*, 1980], probes on-board satellites [*McClure et al*., 1977; Valladares *et al*., 1983], airglow photometers [*Mendillo and Baumgardner*, 1982], scintillation receivers [*Krishnamoorthy et al.*, 1979; *Aarons*, 1982, 1993; *Basu and Basu*, 1985; *Basu et al*., 1996], HF radars [*Jayachandran et al.*, 1993, *Tiwari et al*., 2004] and numerical modeling [*Ossakow*, 1979; *Zalesak and Ossakow,* 1980].

Haerendel [1973] postulated that the largest scales of spread F were produced by a gravitational instability as proposed by *Dungey* [1956] and that the smaller scales resulted from a cascade of instabilities all the way down to meter scales responsible for the radar coherent echoes. He also invoked the role of flux tube integrated, rather than local, density gradients and conductivities in the instability mechanism but even that could not explain the irregularities observed in the topside ionosphere. *Woodman and La Hoz* [1976] proposed that a large (in size) perturbation in the gravitationally unstable bottomside F region would grow non-linearly into a bubble, similar to R-T instability in a neutral fluid. The bubble will rise by the effect of buoyancy and will continue to do so even in regions with gravitationally stable gradients such as in topside ionosphere. This qualitative theory was soon supported by numerical simulations [*Scannapeico and Ossakow,* 1976, *Zalezak et al.,* 1982, *Sekar et al.,* 1997 etc] which reproduce many of the observed features of the bubbles/radar plumes including the role of seed perturbations.

The observation of ESF irregularity structure using two dimensional echo power mapping technique with the Jicamarca VHF backscatter radar by *Woodman and La Hoz* [1976] showed for the first time that ESF can occur either in the bottomside or topside F region when the vertical drift is upward or downward and when density gradient is stabilizing or destabilizing, thereby challenging then existing theories of causative instability mechanisms for ESF. Subsequent long

term Jicamarca radar studies (JULIA) have shown different manifestations of ESF which are classified as topside, bottomside, bottom-type and valley type [*Hysell and Burcham,* 2002] with distinct characteristics (such as spectral widths) and distinct associations with other phenomena. For example, bottom type and valley type spread F do not produce significant spread traces on ionograms or scintillations. Considerable work has been done with in-situ probes on rockets and satellites showing the intensity of the associated plasma depletions by ~ 3 orders of magnitude [*Hanson and Sanatani,* 1971], their composition that is typical of lower altitudes thus revealing their origin [*McClure et al.,* 1977] and their clear temporal and spatial associations with radar plumes [*Tsunoda et al.,* 1982], using the east-west scanning capability of the ALTAIR VHF (155.5MHz) radar at Kwajalein. The Gadanki (6.5^0 N dip) VHF (53MHz) radar in India has revealed many characteristics of spread F irregularities such as spectral characteristics, updrafting and downdrafting structures etc. [*Patra,* 1997]. The EAR in Indonesia (10.36^0 S dip) has the capability to steer to preselected positions in the east - west from pulse to pulse. This enables one to see a Field Aligned Irregularities (FAI) formation west of the radar site before it shifts eastward to the vertical beam and further its development to the east. With this potential, *Yokoyama et al.,* [2004] have observed that plumes start to form very nearer to the E region sunset terminator.

Both ionosonde and scintillation receivers have been used at different locations to determine the temporal, seasonal and geographical distribution of spread F [*Aarons,* 1977, *Basu and Basu,* 1981, *Abdu et al.,* 1988]. The relationship between ionosonde spread F and VHF radar coherent echoes was not established in detail until the work of *Rastogi and Woodman,* [1978].

All such above-mentioned studies have nevertheless given clues of the various possibilities which have led to the present understanding of the gross behavior, but on a case to case basis, the exact mechanism or combination of mechanisms that gives rise to the observed effects is very difficult to pin-point.

Multi-technique observations may considerably improve our understanding of factors responsible for the generation, growth and dynamics of

the destabilized night time F region plasma irregularities. Earlier multi -technique investigations of ESF, such as the CONDOR campaign [*Basu et al.,* 1986] addressed a comparison of vertical wave number spectrum obtained by rocket and UHF scintillation spectrum. More recent Multi - Instrumented Studies of Equatorial Thermosphere Aeronomy (MISETA) campaign in South America [*Basu et al.,* 1996, *Valladares et al.,* 1996, *Mendillo et al.,* 2001] focused on neutral and plasma dynamics. *Kelley et al.,* [1996] were the first to use GPS TEC measurement and VHF backscatter radar measurements at Kwajalein (dip latitude 4.4^0 N) to infer the characteristics of upwelling structures. *Musman et al.,* [1997] used portable radar (CUPRI) and GPS measurements at Alcantara, Brazil near the magnetic equator to bring out clear association between radar plumes and TEC fluctuations. *Valladares et al.,* 2004 have used the observations of Jicamarca radar and a latitudinally distributed chain of GPS receivers to study the altitude-latitude extension of ESF structures. *De Paula et al.,* [2004a, b] used collocated VHF backscatter radar, GPS scintillation and digital ionosonde observations to study ESF manifestations at different spatial scales.

The morphology of equatorial scintillations based primarily on 250 MHz observations and some 1.5 GHz geostationary satellite measurements is reported in several publications [for example, *Aarons*, 1982, 1993; *Basu et al.,* 1980]. The radio beacon satellites transmitting signals in the VHF range have been used to study the scintillations in the Indian longitudes [*Chandra et al.,* 1979, *Krishna Moorthy et al.,* 1979; *Rastogi and Aarons,* 1980, *Dabas et al.,* 1998; *Rama Rao et al, 2005*]. The L-band scintillation measurements using GPS are also used to study the morphology and variability of ionospheric scintillations [For example, *Groves et al., 1997*; *Beach and Kintner,* 1999; *Valladares et al.,* 2004; *Rama Rao et al.,* 2006a,b].

The general morphology of TEC depletions and their association with strong levels of VHF scintillation, over the South American zone, were described by *Das Gupta et al.,* [1983]. Several studies on scintillation phenomena have been carried out with the results that the scintillation mainly occurred during night time, mostly seen during post-sunset and pre-midnight hours, with increased amplitudes

and high occurrence probability during equinoctial months of high solar activity periods and lower amplitudes and minimum occurrence probability during summer months of low solar activity periods [*Das Gupta et al.,* 1981; *Somayajulu et al.,* 1984; *Rama Rao et al.,* 1985].

Kelley et al., [1996] observed the onset of disruptions (in GPS TEC measurements) due to severe irregularity progress from east to west following the terminator. Existence of strong backscatter from regions of low electron density (as seen by TEC depletions) is very important to understand what happens when GPS signals propagate through such a structure. The upwelling turbulent structures lead to severe disruptions (cycle slips or severe scintillations) of GPS signals. Numbers of ESF studies using GPS and radar have been reported in literature. For example *Rodgrigues et al.,* [2004] presented ESF observations using GPS and radar at equatorial station in Brazil. *Aggarwal et al.,* [2007] presented the investigation on dynamics of electron density irregularities of different scale sizes using multi technique observations. They have shown that the plasma bubble irregularities are observed first at Trivandrum (station located at the magnetic equator in India), thereafter by GPS receiver and later by VHF radar (both co-located at off equatorial station), this indicates that the observed plasma bubble is drifting eastward. *Sripathi et al.,* [2008] have presented the simultaneous observations of ESF irregularities using radar and GPS over Indian region.

As mentioned earlier, the similar multitechnique campaign using VHF radar, GPS and TEC scintillation monitor and ionosonde have been conducted to investigate the various characteristics of ESF during equinox season of the years 2005 to 2008 in India. The following sections represent the obtained results and details discussion on it.

4.3 Experimental Setup

Mesosphere-Stratosphere-Troposphere (MST) radar at Gadanki in the ionospheric mode and GPS –TEC and scintillation monitor are operated simultaneously for 4 equinoctial periods during September - 2005 to February - 2008.

The MST radar operated at 53 MHz in ionospheric coherent back scatter mode is used to capture the features of ESF irregularities, if any. As discussed earlier in chapter 2, the nominal beam zenith angle chosen for F regoin experiments is 14.8^0. This beam is perpendicular at 350 km altitudes in the ionosphere. Data recorded from all the satellites visible in view during nighttime with elevation angle higher than 30^0 have been used for the present work. The scintillation index S4 is calculated at every 1 min for all satellites being tracked. Figure 4.3 shows the experimental sites with position of ionosonde, MST radar and GPS receiver in terms of geographical latitudes and longitudes. The red dot in the figure shows the oriented radar beam position. The big black circle shows the coverage by GPS satellite above 30^0 elevations. In addition to the GPS and VHF radar measurements, height of the bottom-side of F-region, h'F and vertical plasma drift are obtained from digital ionosonde, (KEL IPS 42) operated from Trivandrum. The temporal resolution of the ionograms obtained for the present experiments is 15 minutes.

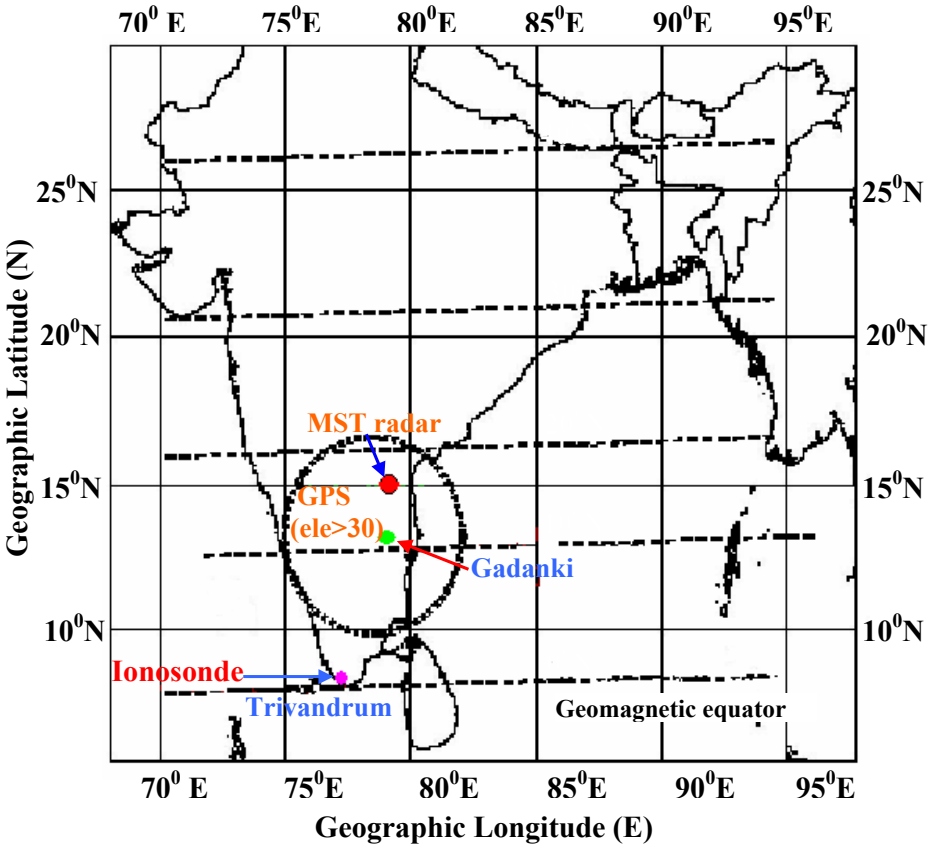

Figure 4.3: Experimental sites showing position of Ionosonde, MST radar and GPS receiver

4.4 A case study to understand an evolution and dynamics of ESF

4.4.1 Observations from the magnetic equator (Trivandrum)

On 21/3/2007, ionosonde observations at Trivandrum revealed that spread F started at 1945 IST, initially as range type spread F and lasted till 2045 IST. Then it became complete spread F from 2100 IST to midnight. From 0030 IST to 0145 IST only range type spread F was observed. From 0200 IST to ~0400 IST frequency spread F was observed.

The height of the base of the F layer (h'F) over Trivandrum during post-sunset period obtained from digisonde data with 15 minute resolution on 21/03/07 is shown in Figure 4.4 (a). The h'F shows a clear evening rise and reached pre reversal peak value of ~300 km at 1930-1945 IST, coinciding with the starting of spread-F on ionogram. The vertical drift velocity (Vz) turns out to be 21 m/s at 1900 IST just before the initiation of ESF as can be seen in the Figure 4.4(b). The vertical drift is computed using dh'F/dt for 15 minutes period. *Basu et al.,* [1996] reported that during solar minimum if drift velocity exceeds 20 m/s then the probabilities of spread-F occurrence are more. Thus, in the present case the observed Vz value of 21 m/s at 1900 IST is sufficient to assist the irregularity generation. The upward and downward movement of h'F can be correlated with the eastward and westward electric field i.e. upward and downward vertical drift velocity respectively in Figure 4.4(a) and (b).

4.4.2 Observations from the low latitude (Gadanki)

The VHF radar at Gadanki can be steered in the N-S directions in order to point the radar 3^0 beam perpendicular to the geomagnetic field at F region heights. The radar beam then intersects the F region (~350 km) over 14.8^0 N and 79.2^0 E (geographic) as shown by the blur circle in Figure 4.5 thus giving an opportunity to probe off magnetic equatorial F region plasma irregularities at ~3 m scale size. Figure 4.5 shows the radar beam position at F region along with the azimuth – elevation path of three satellites (PRN 20, 23, 25) on 21/03/07 over Gadanki.

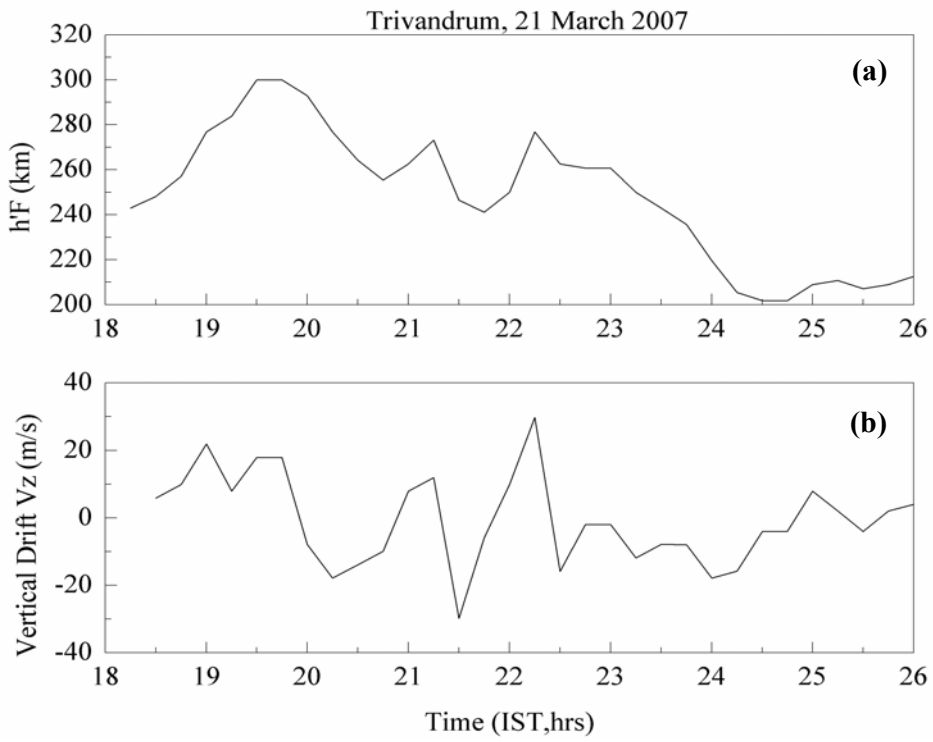

Figure 4.4: Variations of (a) ionospheric F-region height (h'F) in top panel and (b) vertical drift velocity in the bottom panel between 1800 and 2600 IST on 21/03/07 over Trivandrum

The blue dots in each path indicate the epoch when the satellite detects the scintillation (S4) greater than 0.1.

The radar RTI map on 21/3/2007 is shown Figure 4.6 (a). The radar has started to detect the irregularity structures from ~1945 IST onwards i.e. almost simultaneously with Trivandurm ionosonde. According to *Patra* [1997], ESF irregularities appear simultaneously at equatorial station Trivandrum and low latitude station Gadanki. The observed variations on 21/03/07 agree with this.

Figure 4.6 (b) shows the variations of Doppler velocity with height and time and Figure 4.6 (c) shows the variations of spectral width with height and time. The RTI map shows sudden vertically growing plume structures from about 2000 IST. Radar plumes are interpreted as ionospheric bubbles that originate at the base of the F region and may extend over several hundred kilometers in altitude. The striated or elongated blob like multiple plumes are observed in eight different patches (Figure 4.6 (a)). The plumes are extended from about 250 km to 425 km in heights in the beginning. As time progresses, both the bottom and top heights of the plumes are descended by about 50 km by ~ 2245 IST.

A noteworthy feature is that the radar plumes are almost vertical, without any significant tilt, which implies the absence of vertical electric field in the frame of the neutrals that result from a differential motion in the zonal direction between ions and neutrals. The average periodicity of the striations is about 20 minutes.

The periodicity of the upwelling regions (radar bloblike structures of period ~20 min as seen in this case) suggests a wavelike seed process. Such sinusoidal structures organize the plumes in the rest of the radar map. It is interesting to note that a much longer wave length (~700km) modulates the bottomside i.e. h'F and possibly the top of the plumes.

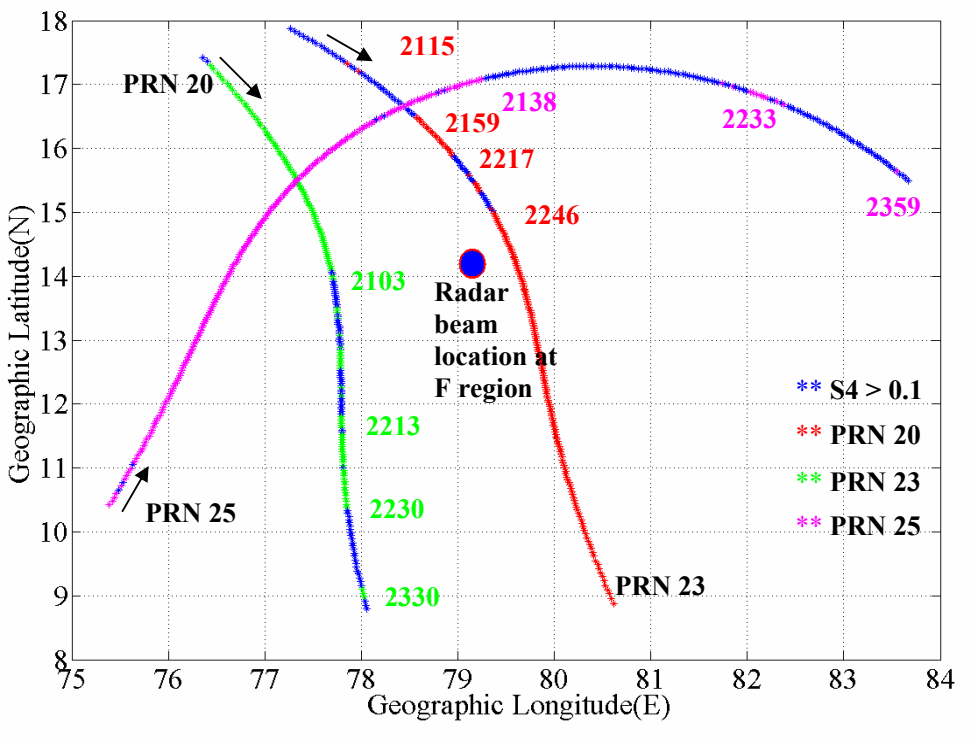

Figure 4.5: Radar beam position at F region along with the azimuth – elevation path of three satellites (PRN 20, 23, 25) on 21/03/07.

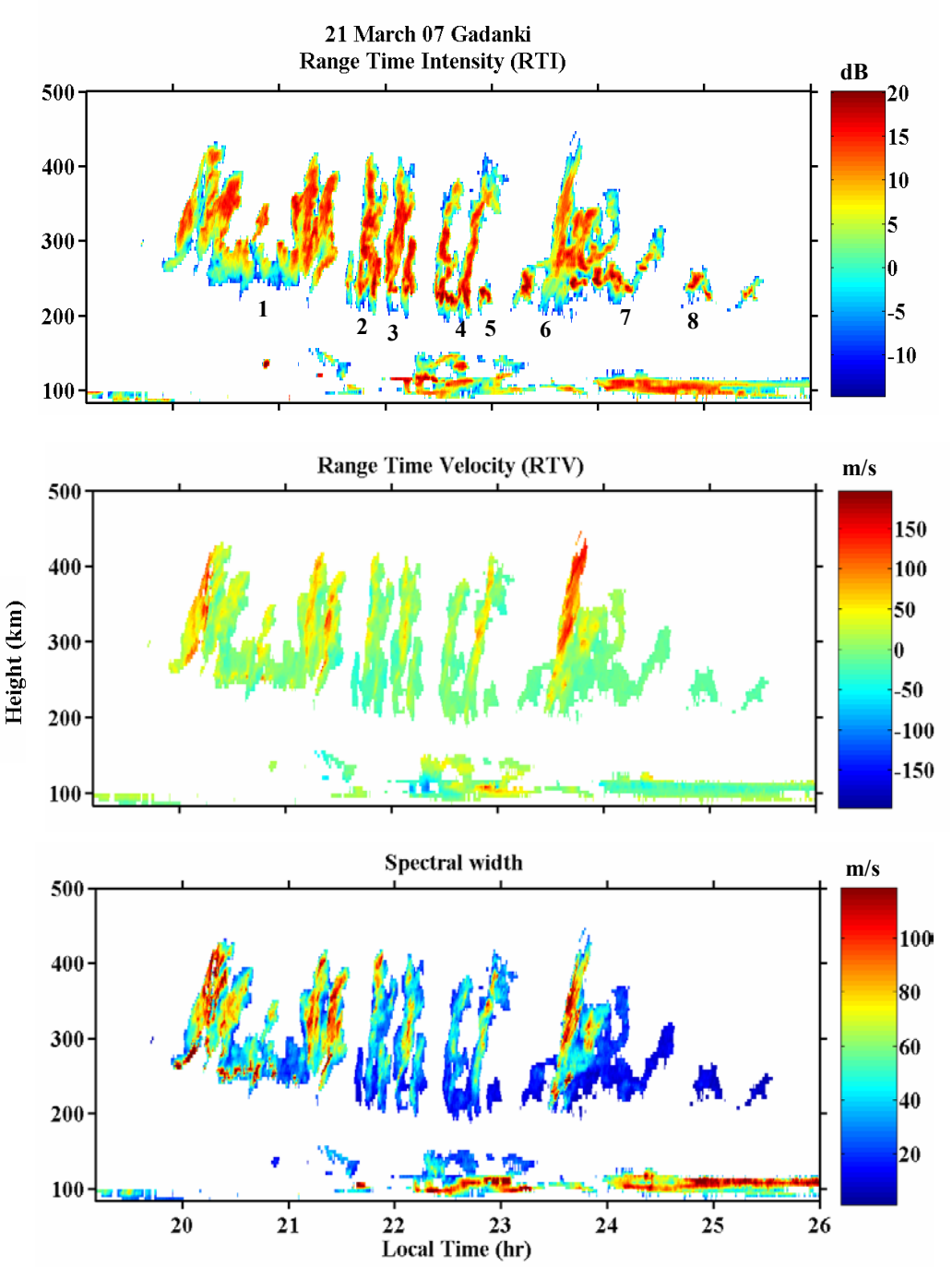

Figure 4.6: (a) Range Time Intensity (RTI) map showing periodic multiple plumes (b) Doppler velocity variations with height and time during the event and (c) Spectral width variations with height and time during the event on 21/03/07, over Gadanki

The multiple plumes seen may be a consequence of the intermodulation of this long wavelength with the shorter wavelengths as also reported by *Kelley et al.,* [1981], *Tsunoda and White,* [1981]. The non linear instability study by *Huang et al.,* [1993] and *Huang and Kelley* [1996] show that periodic seeding of the ionospheric boundary is required for multiple large scale structures to evolve as a result of R-T instability. What we see in the radar maps is the drifting of periodic upwellings across the field of view, essentially unchanged in form –frozen drift effect.

It can be seen from RTI map in Figure 4.6 (a) that when the explosive F region echo development takes place at about 1955 IST, the E region echo disappears and remains absent or weak till about 2130 IST. Weakening of E region field aligned irregularities in association with the F region plume structures have been observed earlier by *Hysell et al.,* [1994] and *Rao et al.,* [1997]. Recently, using Gadanki MST radar observations, *Patra et al.,* [2004] reported that the E region echoes weaken or disappear during the growth phase of the topside F region irregularities at the equator. Using HF and VHF radar observations from equatorial stations, *Patra et al.,* [2005] reported that in the initial phase of plasma bubbles the spectral width is found to be high. The high spectral width values in Figure 4.6 (c) in the intial part of the irregularities between 2000 IST and 2130 IST indicates that these plumes are in development phase. The corresponding high Doppler velocity values also suggest the development phase of irregularities.

As mentioned earlier, here it is observed that the growth of ESF irregularities happens simultaneously along the same magnetic flux tube i.e. simultaneously at low latitude station Gadanki and at the equator. Under these conditions, the mapping of electric field from equatorial valley region to E region over Gadanki may be responsible for the weakening of E region irregularities during the growth phase of ESF at the equator. This agrees with Patra et al., [2004]. They have shown that the weakening or disappearance of E region signals are not directly coupled with the F region irregularities overhead, but linked with the instability processes over the magnetic equator through the magnetic field lines.

The weakening of E region echoes in the later part as can be seen from Figure 4.6 (a), between 2140 IST and 2210 IST and between 2320 IST and 2350 IST, is also correlated with the high Doppler velocities and high spectral width in Figure 4.6(b) and (c) respectively. Though the weakening of E-region is not much clear between 2320 IST and 2350 IST. It can be observed that the correlation between ESF irregularity velocities and E-region echo strength is clearer in the earlier phase than in the later phase. This suggests the local time dependence of the Doppler velocities and also the E region echo strength.These results also agree with the *Patra et al.,* [2004].

GPS receiver to measure TEC and scintillation at L1-frequency (1.575GHz) is simultaneously operated from Gadanki on the day. Figure 4.7 shows the temporal variations of TEC and S4 index observed by three satellites, (a) PRN 20, (b) PRN 23 (c) and PRN 25 on 21/03/07. The latitude and longitude converge of these satellites are also shown in the respective figures. Their ground tracks are shown in Figure 4.5 indicating the IPP being probed by the GPS technique.

PRN 20 shows seven clear depletions in TEC of magnitude ~5-6 TECU between 2100 and 2245 IST. The simultaneous S4 enhancements are also observed. From longitude coverage of PRN 20, it can be seen that PRN 20 is moving in a nearly constant longitudinal path during its passage over Gadanki. The depletions can be associated with the seven clear radar echo structures (patches 2, 3, 4 and 5 in Figure 4.6(a)) between 2130 and 2300 IST. PRN 23 (Figure 4.7 (b)) shows two depletions, though not as deep as in PRN 20, between 2200 and 2300 IST, again associated with strong S4 enhancements. These depletions can be associated with the patches 3 and 4 in Figure 4.6(a).

The first two depletions shown by PRN 23 from ~2115 IST to 2159 IST at the beginning of path in Figure 4.7(b) are at considerably low elevation angles (~30-45, figure not shown here). Thus might be affected through the multipath effect so not taken into consideration.

PRN 25 (Figure 4.7 (c)) also shows multiple depletions and associated S4 enhancments between 2130 IST and 2235 IST at east of Gadanki as can also be seen from its ground tracks in Figure 4.5. From the lat-long information, it appears that PRN 25 is detecting irregularities at quite higher latitudes. It can be seen that at higher latitudes the amplitude of observed L-band scintillation and TEC depletion is more. PRN 20 which is west of radar has detected the irregularities from 2100 IST onwards, almost simultaneously with radar. PRN 25 is observing from 2130 IST but at higher latitudes and east of Gadanki. This infers that the ESF irregularities are drifting east ward and also increasing in zonal dimensions.

PRN 20 and radar are simultaneously observing the plume structures 2 to 5 (Figure 4.6(a)) between 2100 and 2245 IST. PRN 23 and radar are observing the plume structure 3 and 4 between 2224 and 2246 IST simultaneously. PRN 23 has not detected any irregularities after this, though there is an exact path of PRN 23 over the Gadanki at this time. This suggests that the Fresnel scale size irregularities have been decayed and radar is detecting the 3 m scale irregularities generated at the walls of the Fresnel size irregularities through the secondary mechanism.

Plume structures 1, 6, 7, and 8 in Figure 4.6(a) have not been detected by any of the PRNs. As we have discussed earlier, structures 1 and 6 are in initial phase, thus they might not have developed up to Fresnel scale size that can create the L-band scintillation. The post mid night plume structures 7 and 8 can be considered as dead bubbles, it requires further investigation.

Thus, the different scale sizes of ESF irregulariits manifest themselves on different instruments i.e. ionosonde, radar and GPS. Spectral width and Doppler velocity informations reveal the different phases of irregularities i.e. development phase etc. Still, the growth and decay rate of irregularity pattern that can produce the GHz are needed to find out.

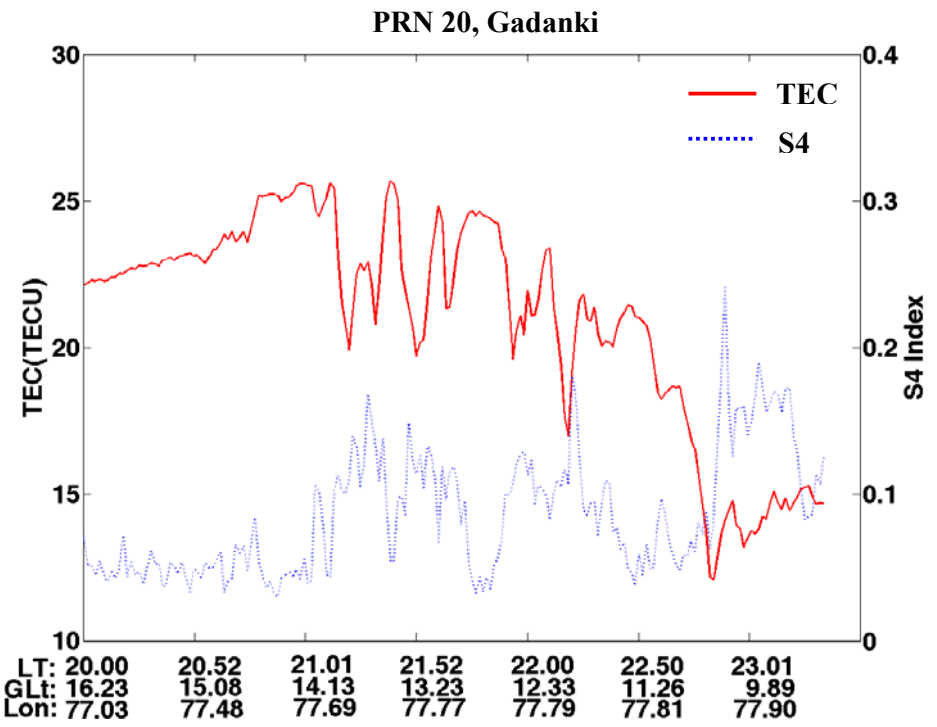

Figure 4.7(a): L-band scintillation and associated TEC depletion as observed by PRN 20 over Gadanki

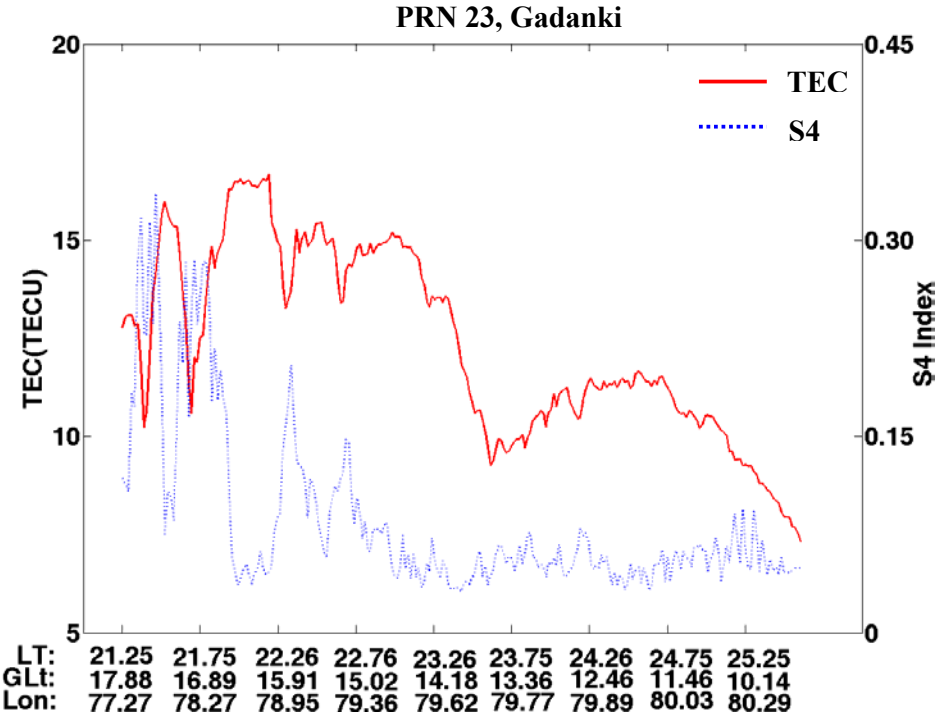

Figure 4.7(b): L-band scintillation and associated TEC depletion as observed by PRN 23 over Gadanki

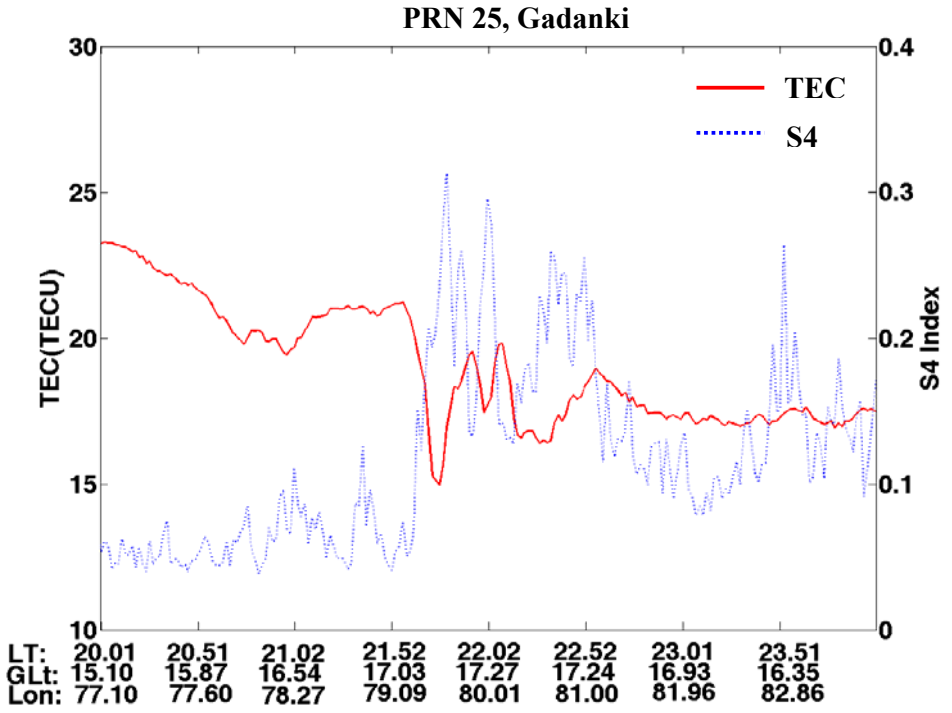

Figure 4.7(c): L-band scintillation and associated TEC depletion as observed by PRN 25 over Gadanki

4.5 TEC enhancement during multiple ESF plume structures

In situ plasma depletions and associated ESF irregularity structures have been studied over the years [e.g. *Hanson and Sanatani,* 1973; *McClure et al.,* 1977; *Tsunoda et al.,* 1982; *Kelley,* 1989; *Kil and Heelis,* 1998]. The observations of localized regions of plasma density enhancements, in addition to plasma depletions, in the night time low latitude F region were reported for the first time by *Oya et al.,* [1986] and *Watanabe and Oya* [1986] using Hinotori satellite measurements. This was substantiated by other satellite measurements [e.g. *Le et al.,* 2003; *Park et al.,* 2003]. These measurements [*Oya et al.,* 1986; *Watanabe and Oya,* 1986] revealed that the density enhancements have similar longitudinal dimensions as plasma depletions and that the enhancements are about a factor of two higher than the background plasma density. The occurrences of these enhancement structures were generally found to maximize at $\pm 20^0$ magnetic latitude. However, the exact mechanism that would give rise to plasma enhancements was not known. *Sekar et al.,* [2001] had shown through numerical simulation of ESF that plasma enhancement can be generated by the interacting electric fields generated by the growth of the R-Taylor instability initiated by large and small scale size perturbations. Subsequently, the presence of plasma enhancements was inferred [*Pimenta et al.,* 2004] using ground based 630.0 nm airglow imager and ionosonde in the anomaly crest region over Brazilian sector. However, *Sekar et al.,* [2004] had shown the evidence for the plasma enhancements associated with ESF extending from base of F- region to beyond 350 km altitude using co-ordinated VHF radar and airglow measurements from Gadanki in India. This evidence was substantiated with subsequent observations using the same techniques [*Sekar et. al.,* 2008].

These plasma depletion and enhancement structures associated with ESF are expected to leave their signatures in TEC measurements. *Tsunoda and Towle* [1979] reported TEC depletions associated with ESF from the dip equatorial region for the first time. Using GPS satellite measurements, a number of investigations [e.g. *Basu and Kelley,* 1979; *Aarons et al.,* 1996; *Kelley et al.,* 1996; *Beach and Kintner,* 1999; *Bhattacharyya et al.,* 2000; *Valladares et al.,*

2004] were carried out to understand TEC depletions and associated scintillations over the low latitude region in the American sector. *Chen et al.,* [2008] presented the night time TEC enhancement near the EIA crest region in China. *Dashora and Pandey* [2005] brought out an evidence for the TEC enhancement during night-time near the EIA crest region. They, however, did not observe any significant scintillation associated with it.

In the present study, a case of TEC enhancement over Gadanki in the Indian zone during an ESF event is reported based on the observations using a number of techniques like TEC measurements (GPS), VHF radar and ionosonde. The observations from PRN 20 on 21/03/07 are reproduced in Figure 4.8. The two subplots at the top reveal the elevation from the GPS observational site and the latitudinal/longitudinal coverage of the satellite. The ray path from the IPP of the PRN20 satellite to the receiver is within 4.1^0N geomagnetic latitude and 77.7^0E geographic longitude (Figure 4.8b) that is 2^0 west of Gadanki, the radar site.

As mentioned in previous section, a few depletions of magnitude ~5 - 6 TECU from 2100 IST to 2245 IST are observed. It can be seen fron Figure 4.8 (c) that after 2142 IST, TEC recovers to the background level (TEC before 2100 IST) close to 25 TECU and subsequently decreases to 20 TECU at 2154 IST Thereafter, a gradual enhancement of VTEC reaching a maximum of 24 TECU at 2206 IST is noticed. In the present section, this enhancement event is focused. The lowermost subplot (d) depicts the variation in the S4 index, the change in the S4 index during enhancement event (2154 IST - 2206 IST boxed region) is not substantial.

The top two panels of Figure 4.9 depict the RTI and RTV maps of ESF irregularities during 2200 – 2300 IST on 21/03/07. It is to be noted that the TEC variations shown in Figure 4.9(c) is time shifted by 30 min in order to take care of the travel time for the plasma structure from the longitude of TEC measurement (77.7^0E) to the longitude (79.2^0E) of the coordinated VHF radar. The time-shift is estimated based on the eastward plasma drift of ~80 m/s as deduced from the bi-directional 777.4 nm airglow measurements (zenith and 45^0 elevation towards west in this campaign).

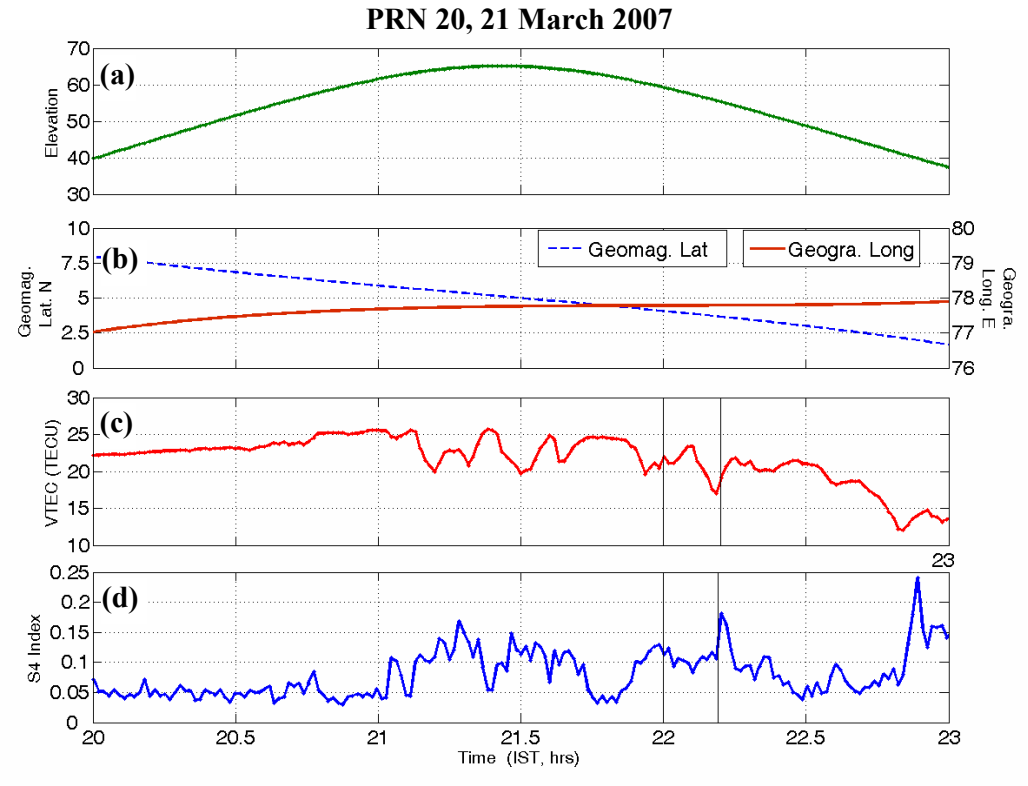

Figure 4.8: The temporal variations of (a) elevation of PRN 20 from the observational site (b) geomagnetic latitude, geographic longitude coverage of it (c) TEC and (d) S4 index as observed by PRN 20

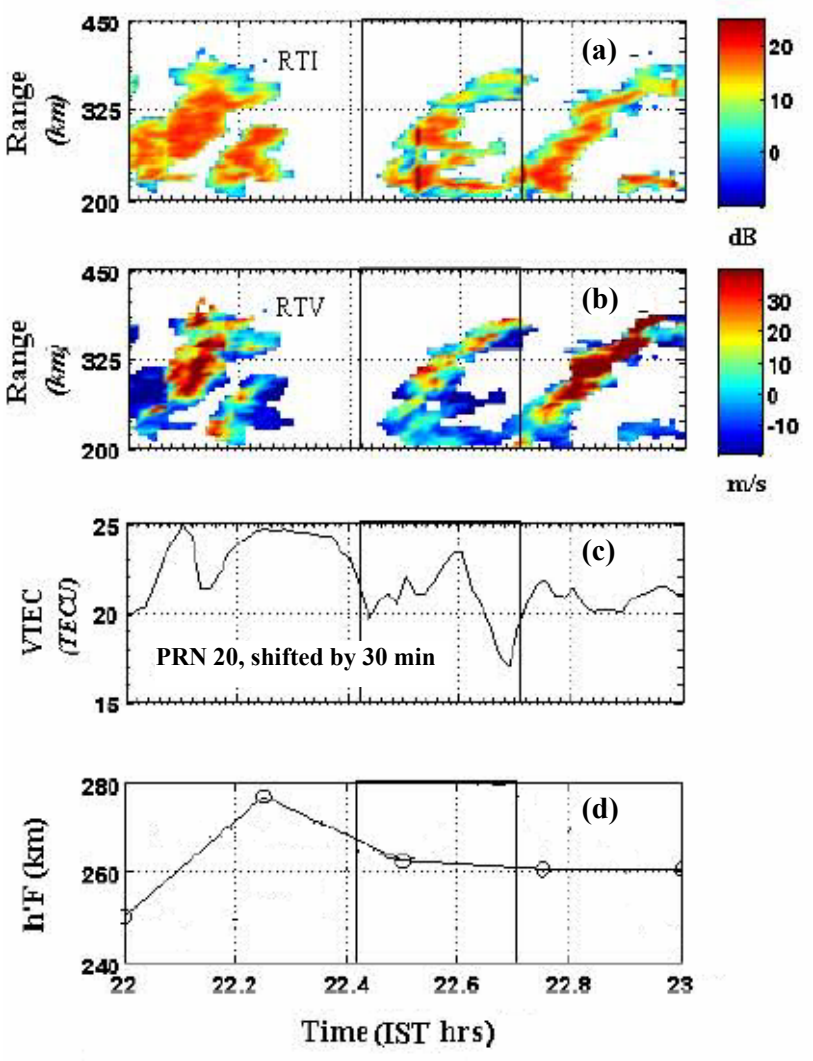

Figure 4.9: (a) RTI map (b) RTV map between 22-23 IST on 21/03/07. The temporal variations of (c) TEC observed by PRN 20 (d) h'F variations over Trivandrum between 22-23 IST on 21/03/07

The 777.4 nm airglow observations are taken using multi-wavelength photometer from the same place on the day by Physical Research Laboratory, Ahmedabad group. A multi-wavelength scanning photometer, with a narrow spectral band capability and a narrow field-of-view, was developed at Physical Research Laboratory to study the nighttime airglow emission intensities from the thermosphere. The details of this photometer can be found in *Sekar et al.,* [2004, 2008].

As mentioned earlier, the plasma enhancements were observed from the regions closer to magnetic equator [*Sekar et al.,* 2004; 2008] and low latitude stations [e.g. *Oya et al.,* 1986]. On the other hand, enhancements in TEC were observed [*Dashora and Pandey,* 2005] closer to the EIA crest region. Further, the origin of that TEC enhancement was believed, not to be associated with ESF as the S4 scintillation index was weak. In contrast to these measurements, the present study provides an evidence for TEC enhancement nearer to the dip equatorial region. Further, the origin of TEC enhancement was shown to be associated with ESF.

In order to understand the enhancement in TEC reported in the present study, VHF radar maps of the corresponding ESF structures are examined. It is rather well known that the echo strength of VHF radar in coherent mode is proportional to square of the electron density fluctuations. Therefore, unequivocal identification of depleted or enhanced plasma regions is not possible using the radar technique alone. The velocity maps obtained from the radar can indicate the nature of the plasma structure as the depleted structures move upward and the enhanced structure move downward. However, the "fossil bubbles" which turn active are also shown [*Sekar et al.,* 2007] to move downward. Thus the VHF radar technique is not sufficient to identify the nature of plasma structure. Combining with TEC observations, the plasma enhancement structure can be identified, as any localized plasma variations in the night time ionosphere should get reflected in TEC.

The observations of VHF radar reveals structures at 200-250 km altitude region that are predominantly moving downward as seen from the RTV maps in

Figure 4.9(b) at around 22.64 IST. It is of interest to note that there are upward and downward velocity variations inside the structure in the boxed region that have correspondence with the modulations in TEC values. The structures in the boxed region corresponding to the plasma enhancements are not stronger and thus the S4 index is weak. The h'F variation in boxed region in Figure 4.9(d) suggests that the height of the equatorial F region is relatively stable ~ 260 km during this time. Finally, in spite of the difficulty in measurement of TEC in vertical direction in the presence of plasma structures, the present set of measurements reveals that the enhancement seen in TEC over equatorial region corresponds to plasma enhancement associated with ESF.

4.6 A case study to understand the latitudinal extent of L-band scintillation

L-band scintillations are mainly due to scattering from Fresnel scale irregularities and it maximizes in amplitude as well as in occurrence around the EIA crests whereas the VHF scintillations are most intense at equatorial regions. The field aligned ESF irregularities are mapped to higher latitudes along with the non-linear evolution of the irregularities in to topside ionosphere [e.g. Whalen, 2002]. Using GPS and radar observations recently, Sripathi et al. [2008] have shown that when irregularities reach to higher altitudes as observed by the Gadanki Indian MST radar during pre mid-night periods, strong L-band scintillations are present at higher latitudes. In contrast to this, when the radar echoes are observed at lower altitudes, weak L-band scintillations are present with small latitudinal extent.

To derive the latitudinal extent of L-band scintillations we have used observations of GAGAN GPS receivers. The details of GAGAN stations can be found in Appendix- I (Table I.1). Figure 4.10 (a) shows the virtual height of the base of the F layer (h'F) over Trivandrum during post-sunset period obtained from digisonde data with 15 minute resolution on 15 September 2005. The h'F starts rising around 1915 IST and goes high up to ~320 km around 2015 IST, indicating that the plasma is drifting upwards and the ambient horizontal electric field is eastward. Thereafter the base started drifting downwards (indicating a reversal of

the ambient electric field) and by 2130 IST the h'F came down to ~260 km. As observed by the ionosonde, the spread F appeared at about 1915 IST at Trivandrum and became strong by 2015 IST. The vertical drift is computed using dh'F/dt for 15 minutes period. Figure 4.10(b) shows that vertical drift is upward and is high, ~25 m/s ~1930 IST at Trivandrum and then becomes downward ~2100 IST indicating a strong eastward electric field around 1930 IST and then electric field becomes westward and the downward drift is also high (~40 m/s). The larger upward EXB drift velocity, late reversal time, and smaller early night downward drift velocity can provide favorable conditions for the generation of spread F [*Fejer et al.,* 1999].

Figure 4.11 shows the RTI map of an ESF event observed on 15 September 2005 over Gadanki. A low altitude thin layer of 3 m irregularities developing from ~220 km at 2145 IST is exploded into a high altitude plume. A steady, vertical, fully grown, strong irregularity region is observed between 250-420 km at ~2200-2240 IST for 40 minutes duration and later confining into a thin layer of about 130 km thickness.

Figure 4.12 (a) shows the spectral width characteristics and (b) shows the Doppler velocity variations with height and time on 15 September 2005. The observed spectral width for the first patch is little high (~40 m/s) between 330 and 350 km in the initial stage with gradual decrease with height and time both. Plasma inside the first patch is descending with the velocity of ~10 m/s in the initial stage as seen in Figure 4.12 (b). The second patch is observed at the lower altitudes up to post midnight with descending velocity. Spectral width and Doppler velocity information says that the bubbles are not freshly generated but drifted in from west.

The day was magnetically active day and characterized by substorm followed by the storm of 11 September 2005 which had prolonged recovery phase. Thus, the generation of ESF on 15 September 2005 may due to storm time prompt penetration electric field during this prolong recovery phase. The prompt penetration phenomenon will be discussed in detail in Chapter 5.

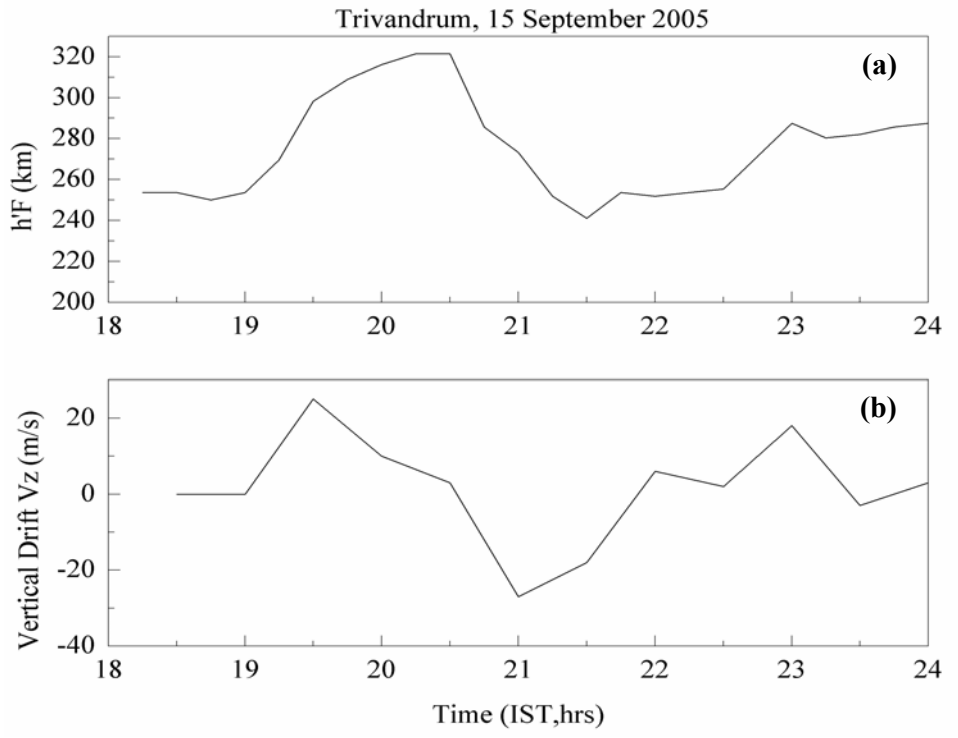

Figure 4.10: Variations of (a) virtual height of the base of the ionospheric F-region (h'F) (b) vertical drift velocity, between 1800 and 2400 IST on 15 September 2005 over Trivandrum

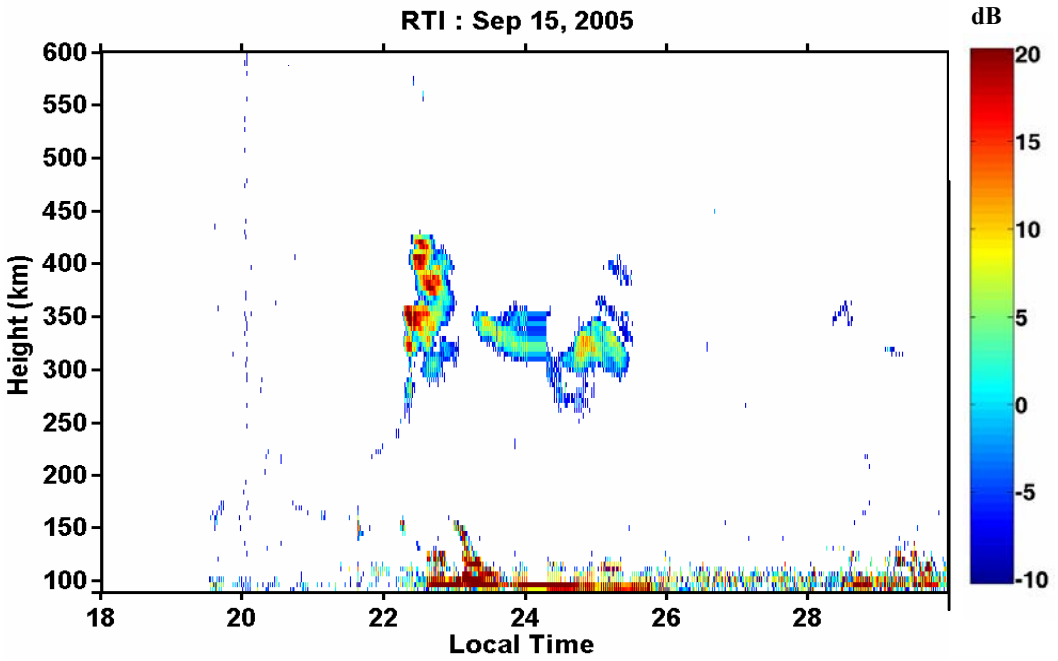

Figure 4.11: RTI map observed on 15 September 2005 over Gadanki

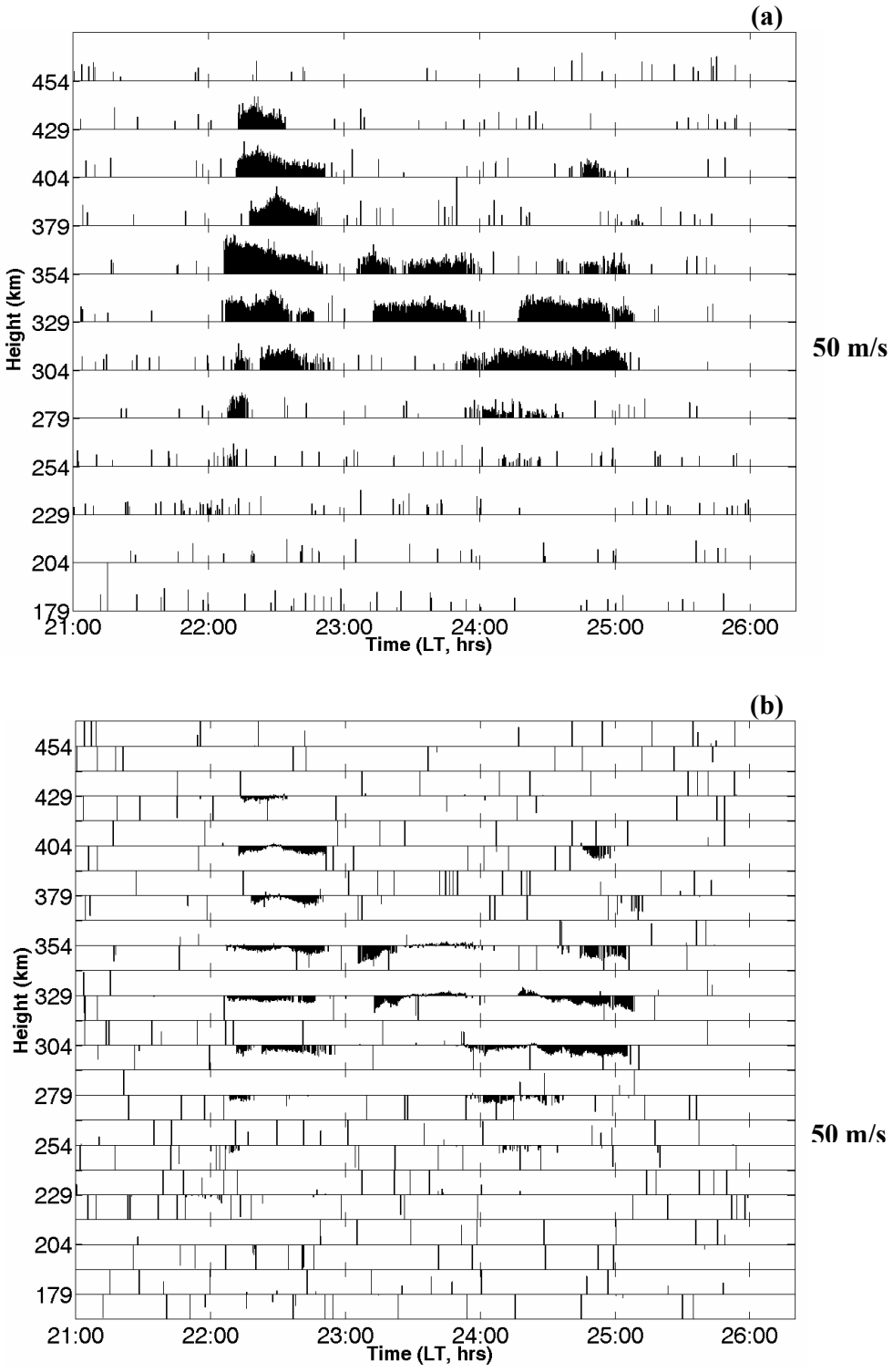

Figure 4.12: Height Time variation of the (a) spectral width and (b) Doppler velocities of the irregularities observed on 15 September 2005

Figure 4.13 (a), (b), (c) and (d) shows observations of PRN 2, 9, 30 and 29 respectively, from GAGAN GPS stations along with the GPS observations from low latitude station Gadanki on 15 September 2005. In Figure 4.13(a), PRN 2 shows the L-band scintillation with S4-index value of ~0.17 at ~2005 IST at Trivandrum. This scintillation is associated with the TEC depletion of ~ 6 TECU. After this, small TEC fluctuations are observed and S4 enhanced to ~0.24 at 2065 IST. At Bangalore, TEC depletion is observed little later at ~2055 IST with value of ~6 TECU and associated L –band scintillation is observed of ~0.24. PRN 2 is not observing any scintillation or TEC depletion beyond Bangalore latitudes.

Figure 4.13(b) shows TEC and S4 variations observed by PRN 9 at Trivandrum, Bangalore, Gadanki and Hyderabad. It can be seen that TEC depletion is observed first at Trivandrum at ~1975 IST and then ~2010 IST and ~2025 IST at Bangalore and Gadanki respectively. The maximum TEC depletion is observed at Bangalore with value of ~ 9 TECU for the first observed structure and associated scintillation is 0.29. But scintillation maximizes at Gadanki with value of ~0.36. This may be due to the fact that Gadanki is surrounded by hilly area and the observed scintillation is at the beginning of the path (elevation ~35), thus may be affected from the multipath effect.

The second structure observed by PRN 9 is of ~7 TECU ~2075 IST at Trivandrum, of ~5 TECU ~2080 IST at Bangalore and of ~10 TECU at ~2080 IST at Gadanki. The observed S4 values are 0.16, 0.21 and 0.37 respectively at Trivandrum, Bangalore and Gadanki. Finally at Hyederabd, TEC depletion of ~ 4 TECU at 2090 IST is observed. This depletion is associated with the S4 value of ~0.17. Beyond this latitude, PRN 9 observations are not showing any scintillation signature e.g. at Delhi. Thus, the plasma bubbles extended up to 17.48^0N (Geographic Lat, 9.48^0N Geomagnetic) i.e. Hyderabad. These observations are pointing towards the fact that scintillation index S4 is consistently increasing from Trivandrum to Gadanki i.e. L-band scintillation maximizes at low latitudes.

Figure 4.13(c), PRN 30 is observing TEC depletion of ~1 TECU at ~2460 IST over Trivandrum, of ~ 1.5 TECU at ~2465 IST over Bangalore and of ~1.5 TECU at ~2475 IST over Gadanki. Here also, the highest scintillation is observed

at low latitude station Gadanki. In Figure 4.13 (d), PRN 29 has observed the depletion and scintillation over Trivandrum only. The L-band scintillation/TEC depletion are found to be absent at other stations, e.g. Gadanki observations are shown in bottom panel of the figure.

Figure 4.14 shows the azimuth-elevation coordinates for GPS satellite PRN 2, PRN 30, PRN 9, and PRN 29 as observed from Gadanki on 15 September 2005. It is obvious that for rest of the stations also the geometry of the satellite will be similar, as all the stations are situated within $\pm 2^0$ longitude difference. It can be said that PRN 2 and PRN 9 are observing pre-midnight L-band scintillation in the east of observing stations while PRN 29 and PRN 30 are observing post-midnight L-band scintillation in east and west of observing stations respectively. The scintillation and TEC depletion are observed to be intensed during pre-midnight hours. During post-midnight hours, the scintillation and TEC depletion are observed to be less intensed.

PRN 29 has detected irregularities only at Trivandrum ~0090 IST. At Gadanki, PRN 29 has not detected any irregularity signatures, but radar is still detecting the irregularities. This says that the irregularity pattern which can create the L-band scintillation might have decayed but 3 m size irregularities are still exist and giving backscatter of radar signals.The irregularities are observed first at Trivandrum (equatorial station) around 1915 IST, then is observed by GPS receiver and then by VHF radar (off-equatorial station) indicating that the observed bubble is drifting eastward.

One more interesting point here is that the general TEC variations as observed by PRN 29 shows decrease from 14 TECU to 8 TECU at Trivandrum. At Gadanki, TEC is observed to be enhanced up to ~0030 IST after an initial decrease. After 0030 IST, a gradual decrease is seen. This may be due to resurge of EIA or due to some wave kind of structures which requires further investigations.

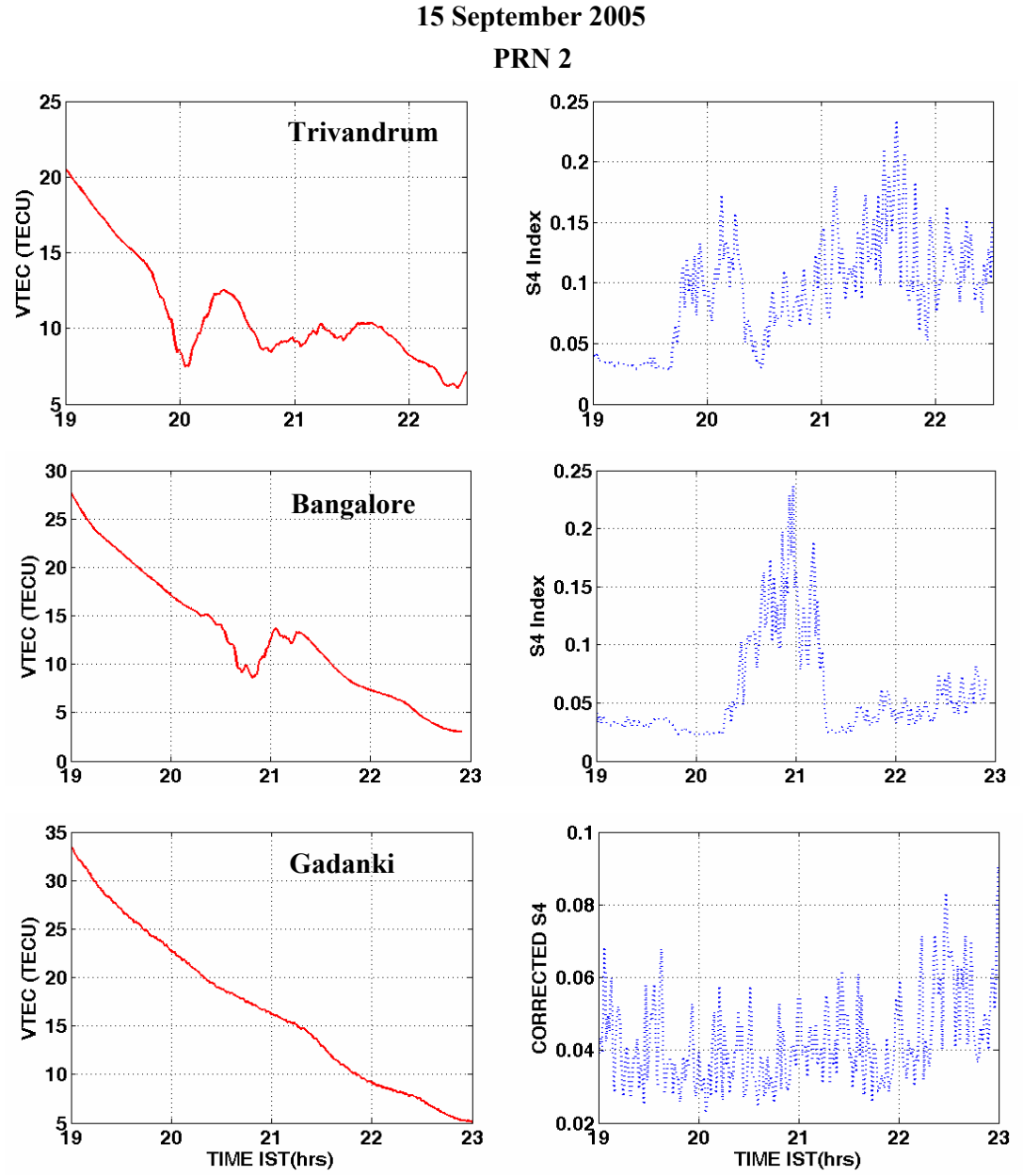

Figure 4.13 (a): L-band scintillation and associated TEC depletion as shown by PRN 2 on 15 September 2010 at Trivandrum, Bangalore and Gadanki

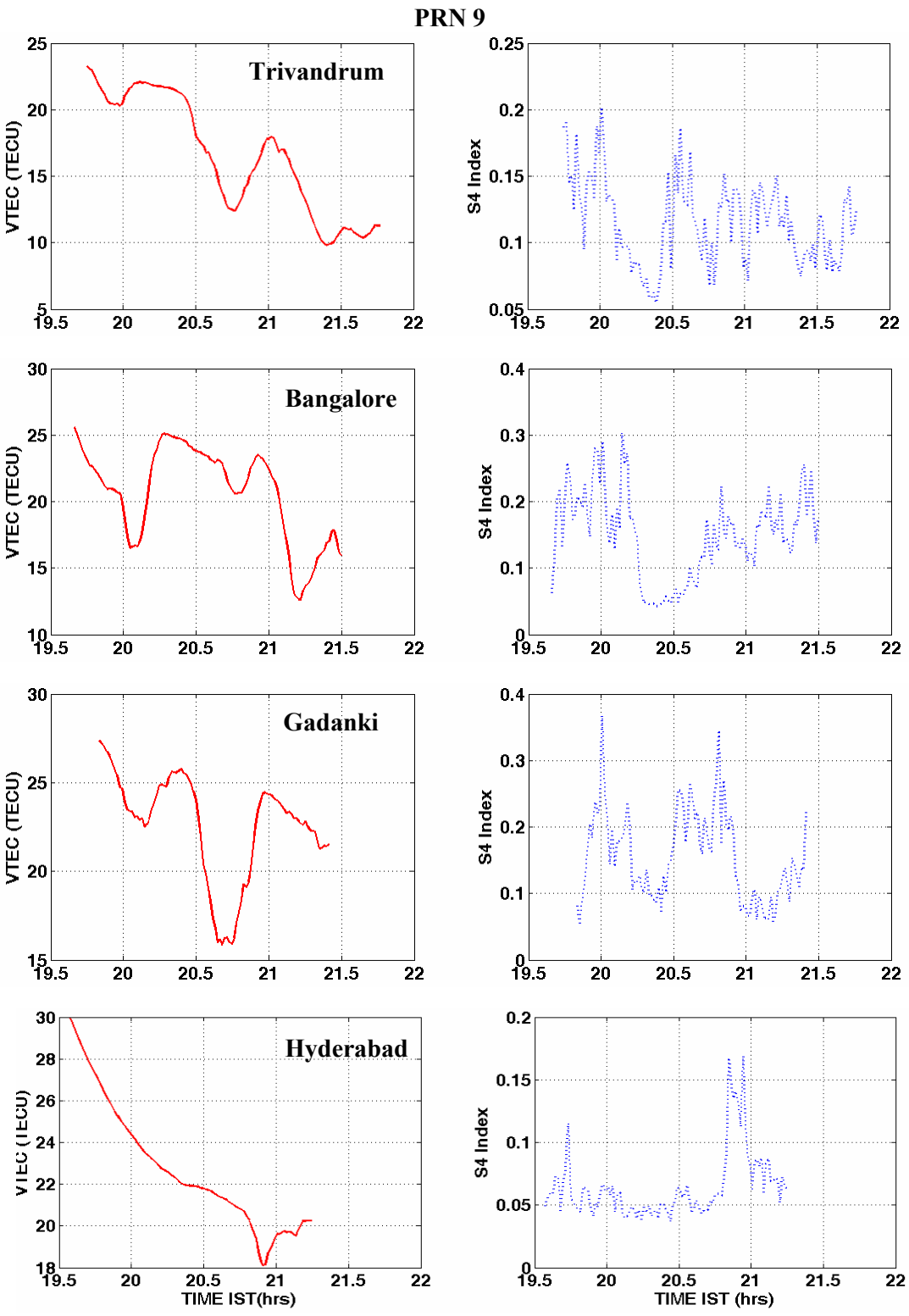

Figure 4.13 (b): L-band scintillation and associated TEC depletion as shown by PRN 9 on 15 September 2010 at Trivandrum, Bangalore, Gadanki and Hyderabad

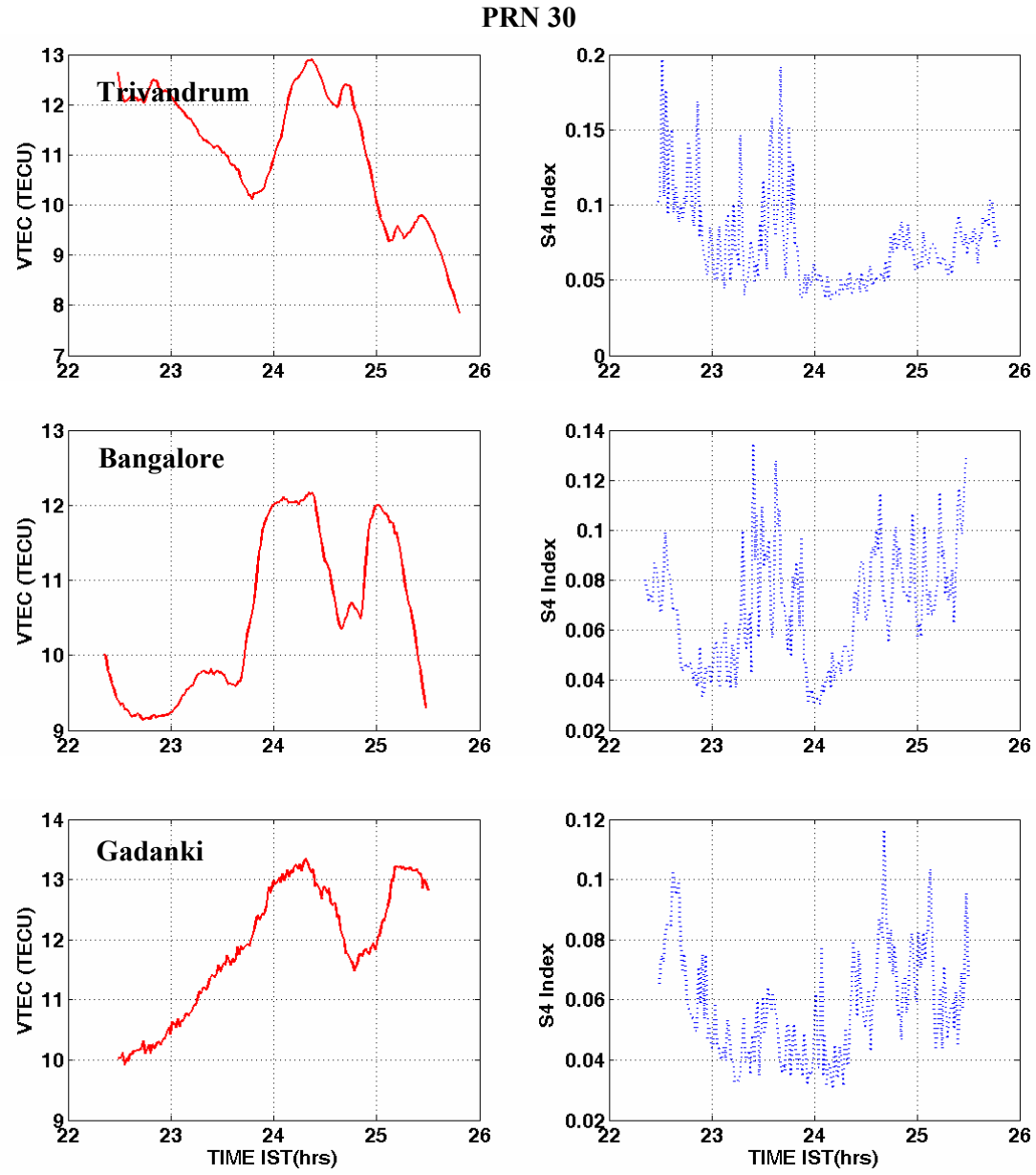

Figure 4.13 (c): L-band scintillation and associated TEC depletion as shown by PRN 30 on 15 September 2010 at Trivandrum, Bangalore and Gadanki

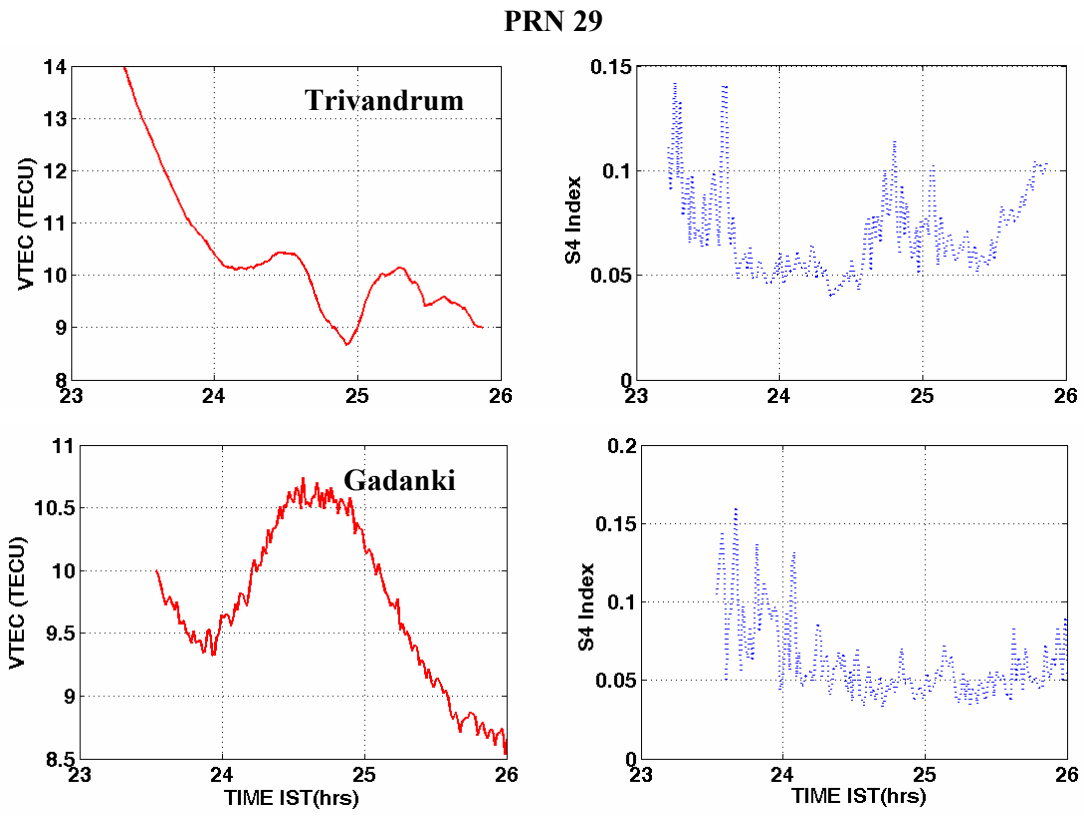

Figure 4.13 (d): L-band scintillation and associated TEC depletion as shown by PRN 29 on 15 September 2010 at Trivandrum and Gadanki

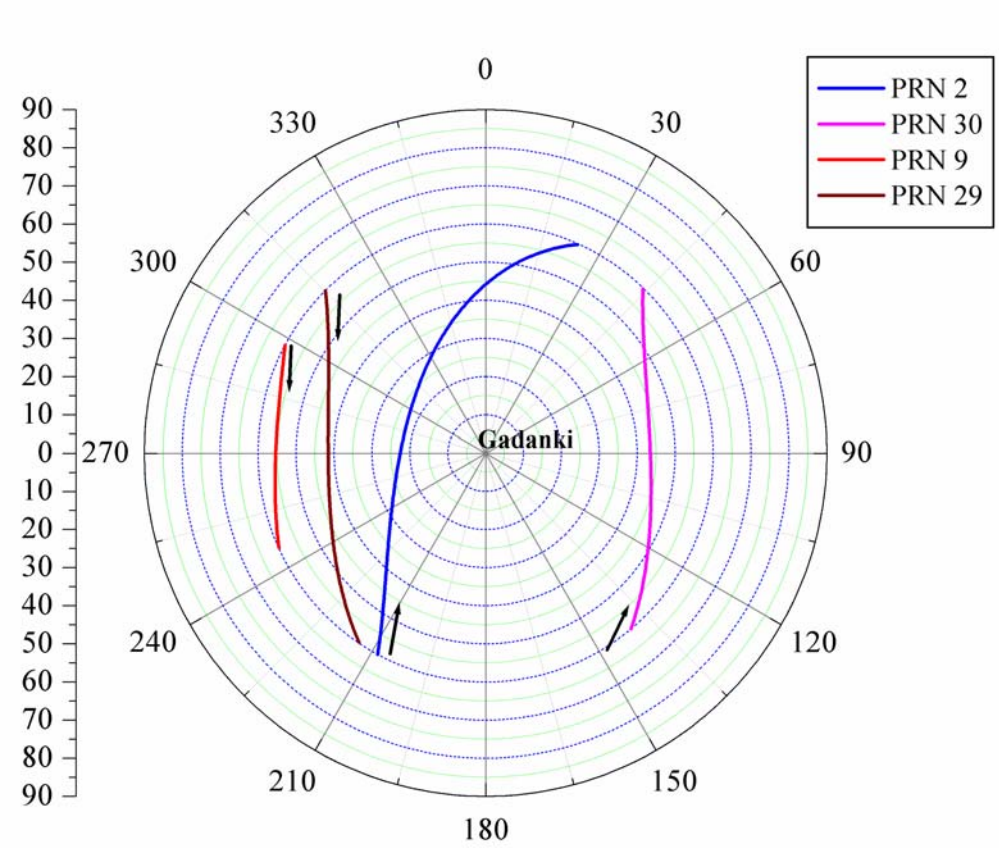

Figure 4.14: Azimuth-elevation coordinates for GPS satellite PRN 2, PRN 30, PRN 9, and PRN 29 as observed from Gadanki on 15 September 2005

4.7 Solar activity dependence of L-band scintillation

The morphology of ESF associated L-band scintillation during solar maximum and solar minimum period was reported by *Basu et al.,* [1988]. They have shown that L-band scintillations are most intense in the low latitude region, moderate at high latitudes and generally absent at mid-latitudes. The occurrence frequency of scintillation is highest during high solar activity period for all latitude regions.

In this section we have tried to study the ESF associated L-band scintillation variations during the descending phase of the solar activity (2005-2008) by using the scintillation data recorded at Gadanki. Figure 4.15(first panel) shows the RTI map observed on 15 September 05. Figure 4.15 (second panel) and Figure 4.15 (third panel) shows the TEC observations and S4 index variations respectively from all the visible satellite in view between 1800 IST and 3000 IST. The elevation mask of 30 degree has been applied to reduce the multipath effect if any. The RTI map on 15 September 2005 is already discussed in the previous section. We can see that only one PRN is showing significant TEC depletion of ~6 TECU accompanied by S4 value of 0.25 at ~20:00 LT and of ~10 TECU accompanied by S4 value of ~0.37 at ~2080 LT.

Figure 4.16(first panel) shows the RTI map on 21 March 2007. The almost vertical periodic multiple plumes creates strong GHz scintillation and associated TEC depletions in multiple PRNs as can be seen in Figure 4.16 (third panel) and 4.16 (second panel) respectively. The plumes recorded by radar between 1900 and 2100 LT are accompanied by disruption of E region irregularities. But the irregularities observed after 2200 LT are accompanied by E region instabilities with descending of plumes towards the E region after mid night. One of the plumes extended to ~450 km of altitude. This event is already discussed in detail in section 4.4 of this chapter. The highest TEC depletion observed on the day is of ~ 8 TECU which accompanied by S4 value of ~0.31.

Figure 4.17(first panel) shows the RTI map observed on 05 February 2008. The ascending westward tilted plume with velocity of ~ 97 m/s is observed between 2000 LT and 2200 LT. The second patch which is connected to the E region in the beginning is raised up to ~ 420 km. This patch is also slightly tilted to the west. The E region irregularities are very weak during most of the time of the event. This ESF event is associated with very weak GHz scintillation as can be seen in Figure 4.17(third panel). There is no significance TEC depletion as can be seen in Figure 4.17 (second panel). The TEC depletion of ~ 1 TECU with S4 value of ~0.15 is observed.

As we have already discussed in chapter 3, that the phase of the solar activity is going down since 2005. The solar flux values presented in Figure 3.5 decreases continuously since 2005. The presented results say that the intensity of GHz scintillation is also decreasing after 2005 showing positive co-relation with solar activity. The magnitude by which the phase of the radio wave signals gets perturbs depends on integrated electron density which in turn controlled by irregularity amplitude and background electron density and its distribution in the ionosphere. It is known from the satellite In situ measurements that though the irregularity amplitude remains almost constant, the background electron density in some regions of the ionosphere experiences a drastic variation with the solar activity variations. This ultimately affects the phase and amplitude scintillation [*Basu et al.,* 1988].

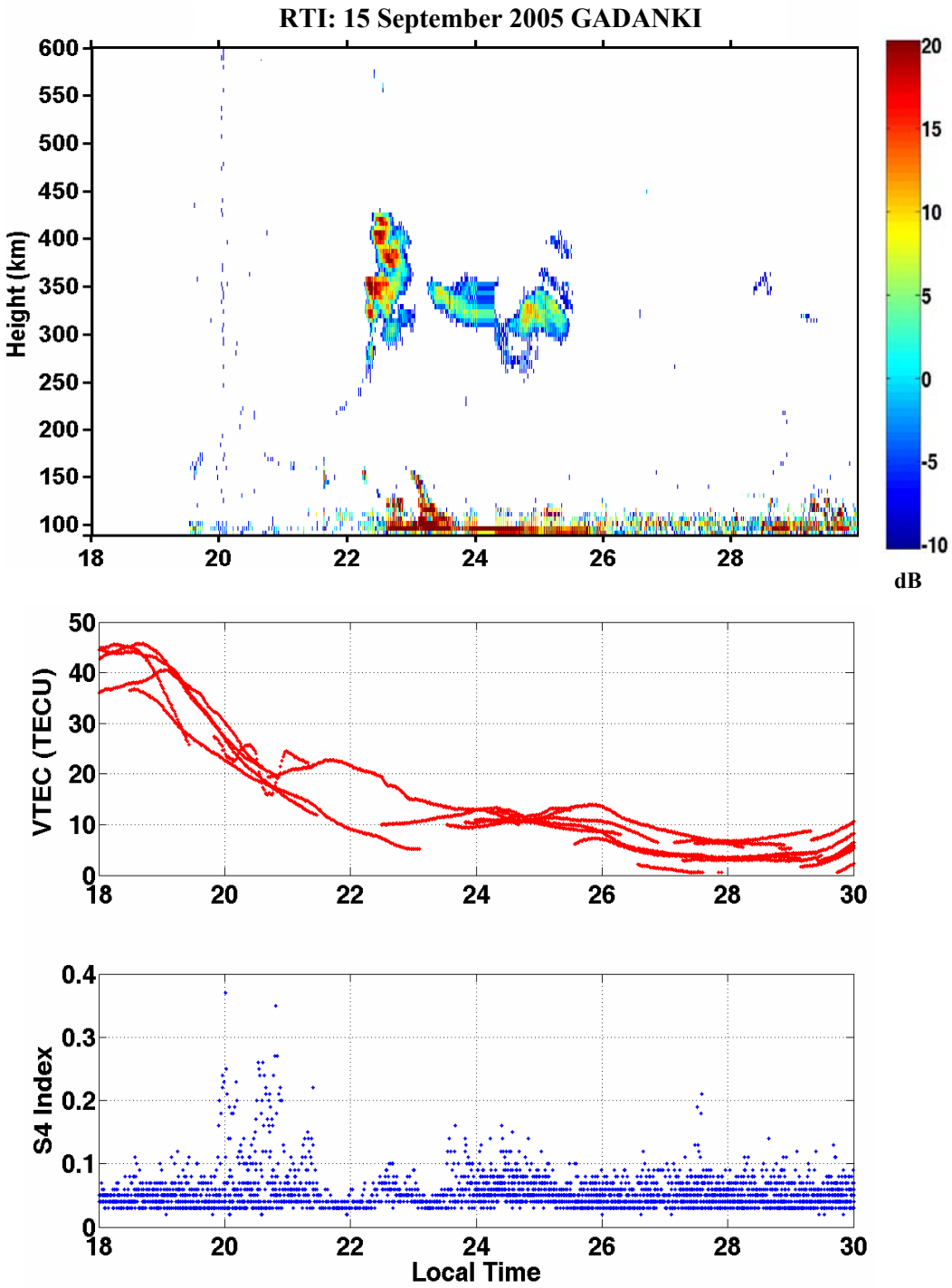

Figure 4.15: RTI map, TEC and S4 observations from all the PRNs in view between 18:00 IST to 30:00 IST on 15 September 2005

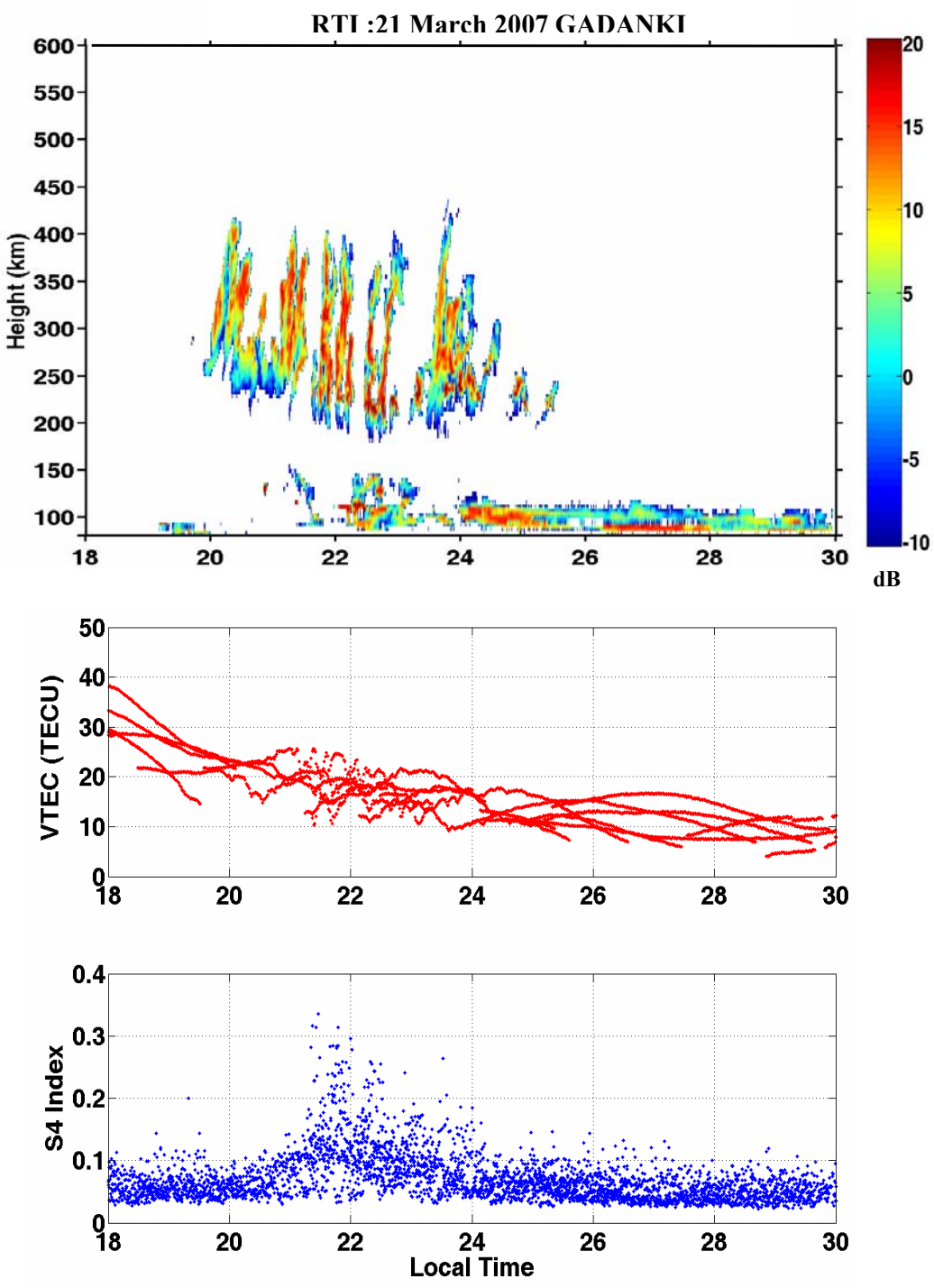

Figure 4.16: RTI map, TEC and S4 observations from all the PRNs in view between 18:00 IST to 30:00 IST on 21 March 2007

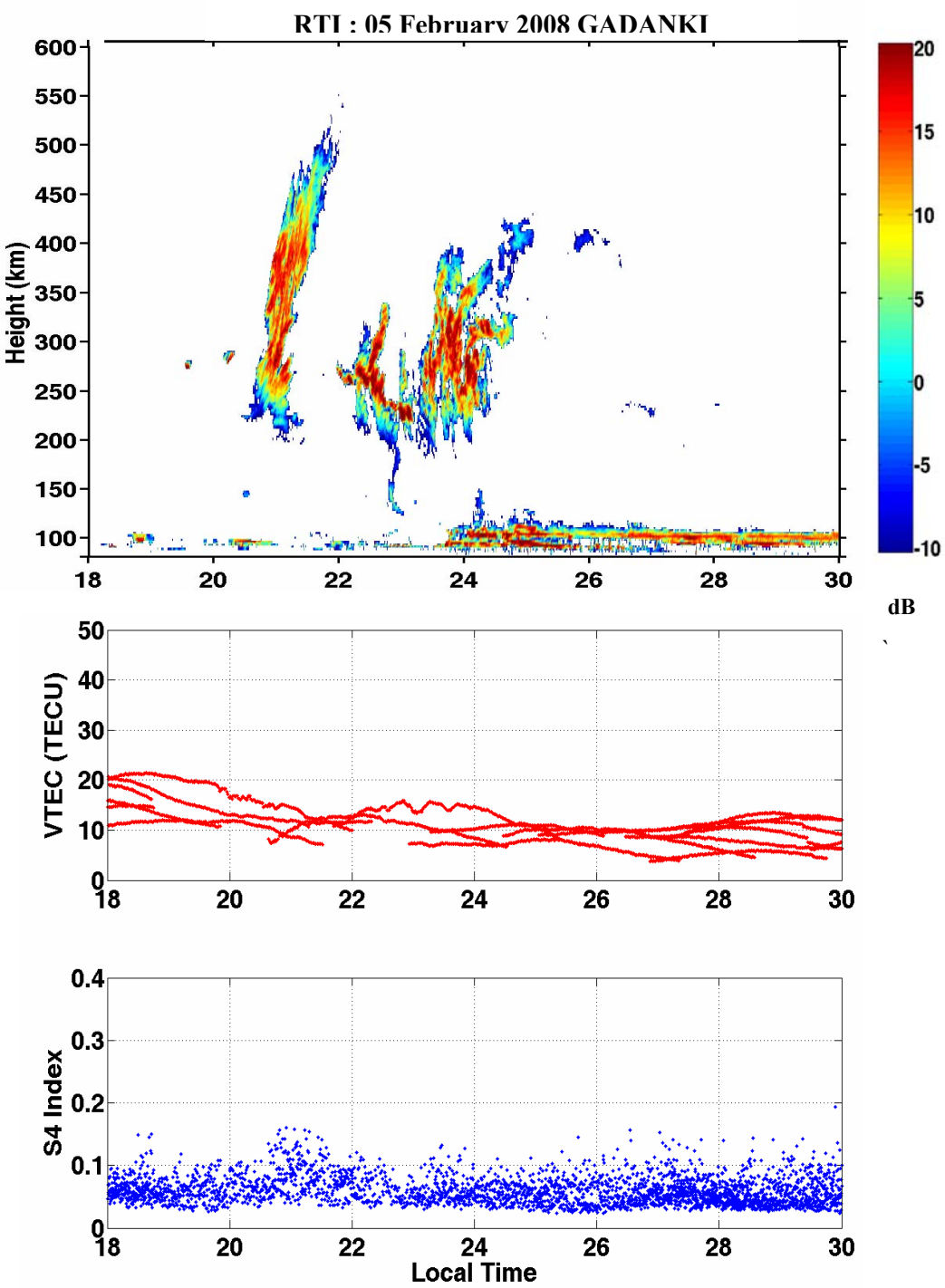

Figure 4.17: RTI map, TEC and S4 observations from all the PRNs in view between 18:00 IST to 30:00 IST on 5 February 2008

4.8 Conclusion

A multitechnique investigation on various characteristics of ESF has been carried out using VHF radar, GPS –TEC and scintillation monitor and ionosonde in India. The evolution of different scale sizes of irregularities manifests themselves on different instruments. On 21/3/07, the ionosonde observations located at equatorial station Trivandrum shows the conditions necessary for ESF irregularity generation. VHF coherent back scatter radar located at low latitude station Gadanki starts showing striated/elongated blob like multiple plumes of irregularities between 1955 and 2600 IST almost simultaneously with the onset of irregularities at Trivandrum. The periodicity of the upwelling regions (radar bloblike structures of period ~20 min) suggests a wavelike seed process. When the explosive F region echo development takes place, the E region echo disappears and remains absent or weak. From the spectral width and Doppler velocity variations, it emerges that the disruption of E region is during the initial phase of ESF. The mapping of electric field from equatorial valley region to E region over Gadanki may be responsible for the weakening of E region instabilities during the growth phase of ESF at the equator.

The multiple depletions which can be associated with the multiple radar plumes are observed in PRN 20 which is moving in a nearly constant longitudinal path during its passage over the Gadanki between 2100 and 2245 IST. PRN 25 has detected irregularities at higher latitudes with higher values of S4 index and strong TEC depletion. The absence of scintillation in PRN 23 after 2246 IST, though it is passing exactly above the Gadanki during this time, reveals that Fresnel scale size irregularities have been decayed and radar is detecting 3 m scale irregularities generated at the walls of the Fresnel size irregularities through the secondary mechanism. The absence of scintillation in PRN 23 after 2300 IST may correspond to the initial phase of ESF irregularities, as inferred from spectral width and Doppler velocity values, which yet not developed to Fresnel scale sizes.

Using multi-technique observations, it is shown that the TEC enhancement observed over Gadanki during an ESF night is due to the plasma enhancement

structure associated with ESF. This suggests the generation of substantial localized plasma enhancement during ESF events that can alter TEC in the ionosphere over dip-equatorial region. The study of latitudinal extent of ESF associated L-band scintillation as observed by a chain of GPS receivers indicates that the maximum of L-band scintillation occurs at low latitudes. The solar activity dependence of L-band scintillation has been clearly seen. The highest scintillation for the span of observations (2005 to 2008) is observed in 2005. The intensity of scintillation has been decreased since 2005 onwards, and minimum of its observed in 2008.

Chapter 5

Low Latitude ionospheric-thermospheric response to storm time electrodynamical coupling between high and low latitudes

5.1 Introduction

The sun's outer atmosphere, the solar corona, is not in hydrostatic equilibrium unlike the earth's atmosphere. It continuously expands with plasma leaving the sun and flowing into interplanetary space. This flow of plasma is known as the solar wind. The solar wind plasma is very tenuous and thus almost collision free. As a result the electrical conductivity of solar wind is very large. It is the case similar that when a perfect conductor moves into the magnetic field, it generates currents that hold the steady internal magnetic field inside the conductor. This says that the solar wind plasma will continue to hold the original magnetic field or in other words the magnetic field is frozen to the solar wind plasma. This magnetic field is known as the Interplanetary Magnetic Field (IMF). The fast solar wind emerges from the Coronal holes. Coronal hole is the region of very low density and the magnetic field in the coronal hole has a single polarity, i.e., the magnetic field lines from it go out in to the interplanetary space rather than looping back to the sun. Thus, the plasma can flow easily along it and this causes fast solar wind streams to develop. The close field line configurations provide a source of slower solar wind. In addition to this, earthward Coronal Mass Ejections (CMEs) and associated solar flares from the coronal hole also produce large fluxes of energetic particles and generate geomagnetic disturbances. These disturbances are known as the geomagnetic storms. However, all storm events cannot be associated with solar flares.

The severity of disturbance depends on the orientation of the meridional component (Bz) of the IMF. If the IMF Bz is southward, reconnection occurs between the earth's magnetic field lines and IMF lines at the magnetopause. Due to the dayside reconnection process, energy, momentum and mass get transferred

from solar wind to the earth's magnetosphere. As the magnetosphere – ionosphere- thermosphere are threaded by the same magnetic field lines, huge amount of energy and momentum is swapped between them at the time of magnetic reconnection process during the geomagnetically disturb conditions. Some of the solar wind energy directly gets transferred to the ionosphere over polar latitudes through polar cusp region and via field aligned currents.

The magnetotail region stores solar wind energy in the form of kinetic and thermal plasma and this is known as one of the major consumers of solar wind energy. There is also a direct precipitation of solar wind particles through the open geomagnetic field lines at the polar ionosphere. Significant part of the magnetic energy gets transferred to the ring current which flows in the equatorial plane due to the trapped solar wind particles by earth's magnetic field. The trapped solar wind particles drift from one field line to another one, gradually moving across the magnetic field lines all the way around the earth. Ions move westward and electrons move eastward forming westward ring current. The magnetic field produced due to the ring current is anti parallel to the existing earth's magnetic field, therefore this causes a decrease in the measured geomagnetic field.

The transferred storm time solar wind electric field at high latitude ionosphere enhances the heat budget there. This electric field when penetrates to low and equatorial latitudes alters the electrodynamics and thus electron density distribution at low and equatorial latitudes. The enhanced heat at high latitudes alters the thermospheric neutral composition globally. Thus the input solar wind energy, especially during geomagnetically disturb conditions, alters the heat budget of magnetosphere, ionosphere and thermosphere globally. All these effects are highly time dependent and their occurrence is totally rely on the local time of SSC at any place on the earth.

In this chapter we have tried to investigate the low latitude ionospheric – thermospheric response to geomagnetic storm time electrodynamical coupling between high and low latitudes. The ionospheric variations are discussed in terms of GPS-TEC. The thermospheric neutral composition variations, mainly a delayed effect of geomagnetic storm, are discussed in terms of $[O]/[N_2]$ ratio, measured

onboard TIMED/GUVI satellite. The different aspects of the observed TEC behavior will be discussed in detail in terms of the responsible physical processes to bring out the storm time electrodynamical coupling between high and low latitudes more comprehensively. The three storms 15 May 2005, 24 August 2005 and 8-9 May 2005 are considered for the present study.

5.2 Historical background

During geomagnetically disturbed conditions, ionospheric electric fields and currents at equatorial and low latitudes have been observed to be modulated by the direct prompt penetration of a dawn-dusk electric field to equatorial and low latitude ionosphere [*Nishida*, 1968, *Spiro et al.*, 1988, *Sastri et al.*, 1997] and by the ionospheric disturbance dynamo electric field [*Blanc and Richmond*, 1980; *Fejer and Scherliess*, 1997]. The storm time ionospheric electric field perturbations often affect the distribution of ionospheric plasma by creating positive ionospheric storm (increased electron density) and/or negative ionospheric storm (decreased electron density) and the occurrence of plasma density irregularities at equatorial and low latitudes [for e.g., *Fejer,* 1986; *Abdu et al.*, 1991, 1997; *Sobral et al.*, 1997; *Sastri et al.*, 2000; *Basu et al*., 2001].

The direct prompt penetration of solar wind/magnetospheric electric fields to low latitudes is short lived (time scales < 1 hour) [e.g., *Kelley et al.*, 1979; *Fejer*, 1986; *Fejer et al.*, 1990a; *Kikuchi et al.*, 1996; *Sastri et al.*, 1997, 2002]. It generally occurs during the period of large and rapid changes in magnetospheric convection and at the time of preliminary geomagnetic sudden commencement and sudden changes in the dynamic solar wind pressure. It creates a dawn-dusk electric field in the equatorial ionosphere which is in general eastward in the dayside and westward in the nightside. Therefore, it enhances the daytime eastward dynamo electric field and vertical drifts at equatorial and low latitude ionosphere which lifts the plasma to higher altitudes, where the ratio of production to loss is large, leading to enhanced electron densities in the dayside sector. The dayside ionospheric response to the prompt penetration electric field is seen as huge enhancement in TEC [*Maruyama et al.,* 2004; *Tsurutani et al.,* 2004] and the

night side response is often observed as a depletion in the TEC [*Abdu et al.,* 2007]. In addition to this, the EIA is found to intensify in amplitude as well as in latitudinal extent in association with the prompt penetration electric field [*Linn et al.*, 2005; *Mannucci et al.*, 2005; *Zhao et al.*, 2005; *Balan et al.*, 2010].

In contrast to prompt penetration electric fields, disturbance dynamo electric fields resulting from the enhanced energy deposition into the high latitude ionosphere are more slowly varying (time scales from a few to several hours) and perturb low latitude electric fields and currents during and up to about a day or two after the onset of geomagnetic storm i.e. long lived electrodynamical disturbances. [*Blanc and Richmond*, 1980; *Fejer et al.*, 1983; *Sastri*, 1988; *Mazaudier and Venkateswaran*, 1990; *Fejer*, 1997]. Disturbance dynamo electric field perturbations are westward in dayside i.e. opposite to the daytime ionospheric dynamo electric field and eastward in the nightside. Hence, it can cause depletion of TEC in dayside [*Tsurutani et al.*, 2004] by generating negative ionospheric storm and also cause suppression of EIA, while on nightside, results are reported showing huge F layer uplift at night time and even resurgence of strong EIA *[Fuller-Rowell et al.*, 2002].

Since the ionosphere and thermosphere behave as a coupled system, the storm time electrodynamical perturbations in ionosphere get reflected in the thermospheric dynamics also and this makes the situation bit complex. Direct particle precipitation in the polar region increases the auroral electrojet (AE) current which results in the generation of atmospheric gravity waves (AGWs) owing to the joule heating by the AE current system. These waves which are known as Traveling Atmospheric Disturbances (TADs) [*Hines*,1960, 1974; *Richmond* 1978; *Jing and Hunsucker*, 1993; *Balthazor and Moffer*, 1997] propagate towards the equator and redistribute the energy and momentum through viscous interactions, heat conduction, and frictional loss due to ion drag with a time delay of 24 hour or more [*Prolss*, 1997; *Fuller-Rowell et al.*, 2002]. The enhanced joule heating over polar latitudes lifts the neutrals and drives them towards the low and equatorial latitudes, thereby changing thermospheric composition globally. The atomic species e.g., O being lighter lifts up first and reaches to lower latitudes earlier, contributing in positive ionospheric storm [e.g.

Burns et al., 1995; *Field et al.*, 1998] while molecular species eg. N_2, O_2 etc. being a heavier reaches later and can cause negative ionospheric storm. The meridional wind circulation changes both in magnitude and direction following a storm. In general, meridional winds flow from the equator to polar region during daytime and the reverse happen during nighttime. During geomagnetic storm these patterns change drastically and wind flows from the poles to the equatorial region during daytime.

In the dusk sector, the zonal electric field perturbations at the equator during geomagnetic storms lead to development/inhibition of ESF irregularities which is determined by the local time dependence of the polarity and amplitude of electric field perturbations due to again prompt penetration and disturbance dynamo electric fields. There are a number of studies reported which explain the development/inhibition of ESF during geomagnetic storm and the role of storm time electric fields perturbations during last three decades [*Aarons*, 1991; *Abdu et al.*, 1995; *Fejer et al.*, 1999; *Basu, Su et al.*, 2001; *Basu, S et al.*, 2001, 2005; *Ram et al.*, 2008].

A comparatively less explained aspect is the significant enhancement in electron density a day before the onset of geomagnetic activity with an amplitude comparable to F_2-layer storm effect and termed as prestorm enhancement [*Buresova and Lastovicka*, 2007] or positive phase before the onset of geomagnetic activity [*Danilov*, 2001; *Kan*e, 1973]. *Liu et al.*, [2008] showed prestorm enhancement in maximum electron density (NmF2) and TEC at low latitudes. They suggested enhanced zonal electric field or vertical plasma drift as the causative mechanism for it. But they were not able to explain the exact cause for the zonal electric field or vertical plasma drift enhancement. Apart from this *Kutiev et al.*, [2006, 2007] observed strong TEC enhancement at the end of recovery phase of geomagnetic storm and they suggested that it can appear 1-3 days after the main phase of the storm. They reported that most of the enhancements are part of the EIA crest region during nighttime and with structures in the whole latitude range considered at daytime. The following sections describe the low latitude ionospheric –thermospheric variations before, during and after the geomagnetic storms.

5.3 Data and Method of analysis

GPS – TEC measurements from low latitude station Rajkot located near the EIA crest, and the GPS - TEC from a chain of ISRO GAGAN GPS receivers along the 77-78^{0}E longitude extending from magnetic equator to the EIA crest and beyond, also in the Indian region, and from Arequipa Laser Station (AREQ), Galapagos Permanent Station (GLPS), Taal Volcano Station (TVST) have been used to study the effects of geomagnetic storm at low and equatorial latitude ionosphere during day and night sectors during 15 May 2005 storm. The details of all these stations are given in Appendix –I (Table I.1 and Table I.2). Jicamarca (-11.57^{0}N, 283.8^{0}E, geomagnetic latitude -1.61^{0}N) radar and ionosonde data (http://jro.igp.gob.pe/madrigal) have also been used to see the behavior of night time ionospheric F-region during 15 May 2005 storm. GPS-TEC measurements from Rajkot are used to study the low latitude ionospheric variations during another two storms i.e. 24 August 2005 and 8-9 May 2005.

For Indian GPS stations, the slant TEC data have been recorded at a sampling rate of 60 seconds and then converted in to the VTEC according to the method described in *Bagiya et al.*, [2009]. The mean of VTEC data from all the visible satellites with elevation mask of 30^0 has been derived at every 15 minutes for a given IPP and presented as a single TEC value for that IPP. Diurnal profiles for that IPP are then derived from the above TEC values with a temporal resolution of 15 minutes. The temporal resolution for AREQ, GLPS and TVST GPS data is 30 seconds. For GLPS and AREQ stations, the TEC values are plotted along with the standard deviation of rate of TEC change index (ROTI) with 5 minutes temporal resolution to show the presence of scintillation if any.

Symmetric ring current index SYM-H values are used to represent the evolution of the storm. The dawn to dusk component of IEF i.e. IEFy, for the SSC day has been calculated using the IMF B_z component and the solar wind velocity V_x. The IMF B_z and V_x values are obtained from Advanced Composition Explorer (ACE) satellite (located at L1 point). The IEFy can be expressed as

$$\mathbf{IEF_y = V_x \times B_z} \qquad (5.1)$$

To translate the electric field values to the earth's ionosphere, appropriate time delay is incorporated by the method described in detail in *Chakrabarty et al.*, [2005]. The time delay comprises of three components. The travel time of the solar wind from the spacecraft to the subsolar bow shock (t_1), propagation time from the bow shock to the magnetopause (t_2), and the Alfven transit time (t_3) along the magnetic field lines from the subsolar magnetopause to the ionosphere. The total time delay during the present storm is found to be varying from 61 minutes to 25 minutes.

The absolute values of the horizontal magnetic field H component from four magnetic observatories extending from equator to mid latitudes around the longitude belt of 77 ± 5^0E have been replotted at a resolution of 1 minute for the SSC day during 15 May 2005 storm to see the signature of prompt penetration electric field to equatorial and low latitudes. The details of these observatories are given in Appendix I (Table I.3). The EEJ strength ($\Delta H_{(TIRUNELVELI)} - \Delta H_{(ALIBAG)}$) has been derived from the ΔH values at Alibag (low latitude) and Trivandrum (magnetic equator) during the storm period as per the method adopted by *Rastogi and Klobuchar* [1990].

To examine the thermospheric neutral composition changes during the storm period, TIMED/GUVI measurements have been extracted for $[O]/[N_2]$ ratio (http://guvi.jhuapl.edu/levels/level3/guvi_on2/plot/gif/2005) and replotted for Indian latitudes-longitudes (lat-long) sectors during 15 May 2005, 24 August 2005 and 8-9 May 2005 storms. As the GUVI observations are not continuous for particular lat-long sector, the exact timing information for these observations is difficult to provide. But we have tried to derive the average time period of the presented GUVI $[O]/[N_2]$ observations and that falls in between 11:30 IST to 14:30 IST during 15 May storm, 10:50 IST to 12:50 IST during 24 August storm and 12:45 IST to 16:30 IST during 8-9 May storm for Indian lat – long sectors.

5.4 Storm of 15 May 2005

The active region 759 of the sun triggered M-8 (Medium Sized) X-ray flare and a CME on 13 May 2005 at 22:30 IST. The MDI image of the sun, Figure 5.1(a), shows the large sunspot active region 759. Figure 5.1 (b) shows the EIT 195 Angstrom (green) image of the sun's corona. The bright area shows the M-8 flare. Figure 5.1(c) shows the Halo CME which was directed towards the earth and impacted on it on 15 May 2005. As a result the earth was influenced the passage of a magnetic cloud which started at 10:50 IST on 15 May and ended at 04:00 IST on 16 May.

The geomagnetic storm of 15 May 2005 is unique in itself as the IEFy on occasion boosted to abnormally high values. Figure 5.2 (a), 5.2(b), 5.2(c) and 5.2(d) show the temporal variations of appropriately time shifted IMF Bz, AE index, Sym-H Index, and appropriately time shifted dawn to dusk component of IEFy respectively on 15 May 2005. The shaded area in Figure 5.2 shows the disturbed period on the day. The storm started with SSC at 08:02 IST (02:30 UT) just after the forward shock with amplitude of 39 nT synchronized with sudden increase in AE index on 15 May 2005.

During the initial phase of the storm the SYM-H values remained steady at the raised value up to 11:53 IST, after this SYM-H started to decrease very fast indicating the commencement of the main phase, and reaching a minimum value of -305 nT at 13:51 IST. The main phase onset coincided in time with the southward turning of IMF Bz (negative), large AE index and a large IEFy values of ~42 mV/m. The data are not available for Vx for the time period when sudden increase in AE index occurred (08:04 IST to 10:45 IST), therefore the initial variation of IEFy, when SSC occurred, cannot be presented. The ionospheric-thermospheric variations before, during and after 15 May 2005 storm are discussed in the following subsections.

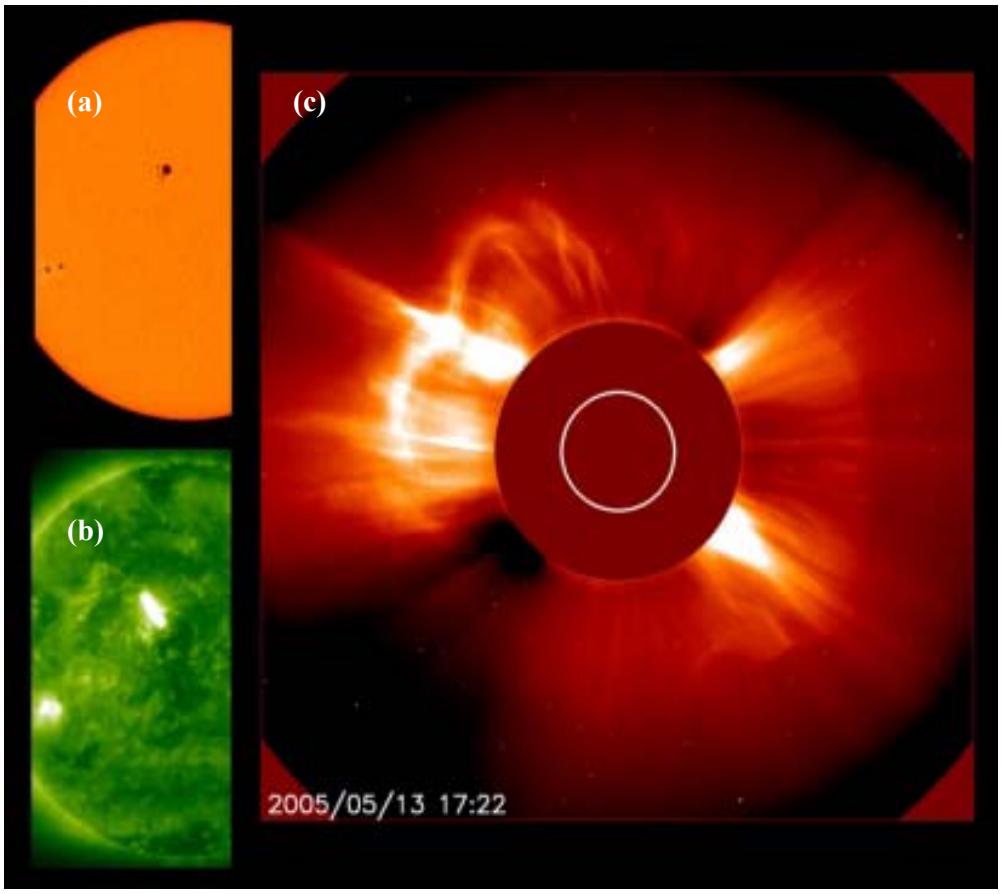

Figure 5.1: (a) Yellow MDI image of the sun shows the active region 759 from which a major class M-8 flare spawned.(b) the EIT 195 Angstrom (green) image of the sun's corona, the bright area shows the flare (c) SOHO satellite image of 13 May 2005 Halo CME

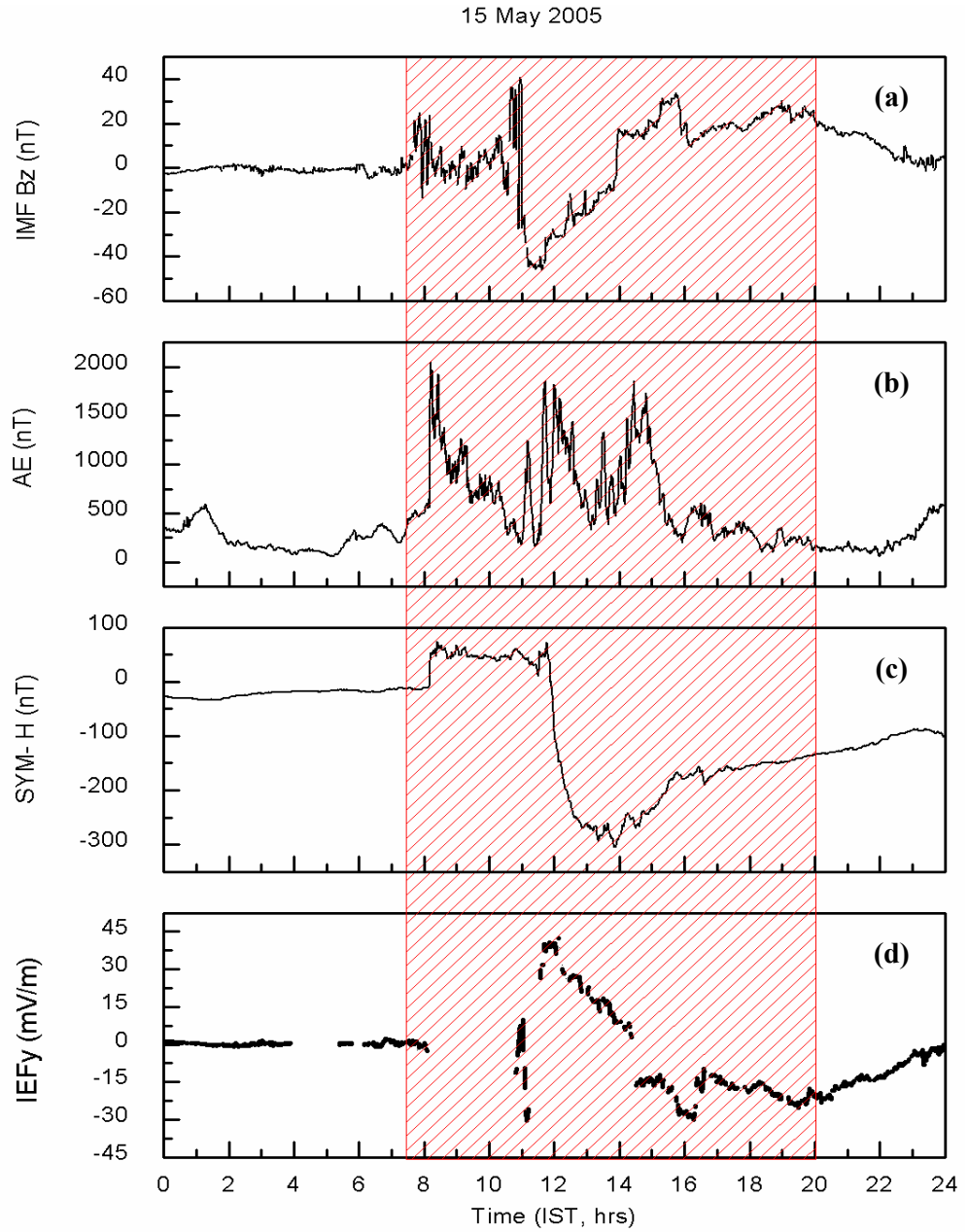

Figure 5.2: Interplanetary and geomagnetic conditions during 15 May 2005 storm. From top the temporal variations of (a) IMF Bz (b) AE index (c) SYM-H index (d) IEFy with time lag correction respectively on 15 May 2005

5.4.1 TEC enhancements on the day preceding the occurrence of SSC

The TEC variation on 14 May 2005, a day before the SSC day for Rajkot and for five GAGAN GPS stations along with the quiet days' (Ap<4) TEC mean of the month is shown in Figure 5.3. It is pertinent to note that on a day prior to the storm (14 May), TEC enhancements of ~ 20 TECU , ~ 15 TECU and ~10 TECU with respect to quiet days' TEC are observed at EIA trough latitudes Trivandrum and Bangalore as well as at Hyderabad respectively. The observed TEC enhancements gradually decrease with increasing latitudes from the equator. At near EIA crest latitudes i.e. Delhi and Rajkot TEC is almost following the quiet days' values. TEC enhancements on 14 May started at ~ 10:00 IST at Trivandrum and ~ 13:00 IST at Bangalore and Hyderabad. At Hyderabad, the enhancement lasted up to ~ 19:30 IST, at Bangalore up to 20:30 IST and at Trivandrum up to almost midnight.

Figure 5.4(a) represents the development of EIA on 14 May at different daytime hours. The corresponding day's EEJ peak value and Ap value are also indicated in it. It can se seen that development of EIA started from 10:30 IST. The EIA maximum occurred at 14:30 IST with peak value of ~50 TECU at 14^0N latitude (geomagnetic). After 14:30 IST, EIA gets weakened gradually. There is one to one correlation between EEJ and EIA i.e. enhanced EEJ results in the strong EIA [*Raghavarao et al.*, 1978]. The moderate EEJ value of ~ 52 nT on quiet day of 14 May as indicated in Figure 5.4(a) also supports the observed moderate EIA behavior. The maximum TEC value is found at Trivandrum (trough latitudes) instead of crest latitudes on the day. TEC enhancement lasted up to almost mid night at Trivandrum which also emphasise that most of the plasma remained on the trough latitudes rather than getting transferred to crest latitudes. The thermospheric response on this day as observed by GUVI in Figure 5.4(b), which represents the variations of $[O]/[N_2]$ for Indian lat-long sectors on 14 May 2005, shows that there is an enhancements in thermospheric $[O]/[N_2]$ below 18^0N (geographic) latitudes around 77-78 ^{0}E longitudes. TEC enhancements below 18^0N (geographic) well coincides with $[O]/[N_2]$ enhancements.

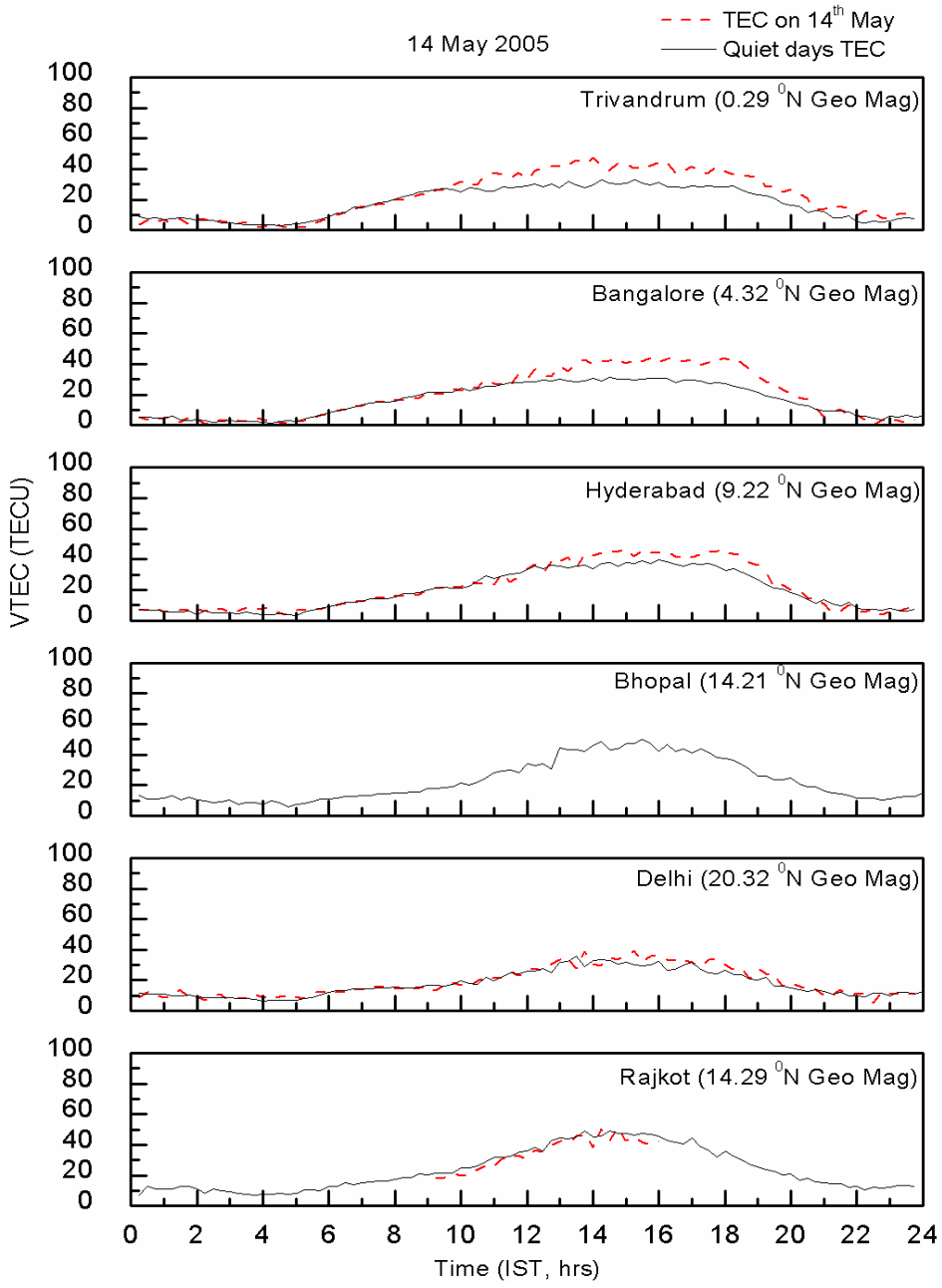

Figure 5.3: Diurnal variation of TEC over the stations, extending from equator to low latitude and beyond it on 14 May 2005 along with quiet days' (Ap<4) mean TEC of the month

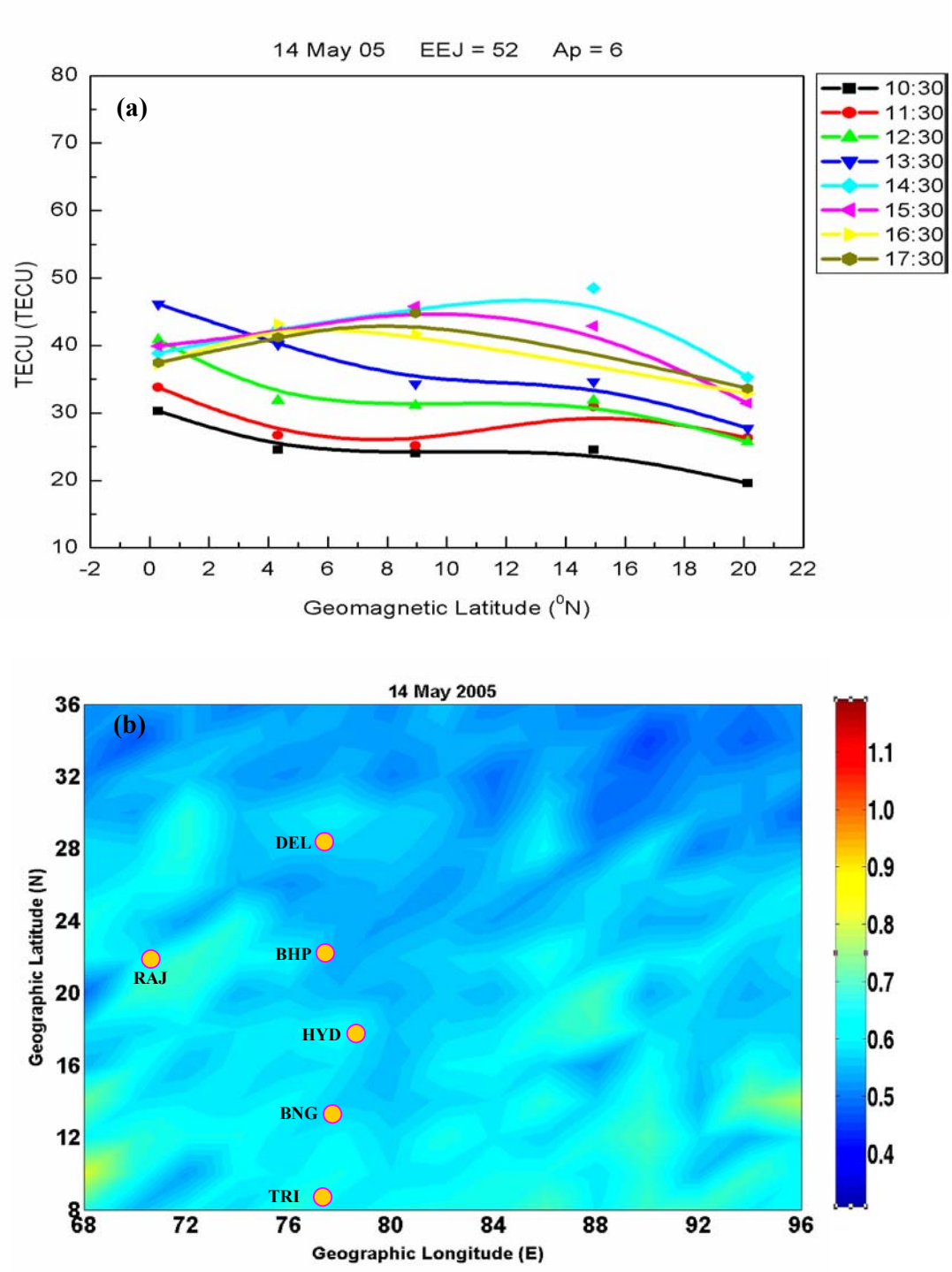

Figure 5.4: (a) Latitudinal profiles of TEC starting from equatorial station Trivandrum (0.5^0 N, Geomagnetic) to low latitude station Delhi (20.38^0 N, Geomagnetic) on 14 May 2005 (b) [O]/[N_2] values between 11:50 IST to 14:50 IST replotted for Indian lat-long sector on 14 May 2005 derived from the observations of GUVI onboard the TIMED NASA satellite

Liu et al., [2008] reported low latitude prestorm enhancements with simultaneous depletion at equatorial latitudes using ionosonde and GPS- TEC measurements along the longitude of 120^0E in the Asia/Australia sectors. They explained that the enhancements were due to enhanced zonal electric field or vertical drifts and the reason for the strong zonal electric fields or vertical plasma drift might be the aftermath of previous geomagnetic activity or direct mapping to the equatorial ionosphere from the solar wind electric fields, effects of planetary waves etc. The present study revealed prestorm enhancements at equatorial latitudes in contrast to what reported by *Liu et al*., [2008] and moderate EIA with absence of any low latitude TEC enhancements.

On the other hand, [*Kutiev et al.*, 2006, 2007] reported the strong TEC enhancements at the end of recovery phase of geomagnetic storms. They speculated that these poststorm enhancements are emerged mainly by disturbance dynamo electric field and some cases which appeared at the end of prolonged period of low geomagnetic activity can be related to direct prompt penetration of IEFy in the equatorial ionosphere.

A double main phase storm is occurred on 8-9 May 2005 which has prolonged recovery phase; seen up to 14 May 2005. This storm is discussed in brief in the later part of the chapter. TEC enhancement on 14 May is more pronounced at equatorial latitudes and less pronounced at low latitudes. EIA is also not showing any remarkable increase. Thus, the observed enhancements might not be due to IEFy penetration as in cases reported by [*Kutiev et al*., 2006, 2007]. But the enhancements can be projected as the effect of penetration of long lived disturbance dynamo electric field during the prolonged recovery phase of 8-9 May 2005 storm which is westward during daytime. This results in the enhanced electron density at trough latitudes.

In addition to this, enhanced AE index of ~ 1100 nT at 14:00 IST on 13 May 2005 might have resulted in storm time thermospheric circulation which redistributes the neutral species in equatorial and low latitude ionosphere. The excess energy deposition over high latitudes changes the neutral composition and temperature globally by producing large scale perturbation in the thermospheric

circulation. Due to the direct precipitation of energetic particles in the polar region through polar cusp, the strength of AE current increases and thus Joule heating enhances. The enhanced Joule heating in the polar region produces large pressure gradients and the resultant is the development of equatorward neutral wind. These neutral winds carry molecular rich air towards mid and low latitudes. N_2 being heavier than O, takes longer time to reach to mid and low latitudes.

The consistent behavior of TEC, $[O]/[N_2]$, and AE index (on 13 May) indicate the post storm thermospheric circulation effect of previous storm. Further the longer duration of enhancements up to midnight may be due to longer life time of chemical changes. The observed TEC enhancements on 14 May can be taken as post storm effect produced by storm time thermospheric neutral composition changes which might have triggered due to geomagnetic active condition of 13 May 2005. But the role of disturbance dynamo electric field penetration, if any, during the recovery phase of 8-9 May storm can not be ruled out.

5.4.2. Positive ionospheric storm on 15-16 May 2005

Figure 5.5 illustrates diurnal variations of TEC over the latitude belt (0.29^0N to 20.30^0N, magnetic) starting from Trivandrum (trough) to Bhopal (crest) and Delhi (beyond the crest) on 15 May 2005 along with the quiet days' (Ap<4) TEC mean of the month. Accompanying the SSC, a remarkable enhancement in TEC appeared almost simultaneously at all the stations. The maximum amplitude of TEC enhancements about 40 TECU with respect to quiet day's TEC appeared at EIA crest region Bhopal. Unfortunately, the data for Rajkot station is not available on this day, so could not be presented. The observed TEC enhancements from the equator to the low latitudes show strong positive ionospheric storm on 15 May. *Pandey and Dashora* [2006] have also observed daytime peak TEC of 100 TECU on 15 May 2005 from Udaipur (26.4^0N 73.7^0E, Geographic, 15.6^0N Geomagnetic), India, another EIA crest station. *Manucci et al.,* [2005] reported the penetration of IEFy to the low and equatorial ionosphere causing ionospheric positive storm during the super storm of 29-30 October 2003.

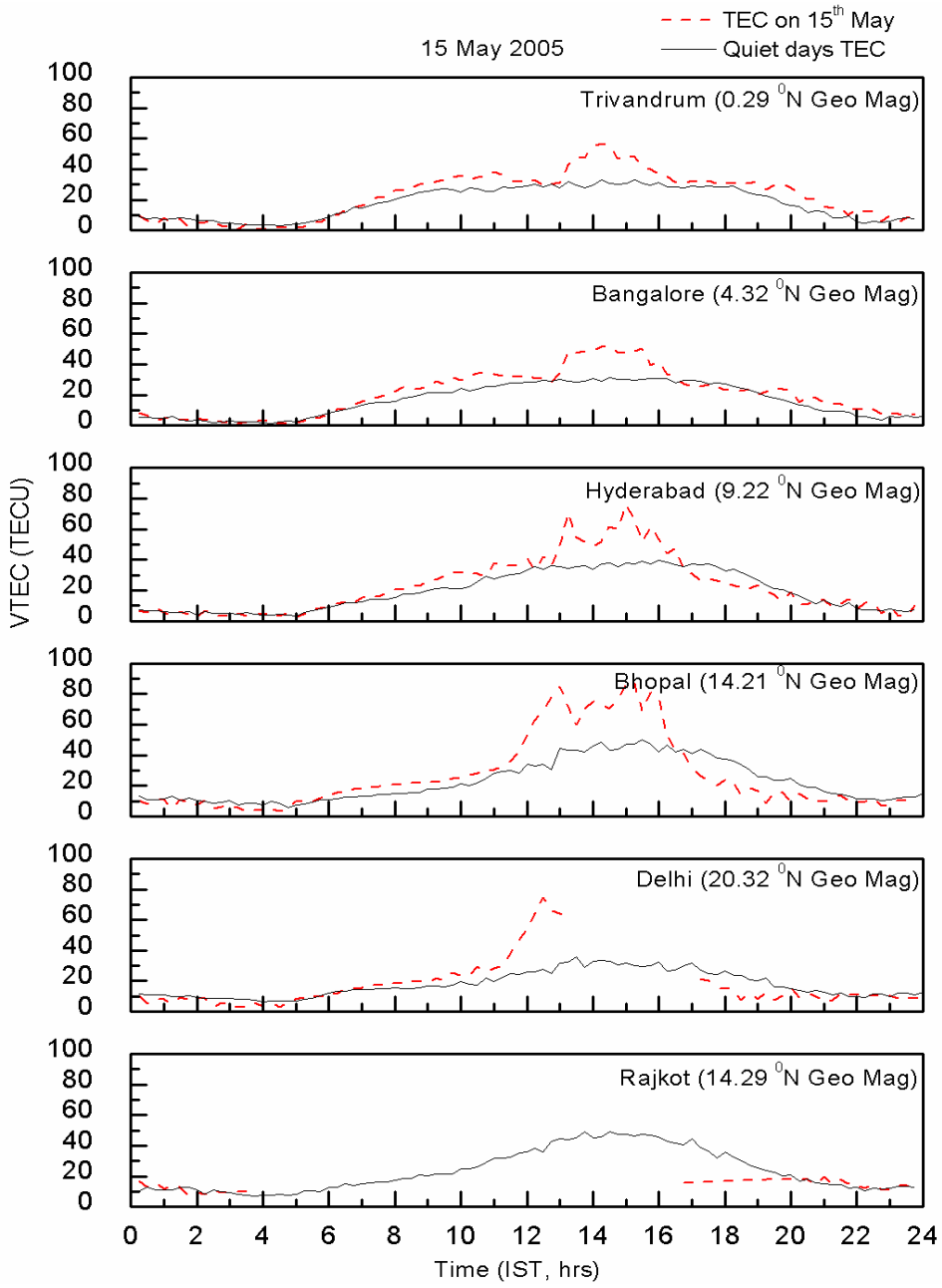

Figure 5.5: Diurnal variation of TEC over the stations, extending from equator to low latitude and beyond it on 15 May 2005 along with quiet days' (Ap<4) mean TEC of the month

Kelley et al. [2003] invoked the penetration of strong high latitude electric field to the mid and low latitudes to explain the resultant day time midlatitude TEC enhancements.

EEJ strength ($\Delta H_{(TIRUNELVELI)} - \Delta H_{(ALIBAG)}$) along with the magnetograms recorded on 15 May 2005 at stations spreading from equator to mid latitudes along the 77 ± 5^0E longitudes are plotted in Figure 5.6. Accompanying the IEFy increase (Figure 5.2(d)), EEJ increase started at 11:00 IST, reached to its maximum values at 11:20 IST, and started to decrease gradually at 11:25 IST. The evolution of EEJ strength indicates that, EEJ maximum of ~220 nT occurred after the epoch when the IEFy increase is started. The absolute horizontal magnetic field values for Tirunelveli (Figure 5.6) also show sharp and significant increase which also almost coincides in time with maximum IEFy values at ~11:45 IST. The observed EEJ strength of ~ 220 nT and simultaneous sharp increase in horizontal magnetic field values at Tirunalveli on 15 May 2005 provide evidence for the daytime prompt penetration of IEFy at low and equatorial latitudes. The penetrated electric field raises the F- region upward over the entire latitude belt, starting from equator to low latitudes. At higher altitudes, the recombination rate will be slow the resultant is the higher electron density at F-region altitudes.

The low and mid latitude magnetograms (Alibag, Alma Ata and Novosibirsk in Figure 5.6) are not showing any significant IEFy signatures. It is known that the low and mid latitude conductivity is low in comparison to the high and equatorial latitudes. *Reddy et al.*, [1978] have stated that the high latitude electric field perturbations penetrate to the equatorial latitudes with reduction factors of ~10 in the longitude sector of the source region. Consequently, smaller electric field perturbations do not produce any significant surface magnetic field variations at mid latitudes. In the present case we can see that the IEFy values boosted to very high amplitude, but still we are not able to see any signatures of it at mid latitudes. The significant depression of H is progressively reduced with increasing distance from the equatorial station. The afternoon CEJ is seen shortly after the EEJ peak value of ~ 220 nT which coincides with the main phase of the storm.

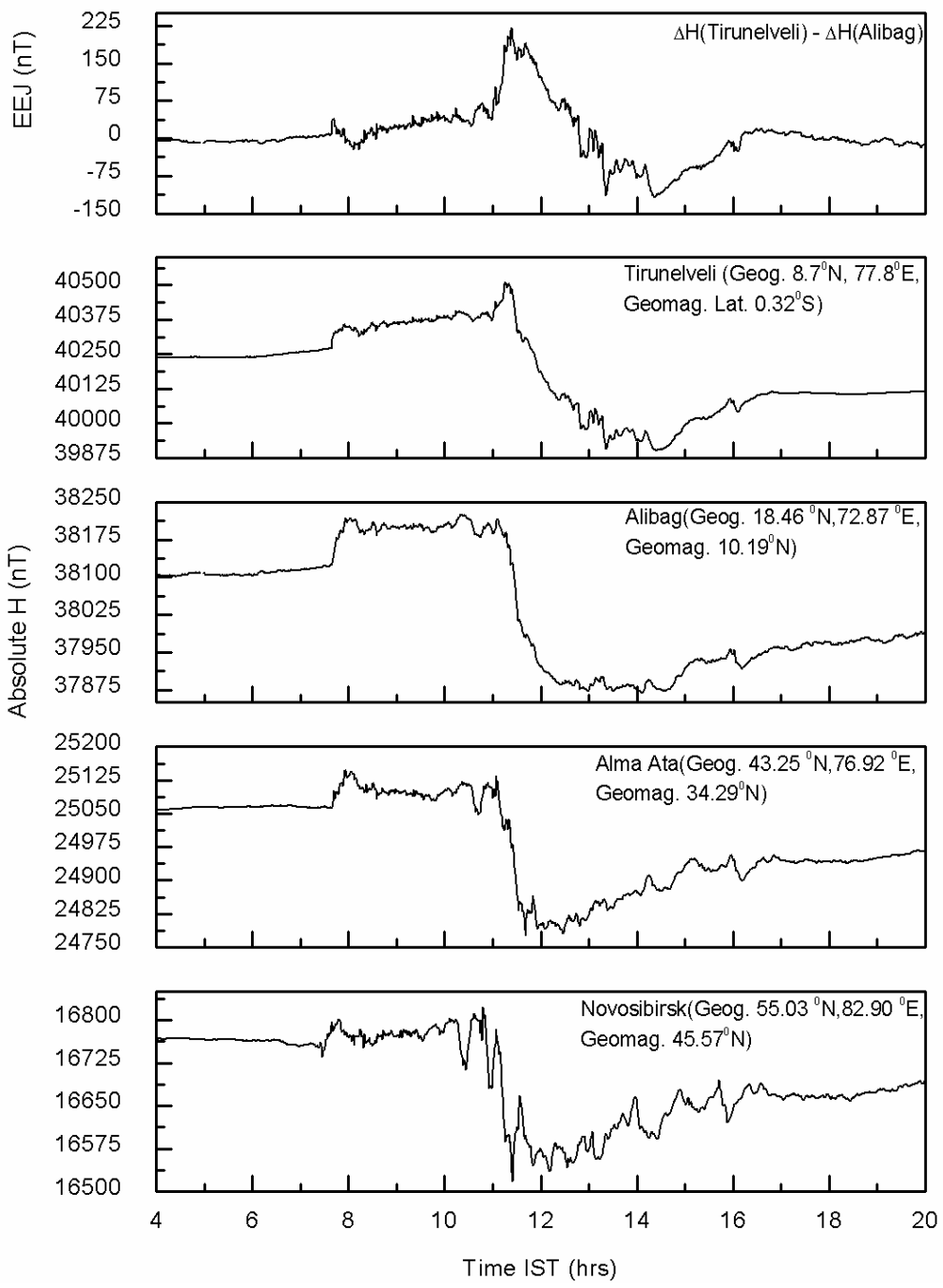

Figure 5.6: From top the diurnal variations of (1) EEJ (2) absolute values of H at equatorial station Tirunelveli (3) absolute values of H at low latitude station Alibag (4) absolute values of H at mid latitude station Alma Ata (5) absolute values of H at another mid latitude station Novosibirsk respectively on 15 May 2005

Rastogi, [1999] suggested that a regular westward electric field is imposed in the equatorial latitudes during the midday hours of geomagnetically disturbed days. This can cause CEJ. As seen in Figure 5.5, depletion in TEC appeared at ~13:00 IST at Trivandrum and Bangalore, simultaneous TEC enhancements developed at Hyderabad, Bhopal and Delhi.

After 13:00 IST, TEC increases at Trivandrum and Bangalore and simultaneous depletion is observed at Hyderabad, Bhopal and Delhi. The observed decrease in TEC at crest regions with simultaneous increase at trough regions on 15 May 2005 may be the effect of CEJ observed in the afternoon on 15 May 2005 (Figure 5.6). The westward electric field during CEJ reverses $\mathbf{E} \times \mathbf{B}$ drifts thus plasma will start to return at trough latitudes due to reverse fountain effect. CEJ started to recover after 14:00 IST. The second and gradual TEC increase at Hyderabad and Bhopal shortly after the depletion at ~ 13:00 IST (Figure 5.5) may be due to recovery of CEJ to the normal condition. The prompt variations of TEC with respect to CEJ show the strong electrodynamical coupling between equatorial and low latitudes. Finally, observed TEC increase at equatorial latitudes is followed by gradual decrease after 16:00 IST. At crest latitudes, the observed TEC depletion is followed by sharp increase between 15:00 and 16:00 IST, after 16:00 IST, TEC shows regular daytime decrease at near crest and crest latitudes also.

Figure 5.7(a) shows the development of EIA on 15 May 2005. EIA gets started to develop after 10:30 IST. The strongest of the EIA occurred at ~12:30 IST shortly after the maximum of EEJ and EIA extended up to ~21^0 N (magnetic) latitudes. The presence of intense EEJ on 15 May 2005 is an indirection of strong vertical $\mathbf{E} \times \mathbf{B}$ drift over the equator required for strong EIA development. As a result, TEC at the EIA crest i.e. Bhopal and beyond crest i.e. Delhi shows remarkable increase with respect to quiet days' mean, with maximum amplitude at Bhopal on the day. The strongest of the EIA on the day at ~12:30 IST is depressed by 13:30 IST. The depressed EIA again redeveloped at ~14:30 IST and then finally gets weakened gradually by ~16:30 IST.

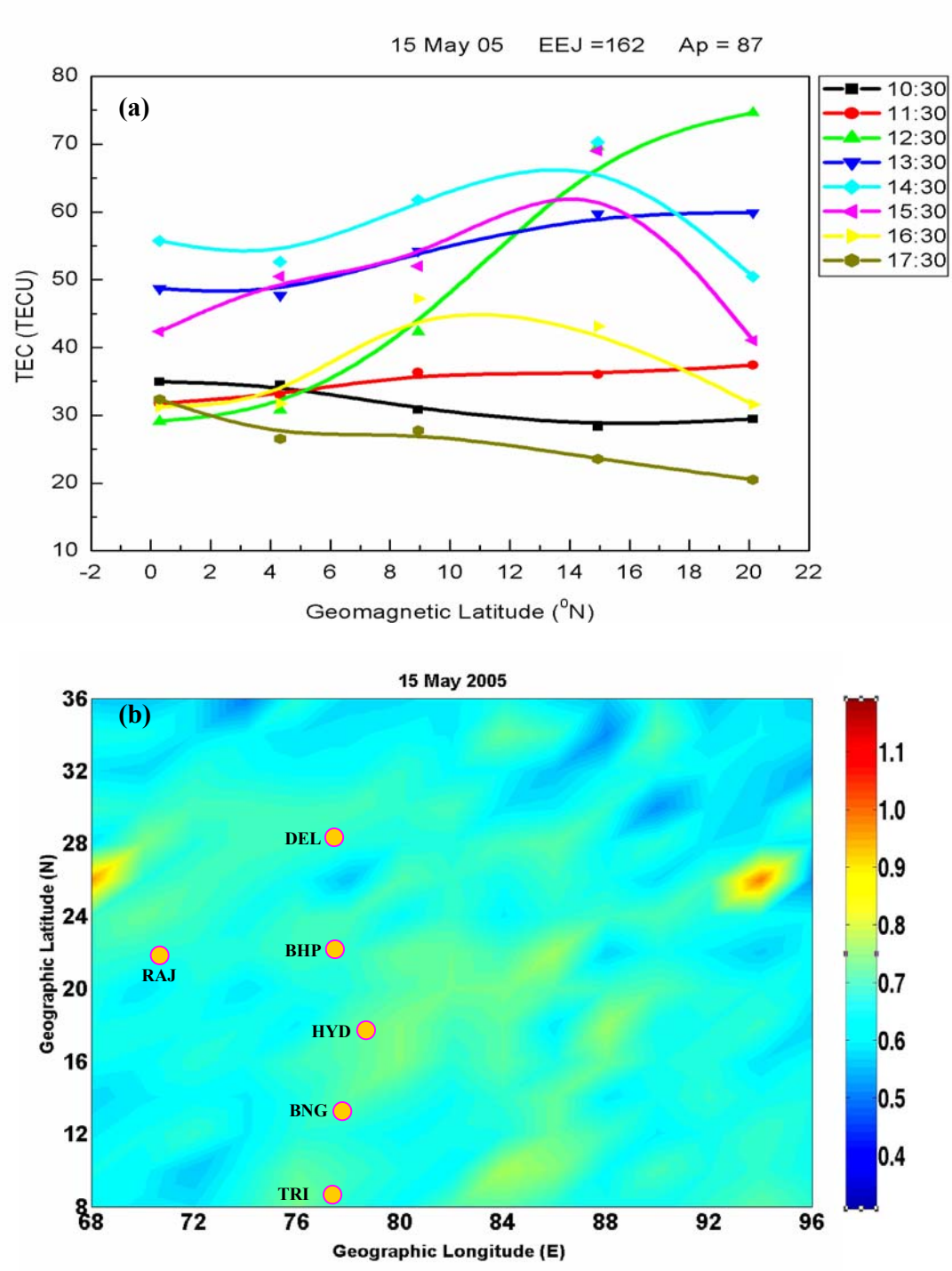

Figure 5.7: (a) Latitudinal profiles of TEC starting from equatorial station Trivandrum (0.5^0 N, Geomagnetic) to low latitude station Delhi (20.38^0 N, Geomagnetic) on 15 May 2005 (b) [O]/[N_2] values between 11:50 IST to 14:50 IST replotted for Indian lat-long sector on 15 May 2005 derived from the observations of GUVI onboard the TIMED NASA satellite

The depression of EIA at 13:30 IST also agrees with the reversal of zonal electric field at the equator. Due to the presence of afternoon CEJ, EIA strength reduces therefore electron density at trough latitudes increases and that at crest latitudes decreases. In latitudinal TEC profile on 15 May (Figure 5.7(a)) TEC values are greater ~13:30, ~14:30 and ~15:30 IST than the values at 12:30 IST at trough latitudes and are lesser at crest latitudes TEC than the values at 12:30 IST. This indicates that intensity of EIA is decreasing after 12:30 IST due to CEJ.

The enhanced Joule heating in the polar region results in the development of equatorward neutral wind. These neutral winds carry molecular rich air towards mid and low latitudes, O being lighter arrives first. Hence, initially an increase in $[O]/[N_2]$ is expected. The storm time thermospheric variations in terms of $[O]/[N_2]$ is shown in Figure 5.7(b). There is significant increase in $[O]/[N_2]$ over the complete latitude belt starting from 8^0N to 36^0N geographic around 77-78^0E longitudes. As O is the major species which builds the F- region ionization, the increased value of $[O]/[N_2]$ contributes positively into the observed TEC enhancements.

In addition to Indian longitude sectors, this study has been extended to other longitude sector also where SSC occurred in day time. Figure 5.8(a) and 5.8(b) represents the TEC diurnal profiles for TVST on 14 and 15 May respectively. Light and dark gray shadows represent nighttime at ionospheric heights. At TVST, the time of SSC is ~10:30 LT (local time). TEC profile on 15 May 2005 at TVST shows that TEC has been increasing gradually after the SSC and the delayed day maximum occurred at ~ 16:00 LT. The maximum TEC values observed are ~120 TECU at ~16:00 LT which is higher by ~ 30 TECU than the TEC values observed on 14 May 2005. The gradual increase in TEC after the SSC is followed by a depletion of ~ 40 TECU at 15:30 LT. This depletion is coincided with the minimum of main phase at TVST. As TVST falls under equatorial latitudes, this depletion is due to transport of plasma from TVST to crest latitudes during fountain effect. This depletion is followed by sharp increase at ~16:00 LT. This may be the effect of penetration of regular westward electric field in the equatorial latitudes [*Rastogi*, 1999] which pulls back the plasma from the crest

latitudes towards the equatorial latitudes, similar to what we have observed for Indian region.

Figure 5.9 shows the diurnal TEC profiles on 16 May 2005 along with quiet days' (Ap<4) mean TEC of the month for Rajkot and GAGAN stations, 5.10(a) represents the latitudinal TEC profiles for different hours of the day on the day and 5.10(b) represents the $[O]/[N_2]$ variations for the Indian lat- long sectors on the day. On 16 May 2005, the day after the SSC event, significant daytime TEC enhancements are seen over the magnetic belt (0.29^0N to 20.30^0N, magnetic) starting from Trivandrum to Delhi with increase of ~20 TECU at Bhopal and ~12 TECU at Rajkot. But on 16 May 2005, increase over trough latitudes is clearer than the crest latitudes.

The observed EIA profile on 16 May 2005, Figure 5.10(a), shows that the EIA developed less pronouncedly with delayed peak at ~13:30 IST. The neutral composition variations in Figure 5.10(b) on 16 May show considerable increase of $[O]/[N_2]$ at trough latitudes around $77\text{-}78^0$E longitudes and this increase is more clearer at trough latitudes. TEC enhancements have also been seen more effective at trough latitudes than the crest latitudes on 16 May 2005. This indicates that TEC enhancements on 16 May are caused by enhancement of O due to storm time neutral composition changes. From moderate EEJ values of 16 May 2005, it appears that there might be penetration of storm time disturbance dynamo electric field which gets activated ~ 4 hours after the SSC phase and lasts up to about a day or two after the onset of geomagnetic storm [*Fejer et al.*, 2002 and reference there in]. The moderate EIA in Figure 5.10(a) agrees with the observed EEJ variations.

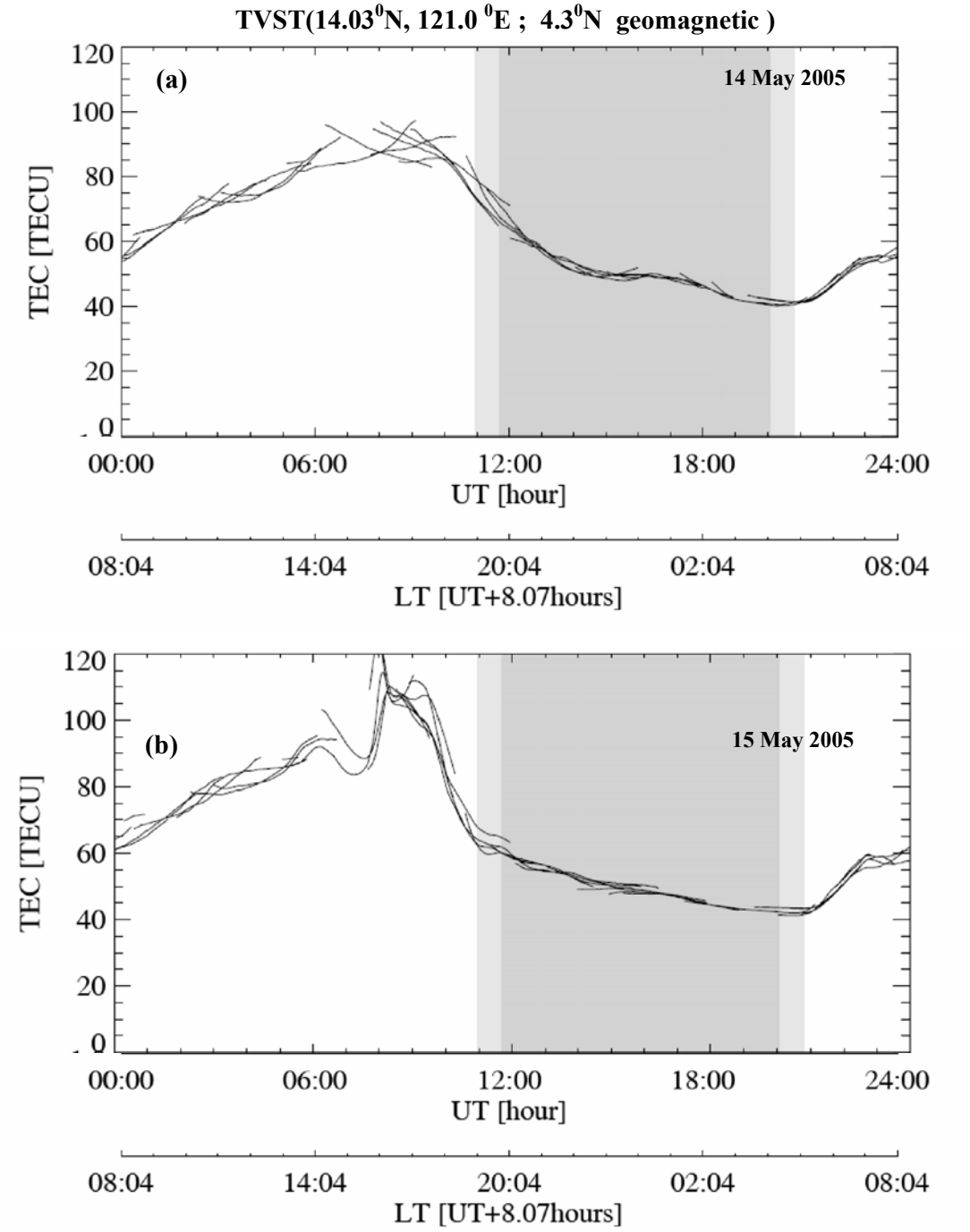

Figure 5.8: (a) Diurnal TEC variations at TVST on 14 May 2005(b) Diurnal TEC variations at TVST on 15 May 2005

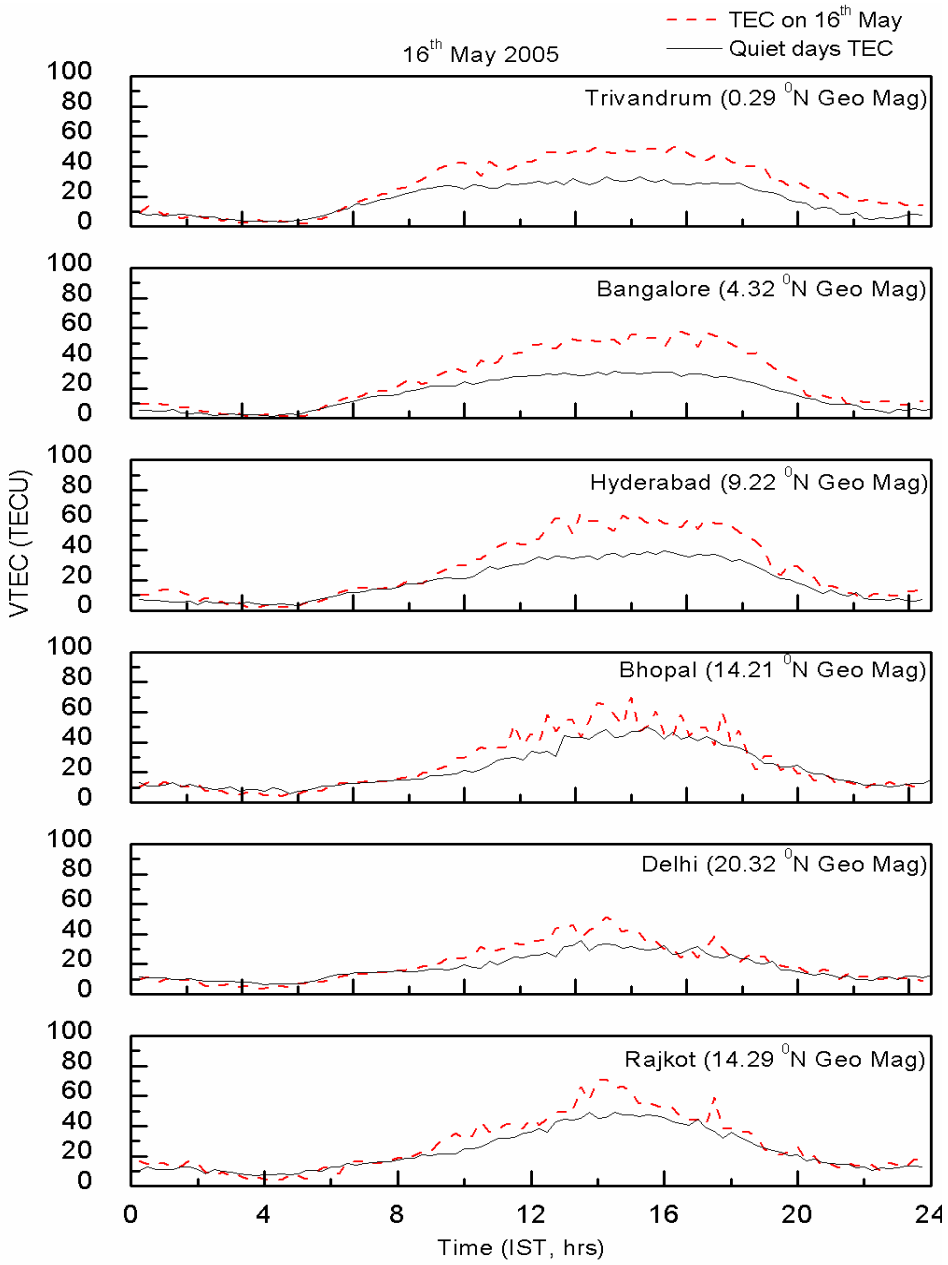

Figure 5.9: Diurnal variation of TEC over the stations, extending from equator to low latitude and beyond it on 16 May 2005 along with quiet days' (Ap<4) mean TEC of the month

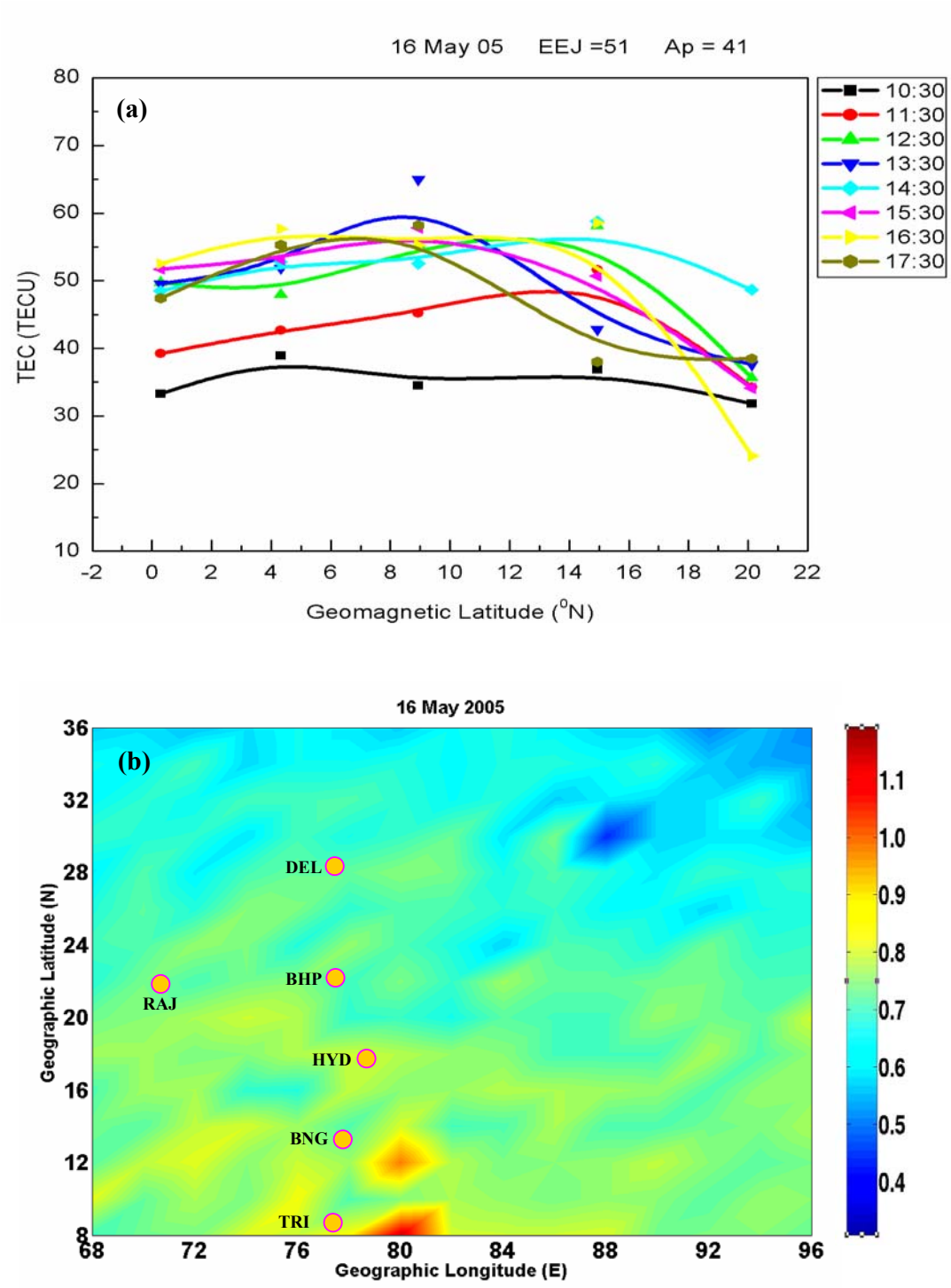

Figure 5.10: (a) Latitudinal profiles of TEC starting from equatorial station Trivandrum (0.5^0 N, Geomagnetic) to low latitude station Delhi (20.38^0 N, Geomagnetic) on 16 May 2005 (b) [O]/[N_2] values between 11:50 IST to 14:50 IST replotted for Indian lat-long sector on 16 May 2005 derived from the observations of GUVI onboard the TIMED NASA satellite

5.4.3 Negative ionospheric storm on 17 May 2005

Figure 5.11(a) illustrates TEC variations over the latitude belt (0.29^0N to 20.30^0N, magnetic) starting from Trivandrum (trough) to Bhopal (crest) and Delhi (beyond the crest) on 17 May 2005 along with the quiet days' (Ap<4) TEC mean of the month. Figure 5.12(a) and 5.12(b) represents the EIA development and thermospheric neutral composition variations on 17 May 2005 respectively. It can be seen that clear increase in TEC on 16 May 2005 is followed by TEC depletion on 17 May 2005 at Rajkot of ~10 TECU and at Delhi of ~20 TECU. The observed TEC depletions represent the negative ionospheric storm and it appeared over low latitudes only and not observed below it

In Figure 5.7(b), the value of $[O]/[N_2]$ was ~ 0.68 on 15 May 2005 over Rajkot region. But on 17 May it decreased to 0.54 from 0.68. The $[O]/[N_2]$ depletion extended up to low latitude region of ~16^0 N (magnetic) from the pole along the longitude belt of 77-78^0 indicating an enhancement of N_2. Electron loss at F_2 peak depends upon the recombination/attachment with N_2; as N_2 density increases, electron density decreases. Thus the observed negative storm at low latitudes on 17 May may be due to storm time neutral composition changes. On 17 May 2005 EIA did not develop due to negative storm effect as seen in Figure 5.12(a).

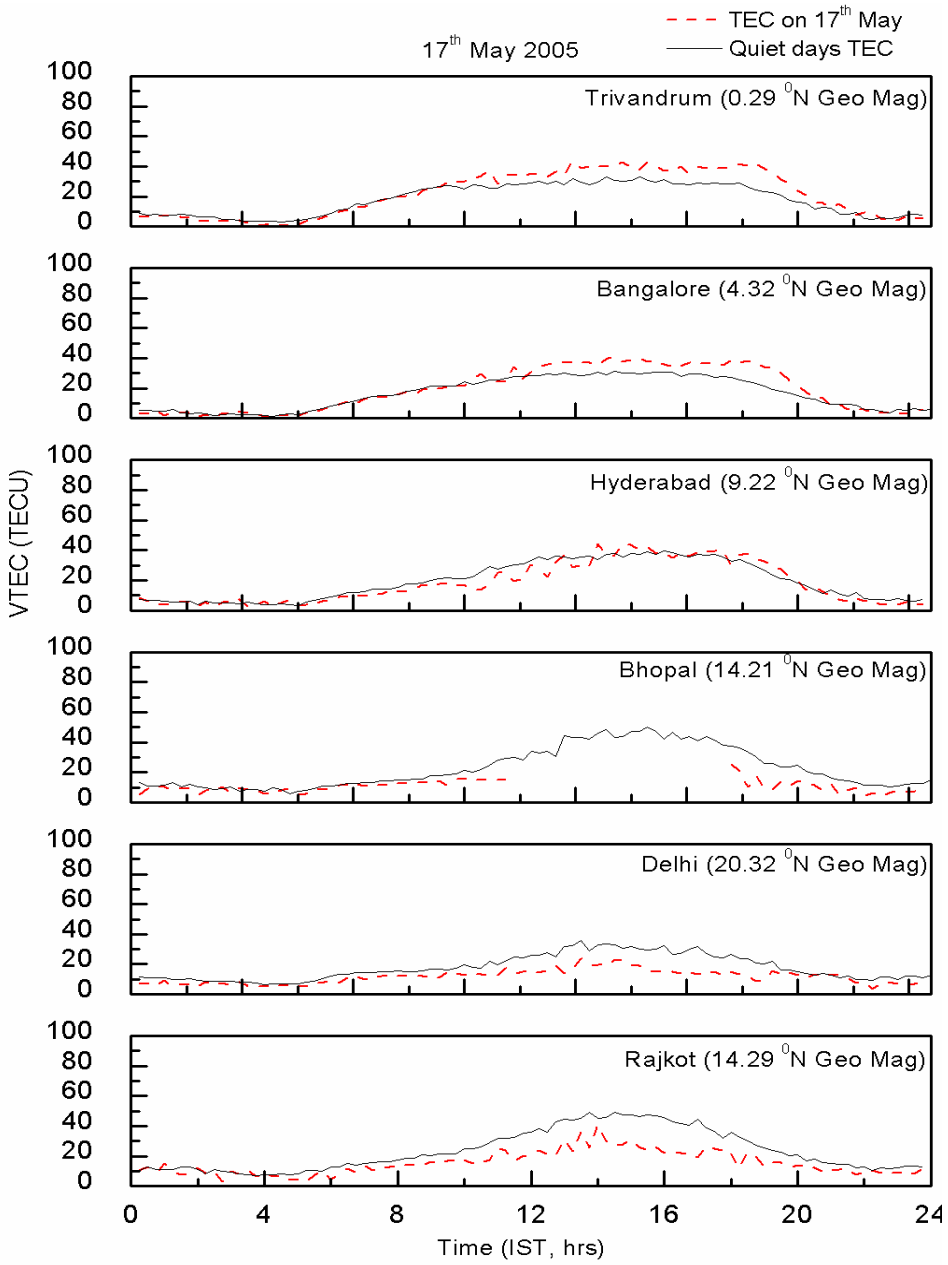

Figure 5.11: Diurnal variation of TEC over the stations, extending from equator to low latitude and beyond it on 17 May 2005 along with quiet days' (Ap<4) mean TEC of the month

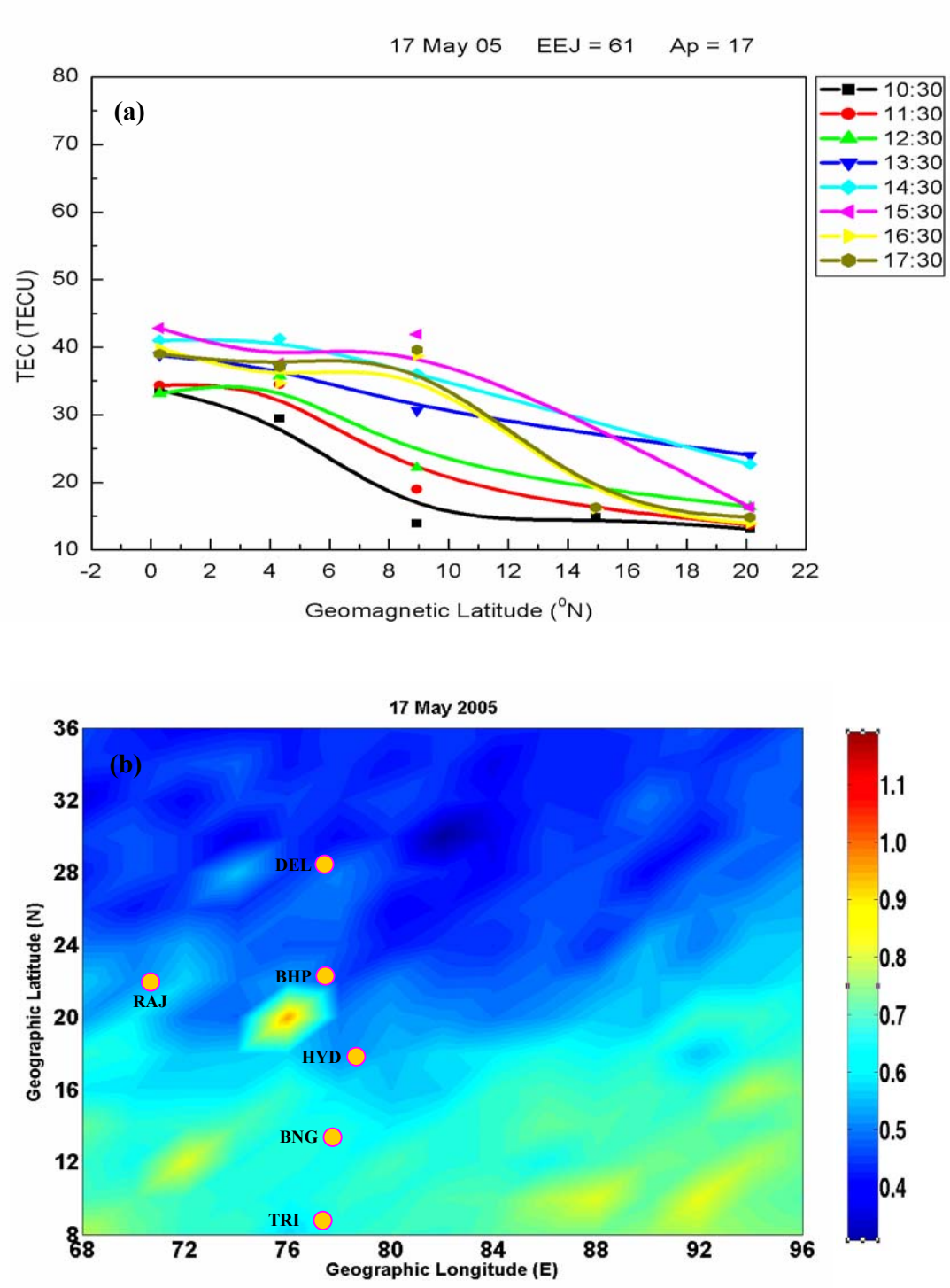

Figure 5.12: (a) Latitudinal profiles of TEC starting from equatorial station Trivandrum (0.5^0 N, Geomagnetic) to low latitude station Delhi (20.38^0 N, Geomagnetic) on 17 May 2005 (b) [O]/[N_2] values between 11:50 IST to 14:50 IST replotted for Indian lat-long sector on 17 May 2005 derived from the observations of GUVI onboard the TIMED NASA satellite

5.4.4 Local time dependent response of ESF/Scintillations

A study has been carried out on the effects of geomagnetic storm over the equatorial and low latitude ionosphere where local time of SSC falls after postsunset hours on 15 May 2005. At Jicamarca the local time of SSC is ~21:30 LT i.e. during pre-midnight hours. Figure 5.13(a) and 5.13(b) shows JULIA RTI map on 13-14 May 2005 (a day before the onset of geomagnetic storm) and on 14-15 May 2005 respectively. On 13-14 May ESF irregularities started to appear from ~19:30 LT in valley-type format between 200 and 300 km with small updrafting patch at ~ 22:00 LT. The ionosonde observations from Jicamarca (Figure 5.14(a)) on 13-14 May 2005 shows pre evening rise in h'F after 18:00 LT. Between 18:00 LT and 19:05 LT, an increase of ~50 km is seen in h'F. This pre-reversal enhancement creates necessary condition for the generation of ESF on the day. GPS observations from AREQ in Figure 5.15 are not showing any significant scintillation on 13-14 May 2005. But at GLPS in Figure 5.17, TEC depletion in multiple PRNs which is associated with the high values of ROTI index is observed.

On 14-15 May 2005 (SSC at ~21:30 LT), Jicamarca ionosonde observations shows gradual rise in h'F after local sunset but significant clear increase is seen at ~21:30 LT which coincides with the onset of geomagnetic storm (Figure 5.14 (b)). In radar backscattere map in Figure 5.13(b), it can be seen that after 21:30 LT, irregularities start to become strong and rising plume structure is seen between 22:00 and 23:00 LT with altitude range of 300 to 450 km. This coincides with the SSC. The rising plume started to descend after 22:45 LT and again a strong band structure is seen up to 00:45 LT. This band structure is ended with huge rising plume at ~ 01:00 LT which coincides with the main phase of the storm. This second plume drifted up to more than 1000 km vertically.

At AREQ the local time of SSC is ~21:45 LT and at GLPS is ~ 20:30 LT. When we look into the GPS observations at AREQ and GLPS, it can be seen that AREQ GPS observation in Figure 5.16 shows significant scintillation and TEC depletion between 23:15 LTand 2:15 LT which coincides with the local time of

main phase at AREQ and second rising plumes of RTI map at Jicamarca. At GLPS TEC depletion and associated scintillation in ROTI values are seen after ~21:00 LT i.e. half an hour after the local SSC time at GLPS (Figure 5.18). On 15 May 2005, the scintillation is absent up to 21:00 LT at GLPS, after 21:00 LT only scintillation is started to develop and significant signatures are seen in ROTI index which are associated with the TEC depletion between 21:00 LT and 01:00 LT. This significant scintillation and associated TEC depletion coincided with the local time of main phase of the storm at GLPS and also with the second rising ESF plume at Jicamarca.

The h'F rise at 21:30 LT and simultaneous generation of ESF as shown in RTI map at Jicamarca instantaneously at SSC time indicates that prompt penetration of eastward electric field immediately after SSC provides platform for ESF generation on 14-15 May at Jicamarca. The second huge plume at 00:45 LT, significant L-band scintillation at AREQ and GLPS before and after midnight provides evidence for the penetration of intense eastward electric fields over the equator which prevailed over the ambient westward electric fields leading to development of strong ESF after mid night. This corroborates with the previous report by *Ram et al.*, [2008]. Using the data from different longitude sectors, they explained the role of storm time prompt penetration of electric field in the occurrence of ESF.

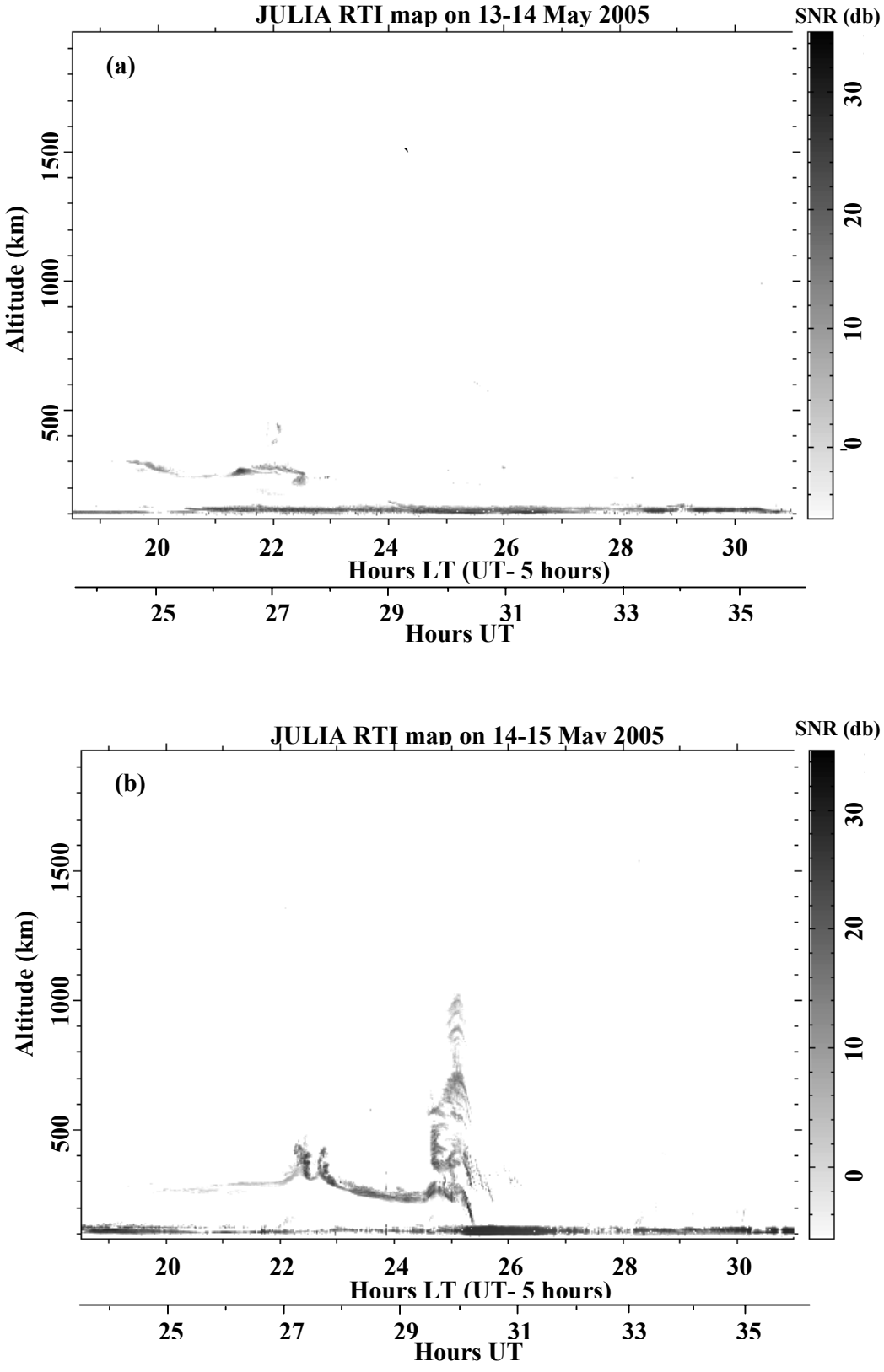

Figure 5.13: JULIA RTI map on (a) 13-14 may 2005 (b) on 14-15 May 2005

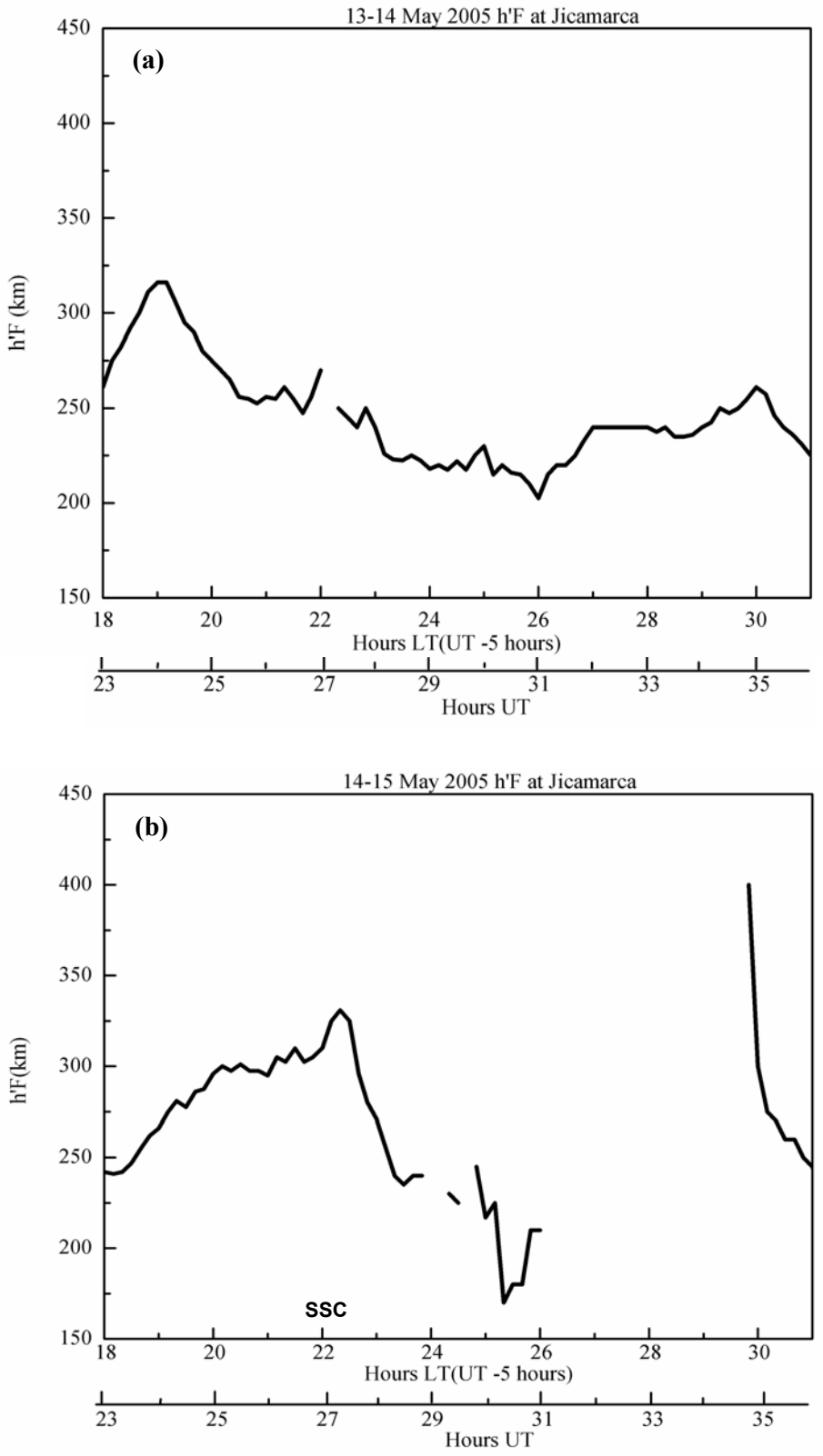

Figure 5.14: (a) h'F variations at Jicamarca on 13-14 May 2005 (b) h'F variations at Jicamarca on 14-15 May 2005

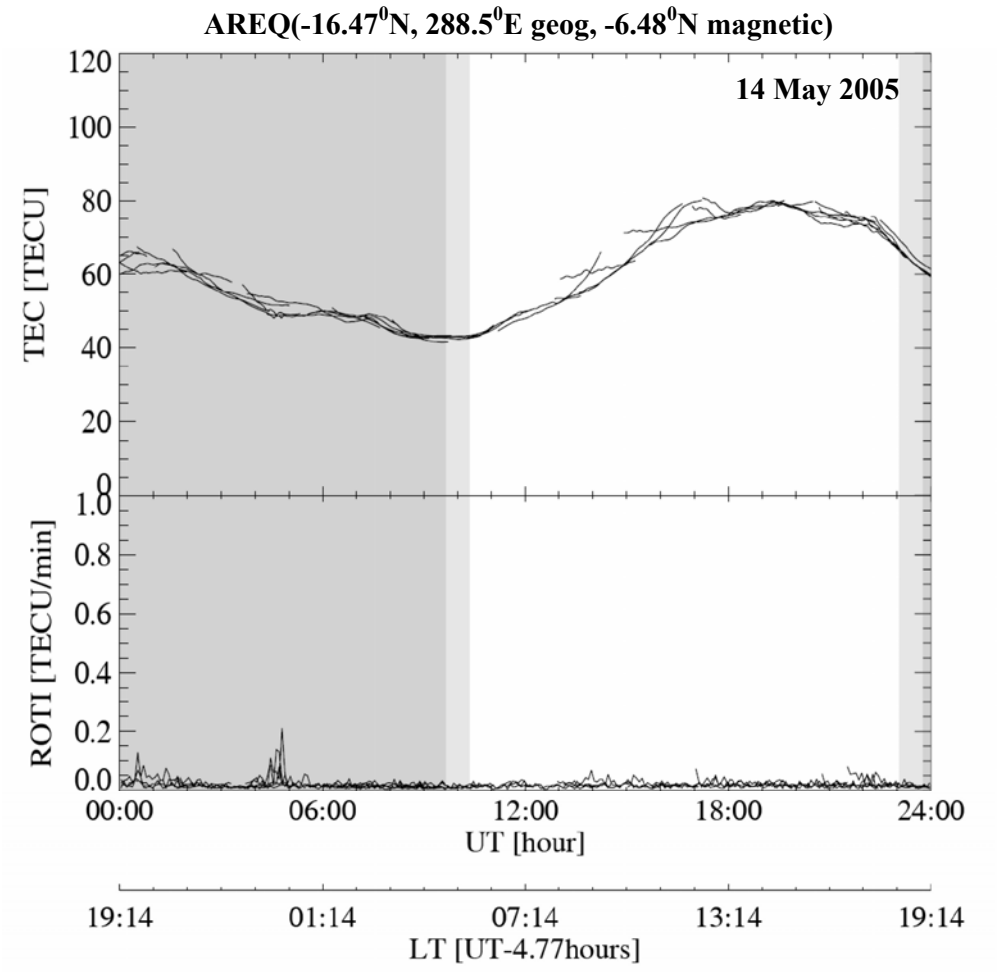

Figure 5.15: Diurnal TEC and ROTI variations at AREQ on 14 May 2005

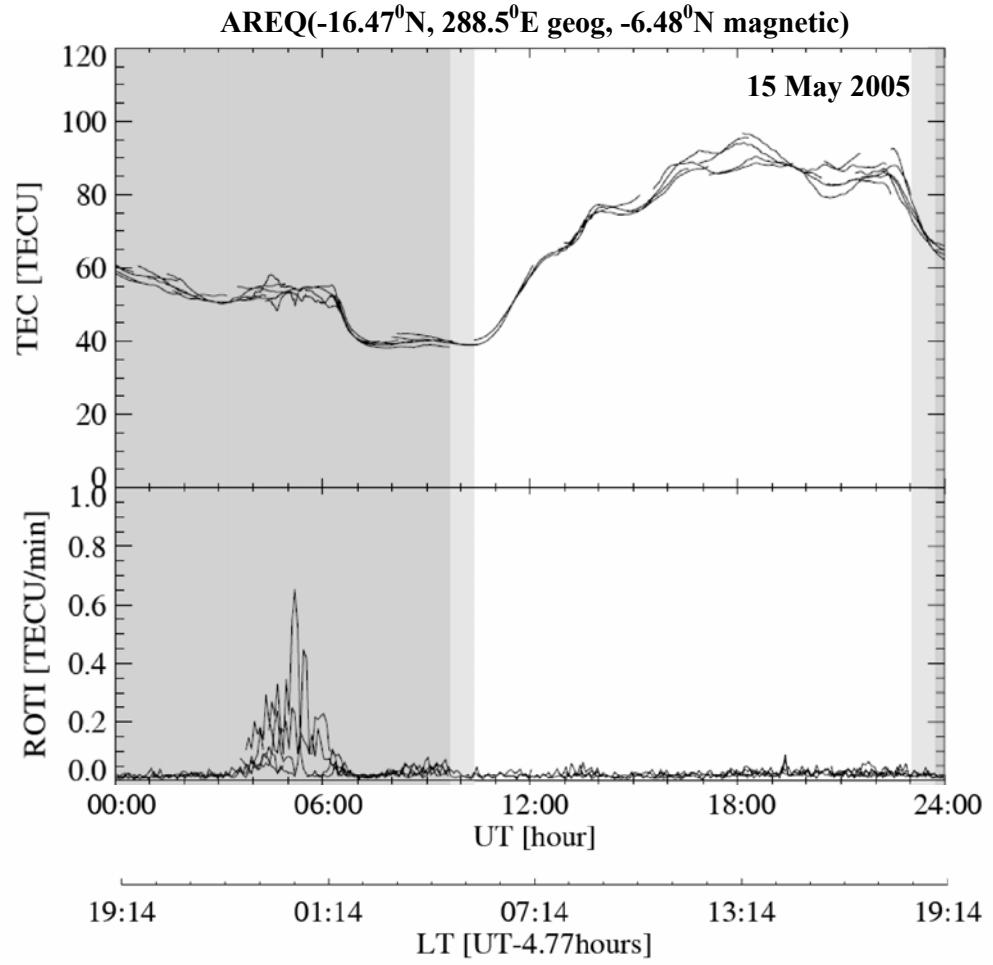

Figure 5.16: Diurnal TEC and ROTI variations at AREQ on 14 May 2005

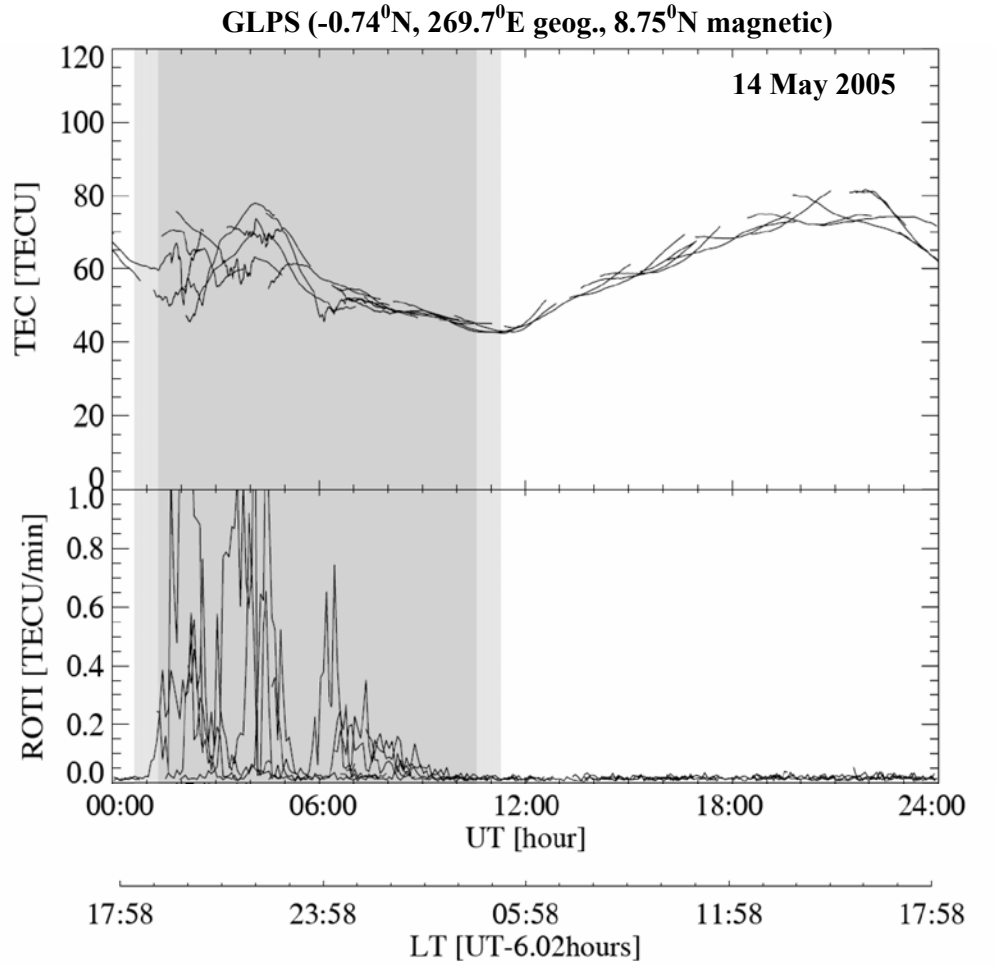

Figure 5.17: Diurnal TEC and ROTI variations at GLPS on 14 May 2005

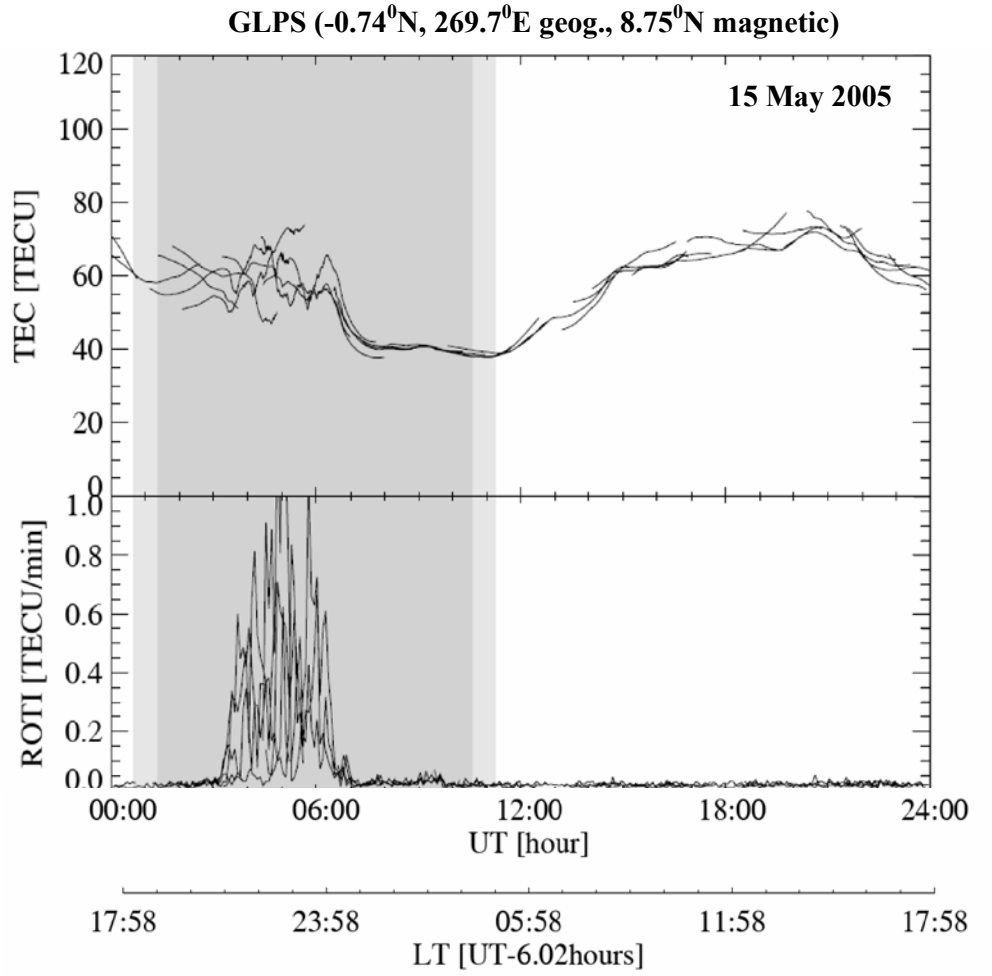

Figure 5.18: Diurnal TEC and ROTI variations at GLPS on 15 May 2005

5.5 Storm of 24 August 2005

The storm of 24 August 2005 probably is the last intense storm of the solar cycle 23. Figure 5.19 shows the interplanetary and geomagnetic conditions during 24 August 2005 storm. The shaded region shows the disturbed condition. The storm started with Bz value of ~-5 nT at ~ 11:18 IST (Figure 5.19(a)). The appropriate time delay is incorporated by the method described in detail in *Chakrabarty et al.*, [2005] to translate the Bz values and IEFy values to the earth's ionosphere. The time delay varies from 30 minutes to 1 hour for the present storm. The AE index started to show the storm signature at ~11:27 IST (Figure 5.19(b)). From SYM-H index variations (Figure 5.19(c)), it can be said that SSC occurred at ~11:55 IST and SYM-H values raised to 62 nT at 12:06 IST. After this, SYM-H values fluctuated for ~2 hours and then descending of SYM- H is started. At 13:55 IST a second commencement in SYM-H is occurred which is accompanied by sudden increase in Bz of ~49 nT at ~14:30 IST. After this Bz turned southward and reached to minimum value of -51 nT at ~15:00 IST. The second commencement in SYM-H reached to 74 nT at ~ 14:55 IST. This increase in SYM-H is followed by initiation of main phase of this storm. A sudden increase in AE of 3078 nT is occurred almost at the same time. During main phase the minimum of SYM-H is occurred at ~17:40 IST with value of -179 nT. The IEFy values boosted to ~31 mV/m on occasion at 15:31 IST. This value decreased to -14 mV/m at ~ 17:00 IST incorporation with northward turning of Bz. Again an increase in IEFy is seen ~17:30 IST and it has reached to value of ~20 mV/m which is incorporation with southward turning of Bz. Finally this IEFy enhancement again decreases to ~17 mV/m at ~18:26 IST and then slowly recovered to normal level by 22:36 IST. These fluctuations of IEFy coincide with the main phase of the storm. The recovery of the main phase started ~18:30 IST.

5.5.1 Low Latitude ionospheric - thermospheric behavior during 24-27 August 2005

The low latitude ionosphere – thermosphere response to the disturbed condition of 24 August 2005 has been analyzed using GPS TEC data recorded at Rajkot and $[O]/[N_2]$ variations observed by GUVI respectively. Figure 5.20 shows

the diurnal variation of TEC at low latitude station Rajkot during 23 to 27 August 2005 along with the quiet days' (Ap<4) mean TEC of the month. On 23 August, on day before the SSC day, TEC almost follows the quiet days' TEC values.

On 24 August, TEC shows an enhancement of 21 TECU at ~15:30 IST with respect to average quiet days' values. This is just after the minimum of Bz and initiation of main phase of the storm. The maximum of IEFy is occurred almost at the same time. The observed TEC enhancement is attributed to prompt penetration of storm time electric field to low latitudes. The rate of change of SYM-H exhibits a sharp negative excursion of -35 nT/10 min at 15:10 IST. The sudden increase in AE index and marked decrease in SYM-H index under southward orientation of IMF Bz creates favorable conditions for the prompt penetration to occur. Figure 5.21 shows the diurnal variations of EEJ on (a) 24 August 2005 (b) 25 August 2005 and (c) 26 August 2005 (d) 27 August 2005. The observed strong EEJ with maximum strength of 69 nT on 24 August (Figure 5.21(a)) also incorporates the IEFy penetration. It can be seen from EEJ variations on 24 August that the diurnal pattern has already started to decrease after 12:00 IST. But at 14:00 IST a sudden increase in EEJ is observed which reached to day maximum of 69 nT at 15:00 IST. The Bz minimum, second commencement and large increase in IEFy are occurred between 14:00 IST and 15:00 IST only. We could not present the EEJ values with high time resolution for this storm. Thus the exact timing information cannot be found. But it can be said that the enhancement in EEJ after 14:00 IST may be due to prompt penetration of storm time electric field to low latitudes.

As it is discussed in the previous case of 15 May 2005 storm that prompt penetration of eastward electric field in the dayside sector results into the development of strong EIA and thus electron density at low latitudes enhances. In addition to this, the penetrated electric field raises the whole ionosphere upward where the recombination rate is low thus the electron density increases.

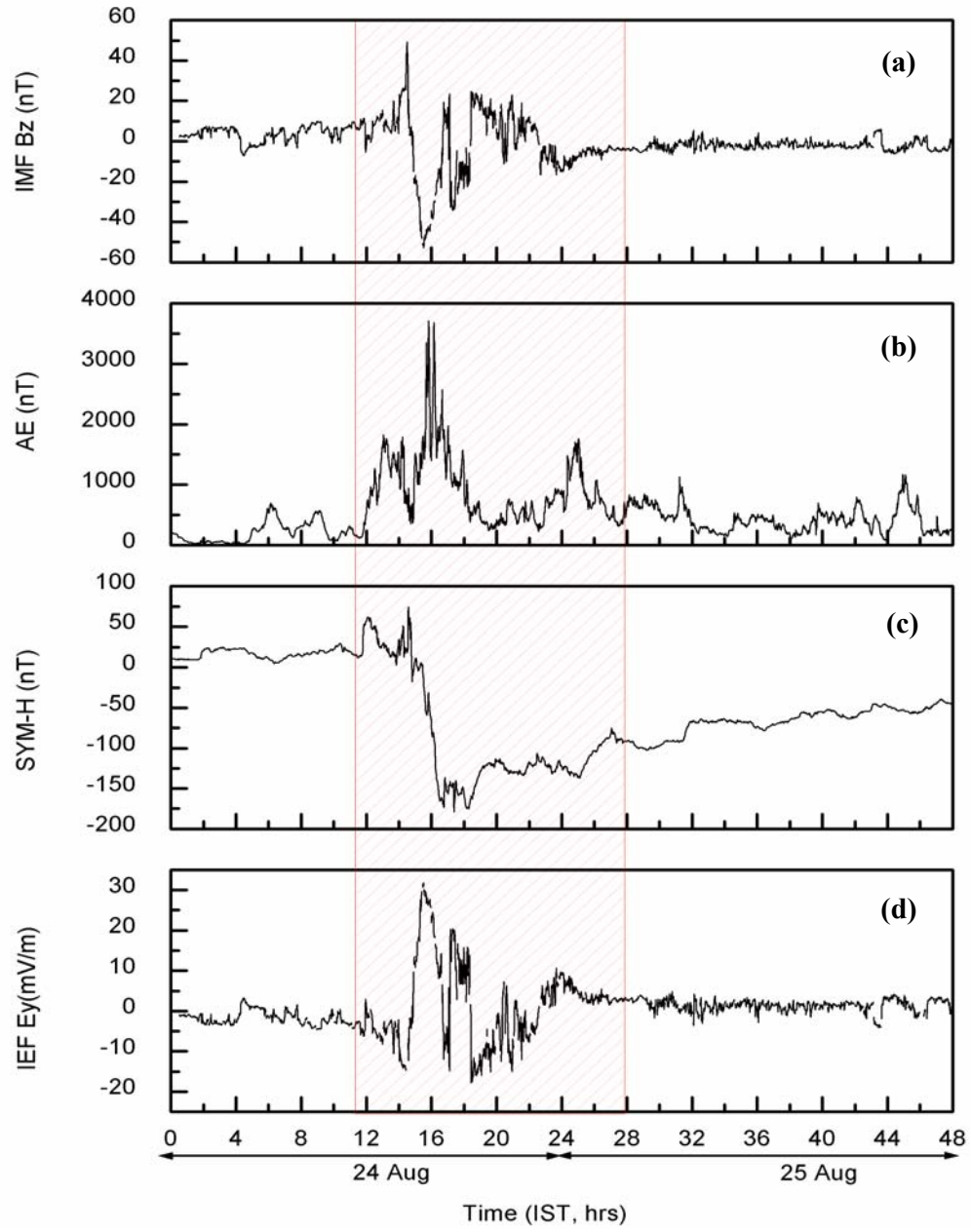

Figure 5.19: Interplanetary and geomagnetic conditions during 24 August 2005 storm. From top the temporal variations of (a) IMF Bz (b) AE index (c) SYM-H index (d) IEFy with time lag correction respectively on 24 and 25 August 2005

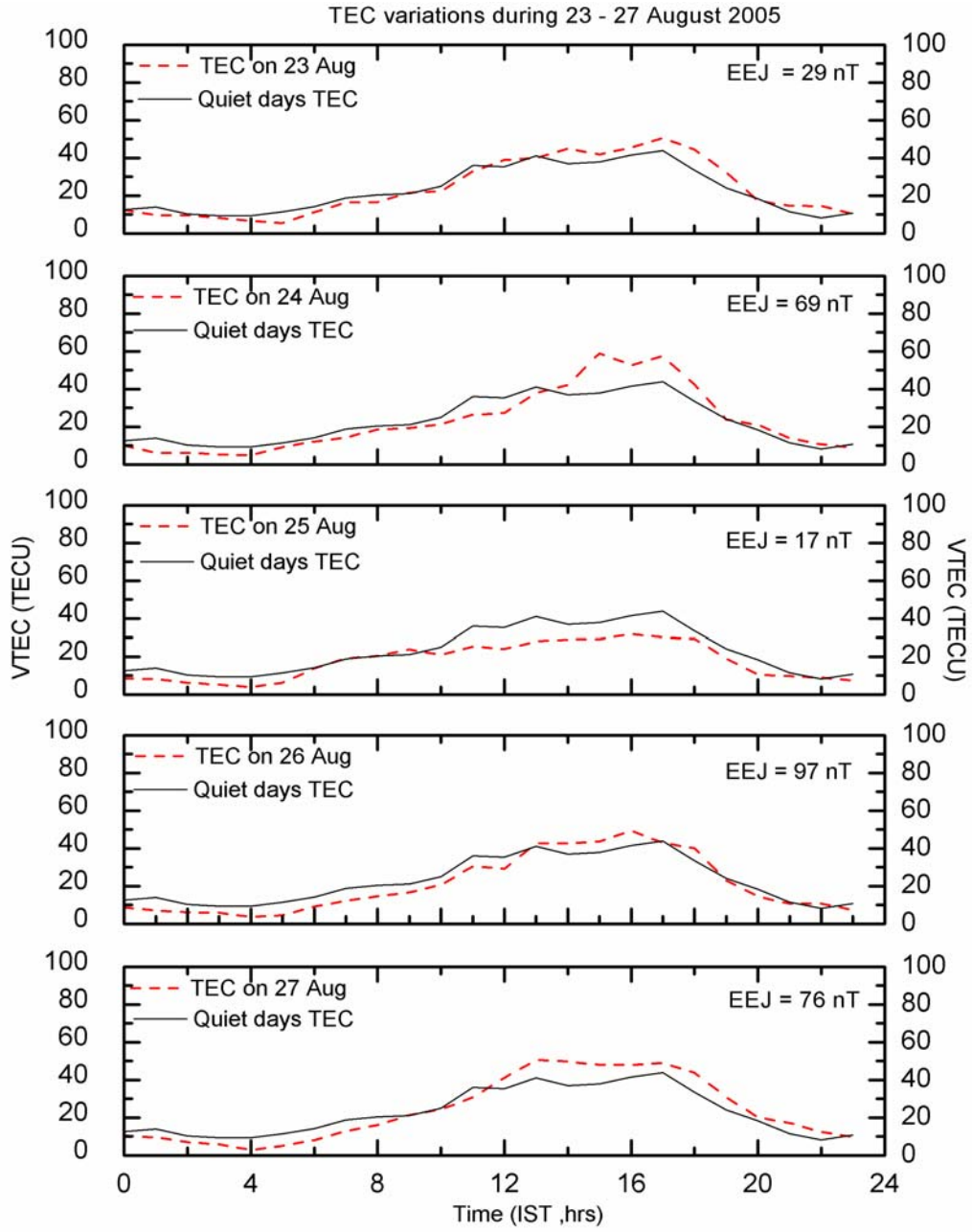

Figure 5.20: Diurnal variations of TEC at low latitude station Rajkot during 23 to 27 August 2005 along with quiet days' (Ap<4) mean TEC of the month

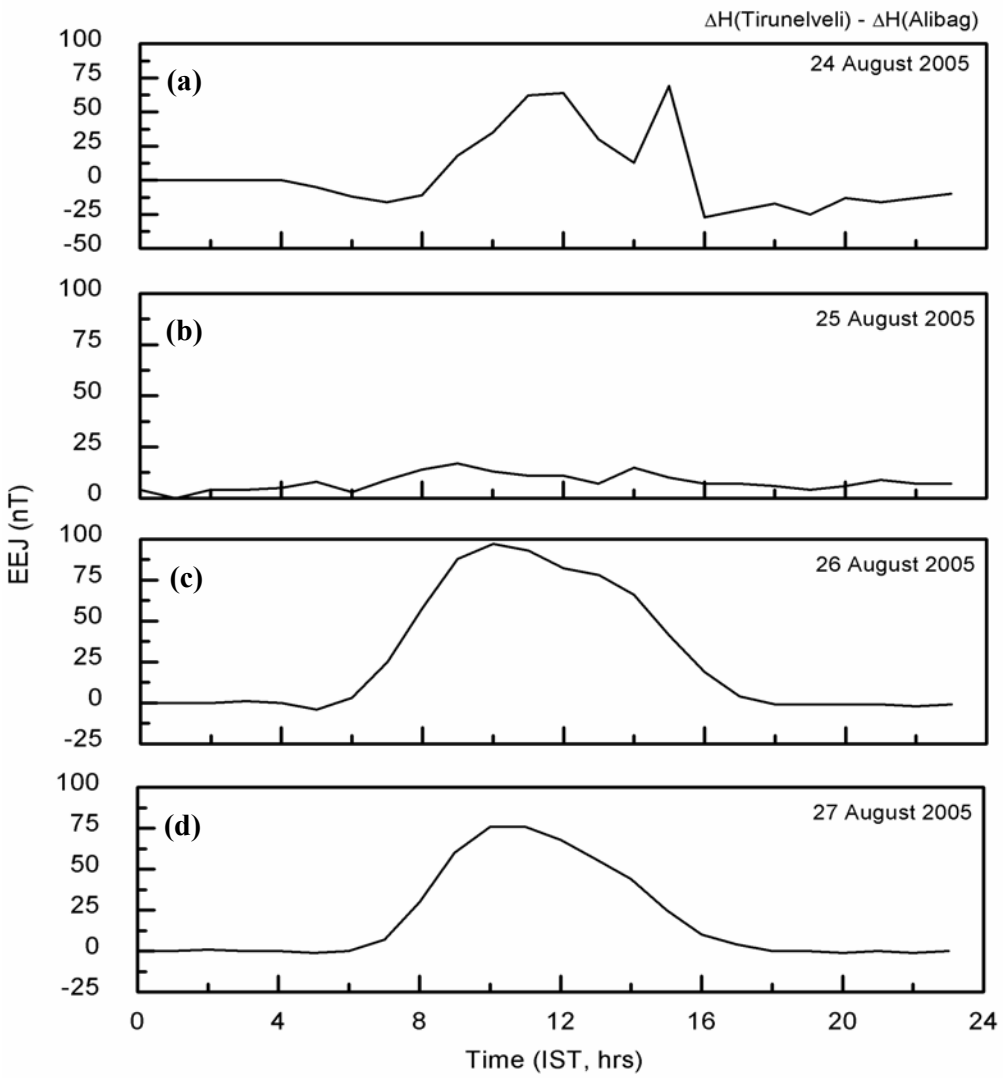

Figure 5.21: Diurnal variations of EEJ on (a) 24 August 2005 (b) 25 August 2005 (c) 26 August 2005 (d) 27 August 2005

On 25 August, TEC decreases with respect to average quiet day's values (Figure 5.20). The maximum depletion is observed of ~18 TECU at 13:00 IST. The observed negative storm is attributed to either long lived disturbance dynamo electric field penetration to low latitudes or neutral composition changes. The EEJ variations on 25 August show the presence of CEJ and day maximum occurred at 17 nT only. The inhibition of EEJ on 25 August is the clear evidence of penetration of storm time disturbance dynamo electric field to low latitudes. Due to the weak EEJ, EIA might not have developed strong. Thus low latitude TEC decreases with respect to average quiet day's values.

To examine the neutral composition $[O]/[N_2]$ variations we have looked in to the TIMED/GUVI images for the day. The continuous TIMED/GUVI data is not available, the temporal domain of the data which we have extracted for this event varies from 10:50 IST to 12:50 IST for Indian region. Figure 5.22 shows $[O]/[N_2]$ variations over Indian region during (a) 24 August 2005 (b) 25 August 2005 (c) 26 August 2005 (d) 27 August 2005 as observed by GUVI onboard the TIMED NASA satellite. On 24 August a clear enhancement in $[O]/[N_2]$ is observed. On 25 August the $[O]/[N_2]$ values are decreasing to 0.411 from 0.683 observed on 24 August 2005. The enhancement in $[O]/[N_2]$ contributes to the observed positive ionospheric storm on 24 August while the depletion in $[O]/[N_2]$ contributes to the observed negative ionospheric storm on 25 August. Thus the observed storm time TEC behavior on 24 and 25 August 2005 is controlled by the electrodynamical as well as neutral dynamical coupling between high and low latitudes.

TEC enhancements on 26 and 27 August with respect to average quiet day's values (Figure 5.20) are the point of special interest in this storm. These enhancements are during the recovery phase of the storm. It can be seen from EEJ variations in Figure 5.21 that on both the days EEJ strength is strong. On 26 August, TEC enhancement of ~6 TECU with respect to quite day's average values is observed. On 27 August, TEC enhancement of ~15 TECU is observed.

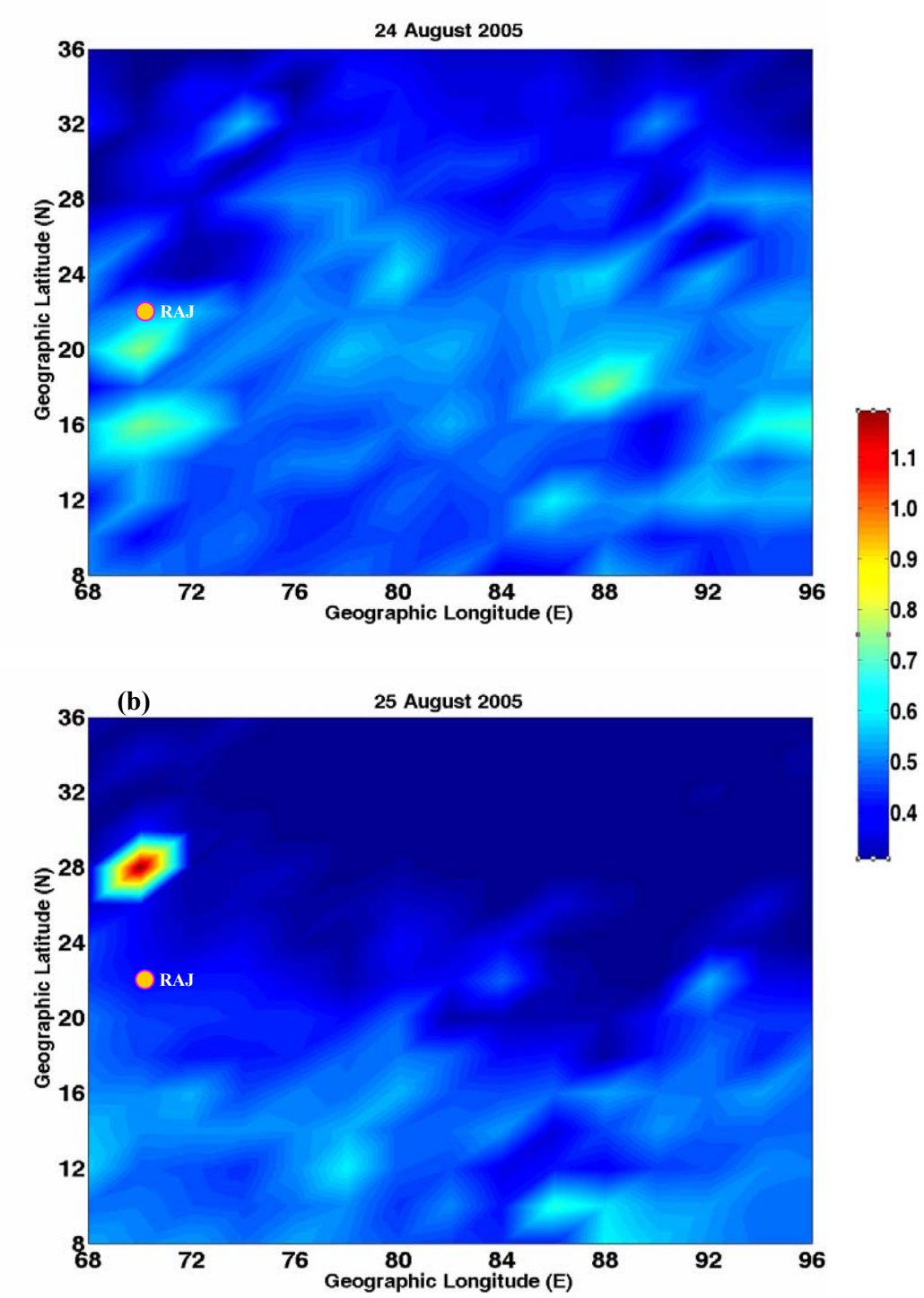

Figure 5.22: [O]/[N_2] variations for Indian lat- long sectors during (a) 24 August 2005 (b) 25 August 2005 observed by GUVI onboard the TIMED NASA satellite

From Figure 5.22(c) and (d) it is observed that $[O]/[N_2]$ values are getting recovery on 26 and 27 August, after decreasing significantly on 25 August at low latitudes. But still on 26 August the effect of excess molecular species is observed in TEC at low latitudes. In the presence of strong EEJ (97 nT), EIA might have developed strongly but the neutral composition variations are dominating the TEC behavior at low latitudes on 26 August.

On 27 August, TEC enhancement is strong. The observed EEJ strength on 27 August is also high (Figure 5.21(d)) which results in to the strong EIA and thus TEC at low latitudes increases. In addition to this, there is a clear increase in $[O]/[N_2]$ around Rajkot region which also contributes in to the observed TEC enhancement.

Fejer and Emmert, [2003] reported low latitude ionospheric electric field perturbations due to both prompt penetration and disturbance dynamo electric fields during the recovery phase of the storm. The observed positive storm on 26 and 27 August may due to prompt penetration electric field during the recovery phase of the storm. The observed strong EEJ strength on both the days also provides strong evidences of prompt penetration electric fields. In addition to this, the recovery in neutral composition variations, after decreasing on 25 August, $[O][N_2]$ values are gradually increasing on 26 August and 27 August, also contributes in to the TEC enhancements at low latitudes.

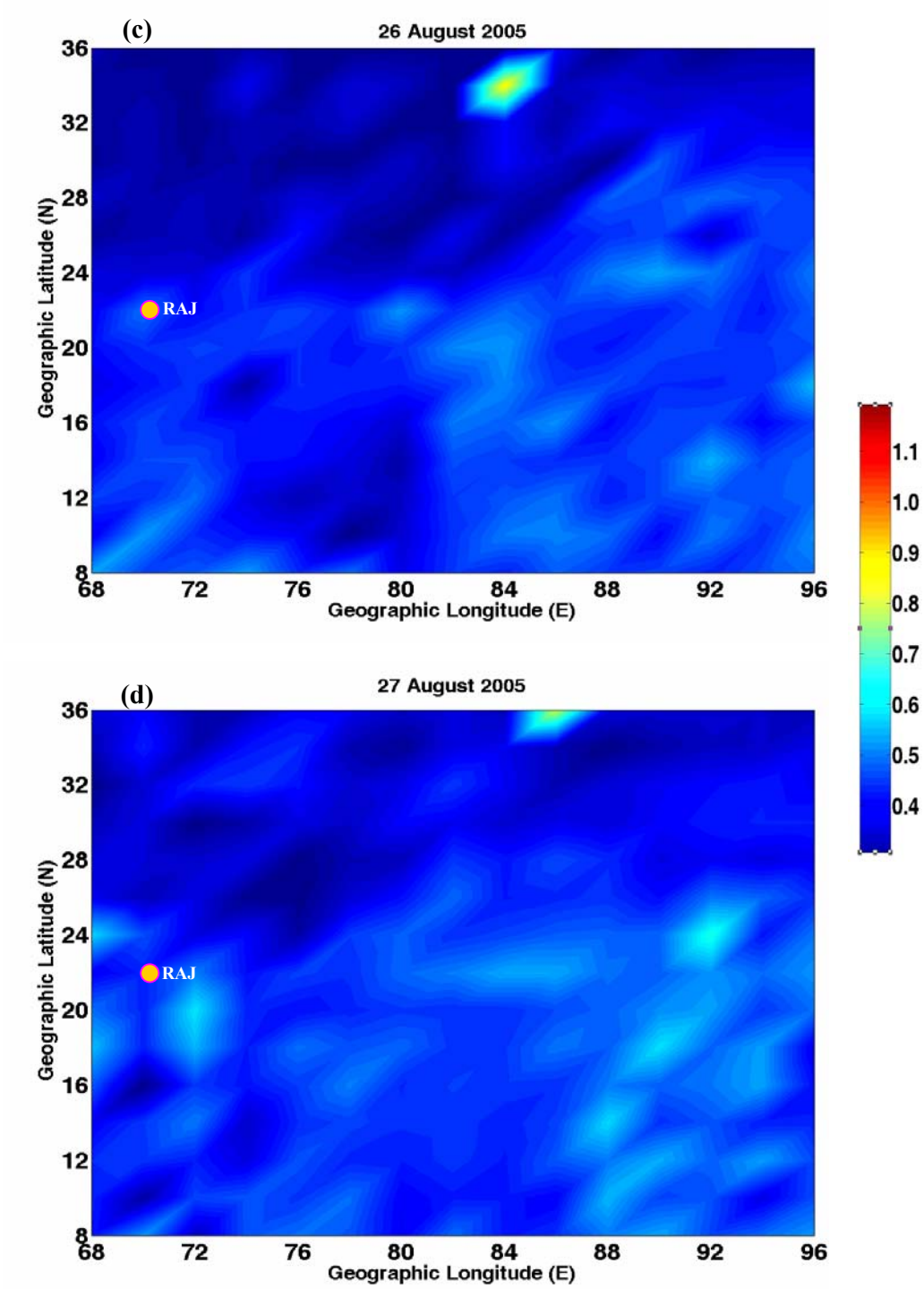

Figure 5.22: [O]/[N_2] variations for Indian lat- long sectors during (a) 26 August 2005 (b) 27 August 2005 observed by GUVI onboard the TIMED NASA satellite

5.6 Storm of 8-9 May 2005

This storm has occurred with two main phases first on 8 May and the second on 9 May as shown in Figure 5.23. The interplanetary and geomagnetic conditions during the storm are shown in Figure 5.23. The first panel from the top shows the temporal variations of IMF Bz, second panel shows the temporal variations of AE index, third panel shows the temporal variations of SYM-H, and fourth panel shows the temporal variations of IEFy at the ionosphere. The IEFy is corrected for the time delay from ACE spacecraft to the earth's ionosphere as per the method described in *Chakrabarty et al.,* [2005].

The IMF Bz turned southward at 20:45 IST on 7 May and first SSC impact for the storm occurred at 01:51 IST on 8 May. The main phase is started with this and SYM-H minimum occurred at 8:52 IST on 8 May with value of -102 nT. The recovery phase is started after this and continued up to 18:00 IST on 8 May. After showing recovery up to 18:00 IST, the second main phase is started and SYM-H reached to a minimum value of -117 nT at 02:30 IST on 9 May. After this prolonged recovery phase started and remained continue up to the date of 13 May (figure not shown here). The main phase on 8 May is accompanied by AE increase of ~1250 nT and main phase of 9 May is accompanied by AE increase of ~2079 nT. The IEFy varies between -15 mV/m to 14 mV/m during this storm.

5.6.1 Low latitude ionospheric- thermospheric response to the storm

To examine the low latitude TEC variations during the storm we have plotted diurnal TEC variations recorded at Rajkot from 7 to 11 May 2005 along with the quiet days' (Ap<4) mean TEC of the month as shown in Figure 5.24. TEC on 7 May follows almost quiet days' values. On 8 May, TEC increase of 8 TECU with respect to quiet days' mean TEC is seen. On 9 May, TEC depletion of 14 TECU with respect to quiet days' mean TEC is observed. On 10 and 11 May, TEC increase of 16 and 11 TECU is observed respectively.

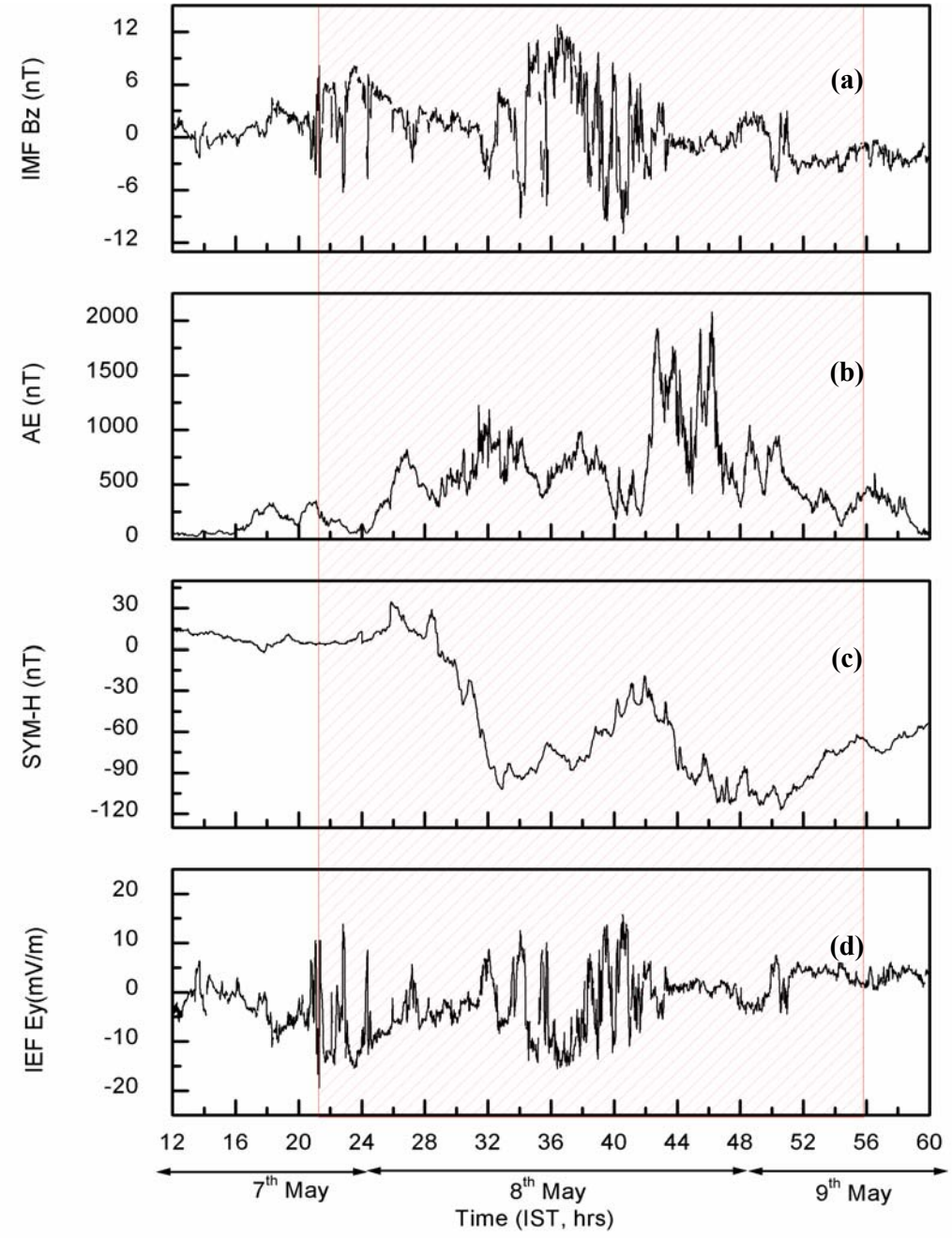

Figure 5.23: Interplanetary and geomagnetic conditions during 8-9 May 2005 storm. From top the temporal variations of (a) IMF Bz (b) AE index (c) SYM-H index (d) IEFy with time lag correction respectively during 7 to 9 May 2005

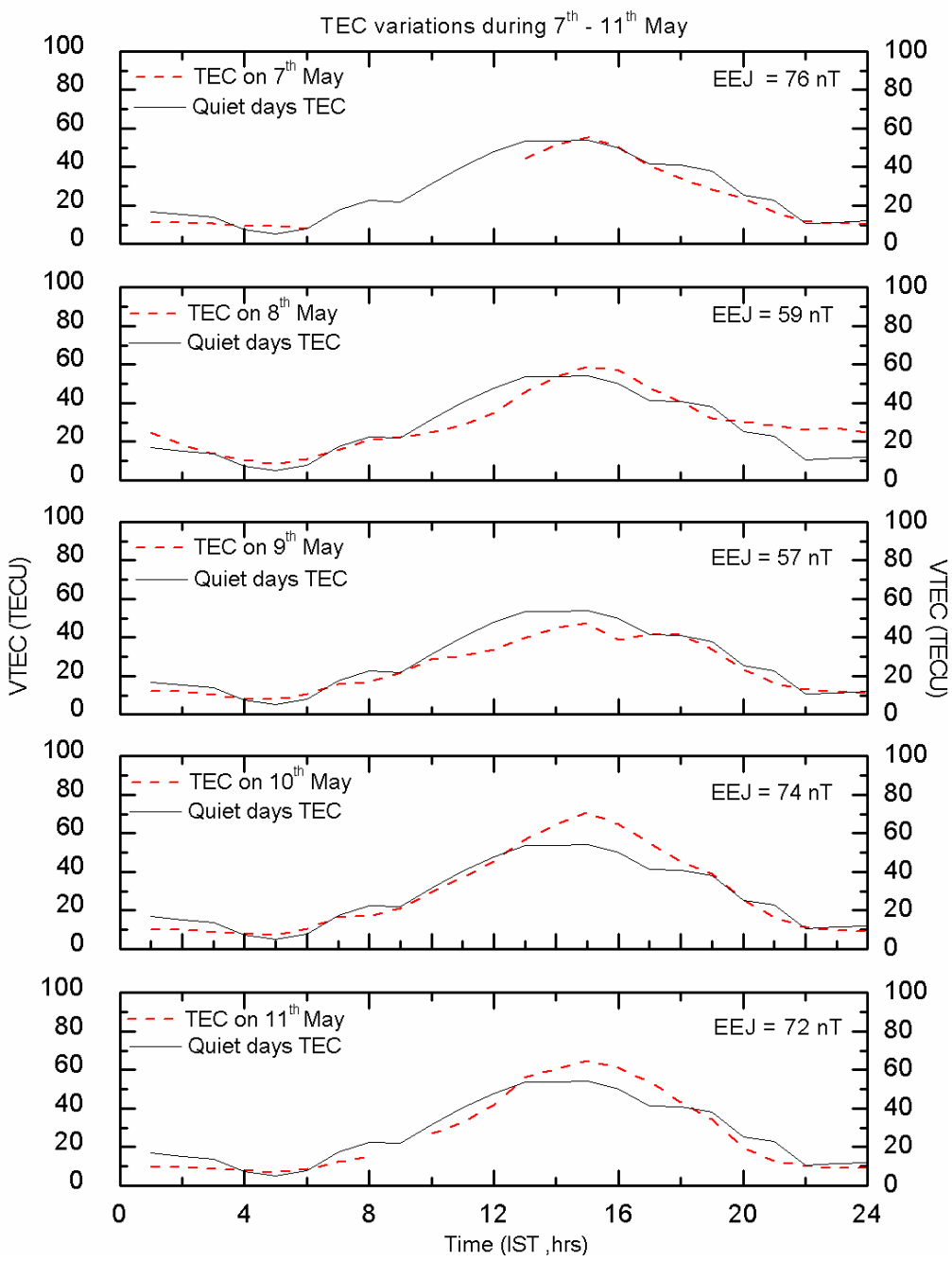

Figure 5.24: Diurnal variations of TEC at Rajkot during 7 May 2005 to 11 May 2005 along with the quiet days' (Ap<4) mean TEC of the month

Figure 5.25 shows the diurnal variations of EEJ on (a) 8 May 2005 (b) 9 May 2005 (c) 10 May 2005 (d) 11 May 2005. To examine the neutral composition $[O]/[N_2]$ variations we have looked in to the TIMED/GUVI images during 8 to 11 May 2005. The continuous TIMED/GUVI data is not available, the temporal domain of the data which we have extracted for this event varies from 12:45 IST to 16:00 IST for Indian region. Figure 5.26 shows the $[O]/[N_2]$ variations for Indian lat- long sectors during (a) 8 May 2005 (b) 9 May 2005 (c) 10 May 2005 and (d) 11 May 2005 as observed by GUVI onboard the TIMED NASA satellite.

Diurnal TEC variations on 8 May shows depletion in TEC with respect to quiet day's mean between 8:00 IST and 12:00 IST. From diurnal pattern of EEJ in Figure 5.25(a), the morning counter electrojet is observed on 8 May. This may be due to penetration of disturbance dynamo electric field which is westward in general and hence reduces the EIA strength. Thus the percentage values of plasma at crest latitudes decrease. The disturbance dynamo electric field usually gets activated after 4-5 hrs of SSC, the SSC for this storm occurred at 01:51 IST on 8 May, the observed EEJ and TEC behavior in morning hours hence provides evidence for the penetration of disturbance dynamo electric field. TEC pattern between 14:00 and 18:00 IST shows noticeable increase in TEC with respect to quite days' mean.This may be due to resurge of EIA in the afternoon hours as the EEJ strength increases with the day time. The $[O]/[N_2]$ variations (Figure 5.26(a)) show the distribution almost equal to quiet period.

The night time L-band scintillation and TEC depletion are observed on 8-9 May 2005 at Rajkot. Figure 5.27(a) – (d) shows the L-band scintillation and TEC depletion as observed by different PRNs on 8-9 May 2005. In Figure 5.27(a), scintillation detected by PRN 23 between 20:58 and 21:20 IST, in Figure 5.27(b) scintillation detected by PRN 13 between 20:25 IST and 21:45 IST are shown. In Figure 5.27(c), scintillation detected by PRN 8 with S4 value of 0.24 and TEC depletion of ~ 5 TECU at ~23:09 IST is shown. In Figure 5.27(d), PRN 28 is also showing significant scintillation around and after the midnight. The observed scintillation is post sunset and seen after the starting of second main phase and second sudden increase in AE index. The prompt penetration of IEFy of 5 mV/m

at ~19:15 IST on 8 May (Figure 5.23 (d)) may be responsible for generation of low latitude spread-F irregularities and hence L-band scintillation.

On 9 May negative ionospheric storm is observed as shown in Figure 5.24. This may be the result of again long lived electrodynamic disturbances due to the disturbance dynamo electric field which is in general westward during day. The moderate EEJ value of 57 nT (Figure 5.25(b)) also aggress with this. The neutral composition variation in terms of $[O]/[N_2]$ ratio show enhancement on 9 May in comparison to 8 May (Figure 5.26(b)) . But no major effects are seen of its in TEC variations.

The strong EEJ values of 74 nT and 72 nT on 10 and 11 May respectively (when storm was in recovery phase) might have resulted in strong EIA. Thus significant TEC increase is seen in terms of positive ionospheric storm on both 10 and 11 May at Rajkot. As discussed in the previous case of 24 August storm, here also the observed positive ionospheric storms during recovery phase on 10 and 11 May might be due to eastward prompt penetration of IEFy. The strong EEJ on both the days also agrees with this. As we have discussed in section 5.4, TEC enhancement on 14 May resulted during the prolonged recovery phase of 8 May storm.

The $[O]/[N_2]$ values are enhanced on 10 May (Figure 5.26(c)) and decreased on 11 May (Figure 5.26 (d)) at low latitudes. The enhanced $[O]/[N_2]$ may be one of the reasons for TEC enhancement on 10 May. Thus for the case of 10 and 11 May, how much neutral composition variations have contributed in positive ionospheric storm that still requires further investigation.

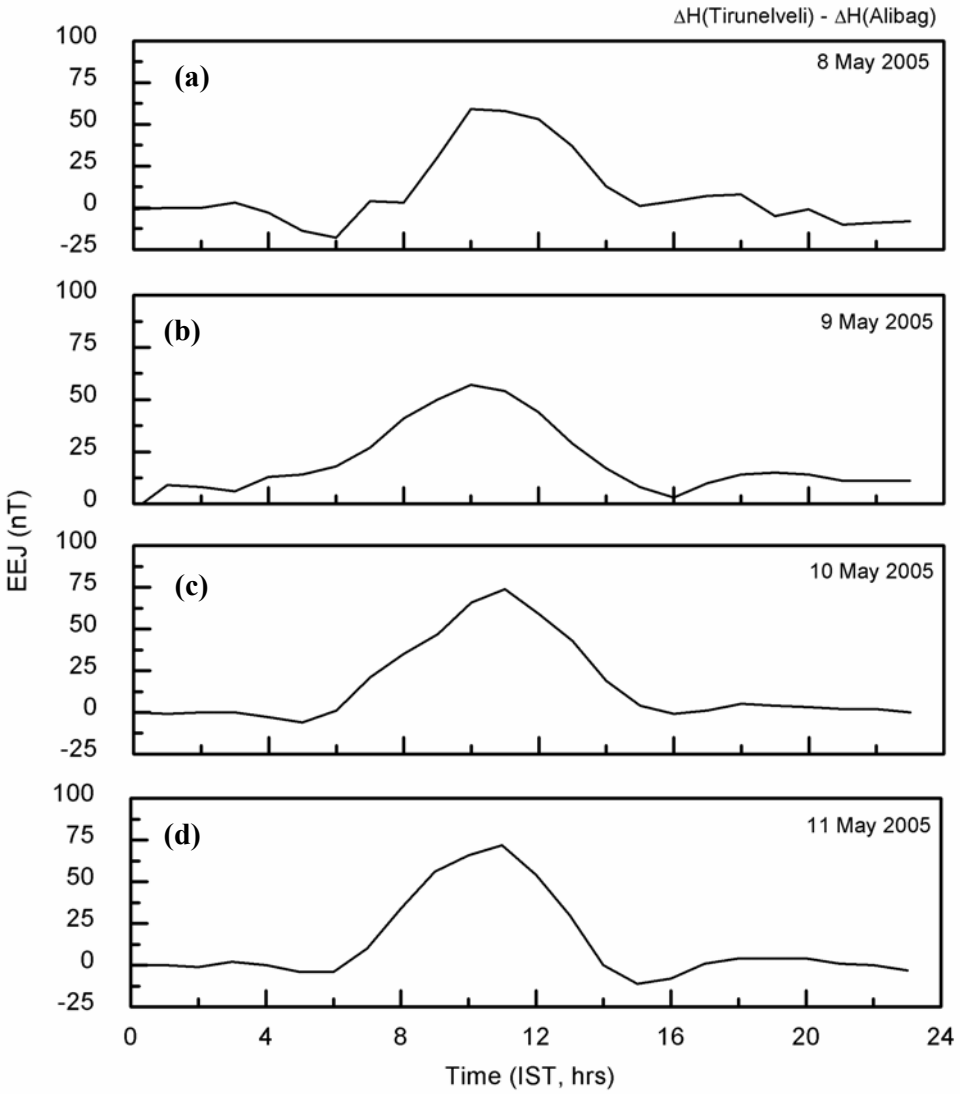

Figure 5.25: Diurnal variations of EEJ on (a) 8 May 2005 (b) 9 May 2005 (c) 10 May 2005 (d) 11 May 2005

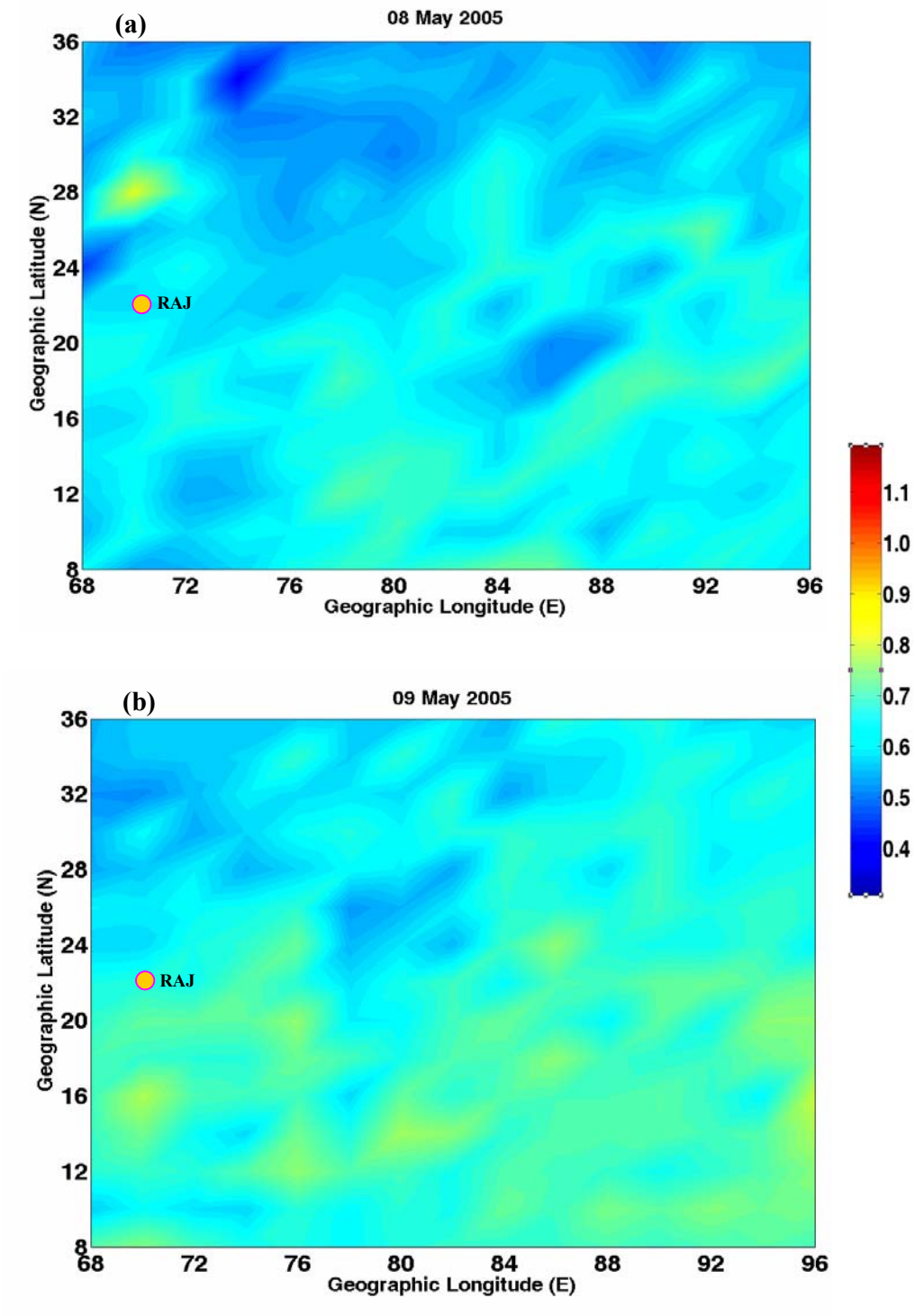

Figure 5.26: [O]/[N_2] variations for Indian lat- long sectors during (a) 8 May 2005 (b) 9 May 2005 observed by GUVI onboard the TIMED NASA satellite

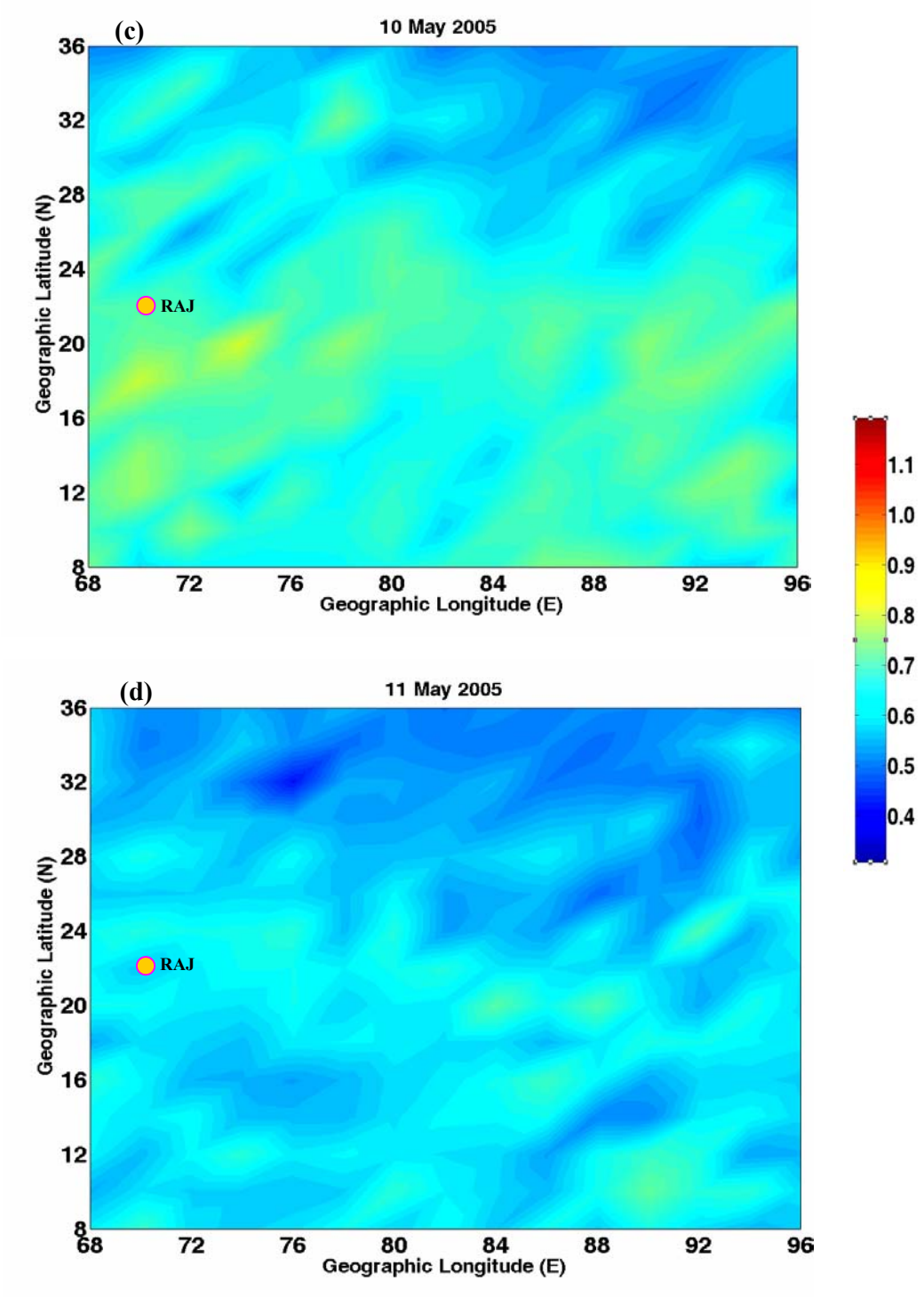

Figure 5.26: [O]/[N_2] variations for Indian lat-long sectors during (c) 10 May 2005 (d) 11 May 2005 observed by GUVI onboard the TIMED NASA satellite

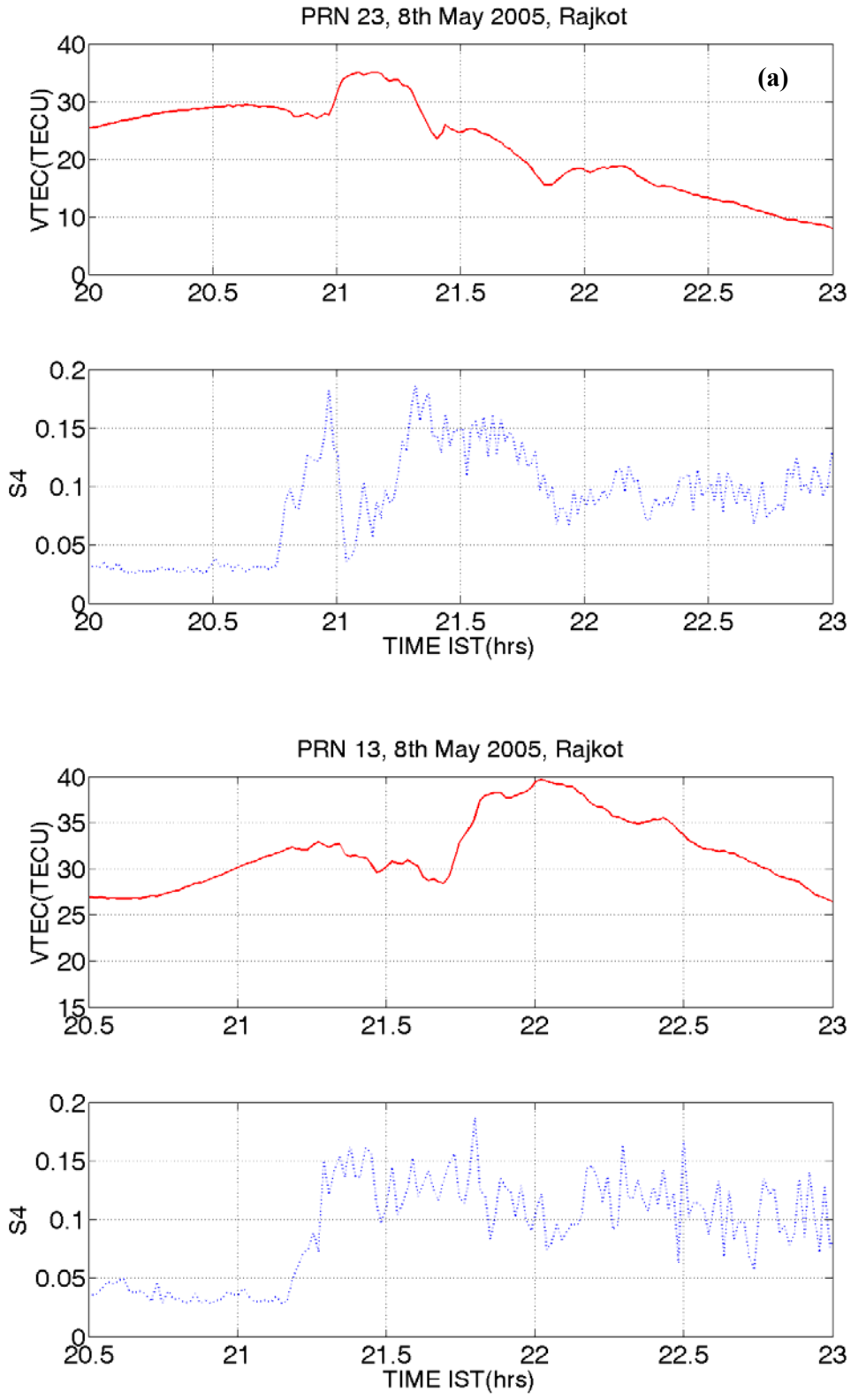

Figure 5.27: L-band scintillation and associated TEC depletion as observed by (a) PRN 23 and (b) PRN 13 on 8 - 9 May 2005

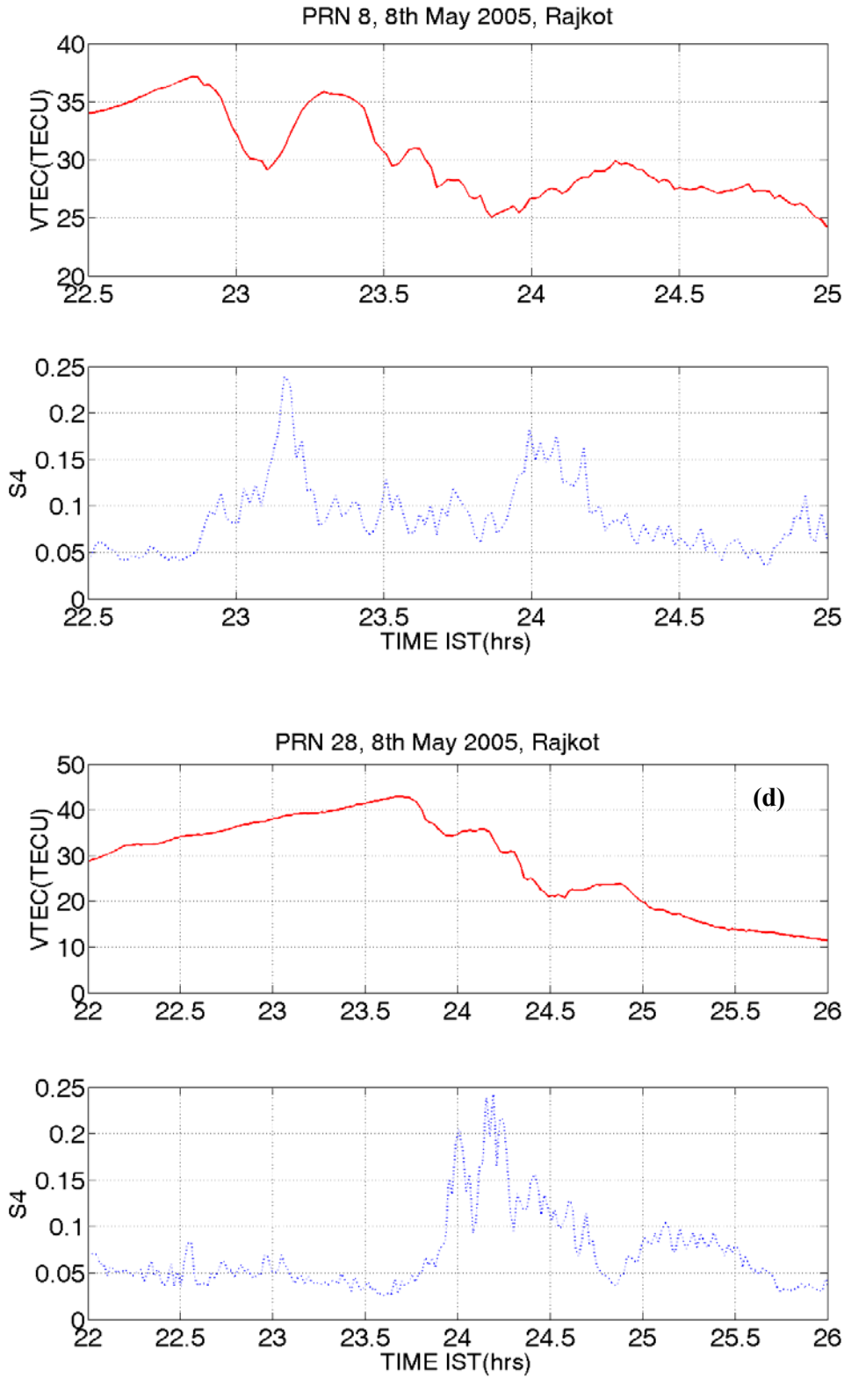

Figure 5.27: L-band scintillation and associated TEC depletion as observed by (c) PRN 8 and (d) PRN 28 on 8 - 9 May 2005

5.7 Conclusion

A detailed investigation is carried out on storm time electrodynamical and neutral dynamical coupling and its influences on the equatorial and low latitude ionosphere – thermosphere system for 15 May 2005, 24 August 2005 and 8-9 May 2005 storm. The results and discussions presented in above sections have shown the storm time ionospheric perturbations due to either prompt penetration electric field or storm time neutral composition changes/disturbance dynamo electric field which leads to positive or negative ionospheric storms respectively. The prompt penetration of eastward electric field to equatorial and low latitude leads to development of strong ESF where conditions was not much conducive for strong ESF generation before the onset of storm. It is shown that storm time thermospheric neutral composition variations have great influence on ionospheric electron density.

The main results of this study can be concluded as follow:

The storm of 15 May:

(1) TEC enhancements at EIA trough latitudes are observed on day before SSC i.e. 14 May 2005 which may be the post effect of high auroral activity on 13 May 2005 in terms of neutral composition variations. But the role of aftermath of previous geomagnetic activity of 8-9 May 2005 in terms of penetration of disturbance dynamo electric field during prolonged recovery phase of 8-9 May can not be ruled out. (2) The prompt penetration of electric field from high to low latitudes on 15 May 2005 as evident by intensified EEJ and sharp rise in absolute horizontal magnetic field values for Tirunelveli results in to strong positive ionospheric storm in different longitude sectors during daytime. The prompt response of the equatorial and low latitude TEC to CEJ variations on 15 May 2005 between 13:00 IST hrs and 16:00 IST hrs shows strong electrodynamical coupling between low and equatorial latitudes. The sharp and correlated fluctuations in AE, H values, EEJ strength and TEC are clear evidence of high-low latitude electrodynamical coupling during the storm. (3) On 16 May 2005, storm time neutral composition variation results in to higher $[O]/[N_2]$ values along 77-78^{0}E

longitudes with more clearer increase at trough latitudes than crest latitudes. (4) Low latitudes TEC shows negative storm effect on 17 May 2005. Delayed effects as on 16 and 17 May 2005 are evidences of thermosphere / neutral dynamic coupling. It is emphasized by the observations that positive effect of neutral composition variations is seen more clearly at equatorial latitudes i.e. atomics species can penetrate up to equatorial latitudes while negative phase is seen only at Delhi and Rajkot, but not at lower latitudes, indicating that the effect of molecular enhancements does not penetrate beyond some limiting latitudes. (5) Vertically rising strong plume at Jicamarca after midnight as on RTI map and L-band scintillation and associated TEC depletion before and after midnight at AREQ and GLPS GPS observations provide evidence for the prompt penetration of intense eastward electric field over the equator which prevailed over the strong westward electric fields leading to development of strong ESF plumes and significant L-band scintillation after midnight.

The storm of 24 August:

(1) The observed TEC enhancement is attributed to prompt penetration of storm time electric field to low latitudes. The rate of change of SYM-H exhibits a sharp negative excursion of -35 nT/10 min at 15:10 IST. The sudden increase in AE index and marked decrease in SYM-H index under southward orientation of IMF Bz creates favorable conditions for the prompt penetration to occur. (2) The negative storm on 25 August is due to the disturbance dynamo electric field penetration to low latitudes. The observed CEJ on the day also provides evidences for the penetration of storm time disturbance dynamo electric field. In addition to this enhanced molecular species at low latitudes also contributes in to the TEC depletion on 25 August. (3) The positive ionospheric storm and strong EEJ on 26 and 27 August may due to prompt penetration of electric field during recovery phase of the storm. The recovery of neutral composition variations towards the normal level on 26 and 27 August also contributes in to the TEC enhancements.

The storm of 8-9 May:

(1) The daytime TEC at Rajkot shows depletion due to storm time disturbance dynamo electric field penetration in the morning hours on 8 May. The resurge of EIA in the afternoon hours enhances the TEC at low latitudes with

respected to quiet days' mean. During 8 May storm SSC occurred in night time. The prompt penetration of storm time IEFy following the SSC causes low latitude L-band scintillation on 8 May. The prompt penetration of storm time IEFy during the second main phase causes the low latitude L-band scintillation on 8-9 May. (2) The negative ionospheric storm on 9 May may be the delayed effect of the storm in terms of disturbance dynamo electric field. (3) On 10 and 11 May the positive ionospheric storm may be due to prompt penetration of IEFy during recovery phase of the storm. The recovery phase extended up to 14 May. Discussions based on the evidences bring out that during 8 May storm electrodynamical coupling between high and low latitudes dominant the low latitude ionosphere and TEC behavior. The storm time neutral composition variations have no major influences on low latitude TEC.

The multi-instrumental and multistation data presented in this chapter shows all the effects of geomagnetic storms over equatorial and low latitude ionosphere-thermosphere system, and it is also seen that the prompt penetration of eastward electric fields into low latitudes and subsequent development of ESF occurred

Chapter 6

Summary

6.1 Summary

Regular studies on the behavior of the ionosphere from the low latitude station Rajkot (22.29^0N 70.74^0E Geographic, sub-ionospheric dip latitude 15.8^0N) in India have been carried out. The major emphasises of the present work are on studying the temporal and spatial variability of ionospheric electron density using the GPS TEC and scintillation monitor technique, understanding the evolution and growth of ESF irregularities and associated L-band scintillation using multitechnique and further elucidating the geomagnetic storm time low latitude ionospheric – thermospheric variations.

Rajkot (22.29^0N 70.74^0E Geographic, sub-ionospheric dip latitude 15.8^0N) is situated near the crest region of the EIA and therefore is one of the most suitable locations to investigate the behavior of the low latitude ionosphere during the passage of crest of the EIA overhead. Using GPS-TEC measurements recorded at Rajkot, the low latitude ionospheric variability during low solar activity period (2005-2009) is investigated. The diurnal variations of TEC show a steady increase from about sunrise to an afternoon maximum and then fall to attain a minimum just before sunrise. A significant day to day variability in diurnal pattern has been observed which decreases with descend phase of solar activity. The seasonal variations of TEC show that TEC values are high in equinoctial months followed by summer and winter. The month to month variations of mean diurnal peak TEC shows semiannual variations with a peak during the equinox period and a trough during the solstice period. The high positive correlation between TEC peak and solar F10.7 flux shows high solar cycle dependence of TEC. The gradual increase in TEC observed in the year 2009 provides the indication of the starting of new solar cycle. The EIA development and EEJ controls on it are explained using the chain of GPS - TEC measurements (starting from equator to north crest of EIA) deployed under GAGAN project in India. Our results indicate that low latitude

TEC magnitude and daily peak time depends on the EEJ conditions. EIA is completely inhibited on the day of morning CEJ, resulting in a lower TEC value at Rajkot. The low latitude L-band scintillation is low both in amplitude as well as occurrence frequency due to the low solar activity period. Most of scintillation events are observed between post sunset and pre-midnight hours.

In the present age of satellite based communication and navigation, the presence of ESF irregularities sometime results into the signal loss of lock and in most of the cases degradation of signal amplitudes. Therefore it is very important to understand the various characteristics of the ESF irregularities in detail.

A multitechnique investigation on ESF irregularities has been carried during 2005 to 2008 using VHF coherent back scatter radar, GPS TEC and scintillation monitor and ionosonde in India. The simultaneous onset of strong ESF irregularities is observed at equatorial (Trivandrum) and off equatorial station (Gadanki) on 21/03/07. The ESF irregularities manifest themselves as periodic multiple plume structures on radar RTI map on this day. These periodic ESF plume structures create multiple TEC depletions and associated L-band scintillation in more than one PRNs in view from the observational site Gadanki. From the spectral width and Doppler velocity information it emerges that the initial phase of ESF irregularities does not affect the L-band signals. The electric field from equatorial valley region might be getting mapped to E region over Gadanki and inhibiting the E region instabilities at Gadanki during the growth phase of ESF at the equator as observed on 21/03/07 as well as on 05/02/08. The TEC enhancement associated with the ESF is also addressed. It is observed that the noticeable localized plasma enhancements during ESF events can occur which can alter the TEC in the ionosphere over dip-equatorial region. The latitudinal extent of L-band scintillation during the presence of ESF is brought out using GAGAN GPS –TEC observations. It is observed that GHz scintillation maximizes at low latitude station. The intensity of GHz scintillation decreases with descending phase of ESF irregularities.

During geomagnetic storm the solar wind electric field directly gets transferred to high latitude ionosphere which enhances the heat budget there. This

electric field when penetrates to low and equatorial latitudes alters the electrodynamics and thus electron density distribution over there. During geomagnetic storm, the ionospheric electron density shows large enhancement (depression) with respect to their quiet days' values which is termed as positive (negative) ionospheric storm. In addition to this, night time ionosphere during storm shows the presence of spread-F irregularities and associated L-band scintillations. The enhanced heat budget at high latitudes changes the thermospheric neutral composition globally. This also affects the ionospheric electron density. The detail studies on low latitude ionosphere-thermosphere response to storm time electrodynamical coupling between high and low latitudes are brought out. All these effects are highly time dependent and their occurrence is totally rely on the local time of SSC at any place on the earth.

The present investigation describes that the storm time ionospheric perturbations are either due to prompt penetration electric field or disturbance dynamo electric field which leads to positive or negative ionospheric storms respectively. The storm time neutral composition changes in terms of enhancements in atomic species shortly after the SSC contributes in to the positive ionospheric storm. The delayed effects of storm time neutral composition changes in terms of enhancements in molecular species are responsible for the negative ionospheric storm. The prompt penetration of eastward electric field to equatorial and low latitudes leads to development of strong ESF where conditions was not much conducive for strong ESF generation before the onset of storm. Discussions based on the evidences bring out that the storm time electrodynamical and neutral dynamical coupling between high and low latitudes dominant the ionospheric – thermospheric behavior at low and equatorial latitudes.

6.2 Suggestions for the future Work

The present work deals with the some of the ionospheric problems associated with satellite based navigation. The TEC which is directly proportional to the delay in satellite signals vary significantly with time and place as we have observed in the presented work also. The presented TEC variability is studied

during the solar minimum. This study can be extended to solar maximum period and the TEC variations during a complete solar cycle can be obtained. This long term data base can be useful to prepare model for ionosphere over low latitudes or even making necessary corrections in the existing ionospheric models.

The presented characteristics of ESF irregularities suggest that the conditions under which the irregularities pattern that creates GHz scintillation exists are still needed to find out. The growth and decay rate of irregularity pattern that can create GHz scintillation is needed to bring out. The present investigation is during the equinox season only, during summer and winter seasons also the ESF investigation is required. A detail investigation on latitudinal variability of L-band scintillation using long term data base during solar maximum and solar minimum up to more extended latitudes are needed in view of the GPS based navigation. The longitudinal variability of L-band scintillation using a chain of global GPS receivers can give clearer picture of global scintillation over equatorial and low latitudes.

From the geomagnetic storm point of view, there are many possible extensions for the present work. For example, the storm time low latitude ionosphere-thermosphere variations presented here are during the summer season only. For better understanding of the equatorial and low latitude ionosphere-thermosphere system variability during the geomagnetic storm, extended investigations under different seasons and different geomagnetic disturbance levels are needed. Further investigation is required to find out the role of neutral composition variations in positive and negative ionospheric storm during the geomagnetic disturbed conditions.

The extension of present investigation up to solar maximum conditions can give clear picture of low latitude ionosphere during different geophysical conditions which is very important from the point of view of satellite based positioning and navigation.

Appendix – I

I.1: Details of GAGAN GPS TEC observation stations

Name of Station	Geographic Latitude	Geographic Longitude	Geomagnetic Latitude
Trivandrum(TRI)	8.55^0N	76.9^0E	0.5^0N
Bangalore (BNG)	12.58^0N	77.4^0E	4.32^0N
Hyderabad (HYD)	17.48^0N	78.4^0E	9.22^0N
Bhopal (BHP)	23.17^0N	77.2^0E	14.21^0N
Delhi (DEL)	28.58^0N	77.2^0E	20.32^0N

I.2: Details of other GPS TEC observation stations

Name of Station	Geographic Latitude	Geographic Longitude	Geomagnetic Latitude
Arequipa Laser Station (AREQ)	-16.47^0N	288.5^0E	-6.48^0N
Galapagos Permanent Station (GLPS)	-0.74^0N	269.7^0E	8.75^0N
Taal Volcano Station (TVST)	14.03^0N	121.0^0E	4.3^0N

I.3: Details of Magnetic observatories

Name of Station	Geographic Latitude	Geographic Longitude	Geomagnetic Latitude
Tirunelveli	8.7^0N	77.8^0E	0.32^0N
Alibag	18.46^0N	72.87^0E	10.19^0N
Alma Ata	43.25^0N	76.92^0E	34.29^0N
Novosibirsk	55.03^0N	82.90^0E	45.57^0N

List of Scientific Publications

1. TEC variations during low solar activity period (2005-2007) near the Equatorial Ionospheric Anomaly Crest region in India

   Mala S. Bagiya, H. P. Joshi, K. N. Iyer, M. Aggarwal , S. Ravindran, B. M. Pathan, Ann. Geophys., 27, 1047–1057, 2009.

2. Evidence of storm time dynamical coupling between high and low latitudes

   Mala S. Bagiya, H.P.Joshi, K.N.Iyer, Sudha Ravindran and B.M.Pathan, Proceedings of the ECAR DST Workshop, IIG, Mumbai, India, 26-27 November, 2008

3. Low Latitude ionospheric-thermospheric response to storm time electrodynamical coupling between high and low latitudes

   Mala S. Bagiya, K. N. Iyer, H. P. Joshi, G. Manju, R.K.Choudhary, R.Sridharan, Sobhana Alex, (Under revision J. Geophys. Res., 2010)

4. Periodic ESF plume structures and their association with TEC depletions and enhancement

   Mala S. Bagiya, K. N. Iyer, H. P. Joshi, A. K. Patra, Sudha Ravindran. (To be communicated shortly to Advance in Space Research)

Papers presented by author in National / International Conferences

1. Effect of Interplanetary Electric field on Total Electron Content over the low latitudes

   Mala S.Bagiya, K.N.Iyer and H.P.Joshi

   presented at : 15th National Space Science Symposium, held at the Astronomy Centre, NCRA – TIFR, Udhagamandalam(Ooty), India during February 26-29, 2008

2. Geomagnetic storm effects on low latitude TEC

   Mala S. Bagiya, Smitha V. Thampi, Malini Aggarwal, Sudha Ravindran, H. P. Joshi, K.N.Iyer, G.Manju, and R. Ravindran,

   presented by G. Manju at: COSPAR 2008, held at Montreal, Canada 13-20 July, 2008

3. Vertical Total Electron Content variations during total Solar eclipse of 22 July 2009

   Mala S. Bagiya, H. P. Joshi, K. N. Iyer, R. R. Ranjan, Sheetal Karia, K. N. Pathak, A. K. Gwal

   presented at :16th National Space Science Symposium, held at the Saurashtra University, Rajkot, India during February 24-27 2010

4. Periodic ESF plume structures and their association with TEC depletions and enhancement

   Mala S. Bagiya, H. P. Joshi, K. N. Iyer, R. Sekar, A. K. Patra, Sudha Ravindaran, P V S Ramarao

   presented at: International Beacon Satellite Symposium held at the Barcelona, Spain during 7-11 June 2010

5. Low latitude ionospheric-thermospheric response to the geomagnetic storm of 15 May 2005: Evidence for electrodynamical coupling between high and low latitudes

   Mala S. Bagiya, H. P. Joshi, K. N. Iyer, Smitha V. Thampi, Takuya Tsugawa, Sudha Ravindaran, B. M. Pathan

   presented at: International Beacon Satellite Symposium held at the Barcelona, Spain during 7-11 June 2010

References

Aarons, J.(1977), Global positioning system phase fluctuations at auroral latitudes, Journal Geophys. Res., 102, 17 219–17 231.

Aarons, J. (1982), Global morphology of ionospheric scintillations, *Proc. IEEE*, 70, 360– 378.

Aarons, J. (1991) The role of ring current in the generation or inhibition of equatorial F-layer irregularities during magnetic storms, Radio Sci., 26, 1131-1149.

Aarons, J. (1993), The longitudinal morphology of equatorial F-layer irregularities relevant to their occurrence, Space Sci., Rev., 63, 209.

Aarons, J. and S. Basu (1994), Ionospheric amplitude and phase fluctuations at the GPS frequencies, In Proceeding of ION GPS-94, Inst. of Navig., Arlington, Va., 1569–1578.

Aarons, J., Mendillo, M., Yantosca, R., and Kudeki, E. (1996), GPS phase fluctuations in the equatorial region during the MISETA 1994 campaign, J. Geophys. Res., 101(A12), 26851-26862.

Abdu, M.A., Reddy, B.M., Walker, G.O., Hanbaba, R.,Sobral, J.H.A., Fejer, B.G., Woodman, R.W., Schunk, R.W., Szuszczewicz, E.P.(1988), Process in the quiet and disturbed equatorial-low latitude ionosphere: SUNDIAL campaign 1984, Annales Geophysicae, 6, 69–80.

Abdu M. A., J. H.A. Sobral, E. R. de Paula and I. S. Batisha (1991), Magnetospheric disturbance effects on the Equatorial Ionization Anomaly (EIA) : An overview, J. Atmos. Terr. Phys., 53, 757-771.

Abdu, M. A., I. S. Batista, G. O. Walker, J. H. A. Sobral, N. B. Trivedi, and E. R. de Paula (1995), Equatorial ionospheric fields during magnetospheric disturbances: Local time/longitudinal dependences from recent EITS Campaigns, J. Atmos. Sol.-Terr. Phys., 57, 1065– 1083

Abdu, M.A. (1997), Major phenomena of the equatorial ionosphere-thermosphere system under disturbed conditions, J.Atmos. Solar-Terres. Phys., 59, 1505 -1519.

Abdu M.A., Takashi Maruyama, Inez S. Batista, Susumo Saito and Maho Nakamura (2007),Ionospheric responses to the October 2003 superstorm: Longitude/local time effects over equatorial low and middle latitudes, Journal of geophysical research, vol. 112, a10306, 18 pp.2007.

Aggarwal M. H. P. Joshi, K. N. Iyer, A. K. Patra, S. V. Thampi(2007) Study of equatorial spread F using L-band and VHF Radar, Bull. Astr. Soc. India (2007) 35, 1-7.

Ananda, M., (1988), The NAVASTAR GPS System, AGARD Lecture Series.

Anderson, D.N., and G. Haerendel (1979), The motion of depleted plasma regions in the equatorial ionosphere, J. Geophys. Res., 84, 4251.

Appleton, E. V., and Barnett M A F (1925), Nature, 115, 333.

Appleton, E. V. (1932),, Inst. Elect. Engr., 71, 642.

Appleton, E.V.(1946), Two anomalies in the ionosphere, Nature, 157, 691.

Bagiya M. S., H. P. Joshi, K. N. Iyer, M. Aggarwal, S. Ravindran, and B. M. Pathan (2009) , TEC variations during low solar activity period (2005–2007) near the Equatorial Ionospheric Anomaly Crest region in India ,Ann. Geophys., 27, 1047–1057.

Baker W.G., and D.F. Martyn (1952), Conductivity of the ionosphere, Nature, 170, 1090.

Baker, W. G. and D. F. Martyn (1953), Electric Currents in the ionosphere. I. Conductivity., Phil. Trans. Roy. Soc. London, A246, 281.

Baker W.G.(1953), Electrical currents in the ionosphere, II, The atmospheric dynamo, Philos. Trans. R. Soc. London, A246, 295.

Balan N., K. Shiokawa, Y. Otsuka, T. Kikuchi, D. Vijaya Lekshmi, S. Kawamura, M. Yamamoto, G. J. Bailey (2010), A physical mechanism of positive ionospheric storms at low latitudes and midlatitudes, J. Geophys. Res., VOL. 115, A02304, 12 PP.

Balan, N. and K. N. Iyer (1983) Equatorial anomaly in ionospheric total electron content and its relation to dynamo currents, J. Geophys.Res., 88, 10259–10262.

Balthazor, R. L. and R. J. Moffett, (1997) A study of atmospheric gravity waves and travelling ionospheric disturbances at equatorial latitudes Ann. Geophys., 15,1048–1056.

Balsley, B.B.(1964), Evidence of a stratified echoing region at 150 kilometers in the vicinity of the magnetic equator during daylight hours, J. Geophys. Res., 69, 1925.

Balsley, B.B.(1969), Some characteristics of non-two stream irregularities in the equatorial electrojet, J. Geophys. Res., 74, 2333.

Balsley, B. B. (1969), Measurement of electron drift velocities in the night-time equatorial electrojet ,J. Atmos. & Terr. Phys., 475-478.

Balsley, B.B., and D.T. Farley (1971), Radar studies of the equatorial electrojet at three frequencies, J. Geophys. Res., 76, 8341.

Balsley, B.B., W.L. Ecklund (1972), VHF power spectra of the radar aurora, J.Geophys. Res., 77, 4746.

Balsley, B.B., G. Haerendel, and R.A. Greenwald (1972), Equatorial spread F: Recent ovsercations and a new interpretation, J. Geophys. Res., 77, 5625.

Balsley, B.B., and D.T. Farley (1973), Radar observations of two dimensional turbulence in the equatorial electrojet, J. Geophys. Res., 78, 7471.

Basu, Su., and M. C. Kelley (1977), Review of equatorial scintillations phenomena in light of recent developments in the theory and measurement of equatorial irregularities, J. Atmos. Terr. Phys., 39, 1229-1242.

Basu, S., and Kelley, M. (1979), A review of recent observations of equatorial scintillations and their relationship to current theories of F region irregularity generation, Radio Sci., 14(3), 471-485.

Basu Su, S, Basu, J.P. Mullen, and A. Bushby (1980), Longterm 1.5 GHz Amplitude scintillation measurements at the magnetic equator, *Geophys. Res. Lett*., 4, 259-262.

Basu Su. and S. Basu (1985), Equatorial scintillations, Advances since ISEA-VI, *J. Atmos. Terr. Phys*., 47, 753.

Basu, S., and S. Basu (1981), Equatorial scintillations - a review, J. Atmos. Terr. Phys., 43, 473-489, doi:10.1016/0021-9169(81)90110-0.

Basu S, Basu S, Senior C, Weimer D, Nielsen E, Fougere P. (1986), Velocity shears and sub-km scale irregularities in the Nighttime Auroral F-region, Geophys Res Lett 13(2):101–104.

Basu, S., E. MacKenzie, and Su. Basu (1988), Ionospheric constraints on VHF/UHF communications links during solar maximum and minimum periods, Radio Sci., 23, 363.

Basu S. et al.(1996), Scintillations, plasma drifts and neutral winds in the equatorial nighttime ionosphere after sunset, *J. Geophys. Res., 101*, 26795.

Basu, S., and B. Coppi (1999), Relevance of plasma and neutral wind profiles to the topology and the excitation of modes for the onset of spread F, *J. Geophys. Res., 104*, 225.

Basu, S., Su. Basu, K. M. Groves, H. C. Yeh, S. Y. Su, F. J. Rich, P. J. Sultan, and M. J. Keskinen (2001), Response of the equatorial ionosphere in the South Atlantic region to the great magnetic storm of July 15, 2000, Geophys. Res. Lett., 28, 3577– 3580

Basu, Su., S. Basu, C. E. Valladares, H.-C. Yeh, S.Y. Su, E. Mackenzie, P. J. Sultan, J. Aarons, F. J. Rich, P. Doherty, K. M. Groves, and T. W. Bullet, (2001) Ionospheric effects of majormagnetic storms during the International Space Weather Periodof September and October 1999: GPS observations, VHF/UHFscintillations, and in situ density structures at middle and equatoriallatitudes, J. Geophys. Res., 106, 30389–30413

Basu, S., Su. Basu, K. M. Groves, E. MacKenzie, M. J. Keskinen, and F. J. Rich (2005), Near-simultaneous plasma structuring in the midlatitude and equatorial ionosphere during magnetic superstorms, Geophys. Res. Lett., 32, L12S05, doi:10.1029/2004GL021678

Basu, Su., S. Basu, C. E. Valladares, H.-C. Yeh, S.-Y. Su, E. MacKenzie, P. J. Sultan, J. Aarons, F. J. Rich, P. Doherty, K. M. Groves and T. W. Bullet (2001), Ionospheric effects of Major Magnetic storms during international space weather period of Sept –Oct, 1999, at middle and equatorial latitudes, J. Geophys. Res., 106, 30389-30413.

Batista, I. S., E. R de Paula, M.A. Abdu., and N. B. Trivedi (1991) Ionospheric effects of the March 13, 1989 magnetic storm at low andequatorial latitudes, J. Geophys. Res., 96, 13943–13952.

Beach T. L and P. M. Kintner, (1999), Simultaneous Global positioning system observations of equatorial scintillations and total electron content fluctuations, *J. Geophys. Res*., 104, 22553.

Berkner, L.V., and H.W. Wells (1934), F region ionospheric investigation at low latitudes, Terr. Magn. Atmos. Elec., 39, 215.

Berkner, L.V., and H.W. Wells (1937), Abnormal ionization of the E region of the ionosphere, Terr. Magn. Atmos. Elec., 42, 73.

Becker-Guedes, F. Y. Sahai, P. R. Fagundes, E. S. Espinoza, V. G. Pillat, W. L. C. Lima, Su. Basu, Sa. Basu, Y. Otsuka, K. Shiokawa, E. M. MacKenzie, X. Pi, and J. A. Bittencourt (2007) The ionospheric response in the Brazilian sector during the supergeomagnetic storm on 20 November 2003, Ann. Geophys., 25,863–873, http://www.ann-geophys.net/25/863/2007/.

Bhattacharyya, A., Beach, T., Basu, S., and Kintner, P. (2000), Nighttime equatorial ionosphere: GPS scintillations and differential carrier phase fluctuations, Radio Sci., 35(1), 209-224.

Bhattacharyya, A., S. Basu, K. M. Groves, C. E. Valladares, and R. Sheehan (2001) Dynamics of equatorial F region irregularities from spaced receiver scintillation observations, Geophys. Res. Lett., 28(1), 119-122, doi:10.1029/2000GL012288.

Bhuyan P. K. and Borah R. R (2007), TEC derived from GPS network in India and comparison with the IRI, Adv. Space Res., 39, 830-840.

Biondi, M. A., and D. P. Sipler (1985), Horizontal and vertical winds and temperatures in the equatorial thermosphere: Measurements from Natal, Brazil during August-September, Planet. Space. Sci., 33, 817.

Blanc, M. and A. D. Richmond (1980), The ionospheric disturbance dynamo, J. Geophys. Res., 85, 1669-1686.

Bowles, K. L., R. Cohen, G. R. Ochs, and B. B. Balsley (1960), Radio Echoes from Field-Aligned Ionization above the Magnetic Equator and Their Resemblance to Auroral Echoes, Journal of Geophysical Research, 65 (A6), 1853-1855.

Bowles, K. L., and Cohen, R. (1962), Ionospheric Sporadic E, edited by S. Matsushita, Pergamon press, New York.

Booker, B.B., and H.W. Wells (1938), Scattering of radio waves by the F region of the ionoaphere, J.Geophys. Res., 43, 249.

Bowles, K. L., Balsley, B. B., and Cohen, R. (1963), J. Geophys. Res., 68, 2485.

Breit G. and M. A. Tuve (1925), A Radio Method of Estimating the Height of the Conducting Layer, Nature, 116, 357-357, doi:10.1038/116357a0

Breit G. and M. A. Tuve (1926), A test of the existence of the conducting layer, Phys. Rev. 28, 554-75.

Browne, I.C., Evans, J.V., Hargreaves, J.V., and Murray,J.A.W. (1956), Radio echoes from moon, Proceedings of phys soc., B 69, 901-920.

Buresova, D., and J. Lastovicka (2007), Pre-storm enhancements of foF2 above Europe, Adv. Space Res., 39(8), 1298– 1303.

Burns, A. G., T. L. Killeen, W. Deng, G. R. Carignan, and R. G. Roble (1995), Geomagnetic storm effects in the low- to middle-latitude upper thermosphere, J. Geophys. Res., 100(A8), 14,673– 14,691.

Calvert, W., and R. Cohen (1961), The interpretation and synthesis of certain spread F configurations appearing on equatorial ionogram, J. Geophys. Res., 66, 3125.

Calvert, W. (1963), Instability of the equatorial F layer after sunset, J. Geophys. Res., 68(9), 2591.

Chakrabarty, D., R.Sekar, R. Narayanan, C.V.Devasia, and B.M.Pathan (2005), Evidence for interplanetary electric field effect on the OI 630.0nm airglow over low latitudes, J. Geophys. Res., 110, A11301, doi:10.1029/2005JA011221.

Chandra, H., and R. G. Rastogi (1970), Solar cycle and seasonal variation of spread F near the magnetic equator, *J. Atmos. Terr. Phys*., 32, 439.

Chandra, H., G. Rajaram, and R. G. Rastogi (1973b), Electron density distribution over the magnetic equator, Ind. J. Radio and Space Phys., 2, 243-250.

Chandra H., H. O. Vats, G. Sethia, M. R. Deshpande, R. G. Rastogi and J. H. Sastri (1979), Ionospheric scintillations associated with features of equatorial ionosphere, *Ann. Geophys.*, 35, 145-151.

Chapman, S.,(1931) The absorption and dissocaitive or ionizinig effect of ionochromatic radiation in an atmosphere on a rotating earth, proc.phy.soc (Londan), 43,26-45.

Chapman, S. (1951a), Some phenomena of the upper atmosphere, Proc. Phys. Soc. London, B, 64, 833–843.

Chapman, S. 1956, The electrical conductivity of the ionosphere: A review, Nuovo Cimento, 4(10), 1385.

Chamberlain, J. W. (1958), Oxygen red lines in the airglow, I, Twilight and night excitation processes, Astrophys. J., 127, 54-66.

Chaturvedi, P., and P. K. Kaw (1976), An interpretation for power spectrum of spread F irregularities, *J. Geophys. Res*., 81, 3257.

Chaturvedi, P.K., and S.L. Ossakow (1978), Nonlinear theory of the collisional Rayleigh-Taylor instability in equatorial spread F, J. Geophys. Res., 83, 4219.

Chen Y., Guanyi Ma, Wengeng Huang, Hua Shen, Jinghua Li (2008), Night-time total electron content enhancements at equatorial anomaly region in China, Adv. Space Res., 41 , 617-623.

Christensen, A. B., et al. (2003), Initial observations with the Global Ultraviolet Imager (GUVI) in the NASA TIMED satellite mission, J. Geophys. Res. 108(A12), 1451, doi:10.1029/2003JA009918.

Cohen, R., Bowles, K. L., and Colvert, W. (1962), J. Geophys. Res., 67, 965.

Cohen, R., and K. L. Bowles (1967), Secondary irregularities in the equatorial electrojet, J. Geophys. Res., 72, 885.

Costa, E., and M.C. Kelley (1978), On the role of steepened structures and drift waves in equatorial spread F, J. Geophys. Res., 83, 4359.

Costa, E., and M.C. Kelley (1978), Linear theory for the collisionless drift wave instability with wavelengths near the ion gyroradius, J. Geophys. Res., 83, 4365.

Cowling, T. G. (1945), The electrical conductivity of an ionized gas in a magnetic field, with applications to the solar atmosphere and the ionosphere, Proc. Roy. Soc. London, A183, 453.

Croom, S., A. Robbins, and J. O. Thomas (1959), Two anomalies in the behaviour of the F_2 layer of the ionosphere, Nature, 184, 2003-2004.

da Rosa, A. V., H. Waldman, J.Bendito, and O. K.Garriott (1973) Respons of the ionospheric electron content to fluctuations in solar activity, J. Atmos. Terr. Phys., 35, 1429–1442.

Dabas, R. S., P. K.Bhuyan, T. R.Tyagi, R. K. Bhardwaj, and J. B.Lal (1984) Day-to-day changes in ionospheric electron content at low latitudes, Radio Sci., 19, 749–756.

Dabas, R. S., D. R. Lakshmi, B. M. Reddy (1998), Day-to-day variability in the occurrence of equatorial and low-latitude scintillations in the Indian zone, *Radio Sci*., 33(1), 89-96, 10.1029/97RS02103.

Dagg, M. (1957), The origin of the ionospheric irregularities responsible for radio-star scintillation and spread F. I. Review of existing theories. II. Turbulent motion in the dynamo region, J. Atmos. Terr. Phys., 11, 133, 139.

Danilov, A. D. (2001), F2-region response to geomagnetic disturbances, J. Atmos. Sol. Terr. Phys., 63, 441–449.

Das gupta, A. and A.Basu (1973) Investigation of ionospheric electroncontent in the equatorial region as obtained by orbiting beacon satellites, Ann. Geophys., 29, 409–419.

DasGupta, J. Aarons, J. A. Klobuchar, Santimay Basu, A. Bushby (1982), Ionospheric electron content depletions associated with amplitude scintillations in the equatorial region, Geophysical Research Letters, Vol. 9, No. 2, pp. 147-150, doi:10.1029/GL009i002p00147.

Das Gupta, A., Santimay Basu, Aarons, J., Klobuchar, J. A., Sunanda Basu and Bushby, A.(1983),VHF amplitude scintillations and associated electron content depletions as observed at Arequipa, Peru, J. Atmos. Terr. Phys, 45, 15–26.

DasGupta A., Paul, A., Ray, S., Das, A., Ananthakrishnan, S. (2006), Equatorial bubbles as observed with GPS measurements over Pune, India, Radio Sci., 41, RS5S28, doi:10.1029/2005RS003359.

Dashora, N. and Pandey, R.(2005), Observations in equatorial anomaly region of total electron content enhancements and depletions, Ann. Geophys., 23, 2449-2456.

Davies, K., R. F.Donnelly, R. N., Grubb, and P.V.S. Rama Rao (1979) ATS-6 satellite radio beacon measurements on Ootacamund,India, Radio Sci., 14, 85–95.

Davies,K. (1980) Recent progress in satellite radio beacon studies with particular emphasis on the ATS-6 Radio beacon experiment,Space Sci. Rev., 25, 357–430.

de Paula E. R., K. N. Iyer, D. L. Hysell, F. S. Rodrigues, E. A. Kherani1, A. C. Jardim, L. F. C. Rezende, S. G. Dutra, and N. B. Trivedi (2004), Multi-technique investigations of storm-time Ionospheric irregularities over the Sao Luıs equatorial station in Brazil, , J. Geophys. Res., 22: 3513–3522.

Dungey, J.W. (1956), Convective diffusion in the equatorial F region, J. Atmos. Terr. Phys., 9, 304.

Eccles, J. V. (1998), Modeling investigation of the evening prereversal enhancement of the zonal electric field in the equatorial ionosphere, *103*, 26,709-26,719.

Farley, D. T., E. Bonelli, B. G. Fejer and M. F. Larsen (1986), The prereversal enhancement of the zonal electric field in the equatorial ionosphere, J. Gephys. Res., 91, 13723-13728.

Feichter, E. and R.Leitinger (1997) A 22-year cycle in the F layer ionization of the ionosphere, Ann. Geophys., 15, 1015–1027, http://www.ann-geophys.net/15/1015/1997/.

Fejer, B.G., and M.C. Kelley (1980), Ionospheric irregularities, Rev. Geophys. Space Phys., 18, 401.

Fejer, B.G., D.T. Farley, C.A. Gonzales, R.F. Woodman, and C. Calderon (1981), F region east-west drifts at Jicamarca, J. Geophys. Res., 86, 215.

Fejer, B. G., M. F. Larsen, and D. T. Farley (1983), Equatorial disturbance dynamo electric fields, Geophys. Res. Lett., 10, 537– 540.

Fejer B. G., (1986), Equatorial ionospheric electric fields associated with magnetospheric disturbances, in Solar Wind Magnetosphere Coupling, edited by Y. Kamide and J. A. Slavin, pp. 519-545, Terra Sci., Tokyo

Fejer, B. G., et al. (1990a), Low -and Mid –latitude ionospheric electric fields during the January 1984 GISMOS campaign, J. Geophys. Res., 95, 2367.

Fejer, B.G., E.R. de Paula, S.A. Gonzalez, and R.F. Woodman (1991), Average vertical and zonal F region plasma drifts over Jicamarca, J. Geophys. Res., 96, 13901.

Fejer, B. G. (1997), The electrodynamics of the low-latitude ionosphere: Recent results and future challenges, J. Atmos. Sol. Terr. Phys., 59, 1465– 1482.

Fejer B. G. and L. Scherliess (1997), Empirical models of storm time equatorial zonal electric fields, J. Geophys. Res., 102, 24,047-24,056.

Fejer, B. G., L. Scheerliess, and E. R. de Paula (1999), Effects of the vertical plasma drift velocity on the generation and evolution of equatorial spread F, *J. Geophys. Res.*, 104, 19859.

Fejer, B. G., Emmert, J. T., and Sipler, D. P. (2002) Climatology and storm-time dependence of nighttime thermospheric neutral winds over Millstone Hill, J. Geophys. Res.,107, pp. SIA 3–1, CiteID 1052, DOI 10.1029/2001JA000300/.

Fejer, B. G. and J. T. Emmert (2003) Low-latitude ionospheric disturbance electric field effects during the recovery phase of the 19–21 October 1998 magnetic storm, J. Geophys. Res., 108(A12),1454, doi:10.1029/2003JA010190.

Field, P. R., H. Rishbeth, R. J. Moffett, D. W. Idenden, T. J. Fuller-Rowell, G. H. Millward, and A. D. Aylward (1998), Modelling composition changes in F-layer storms, J. Atmos. Sol. Terr. Phys., 60, 523– 543.

Fuller-Rowell, T. J., G. H. Millward, A. D. Richmond, and M. V. Codrescu (2002), Storm-time changes in the upper atmosphere at low latitudes, J. Atmos. Sol.-Terr. Phys., 64, 1383 – 1391.

Greenspan, M. E., C. E. Rasmussen, W. J. Burke, and M.A. Abdu (1991) Equatorial density depletions observed at 840 km duringthe great magnetic storm of March 1989, J. Geophys. Res.,96, 13931–13942

Groves K. M. et al. (1997), Equatorial scintillations and systems support, *Radio Sci*., 32, 2047.

Gupta, J. K. and L. Singh (2000) Long term ionospheric electron contentvariations over Delhi, Ann. Geophys., 18, 1635–1644, http://www.ann-geophys.net/18/1635/2000/.

Gouin, P., and P. N. Mayaud (1967), A propos de l' existence possible d' un contre electrojet and latitudes magnetiques equatorials, Ann. Geophys., 23, 41.

GSV4004/GSV4004A (2003), GPS Ionospheric Scintillation & TEC Monitor, User's Manual, 1131 Seena Avenue, Los Altos, CA 94024, USA.

Haerendel, G. (1973), Theory of equatorial spread F, report, Max-Planck Inst. fur Phys. and Astrophys., Munich.

Haerendel, G. (1974), Report-Theory of equatorial spread-F, Max-Planck Inst. fur Phys. und Astro-phys., Garching, Germany.

Haerendel, G., O.H. Bauer, S. Cakir, H. Foppl, E. Rieger, and A. Valenzuela (1983), Coloured bubbles- an experiment for triggering equatorial spread F, Eur. Space Agency, ESA SP-195, 295.

Hargreaves, J. K.(1992), The solar terrestrial environment, Cambridge University Press.

Heaviside O. (1902), Telegraphy, Sect. 1, Theory Encyc. Brit.10th ed. London 9: 213–218.

Hanson, W. B., and Sanatani, S. (1973), Large Ni Gradients below the Equatorial F Peak, J. Geophys. Res., 78(7), 11671173.

Hanson, W. B., and S. Sanatani (1971), Relationship between Fe^{+} ions and equatorial spread F", J. Geophys. Res., 76, 7761.

Heelis, R.A., P.C. Kendall, R.J. Moffett, D.W. Windle, and H. Rishbeth (1974), Electricalcoupling of the E and F regions and its effect on F region drifts and winds, Planet. Space Sci., 22, 743.

Hines, C. O. (1960), International atmospheric gravity waves at ionospheric heights, Can. J. Phys., 38, 1441-1481.

Hines, C. O. (1974), The upper atmosphere in motion, Geophysical Monograph, American Geophysical Union.

Hofmann-W, B.ellenhof, H. Lichtenegger, and J.Collins, (1992) Global Positioning System, Theory and Practice, 4th edition, Springer-Verlag, Berlin, Heidelberg, New York, 389 pp.

Huang C.S. and M. C. Kelley (1996), Nonlinear evolution of equatorial spread-F 1 On the role of plasma instabilities and spatial resonance associated with gravity wave seeding, J. Geophys. Res., 101, 283.

Huang, C.S. M. C. Kelley and D. L. Hysell, Nonlinear evolution of Rayleigh-Taylor instabilities, Atmospheric gravity waves and equatoria spread-F, J. Geophy. Res., 98, 15361.

Huba, J.D., P.K. Chaturvedi, S.L. Ossakow, and D.M. Towle (1978), High frequency drift waves with wavelengths below the ion gyroradius in equatorial spread F, Geophys. Res. Lett., 5, 695.

Huba, J.D., and S.L. Ossakow (1981b), Phhysical mechanism of the lower-hybrid drift instavility in a collisional plasma, J. Atmos. Terr. Phys., 43, 775.

Hudson, M.K., and C.F. Kennel (1975), Linear theory of equatorial spread F, J. Geophys. Res., 80, 4581.

Hysell, D.L., M.C. Kelley, W.E. Swartz, and R.F. Woodman (1990), Seeding and layering of equatorial spread F by gravity waves, J. Geophys. Res., 95, 17253.

Hysell, D.L., M.C. Kelley, W.E. Swartz, R.F. Pfaff, and C.M. Swenson (1994), Steepened structures in equatorial spread F, 1. New observations, J. Geophys. Res., 99, 8827.

Hysell, D. L. and J. Burcham (1998), JULIA radar studies of equatorial spread F, *J. Geophys. Res*., 103, 29155.

Hysell, D. L., and J. Burcham (2002), Long term studies of equatorial spread F using the JULIA radar at Jicamarca*, J. Atmos. Terr. Phys*., 64, 1531.

Jakowaski, N., S. Schluter, and E. Sardon , (1999) Total Electron Content of ionosphere during the geomagnetic storm of January 1997, J.Atmos. Sol. Terr. Phys., 61, 299–307.

Jayachandran, B., N. Balan, P. B. Rao, J. H. Sastri, G. J. Bailey(1993), HF Doppler and ionosonde observations on the onset condition of equatorial spread F, *J. Geophys. Res*., 98(A8), 13741-13760, 10.1029/93JA00302.

Jing, N. and R. D. Hunsucker, (1993) A theoretical investigation of sources of large and medium scale atmospheric gravity waves in the auroral oval (1993), J. Atmos. Terr. Phys., 55, 1667–1679.

Kane, P.R. (1973), Global evolution of F2-region storms. Journal of Atmospheric and Terrestrial Physics 35, 1953–1966.

Kennelly A. E. (1902), On the Elevation of the Electrically-Conducting Strata of the Earth's Atmosphere," Elec. World mid Engr., XXXIX (March 15), p. 473.

Kelley, M C., B. G. Fejer, and C. A. Gonzales (1979), An explanation for anomalous ionospheric electric fields associated with a northward turning of the interplanetary magnetic field, Geophys. Res. Lett., 6, 301.

Kelley, M.C., M.F. Larson, C. LaHoz, and J.P. McClure (1981), Gravity wave initiation of equatorial spread F: A case study, J. Geophys. Res., 86, 9087.

Kelley, M. C. (1989), The Earths ionosphere: Plasma physics and electrodynamics, International Geophysics Series, vol. 43, Academic Press.

Kelley, M., Kotsikopoulos, D., Beach, T., Hysell, D., and Musman, S. (1996), Simultaneous Global Positioning System and radar observations of equatorial spread F at Kwajalein, J. Geophys. Res., 101(A2), 2333- 2341.

Kelley, M. C., J. J. Makela, J. L. Chau, and M. J. Nicholls (2003) Penetration of the solar wind electric field into the magnetosphere/ionosphere system Geophys. Res. Lett., 30(4), 1158, doi:10.1029/2002GL016321.

Keskinen, M.J., S.L. Ossakow, and P.K. Chaturvedi (1980a), Preliminary report of numerical simulations of intermediate wavelength collisional Rayleigh-Taylor instability in equatorial spread F, J. Geophys. Res., 85, 1775.

Kikuchi, T., H. Luhr, T. Kitamura, O. Saka and K. Schlegel (1996), Direct penetration of the polar electric field to the equator during a DP2 event EISCAT radar, J. Geophys. Res., 101, 19, 643.

Kil, H., and Heelis, R. A. (1998), Equatorial density irregularity structures at intermediate scales and their temporal evolution, J. Geophys. Res., 103(A3), 39693981.

Klobuchar, J. (1986) Design and characteristics of the GPS ionospherictime-delay algorithm for single frequency users, in: Proceedings of PLANS'86 – Position Location and Navigation Symposium, Las Vegas, Nevada, p. 280–286.

Krishna Murthy, B. V. and Sen Gupta, K. (1972), Disappearance of equatorial Es associated with magnetic field depression, Planet Space Sci., 20, 371–378.

Krishna Moorthy, K., Ragha Reddi, C., and Krishna Moorthy, B. V.(1979), Night-time ionospheric scintillations at the magnetic equator, *J. Atm. Terr. Phys*, 41, 123–134.

Kulkarni, P.V. (1975), 6300 Å night airglow and the geomagnetic control of the equatorial anomaly, Proc. Indian Acad. Sci. (Earth and Planet Sci.), 82, 46-54.

Kutiev, I., Y. Otsuka, A. Saito, and S. Watanabe (2006), GPS observations of post-storm TEC enhancements at low latitudes, Earth Planet. Space, 58, 1479–1486.

Kutiev, I., Y. Otsuka, A. Saito, and S. Watanabe (2007), Low-latitude total electron content enhancement at low geomagnetic activity observed over Japan, J. Geophys. Res., 112, A07306, doi:10.1029/2007JA012385.

Le G., Huang, C.-S., Pfaff, R. F., Su, S.-Y., Yeh, H.-C., Heelis, R. A., Rich, F. J., and Hairston, M. (2003), Plasma density enhancements associated with equatorial spread F: ROCSAT-1 and DMSP observations, J. Geophys Res., VOL. 108, NO. A8, 1318, doi:10.1029/2002JA009592.

Lee, C. C., J. Y. Liu, B. W. Reinisch, W. S. Chen, F. D. Chiu (2005), The effects of the pre-revversal drift, EIA asymmetry and magnetic activity on ESF during solar minimum, *Ann. Geophys*., 23, 745.

Linn, C. H., A. D. Richmond, J. Y. Liu, H. C.Yeh, L. J.Paxton, G. Lu and H. F. Tsai (2005), Large scale variations of low latitude ionosphere during Oct-Nov 2003 superstorm: Observational results, J. Geophysical Res., 110, a09S28 doi:10.1029/2004JA010900.

Liu Libo, Wan Weixing, Zhang Man-Lian, Zhao Biqiang, andNing Baiqi (2008) Prestorm enhancements in NmF2 and total electron content at low latitudes, J. Geophys. Res., 113, A02311,doi:10.1029/2007JA012832

Lousie K. Harra and Keith O.mason (2004), "Space Science", Imperial college press.

Lockwood, G. E. K., and G. L. Nelms (1964), Topside sounder observations of the equatorial anomaly in the 75^{o} W longitude zone, J. Atmos. Terr. Phys., 26, 569—580.

Lu G., L. P. Goncharenko, A. D. Richmond, R. G. Roble, and N. Aponte (2008), A dayside ionospheric positive storm phase driven by neutral winds, J. Geophys. Res., 113, A08304, doi:10.1029/2007JA012895.

Lyon, A. J., and L. Thomas (1963), The F_2-region equatorial anomaly in the African, American, and East Asian sectors during sunspot maximum, J. Atmos. Terr.Phys., 25, 373-386.

Mannucci, A. J., B. T. Tsurutani, B. A. Iijima, A. Komjathy, A. Saito, W. D. Gonzalez, F. L. Guarnieri, J. U. Kozyra, R. Skoug (2005), Dayside global ionospheric response to the major interplanetary events of October 29–30, 2003 ''Halloween Storms''. Geophys. Res. Lett. 32, L12S02, doi:10.1029/2004GL021467.

Maruyama, T., G. Ma, and M. Nakamura (2004) Signature of TEC storm on 6 November 2001 derived from dense GPS receiver network and ionosonde chain over Japan, J. Geophys. Res., 109, A10302,doi:10.1029/2004JA019451

Martyn, D.F. (1947), Atmospheric tides in the ionosphere, I. Solar tides in the F_2 region, Proc. Roy. Soc. London, A189, 241.

Martyn, D.F. (1959), Large scale movements of ionization in the ionosphere, J. Geophys. Res., 64, 2178.

Matsushita, S. (1957), J. Atmos. Terr. Phys., 10, 163.

Mathews, J. D. (1998), Sporadic-E: Current views and recent progress, J. Atmos. Terr. Phys., 60, 413.

Mazaudier, C., and S. V. Venkateswaran (1990), Delayed ionospheric effects of the geomagnetic storms of March 22, 1979, studied by the sixth coordinated data analysis workshop (CDAW-6), Ann. Geophys., 8, 511– 518.

McClure J. P., W. B. Hanson, and J. H. Hoffman (1977), Plasma bubbles and irregularities over the equatorial ionosphere, J. Geophys., Res., 82, 2650.

Meier, R. R., G.Crowley, D. J.Strickland, A. B.Christensen, L. J. Paxton, D. Morrison, and C.L. Hackeert (2005) First look at the 20 November superstorm with TIMED/GUVI: Comparisons with a thermospheric global circulation model, J. Geophys. Res.,110, A09S41, doi:10.1029/2004JA010990.

Mendillo, M., J. Baumgardner, Pi. Xiaoquing, P. J. Sultan, and R. T. Tsunoda (1992), Onset conditions for equatorial spread F, J. Geophys. Res., 97, 13865.

Mendillo M. and Tyler A. (1983),Geometry of Depleted Plasma Regions in the Equatorial Ionosphere, Journal of geophysical research, vol. 88, no. a7, pp. 5778-5782, doi:10.1029/ja088ia07p05778.

Mendillo, M., J. Meriwether, and M. Biondi (2001), Testing the thermospheric neutral wind suppression mechanism for day-to-day variability of equatorial spread F, *J. Geophys. Res*., 106, 3655.

Mitra, S.K. (1946), Geomagnetic control of region F_2 of the ionosphere, Nature, 158, 668.

Mitra, S. N. (1949), A radio method of measuring winds in the ionosphere, Electrical Engineers, Journal of the Institution of, 11, 277.

Modi, R. P. and K.N. Iyer (1989) IEC and slab thickness near the peak,Indian J. Radio Space Phys., 18, 23–26.

Mukherjee S., Shivalika Sarkar, P.K. Purohit and A.K. Gwal (2010), Seasonal variation of total electron content at crest of equatorial anomaly station during low solar activity conditions, Vol. 46, Issue 3, Advan. In Space Research, doi: 10.1016/j.asr.2010.03.024.

Musman, S., Jahn, J. M., LaBelle, J., and Swartz, W. E. (1997), Imaging spread- F structures using GPS observations at Alcantara, Brazil, Geophys. Res. Lett., 24, 1703–1706.

Narayanan, R., J. N. Desai, N. K. Modi, R. Raghavarao and R. Sridharan (1989), Dayglow Photometry: a new approach, Appl. Opt., 28, 2138-2142.

Nishida, A. (1968), Coherence of geomagnetic DP2 fluctuations with interplanetary magnetic variations, J. Geophys. Res., 73(17), 5549.

Ossakow, S. L., S. T. Zalesak, B. E. McDonald, and P. K. Chaturvedi (1979), Nonlinear equatorial spread-F: Dependence on altitude of the F-peak and bottomside background electron density gradient scale length, J. Geophysics. Res., 84, 17-29.

Ossakow, S.L.(1979), Ionospheric irregularities, Rev. Geophys. Space Phys., 17, 521

Ossakow, S. L. (1981), Spread-F theories- A review, J. Atmos. Terr. Phys., 43, 437-452.

Ott, E. (1978), Theory of Rayleigh-Taylor bubbles in equatorial ionosphere, J. Geophys. Res., 83, 2066.

Oya, H., Takahashi, T., and Watanabe, S. (1986), Observation of low latitude ionosphere by the impedance probe on board the Hinotori satellite, J. Geomagn. Geoelectr., 38, 111.

Pallam Raju D., R. Sridharan, S. Gurubaran, and R. Raghavarao (1996), First results from ground based daytime optical investigations of the development of equatorial ionisation anomaly, Ann. Geophys., 14, 238.

Pandey, R. and N. Dashora (2006), Space weather studies at the crest of the equatorial ionization anomaly using GPS receiver, Paper presented at XXVIIIth URSI General 486 Assembly, New Delhi, India, 23 to 29 October, 2005. 487.

Pant T. K. (1998), Study of the thermosphere ionosphere coupling under varying geophysical conditions.

Park J., Kyoung Wook Min, Jae-Jin Lee, Hyosub Kil, Vitaly P. Kim, Hee-Jun Kim, Ensang Lee, and Dae Young Lee (2003), Plasma blob events observed by KOMPSAT-1 and DMSP F15 in the low latitude nighttime upper ionosphere, Geophys. Res. Lett., VOL. 30, NO. 21, 2114, doi:10.1029/2003GL018249.

Patra A. K. (1997), A Study of low-latitude ionospheric irregularities using VHF coherent backscatter radar.

Patra, A. K., P. B. Rao., V. K. Anandan and A. R. Jain (1997), Radar observations of 2.8 m equatorial spread F irregularities, *J. Atmos. Terr. Phys*., 59, 1663-1641.

Patra A. K., S. Sripathi, and D. Tiwari (2004), Coupling effect of the equatorial F region irregularities on the low latitude E region instability processes, Geophy. Res. Lette., Vol.31, L17803, doi:10.1029/2004GL020486.

Patra, A. K., Tiwari, D., Sripathi, S., Rao, P. B., Sridharan, R., Devasia, C. V., Viswanathan, K. S., Subbarao, K. S. V., Sekar, R., and Kherani, E. A.(2005.), Simultaneous radar observations of meter-scale F region irregularities at and off the magnetic equator over India, J. Geophys. Res., 110, A02307, doi:10.1029/2004JA010565.

Patricia H. Doherty, Susan H. Delay and Cesar E. Valladares (2000), Ionospheric scintillation effects in the Equatorial and Auroral regions, Proc. Of ION GPS, 662.

Paxton, L. J., et al. (1999), Global ultraviolet imager (GUVI) : measuring composition and energy inputs for the NASA Thermosphere Ionosphere Mesosphere Energetics and Dynamics (TIMED) mission, SPIE Opt. Spectrosc. Tech. Instrum. Atmos. Space Res., 3756, 265.

Paxton, L. J., et al. (2004), GUVI: A hyperspectral imager for geospace, Proc. SPIE, 5660,227-240, doi: 10.1117/12/579171.

Pimenta A. A., Sahai, Y., Bittencourt, J. A., Abdu, M. A., Takahashi, H., and Taylor, M. J. (2004), Plasma blobs observed by ground-based optical and radio techniques in the Brazilian tropical sector, Geophys. Res. Lett., VOL. 31, L12810, doi:10.1029/2004GL020233.

Prolss, G. W. (1997), Magnetic storm perturbations of the upper atmosphere, in Magnetic Storms, Geophys. Monogr. Ser., vol. 98, edited by B. T. Tsurutani et al., pp. 227– 241, AGU, Washington, D. C.

Raghavarao R., P. Sharma and M. R. Sivaraman (1978), Correlation of the Ionization anomaly with the intensity of the electrojet, Space Res., XVIII, 277-280.

Raghavarao, R., S. P. Gupta, R. Sekar, R. Narayanan, J. N. Desai, R. Sridharan, V. V. Babu, and V. Sudhakar (1987), In situ measurements of winds, electric fields and electron densities at the onset of equatorial spread-F, J. Atmos. Terr. Phys., 49, 485.

Raghavarao, R., W. R. Hoegy, N. W. Spencer, and L. Wharton (1993), Neutral temperature anomaly in the equatorial thermosphere- A source of vertical winds, *Geophys. Res. Lett* 20, 1023.

Ram T. S., P. V. S. Ramarao, D. S. V. V.D. Prasad, K. Niranjan, S. Gopikrishna, R. Sridharan and Sudha Ravindran (2008), Local time dependent response of post sunset ESF duing geomagnetic storms, J. Geophys. Res., Vol. 113, A07310, doi:10.1029/ 2007JA012922.

Rama Rao, P. V. S., M.Srirama Rao, and M.Satyam (1977) Diurnal and seasonal trends in TEC values observed at Waltair, Indian J. Radio Space Phys., 6, 233–235.

Rama Rao, P. V. S., D.Nru, and M.Srirama Rao (1980) Proc.COSPAR/URSI Symp.Warsaw, Poland, edited by: Wernik, A.W., p. 51.

.

Rama Rao, P. V. S., A.Das Gupta, J. A. Klobuchar, and R.G. Rastogi (1983) Proc. Int. Beacon Satellite Symposium Physical Lab., NewDelhi, India, p. 393.

Rama Rao, P. V. S., K.Niranjan, B.V. Ramana Rao, B.V. P.S. Rao, and D. S. V. V. D. Prasad (1985) Proc. URSI/IPS Conference on the Ionosphere and Radiowave Propagation Sydney, Australia.

Rama Rao, P. V. S., P. Sri Ram, P. T. Jayachandran, and D. S. V. V. D. Prasad (1996), Multistation VHF scintillation studies at low latitudes. Planet. Space Sci., 44,1209-1217.

Rama Rao, P. V. S., S. Tulasi Ram, K. Niranjan, D. S. V. V. D. Prasad, S. Gopikrishna, and N.K.M. Lakshmi, (2005), VHF and L-band scintillation

characteristics over Indian low-latitude station, Waltair, *Ann. Geophys*., 23, 2457-2464.

Rama Rao, P. V. S., S.Gopi Krishna, K.Niranjan, and D.S.V.V.D. Prasad (2006) Temporal and spatial variations in TEC using simultaneous measurements from the Indian GPS network of receivers during the low solar activity period of 2004–2005, Ann. Geophys.,24, 3279–3292, http://www.ann-geophys.net/24/3279/2006/.

Rama Rao, P. V. S., S. Gopikrishna, K. Niranjan, and D. S. V. V. D. Prasad, (2006a), Study of spatial and temporal characteristics of L-band scintillations over the Indian low latitude region and their possible effects on GPS navigation, *Ann. Geophys*., 24, 1567-1580.

Rama Rao, P. V. S., S. Tulasi Ram, S. Gopikrishna, K. Niranjan, and D. S. V. V. D. Prasad, (2006b), Morphological and spectral characteristics of L-band and VHF scintillations and their impact on trans-ionospheric communication, Earth Planets, Space, 58, 895-904.

Rama Rao, P. V. S., S. Tulasi Ram, S. Gopikrishna, K. Niranjan, and D. S. V. V. D. Prasad, (2006a), Morphological and spectral characteristics of L-band and VHF scintillations and their impact on trans-ionospheric communication, *Earth Planets, Space,* 58, 895-904.

Rao, P. B., A. R. Jain, P. Kishore, P. Balamuralidhar, S. H. Damle, and G. Viswanathan (1995), Indian MST radar: l. System description and sample vector wind measurements in ST mode, Radio Sci., 30, 1125.

Rao P. B., A. K. Patra, T. V. Chandrasekhar Sarma, B. V. Krishnamurthy, K. S. V. Subbarao and S. S. Hari (1997), Radar observations of updrafting and downdrafting plasma depletions associated with the equatorial spread-F, Radio Sci., 32, 1215.

Rao, P. B., and A. K. Patra (1998), Recent advances on equatorial spread F, Proc. Indian Acad. Sci., 127.

Rao, C. S. R., and P. L. Malhotra (1964), A study of geomagnetic anomaly during I. G. Y., J. Atmos., Terr. Phys., A26, 1075-1085.

Rastogi, R. G. and R.P.Sharma, (1971) Ionospheric electron content at Ahmedabad (near the crest of equatorial anomaly) by using beacon satellite transmission during half a solar cycle, Planet, Space Sci., 19, 1505–1517

Rastogi, R. G., Chandra, H., and Chakravarty, S. C. (1971), The disappearance of equatorial Es and the reversal of electrojet current, Proc. Indian Acad. Sci. Sect. A, 74, 62–67.

Rastogi, R. G., H. Chandra, and S. C. Chakravarty (1971a) , The disappearance of equatorial Es and the reversal of electrojet current, Proc. Ind. Acad. Sci., 73, 62–67.

Rastogi, R. G. (1972), Sudden disappearance of Esq and the reversal of the equatorial electric fields, Ann. Geophys., 28, 717–728.

Rastogi, R. G., R. P.Sharma, and V.Shodan (1973) Total electron content of the equatorial ionosphere, Planet Space Sci., 21, 713–720.

Rastogi, R. G., K. N. Iyer and J. C.Bhattacharya (1975) Total Electroncontent of the ionosphere over the magnetic equator, Current Science, 44, 531–533.

Rastogi, R. G. (1980), Equatorial storm sudden commencement and interplanetary magnetic field, Ind. J Radio & Space Phys., 9, 173–181, 1980.

Rastogi, R. G. and Aarons, J (1980), Nighttime ionospheric radio scintillations and vertical drifts at the magnetic equator, *J. Atmos. Terr. Phys*., 42, 583–591.

Rastogi R..G. and R..F. Woodman (1978), VHF radio wave scattering due to range and frequency types of equatorial spread-F, Journal of Atmospheric and Terrestrial Physics, Volume 40, Issue 4, Pages 485-489, 491.

Rastogi, R. G., and J. A. Klobuchar (1990), Ionospheric electron content within the equatorial F_2 layer anomaly belt, J. Geophys. Res., 95, 19045-19052.

Rastogi, R. G. (1999), Geomagnetic storm effects at low latitudes, Ann. Geophysicae 17, 438-411.

Ratcliffe, J. A. (1956), The formation of the ionospheric layers F-1 and F-2, J. Atmos. Terr. Phys., 8, 260.

Reddy, C. A. and C. V. Devasia (1981), Height and latitude structure of electric fields and currents due to local east-west winds in the equatorial electrojet, J. Geophys. Res., 86, 5751-5767.

Reddy C. A., V. V. Somayajulu and C. V. Devisia, (1978), Global scale electrodynamical coupling of the auroral and equatorial dynamo regions, J.Atmos. Solar-Terres. Phys. 41, 189-201.

Richmond, A. D. (1978) Gravity wave generation, propagation, and dissipation in the thermosphere, J. Geophys. Res., 83, 4131–4145.

Rishbeth, H., and O. K. Garriott (1969*),* Introduction to ionospheric physics, Academic Press, New York.

Rishbeth, H. (1971), Polarization fields produced by winds in the equatorial F-region, Planet. Space Sci., 19, 357-369.

Rush, C. M., and A. D. Richmond (1973), The relationship between the structure of the equatorial anomaly and the strength of the equatorial electrojet, J. Atmos. Terr. Phys., 35, 1171– 1180.

Rodrigues, F. S., de Paula, E. R., Iyer, K. N., Kintner, P. M., Abdu, M. A., and Jardim, A. C.(2004), Equatorial spread F irregularity characteristics over S˜ao Lu´ıs, Brazil, using VHF radar and GPS scintillations techniques, Radio Sci., 39, No 1, RS1S31, doi:10.1029/2002RS002826.

Rohrbaugh, R. P., Hanson, W. B., Tinsley, B. A., Cragin, B. L., and McClure, J. P. (1989), Images of transequatorial bubbles based on fieldaligned airglow from Haleakela in 1984–1986, *J. Geophys. Res*., 94, 6763–6770.

Sahai, Y., P.R.Fagundes, F.Becker-Guedes, M. J. A. Bolzan, J. R.Abalde, V. G. Pillat, R.de Jesus, W. L. C. Lima, G.Crowley, K.Shiokawa, J.W. MacDougall, H.T. Lan, K.Igarashi, and J.A.Bittencourt (2005), Effects of the major geomagnetic storms of October 2003 on the equatorial and low-latitude F region in two longitudinal sectors, J. Geophys. Res., 110, A12S91,doi:10.1029/2004JA010999.

Sales, G. S., B. W. Reinisch, J. L. Scali, and C. Dozois (1996), "Spread F and the structure of equatorial ionization depletions in the southern anomaly region", J. Geophys. Res., 101, 26,819–26,827.

Sastri, J. H. (1988), Equatorial electric fields of ionospheric disturbance dynamo origin, Ann. Geophys., 6, 635–642.

Sastri, J. H., M. A. Abdu, and J. H. A. Sobral (1997), Response of equatorial ionosphere to episodes of asymmetric ring current activity, Ann. Geophys., 15, 1316–1323.

Sastri J. H., N. Jyoti, V. V. Somayajulu, H. Chandra and C. V. Devasia (2000), Ionospheric storm of early November 1993 in the Indian equatorial region, J. Geophys. Res., 105, 18,443-18, 445.

Sastri J. H., K. Niranjan, and K. S. V. Subbarao, (2002) Response of the equatorial ionosphere in the Indian (midnight) sector to the severe magnetic storm of July 15, 2000 Geophys. Res. Lett., 29(13), 1651, doi:10.1029/2002GL015133.

Scannapieco, A.J., and S.L. Ossakow (1976), Nonlinear equatorial spread F, Geophys. Res. Lett., 3, 451.

Sekar, R., and R. Raghavarao(1987), Role of vertical winds on the Rayleigh-Taylor mode instabilities of the nighttime equatorial ionosphere, J. Atmos. Terr. Phys., 49, 981.

Sekar, R., R. Suhasini, and R. Raghavarao(1995), Evolution of plasma bubbles in the equatorial F-region with different seeding conditions, Geophys. Res. Lett., 22, 885-888.

Sekar, R., and R. Raghavarao (1995), Critical role of the equatorial topside F-region on the evolutionary characteristics of the plasma bubbles, Geophys. Res. Lett., 22, 3255.

Sekar R., R. Sridharan and R. Raghavarao (1997), Equatorial plasma bubble evolution and its role in the generation of irregularities in the F region, J. Geophys. Res., 102, 20,063.

Sekar, R., Kherani, E., Rao, P. B., and Patra, A. K. (2001), Interaction of two long-wavelength modes in the nonlinear numerical simulation model of equatorial spread F, J. Geophys. Res., 106(A11), 24765-24775.

Sekar, R., Chakrabarty, D., Narayanan, R., Sripathi, S., Patra, A. K., and Subbarao, K. S. V. (2004): Characterization of VHF radar observations associated with equatorial Spread F by narrow-band optical measurements, Ann. Geophys., 22, 3129-3136.

Sekar, R., Chakrabarty, D., Sarkhel, S., Patra, A. K., Devasia, C. V., and Kelley, M. C. (2007), Identification of active fossil bubbles based on coordinated VHF radar and airglow measurements, Ann. Geophys., 25,2099-2102.

Sekar, R., Chakrabarty, D., Narayanan, R., and Patra, A. K.(2008): Equatorial Spread F structures and associated airglow intensity variations observed over Gadanki, Ann. Geophys., 26, 3863-3873.

Sethia G., R.G. Rastogi, M.R.Deshpande, and H.Chandra (1980) Equatorial electrojet control of the low latitude ionosphere, J.Geomag. Geoelectr., 32, 207–216.

Sivaraman, M. R., R. Suhasini and R. Raghavarao (1976), Role of ambipolar diffusion in the development of equatorial anomaly in solar maximum and minimum period, Ind. J. Radio Space Phys., 5, 136-144.

Sharma, P. and R. Raghavarao (1989), Simultaneous occurrence of ionization ledge and counterelectrojet in the equatorial ionosphere: observational evidence and its implications, *Can. J. Phys.*, 67, 166–172.

Smith, E. K., 1957, NBS Circular No. 582.

Sobral, J. H. A., M. A. Abdu, W. D. Gonzalez, B. T. Tsurutani, I. S. Batista, and A. C. de Gonzalez (1997), Effects of intense storms and substorms on the equatorial Ionosphere/Thermosphere system in the American sector from ground based and satellite data, J. Geophys. Res., 102, 14,305– 14,313.

Somayajulu, V. V., Ligi Cherian, K. Rajeev, Geetha Ramkumar and C. Raghava Reddi (1993), Mean winds and tidal components during counter electrojet events, Geophys. Res. Lett., 20, 1443-1446.

Somayajulu, Y. V., S. C. Garg, R. S. Dabas, L. Singh, T. R. Tyagi, B. Lokanadham, S. Ramakrishna, and G. Navneeth, 1984: Multistation study of nighttime scintillations in low latitudes : Evidence of control by equatorial F-region irregularities. *Rad. Sci.,* 19, 707-718.

Spencer. M (1955), The Shape of Irregularities in the Upper Ionosphere, Proc. Phys. Soc, B, 68, 493.

Sridharan, R., R. Narayanan, N. K. Modi, and D. Pallam Raju (1993), Novel mask design for Multiwavelength dayglow photometery, Appl. Opt., 32, 4178-4180.

Sridharan, R., R. Sekar and S. Gurubaran (1993a), Two dimensional high resolution imaging of the equatorial plasma fountain, J. Atmos. Terr. Phys. 55, 1661-1665.

Sridharan, R. N K Modi, D Pallam Raju, R Narayanan, Tarun K Pant, Alok Taori and D Chakrabarty (1998), Multiwavelength Daytime photometer- A new tool for the investigation of atmospheric processes, Measurement Sci. Tech.,9, 585-591.

Spiro, R. W., R.A.Wolf, and B.G.Fejer (1988) Penetration of high latitude-electric-field effects to low latidudes during SUNDIAL 1984, Ann. Geophys., 6, 39–50, http://www.ann-geophys.net/6/39/.

Sripathi, S., S. Bose, A. K. Patra, T. K. Pant, B. Kakad, and A. Bhattacharyya (2008) Simultaneous observations of ESF irregularities over Indian region using radar and GPS, Ann. Geophys., 26, 3197-3213.

Stewart, B., Encyclopedia Britannica, 9th Ed., 16, 181, 1882.

Tiwari, D., A. K. Patra, C. V. Devasia, R. Sridharan, N. Jyoti, K. S. Viswanathan, and K. S. V. Subbarao (2004), Radar Observations of 8.3-m scale equatorial spread F irregularities over Trivandrum, *Ann. Geophys*.,22,911–922.

Tsurutani, B. T. et al, (2004), Global dayside ionospheric uplift and enhancement associated with Interplanetary electric field, J.Geophys. Res., 109, A08302, doi:10.1029/2003JA010342.

Tsurutani, B. T., O. P. Verkhoglyadova, A. J. Mannucci (2008) et al Prompt Penetration Electric Field (PPEF) and their ionospheric effects during great geomagnetic storm of 30–31 October, 2003 J. Geophys. Res., 113, A05311, doi:10.1029/2007JA012879.

Tsunoda, R. T. (1980), Backscatter measurements of 11 cm equatorial spread F irregularities, *Geophys. Res. Lett*., 7, 848.

Tsunoda, R., and Towle, D. (1979), On the Spatial Relationship of 1-Meter Equatorial Spread-F Irregularities and Depletions in Total Electron Content, Geophys. Res. Lett., 6(11), 873-876.

Tsunoda, R. T., Livingston, R. C., McClure, J. P., and Hanson,W. B. (1982), Equatorial Plasma Bubbles: Vertically Elongated Wedges From the Bottomside F Layer, J. Geophys. Res., 87(A11), 91719180.

Tsunoda, R. T. and White, B. R. (1981), On the generation and growth of equatorial backscatter plumes – 1. Wave structure in the bottomside F layer", J. Geophys. Res., 86, 3610–3616.

Van Velthoven, P. J. (1990) Medium-scale irregularities in the ionospheric electron content, Ph.D. Thesis, Technische Universiteit Eindhoven.

Valladares et al. C. E., W. B. Hanson, J. P. McClure, and B. I. Cragin (1983), Bottomside sinusoidal irregularities in the equatorial F-region, J. Geophys. Res., 88, 8025.

Valladares, C. E., Sheehan, R., Basu, S., Kuenzler, H., and Espinoza (1996), The multi-instrumented studies of equatorial thermosphere aeronomy scintillation system: Climatology of zonal drifts, J. Geophys. Res., 101, 26 939.

Valladares, C. E., J. Villalobos, R. Sheehan and M. P. Hagan (2004) Latitudinal extension of low latitude scintillations measured with a network of GPS receivers, Ann. Geophys., 22, 3155-3175.

Woodman, R. F., and La Hoz C. (1976), Radar observations of F-region equatorial irregularities., J. Geophys. Res., 41, 5447.

Walker, G. O., J. H. K. Ma., R. G. Rastogi, M. R. Deshpande and H. Chandra (1980), Dissimilar forms of the ionospheric equatorial anomaly observed in East Asia and India, J. Atmos. Terr. Phys., 42, 629- 635.

Walker, G. O., J. H. K. Ma., and E. Gotton (1994), The equatorial ionosphere anomaly in electron content from solar minimum to solar maximum from South-East Asia, Ann. Geophysicae, 12, 195-209.

Warnant, R. (2000) The increase of ionospheric activity as measured by GPS, Earth Planets Space, 52, 1055–1060.

Watanabe, S., and Oya, H. (1986), Occurrence characteristics of low latitude ionosphere irregularities observed by impedance probe on board Hinotori satellite, J. Geomagn. Geoelectr., 38, 125.

Weber, E. J., Buchau J., Ether H., and Mende S. B. (1978), North-South aligned equatorial airglow depletions, J. Geophys. Res., 83, 712.

Whalen, J. A. (2001), The equatorial anomaly: Its quantitative relation to equatorial bubbles, bottomside spread F and ExB drift velocity during a month at solar maximum*, J. Geophys. Res*., 106, 29125.

Whalen, J. A. (2002), Dependence of the equatorial bubbles and bottomside spread F on season, geomagnetic activity, and E×B drift velocity during solar maximum, J. Geophys. Res., 107, doi:10.1029/2001JA000039.

Whitehead, J.D. (1970), The gradient drift instability in bounded ionospheric layers, J. Atmos. Terr. Phys., 32, 1283.

Woodman, R.F., and C. LaHoz (1976), Radar observations of F region equatorial irregularities, J. Geophys. Res., 81, 5447.

Wu, Chin-Chun, K.Liou, Shao-Ju, Shan, and C. L. Tseng (2008) Variation of Ionospheric Total Electron Content in Taiwan Region of the Equatorial Anomaly from 1994–2003, Adv. Space Res., 41, 611–616.

Yeh, K.C., and C-H. Liu (1982), Radio wave scintillation in the ionosphere, Proc IEEE, *70,* 324-360/.

Yokoyama T., M. Yamamoto, S. Fukao (2005), T. Takahashi, and M. Tanaka, "Numerical simulation of mid-latitude ionospheric E-region based on SEEK and SEEK-2 observations", Annales Geophysicae, 23, 2377–2384.

Zalesak, S. T., and S. L. Ossakow (1980), Nonlinear equatorial spread F: Spatially large bubbles resulting from large scale initial perturbations, *J. Geophys. Res*., 85, 2131.

Zhao, B., W. Wan, and L. Liu (2005), Response of equatorial anomaly to the October–November 2003 superstorm, Ann. Geophys., 23, 693– 706.